Department of Civil Engineering

University of Nottingham

Composite Steel Beams Using Precast Concrete Hollow Core Floor Slabs

by

Dennis Lam

Thesis submitted to the University of Nottingham for the degree of

Doctor of Philosophy

March 1998

Contents

Appendix A

Acknowledgement

I would first like to thank my supervisors, Professor David Nethercot and Dr. Kim Elliott, for their guidance and support throughout the course of my research for which I am greatly indebted.

I would also like to thank Mr. Mike Bettison for his assistance with the testing. Thanks are also due to the technicians Mr. G. Mitchell and Mr. C. Lambert who helped with the fabrication and casting of the specimens. Assistance from all other technical staff in the Department is also acknowledge.

I would like to express my gratitude to University of Nottingham for providing the experimental, computing and other facilities.

Thanks are due to Engineering and Physical Science Research Council for sponsoring the testing, Bison Floors Limited for providing the hollow core units, J.N. Rowen Limited and Bison Structures Limited for supplying the steelwork.

I would also like to thank City of Wakefield Metropolitan District Council and University of Leeds for financial support and allowing time off to conduct the research for which I am very grateful.

Finally thanks are due to my wife Josephine, my daughter Anthea and my son Kyle for their patience, support and encouragement throughout the duration of my research. It would have been impossible for me to complete this thesis in such a manner without their support.

Declaration

I declare that this thesis is the result of my own work. No part of this thesis has been submitted to any other University or other educational establishment for a Degree, Diploma or other qualification.

(Dennis Lam)

Abstract

The main aim of this thesis is to develop an insight into the behaviour of composite floors that utilise steel beams acting in combination with precast concrete hollow core floor slabs and to produce design recommendations for use by industry for this type of construction.

Full scale bending tests of proprietary precast prestressed concrete hollow core unit floor slabs attached through 19mm diameter headed shear studs to steel Universal Beams (UB) have been carried out to determine the increased strength and stiffness when composite action is considered. The results show the bending strength of the composite beam to be twice that of the bare steel beam, and its flexural stiffness to be more than trebled.

In addition to the beam tests, isolated push-off tests and horizontal eccentric compression tests were used to study the horizontal interface shear resistance of the headed studs and the strength of the slab, respectively. Maximum resistances were compared with the predictions of the Eurcode EC4, and a reduction formula for the precast effect derived.

In addition to the experimental investigations, finite element (FE) studies were also conducted using the FE package ABAQUS to extend the scope of the

experimental work. Results show a 2-dimensional plane stress analysis to be sufficiently accurate, providing the correct material input data obtained from isolated push-off and compression tests are used. The FE model for the composite beam was designed and validated using the full scale beam tests. A parametric study, involving 45 analyses, was carried out to cover the full range of UB sizes and floor depths used in practice. From the finite element work, design charts are formulated which may be used to simplify the design rules.

Given the results of this work, a full interaction composite beam design may be carried out using the proposed design equations. The results show that precast slabs may be used compositely with steel UB's in order to increase both flexural strength and stiffness at virtually no extra cost, except for the headed shear studs. The failure mode is ductile, and may be controlled by the correct use of small quantities of transverse reinforcement and insitu infill concrete.

List of Figures

Chapter 1

Chapter 2

Chapter 3

Chapter 4

Chapter 5

Chapter 6

Chapter 7

Chapter 8

Appendix A

List of Tables

Chapter 3

Chapter 4

Chapter 5

Chapter 6

Chapter 7

Chapter 8

Appendix A

Notation

A	area of combined section
A_c	area of concrete
A_{conc}	area of concrete element
A_d	cross sectional area of the stud
A_s	area of transverse reinforcement
A_{steel}	area of steel element
b_{eff}	effective breadth of concrete slab
b_l	half the transverse spans of the slab on the left of the steel beam
b_r	half the transverse spans of the slab on the right of the steel beam
d	diameter of headed shear stud
d_p	depth of concrete slab
D	depth of steel section
e	eccentricity from the slab neutral axis
E	modulus of elasticity of combined section
E_c	static modulus of elasticity of the insitu infill concrete
E_{cp}	average value of elastic modulus of the insitu and precast concrete
E_s	modulus of elasticity of steel
f_b	bearing stress of headed stud

f_c	concrete cylinder compressive strength
f_{ck}	characteristic concrete cylinder compressive strength specified in EC4
f_{cp}	average concrete cylinder strength of the insitu and precast concrete
f_{ct}	concrete tensile strength
f_{cu}	characteristic concrete cube strength
f_t'	effective tensile strength
f_u	ultimate tensile strength of the headed stud material
f_y	characteristic strength of reinforcement
F	applied eccentric load
F_{con}	resistance force of shear connector
F_{conc}	resistance force of concrete flange
F_{flange}	axial capacity of one steel flange of thickness T
F_{shear}	total shear force on the shear connectors in the shear span
F_{steel}	resistance force of steel beam
g	gap width between ends of hollow core unit
h	overall length of stud
h_p	height of profiled deck
h_c	centroid of the concrete element from the steel/concrete interface
h_s	centroid of the steel element from the steel/concrete interface
H	height of stud connector in rib
I	second moment of area of the combined section

I_c	second moment of area of the concrete element about its centroidal axis
I_{com}	second moment of area of the composite section
I_s	second moment of area of the steel element about its centroidal axis
k_s	shear stiffness of headed stud
K_i	initial shear stiffness
l	width of concrete slab
L_s	length of shear plane
M	moment
M_c	measured moment capacity
M_{com}	composite moment
M_{comp}	moment capacity of the composite beam
M_R	moment capacity
$M_{R(steel)}$	plastic moment capacity of the fully restrained steel beam
M_y	moment at maximum load
n	number of shear connector in half span
N	number of studs per rib
p	confinement pressure
P	applied load per headed stud
P_D	shear capacity of tie bars

P_{RD}	shear resistance of shear stud
p_r	transverse reinforcement stress
p_y	material yield strength of steel UB
q	shear force transmitted per unit length of beam
Q_k	characteristic shear force resistance of shear stud specified in BS 5950
Q_{rib}	shear strength of connection in profiled deck
Q_{sol}	shear strength of a connector in a solid slab
Q_T	shear capacity of headed stud
Q_u	ultimate shear force resistance of the headed studs
R	geometric ratio
s	slip of shear stud
S	slip coefficient
S_x	plastic modulus of steel beam
T	thickness of steel flange
v_{dow}	dowel strength of the transverse reinforcement
v_{fric}	shear resistance by friction
v_{lock}	shear resistance through interface interlock
v_u	total shear strength across the shear plane
V_u	shear force across the shear plane
w	width of hcu
w_r	average rib width of profiled deck

x	coordinate transverse to the centreline of the steel
Z_c	elastic modulus of concrete slab
α	coefficient for headed stud
α_e	ratio of the elastic moduli of steel to concrete (modular ratio)
β	gap width factor
δ	deflection of beam
δ_{full}	deflection of composite beam with full interaction
δ_{part}	deflection of composite beam with part interaction
ε_c	elastic strain at the bottom of the concrete element
ε_s	elastic strain at the top of the steel element
ϕ	diameter of transverse reinforcement
γ_v	partial safety factor
η	stud spacing
κ	curvature of composite beam
λ	transverse reinforcement factor
μ	coefficient of friction
ρ	percentage of transverse reinforcement to area of concrete
σ_{max}	maximum stress
σ_c	maximum concrete stress at the extreme fibre
σ_t	maximum tensile stress
σ_u	ultimate compressive strength

σ_x	curvilinear stress
ω	transverse joint factor

F.E. notations used in Chapter 6 were not included and will be introduced at the relevant sections.

Abbreviations

DG	dial gauges
ERSG	electrical resistance strain gauges
FE	finite element
M-D	moment-deflection
N.A.	neutral axis
POT	linear voltage displacement potentiometers
hcu	hollow core unit

Chapter 1

Introduction

1.1 Background

One of the most effective ways to improve structural efficiency is to utilise the favourable structural properties of the basic components and connectors and to combine them in a manner which leads to maximum performance in a safe and cost effective way. Composite action between steel beams and concrete slabs by the use of shear connectors is responsible for a considerable increase in the load-carrying capacity and stiffness of the steel beams, which when utilised in design, can result in significant saving in steel weight and in construction depth. These economies have largely accounted for the dominance of composite steel frame construction in the commercial building sector in the UK in recent years. Composite construction of steel frames with profiled steel decking to support floor slabs is now common in multi-storey steel frame construction, but the use of precast concrete hollow core units (hcu) in conjunction with the steel frame to provide composite action is relatively new and unknown.

Precast concrete hcu floors are already used extensively in long span steel framed buildings. The precast hcu is considered in isolation from the beam and no

composite action is assumed. Tie steel is placed on site into the milled slots made at the top of the hollow cores, which are filled with grade C25 (minimum) insitu concrete. The slab sits directly on the top flange of the steel beam as shown in Fig. 1.1 and there is no mechanical (or otherwise) connection to the beam.

In the case of composite floor construction with profiled steel decking to support the floor slab, headed stud shear connectors are welded through the steel decking and into the top flange of the steel beam before the concrete floor slab is poured. The disadvantages are associated with the operation and cost of welding the connectors through the decking on site, limitations to maximum spans of about 3.5m without propping or the addition of framing, and a 'wet-trade' is involved for pouring the concrete floor that prevents a dry construction environment.

Composite construction incorporating hcu's is intended to complement the now traditional steel frame / steel decking method and to offer advantages where for reasons of design or environmental considerations a steel decking system may be precluded. The main advantages of this form of construction are that precast concrete slabs can span up to 15 metres without propping. The erection of 1.2 metres wide precast concrete units is simple and quick. Shear studs are pre-welded on beams before delivery to site, thereby offering additional savings associated with shorter construction times. Because no return is received from money invested in the construction of a multi-storey building until the building is occupied, the loss of income from capital may be 10% of the total cost of the

building for a construction time of two years; that is, about one-third of the cost of the structure.

Fig. 1.2 shows the details of the precast-insitu joint of the composite beam with hcu. The longitudinal and transverse joint between the hcu's is filled insitu with grout or concrete so that horizontal compressive membrane forces can be transferred through the slab. A minimum 28 day compressive cube strength of the infill of 25 N/mm^2 is used in design. The infill is placed manually and without mechanical vibration, the ease of placing which depends on the edge profile of the slab. Manufacturers have responded to the calls to make the width of the gap about 40 to 50 mm at the top and not less than 20mm at its narrowest. The FIP design recommendations[1] are shown in Fig. 1.3, and in general most of the slabs conform to these requirements.

Shear connectors are pre-welded to the steel beams and an adequate amount of concrete is to be placed and compacted around the shear connectors. The spacing of the shear connectors is determined from the requirements of the shear force interaction along the plane A-A as shown in Fig. 1.2. The modern form of shear connector is the headed stud, the most popular of which is 19mm diameter and 125mm height and this was used for all the tests. To allow the placing of insitu concrete, the ends of the hcu are shaped on the casting bed to the profile shown in Fig. 1.2 and 1.4. The tops of the hollow cores in the slabs are left open at 400mm

centres for 500mm in length to permit the placement of transverse reinforcement spanning across the longitudinal joint.

1.2 Hollow core units

Hollow core units (hcu) are now the most widely used type of precast floor; in Europe annual production is about 20 million m^2, representing 40 to 60 per cent of the precast flooring market. This success is largely due to the highly efficient design and production methods, choice of unit depth and structural efficiency.

The design of dry cast hcu originated in the United States in the late 1940s following the development of the high strength strand that could be reliably pre-tensioned over distances of 100m to 150m. This coincided with advancements in zero slump (hence the term 'dry') concrete production which inevitably led to factory made hcu. Hcu have longitudinal voids and are produced on a long prestressing bed either by slip form or extrusion and are then saw cut to length. The degree of prestress and the depth of unit are the two main design parameters. The depth ranges from 150 to 400mm, with the performance limited to a maximum span / depth ratio of around 50, although 35 is more usual for normal office loading conditions. A 75mm (nominal) dry bearing length is used onto concrete, although the British Standard BS8110[(2)] permits an absolute minimum bearing length of 40mm where saw cut units bear onto steel surfaces. Dimensional

deviations are less than ± 5mm in depth and width, and ± 10mm in length. Cross section, concrete strength and surface finish are standard to each system of manufacture. Hcu's manufactured by the slip forming technique by Bison Floor Ltd. have been used for all the experimental work throughout. The width of units are based on a nominal 1200mm. More than 95 per cent of units produced are 1200mm wide. The actual width of 1197 mm allows for constructional tolerances and prevents overrunning of the floor layout due to accumulative errors. Openings and cut-outs are easily formed by circular saw whilst the concrete is 'green', i.e. less than 12 hours old.

1.3 Objectives of the research

The use of hcu with steel beams in composite construction is relatively new, with little research having been conducted in this area. The main purpose of the present research is to develop an understanding of the behaviour of this form of construction and to demonstrate the advantages in utilising the composite action which takes place between hcu slabs and steel beams. Specifically, the objectives of the research are:

[1] To study the interaction between precast prestressed hcu slabs and structural steelwork beams.

[2] To determine the flexural strength and stiffness and the horizontal shear capabilities of floors.

[3] To propose design recommendations for composite steel beam - precast hcu slab construction.

1.4 Scope of the thesis

To study the flexural behaviour of the hcu slabs and steel beam composite construction, the major issues were (a) the compression behaviour of the hcu slabs, and (b) the transfer of the horizontal shear forces between the steel beam and the concrete slab. To achieve this full scale bending tests were supplemented by (a) horizontal eccentric compression tests and (b) horizontal push-off tests, as shown in Fig. 1.5. In addition to the experimental work described, analytical studies using the finite element technique were employed to carry out parametric studies. The work is arranged into nine chapters.

Chapter 2 describes previous work related to composite beams with solid slab and metal decking construction. A review of current work on composite beams with hcu is also presented. The test programme of this study is reported in Chapters 3, 4 and 5. Chapter 3 covers the horizontal compression tests of the hcu and Chapter 4 describes the push off tests. Full scale composite beam tests are reported in Chapter 5. In Chapter 6, the finite element method is used to simulate the behaviour of the composite beam. The results from the FE work are compared and validated against the experimental work. Parametric studies for the composite

beam using the finite element model are reported in Chapter 7. Finally, all the major findings are discussed in Chapter 8 with conclusions and recommendations given in Chapter 9.

1.5 References

1. BS8110, Part 1 (1997) Structural Use of Concrete, British Standards Institution, London.
2. Federation Internationale de la Precontrainte recommendations - Precast prestressed hollow core floors, Thomas Telford, London, 1988.

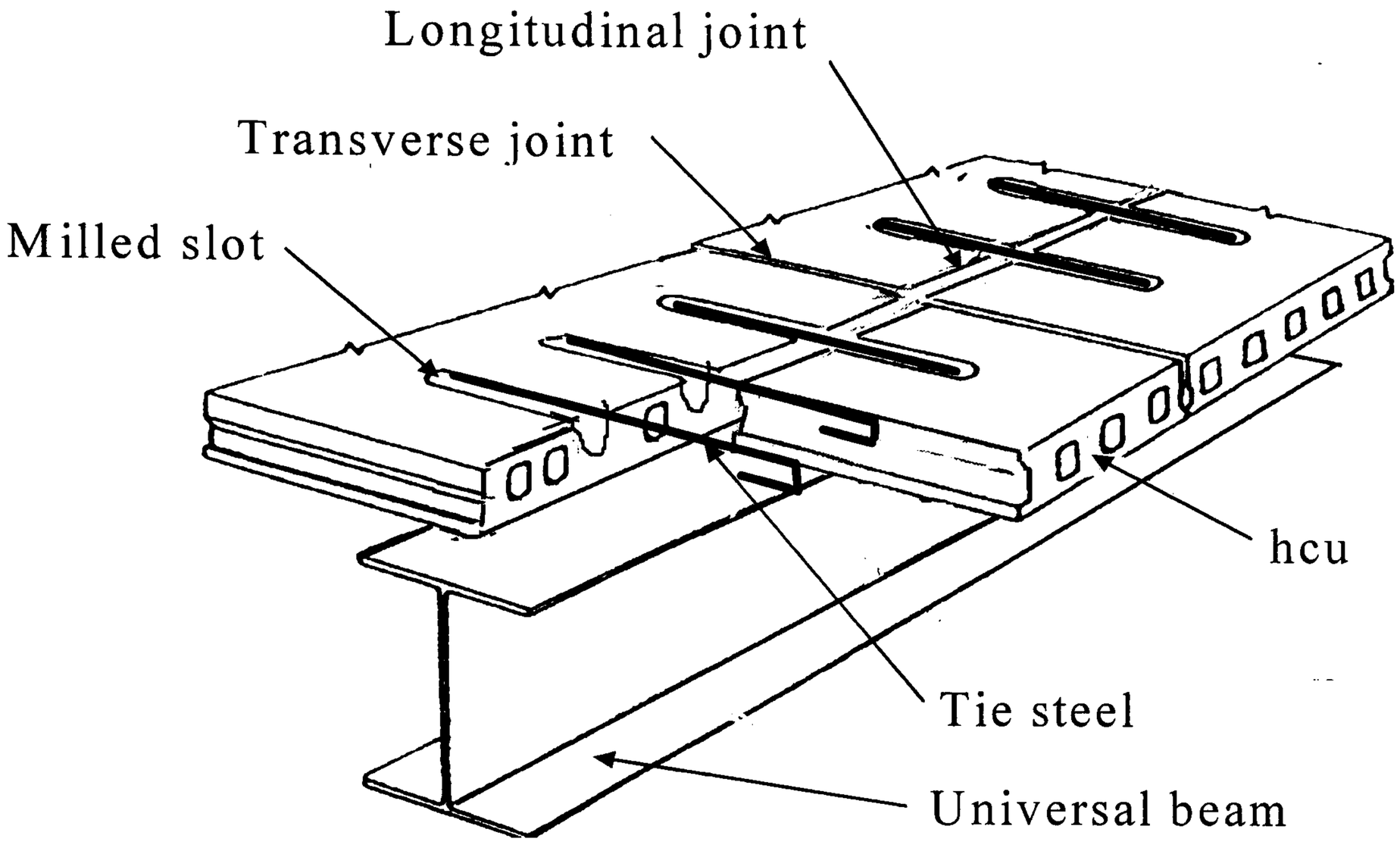

Fig. 1.1 Non composite beam with hollow core slab

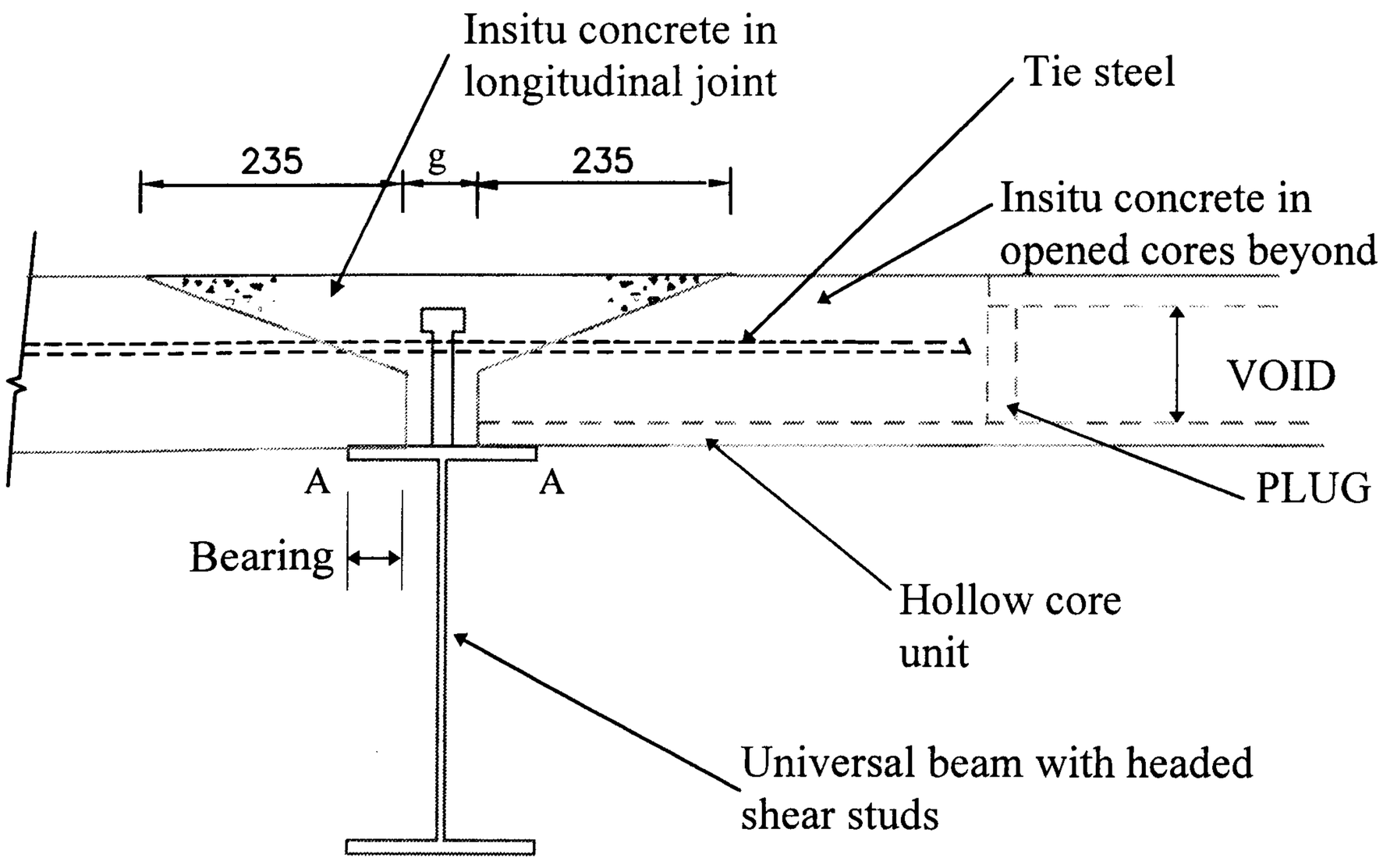

Fig. 1.2 Details of the precast-insitu joint of composite beam with hollow core unit

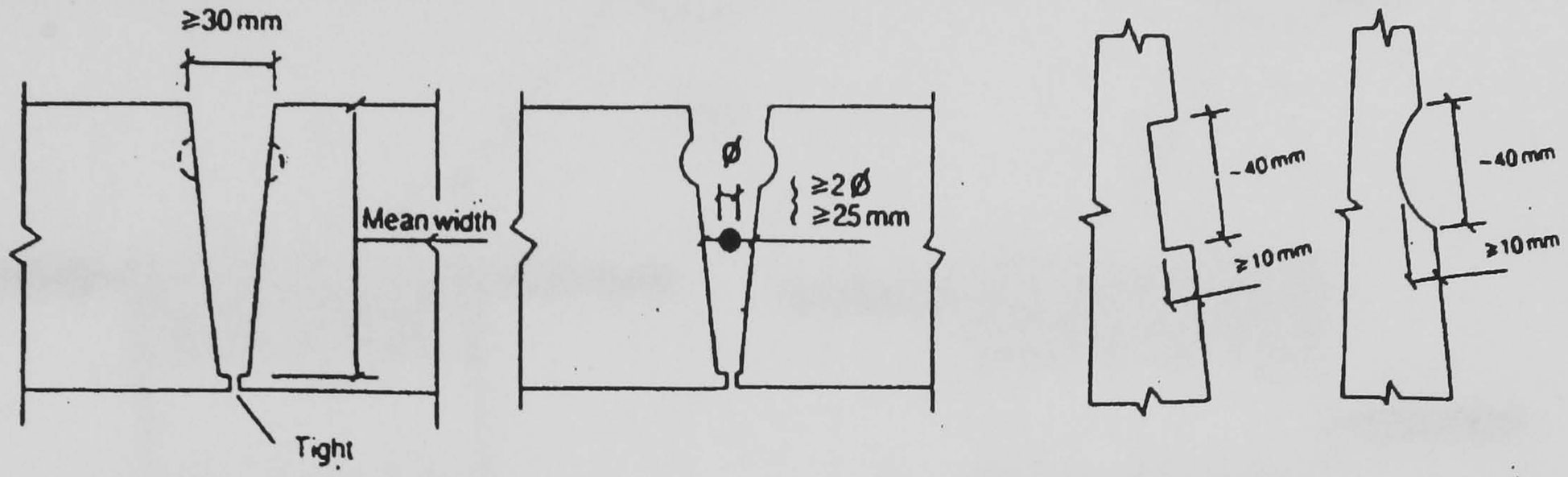

Fig. 1.3 Edge profile of hollow core slab

Fig. 1.4 Precast hollow core units with milled slots and shaped ends

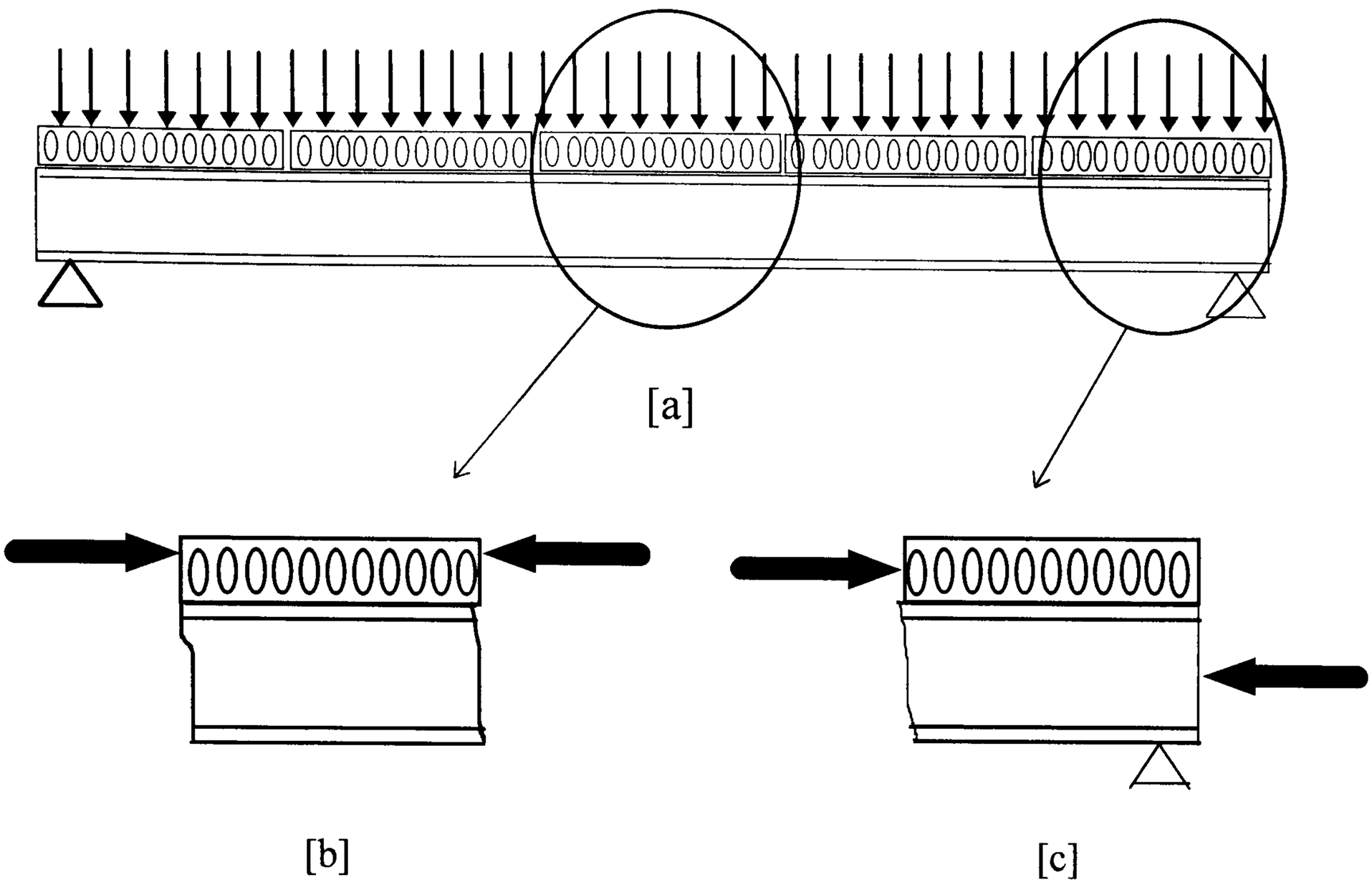

Fig. 1.5 Simplification of testing regime for [a] full scale bending test
[b] isolation eccentric compression slab tests [c] isolated push-off tests

Chapter 2

Review of literature

2.1 Historical review

The use of steel-concrete composite construction was first investigated in the early twentieth century. The early investigators of composite beams were concerned primarily with the interaction between the steel and concrete from the natural bonding between the two materials. The first beam tests were carried out in Canada and reported by MacKay, Gilespie and Leluau in 1923[1]. Two beam tests were carried out and each consisted of two steel I beams encased in concrete and a concrete slab. Further tests on composite beams without shear connectors were carried out between 1923 - 1939 in the United State, mainland Europe and the UK. Good interaction between the encased steel beam and the slab was observed. The most comprehensive experimental study on composite beams relying primarily on natural bond was reported by Batho, Lash and Kirkham in 1939[2]. The investigators concluded that the theory for reinforced concrete is applicable to composite beams as long as bond is present; all beams failed as soon as slippage occurred between the steel beam and concrete encasement. These early investigations have indicated further that the weakness of bond may be remedied by mechanical connectors attached to the top flange of the steel beam and

embedded in the concrete of the slab. A review on composite beams without shear connectors is reported in detail by Viest[3].

The first systematic studies with mechanical connectors were made in Switzerland using spiral shear connectors by Voellmy in 1930's. By 1940, practically all investigation of composite action utilised mechanical connectors. This early work on the concept of composite action with shear connectors was centred mainly on the studies into suitable forms of shear connector. Sixteen push-off specimens, four with spirals, four with flexible angles, four with flexible channels and four with stiff H-sections, were tested at Lehigh University in 1943, to make a comparative study of the behaviour of connectors. Further studies on spiral connectors, rigid connectors such as inclined hooks and bar and flexible angles and channels were made between 1943 to 1958. While European practice in Switzerland and Germany turned toward hooks and stiff connectors, American engineers showed a preference for flexible connectors that required less fabrication. A full review on this area has been presented by Viest[3].

Studies of stud connectors did not begin until 1954. Push off tests on stud connectors were first carried out at the University of Illinois by Viest[4]. The study used straight studs with an upset head of diameters ranging from 0.5 in. to 1.25 in. Fatigue and static tests were also performed by Thurlimann[5] at Lehigh University in 1958. These push-off studies used 0.5 in. diameter bent studs and, to a lesser extent, 0.75 in. diameter straight studs with an upset head. All the push-off tests

showed that steel studs are suitable for use as a shear connector and that the behaviour of a stud connector is similar to that of a flexible channel connector. The shear capacity was found to be a function of the diameter and height of the stud and of the strength of concrete.

Investigations for use of a headed shear stud were first carried out by Chapman and Balakrishnan[6,7] at Imperial College in 1964. Nine push-off tests with headed studs of ½ in. and ¾ in. diameter were carried out together with three tests with bent studs and T's for comparison. Results showed that the capacity of headed studs are comparable to the bent studs. In addition, a series of beam tests were carried out at the same time using headed studs with a solid slab. The shear strength of the headed stud connector was not presented until 1971 after extensive push-off tests were carried out by Ollgaard et al[8] at Lehigh University and by Menzies[9] at the Building Research Station (BRE).

The composite beam with metal deck was first studied in 1969 by Robinson[10] in Canada whilst similar tests were carried out at Lehigh University in 1971. Seventeen full scale beam tests were carried out at Lehigh with a light weight concrete slab cast on a metal deck and connected by ¾ in. diameter headed studs. The tests were reported in detail by Grant, Fisher and Slutter[11]. Tests on composite beams with ribbed metal deck were conducted by Robinson[12] in 1987, two full scale beam tests and seventeen push-off tests were carried out. In the UK, research on composite beams with metal decking was first carried out at Cardiff

University by Wright[13] and at Warwick University by Johnson[14] in 1990. Thirty-five push-off tests using through-deck welded head studs were carried out by Johnson while four full scale beam tests were conducted by Wright. Insitu testing of a composite floor system with profiled deck was also carried out by Wright[15] in Cardiff. In addition to the above work done on profiled deck with welded headed stud connectors, research on composite beams with profiled deck and non-welded shear connectors was carried out by O'Leary[16] at Salford University in 1988 and Crisinel[17] at EPFL, Lausanne in 1990. Since the early 1990's, research work on composite construction has moved towards connections and frame stability.

Although the use of precast hollow core units (hcu) dates back to the 1940's, research on composite construction incorporating steel beams with a hcu floor is relatively new. Some commercial testing in this area was carried out at Salford University and reported by Hamilton[18] in 1989. Very recently, research on shear connector strength in precast solid concrete planks was carried out by Moy[19] and work on composite beams with precast planks for car parks was carried out by Jolly[20] at Southampton University in 1994 and 1996, respectively.

2.2 Previous studies on shear strength of headed stud connector

In steel-to-concrete composite construction longitudinal shear forces are transferred across the steel - concrete interface by the mechanical action of shear connectors, such as headed studs welded to the flanges of the steel beams. The shear strength and stiffness of the connection is not only dependent on the strength of the stud itself, but also on the resistance of the concrete slab against longitudinal cracking caused by the high concentration of shear force at each stud. The resistance of the concrete is a function of its splitting strength, which is directly related to the nature of concrete construction around the stud.

Present knowledge of this behaviour is limited to headed studs in solid reinforced concrete slabs and profiled deck slabs. No research has determined the capacity of the connectors in a composite beam consisting of hcu slabs. A feature of these floor units, as shown in Fig. 2.1, is that no projecting reinforcement is available at the ends of the units to tie the concrete across the line of the studs. As a consequence of this construction, special arrangements must be used to provide a suitable force transfer mechanism.

The strength of shear studs in solid reinforced concrete slabs was first presented as an empirical formula in 1971 by Ollgaard et al[8] after carrying out 48 push-off tests. Fig. 2.2 shows a typical load-slip curve of 19mm headed stud in reinforced

concrete slab. The ultimate shear force resistance Q_u (in N units) of the headed studs was given as follows:-

$$Q_u = 0.5 A_d \sqrt{(f_c E_c)} \qquad (2.1)$$

where A_d= cross sectional area of the stud diameter d (mm^2). See Fig. 2.3.

f_c = concrete cylinder compressive strength (N/mm^2).

E_c = static modulus of elasticity of the concrete (N/mm^2).

This equation, which was adopted in CP 117 [21], assumes a concrete crushing failure rather than a shear failure of the headed stud.

Menzies[9] at BRE carried out thirty-four push-off tests with normal-density concrete slabs to elucidate the discrepancies between the observed static strengths of shear connectors and the value specified in CP117. Test results showed in the case of headed stud connectors, that connector strength was less than the appropriate values specified in the CP117. The evidence of the low strength observed in the tests suggested some reduction of the static strengths of the headed stud connectors specified in CP117 was desirable. Later in BS 5950[22], data presented by Menzies[9] were used to develop the characteristic shear force resistance Q_k. There is no theoretical basis to these data, and values given in *Table 5* in this code reflect only the size of the stud and strength of the concrete, e.g. for 19 mm diameter x 100 mm long headed stud in grade C25 concrete, the

characteristic shear capacity, Q_k is given as 95 kN. Using similar material data equation 2.1 gives Q_u = 100 kN.

In Eurocode EC4[23] the resistance P_{RD} is defined in clause 6.3.2.1. using two equations; the first representing concrete failure, and the second corresponding to failure of the stud at its collar. The lesser of the following values should be used in design:-

$$P_{RD} = 0.29\alpha d^2 \sqrt{f_{ck} E_c} / \gamma_v \qquad (2.2)$$

$$P_{RD} = 0.8 f_u \frac{\pi d^2}{4\gamma_v} \qquad (2.3)$$

where $\alpha = 0.2\ (h/d + 1) < 1.0$. See Fig. 2.3

h = overall length of stud

f_{ck}= concrete cylinder compressive strength (N/mm^2) specified in Table 3.1 of EC4

f_u = ultimate tensile strength of the headed stud material, e.g. 450 N/mm^2

γ_v = partial safety factor, taken as 1.25 at ultimate.

These equations are based on connections in solid concrete slabs by Johnson[14]; there again being no data for precast composite construction.

For shear strength of headed stud in profile decking, a reduction formula was presented by Grant, Fisher and Slutter[11]:

$$Q_{rib} = \frac{0.85}{\sqrt{N}}\left(\frac{h - h_p}{h_p}\right)\left(\frac{w_r}{h_p}\right)Q_{sol} \leq Q_{sol} \qquad (2.4)$$

where Q_{rib} = shear strength of connection in profiled deck

N = number of studs per rib

h = height of stud connector

h_p = height of profiled deck

w_r = average rib width of profiled deck

Q_{sol} = shear strength of a connector in a solid slab

This reduction factor is adopted by the recent Codes of Practice for composite beams in buildings[22,23].

2.3 Previous studies on composite beam with solid slab and headed stud connector

The most extensive study on composite beams with a solid slab and headed studs was carried out at Imperial College by Chapman[7]. Fifteen flexural beam tests with headed studs were conducted with a central point load or uniformly

distributed load. In addition, nine push-off tests were also performed. A typical load-slip curve of 19mm headed stud in solid r.c. slab is shown in Fig. 2.4. All beams failed at a load exceeding that calculated on the basis of a simple rectangular concrete stress distribution, using the measured yield stress for steel and cylinder strength of the concrete. All beams failed by crushing of the concrete slab except those beams where the connector was designed to fail before the ultimate moment of the composite beam was reached. The effect of interface slip in the elastic range was small, and the end slip at maximum load for all beams was no more than 3.0mm. Chapman also discovered that although the ultimate capacity of the shear connector found from a push-off test differs little from that found in the beam test, the slip is less in the beam test than in a corresponding push-off test.

A series of push-off tests and beam tests with headed studs carried out by Slutter and Driscoll[24] in 1965 at Lehigh University, concluded that the force in the concrete is resisted by the sum of the ultimate strengths of the individual shear connectors. The magnitude of slip might affect the magnitude of deflection at which ultimate moment occurred, but slip does not affect the magnitude of the ultimate moment. The conclusion was also reached that connectors have a higher ultimate strength in beams than in push-off specimens. Uniform spacing of shear connectors is satisfactory for beams supporting a uniform load if an adequate number of connectors is provided.

Composite beams with a solid slab were also tested at the University of Cambridge by Johnson[25,26]. Six simply supported beams over 12-ft span and loaded at two points 1½-ft either side of the centre line were tested. The beams consisted of an 8 x 5¼ in. x 20 lb. per ft steel section and a 5 in. thick slab. The shear connection was provided by ½ in. diameter studs. The results showed that composite beams under static loading have a large reserve of strength beyond first yielding of the steel beam and exhibit large deflection prior to failure. Longitudinal cracking might occur and this could lead to premature failure if insufficient transverse reinforcement is provided. This finding is also confirmed by Davies[27] where four composite beams with solid r.c. slab were tested with variation in transverse reinforcement and the results concluded that the ultimate moment capacity of the composite beam is influenced to some considerable extent by the amount of transverse reinforcement in the slab. Inadequate transverse reinforcement allowed longitudinal splitting along the line of the shear connectors, thus permitting loss of interaction.

2.4 Previous studies on composite beam with precast slab and headed stud connector

Full scale commercial beam tests were carried out at Salford University and reported by Hamilton[18] in 1989. Beam tests were carried out using 150mm hcu's and 406 x 178 x 60 UB with 19mm diameter x 120mm long headed studs. The

results showed more than a 70% increase in ultimate moment capacity compared with the steel section. Failure was caused by studs shearing off from the beam.

Research on the shear strength of headed studs in precast concrete planks was investigated by Moy and Tayler[19] at Southampton University. A 65mm solid precast plank was used with 19mm diameter headed studs. 27 push-off tests were carried out, the results showed a reduction in strength as the volume of insitu concrete decreases (i.e. the bearing length onto the steel beam increases). A typical load-slip curve of 19mm headed stud in solid precast plank is shown in Fig. 2.5. It is recommended that the width of insitu concrete on the flange be a minimum of 100mm to avoid reductions in shear strength of the stud connector. It is also recommended that two layers of reinforcement must be used in the slab to avoid concrete splitting.

Work on long span composite beams for car parks was carried out by Jolly[20] at Southampton University. A 16m span composite beam with 110mm deep precast concrete planks was tested. The results showed the dynamic response of long span, shallow composite construction to comply with the requirements of BS5950 without the need to increase from the minimum number of shear connectors specified in the code.

2.5 Conclusions

Although representative work carried out in the United State, mainland Europe and the UK clearly suggested a greatly enhanced flexural capacity due to composite action, the majority of this research on composite action is not directly relevant to composite beams with hcu floor slabs. For example, the need for high degrees of reinforcement and insitu structural topping may well cancel out the structural benefits achieved in employing the composite action with hcu slab. Therefore, this project is designed to investigate the potential benefits of composite beams with hcu slabs without significant change to normal practice when such an arrangement is designed non-compositely - apart from the use of shear studs.

2.6 References

1. Mackay, H.M., Gillespie, P. and Leluau, C., 'Report on the strength of steel I-beams haunched with concrete', *Engineering Journal, Eng. Inst. Of Canada*, Vol. 6, No. 8, 1923, pp365-369.

2. Batho, C., Lash, S.D. and Kirkham, R.H.H., 'The properties of composite beams, consisting of steel joists encased in concrete, under direct and sustained loading', *Journal, Institution of Civil Engineering*, Vol. 11, No. 4, 1939, pp61-114.

3. Viest, I.M., 'Review of research on composite steel-concrete beams', *Journal of the Structural Division, Proceedings of American Society of Civil Engineers*, Vol. 86, No. ST6, June, 1960, pp1-21.

4. Viest, I.M., 'Investigation of stud shear connectors for composite concrete and steel T-beams', *Journal, American Concrete Institute,* Vol. 27, No. 8, 1956, pp875-891.

5. Thürlimann, B., 'Fatigue and static strength of stud shear connectors', *Journal, American Concrete Institute,* Vol. 30, No. 12, 1959, pp1287-1302.

6. Chapman, J.C., 'Composite construction in steel and concrete - The behaviour of composite beams', *The Structural Engineer*, Vol. 42, No. 4, April, 1964, pp115-125.

7. Chapman, J.C. and Balakrishnan, S., 'Experiments on composite beams', *The Structural Engineer*, Vol. 42, No. 11, November, 1964, pp369-383.

8. Ollgaard, J.G., Slutter, R.G. and Fisher, J.W., 'Shear strength of stud connectors in lightweight and normal weight concrete', *Engineering Journal, American Institute of Steel Construction*, Vol. 8, No.2, April, 1971, pp55-64.

9. Menzies, J.B., 'CP117 and shear connectors in steel-concrete composite beam made with normal-density or lightweight concrete', *The Structural Engineer*, Vol. 49, No.3, March, 1971, pp137-154.

10. Robinson, H., 'Composite beam incorporating cellular steel decking', *Journal of the Structural Division, Proceedings of American Society of Civil Engineers*, Vol. 95, No. ST3, 1969, pp355-380.

11. Grant, J.A., Fisher, J.W. and Slutter, R.G., 'Composite beams with formed steel deck', *Engineering Journal, American Institute of Steel Construction*, First Quarter, 1977, pp24-42.

12. Robinson, H., 'Multiple stud shear connections in deep ribbed metal deck', *Canadian Journal of Civil Engineering*, Vol. 15, 1988, pp553-569.

13. Wright, H.D. and Francis, R.W., 'Tests on composite beams with low levels of shear connection', *The Structural Engineer*, Vol. 68, No.15, August, 1990, pp290-298.

14. Mottram, J.T. and Johnson, R.P., `Push tests on studs welded through profile steel sheeting', *The Structural Engineer*, Vol. 68, No.10, May, 1990, pp188-192.

15. Lloyd, R.M. and Wright, H.D., 'In situ testing of a composite floor system', *The Structural Engineer*, Vol. 70, No.12, June, 1992, pp211-219.

16. Thomas, D.A.B. and O'Leary, D.C., 'Composite beams with profile-steel sheeting and non-welded shear connectors', *Steel Construction Today*, Vol. 2, No. 4, August, 1988, pp117-121.

17. Crisinel, M., 'Partial-interaction analysis of composite beams with profiled sheeting and non-welded shear connectors', *Journal of Constructional Steel Research,* Vol. 15, No. 1 & 2, 1990, pp65-98.

18. Hamilton, T.R., 'Composite steel and precast concrete slab construction', Thesis for admission to corporate membership, Institution of Structural Engineers, February, 1989.

19. Moy, S.S.J. and Tayler, C., 'The effect of precast concrete planks on shear connector strength', *Journal of Constructional Steel Research*, Vol. 36, No.3, 1996, pp201-213.

20. Jolly, C.K., 'Long span composite beams for car parks', *Joint IStructE / City University International Seminar, City University, London*, 1-3, July, 1996, pp57.1-57.8.

21. CP117, Part 1 (1965) Composite construction in structural steel and concrete, British Standards Institution, London.

22. BS5950, Part 3.1 (1990) Structural Use of Steelwork in Building, British Standards Institution, London.

23. DD ENV 1994-1-1 (1994) Eurocode 4: Design of composite steel and concrete structures, British Standards Institution, London.

24. Slutter, R.G. and Driscoll, G.C., 'Flexural strength of steel-concrete composite beams', *Journal of the Structural Division, Proceedings of American Society of Civil Engineers*, Vol. 91, No. ST2, April, 1965, pp71-99.

25. Barnard, P.R. and Johnson, R.P., 'Ultimate strength of composite beams', *Proceedings of The Institution of Civil Engineers*, Vol. 32, December, 1965, pp161-179.

26. Barnard, P.R., 'A series of tests on simply supported composite beams', *Journal, American Concrete Institute,* Vol. 62, No. 3, April, 1956, pp443-455.

27. Davies, C., 'Tests on half-scale steel-concrete composite beams with welded stud connectors', *The Structural Engineer*, Vol. 47, No.1, January, 1969, pp29-40.

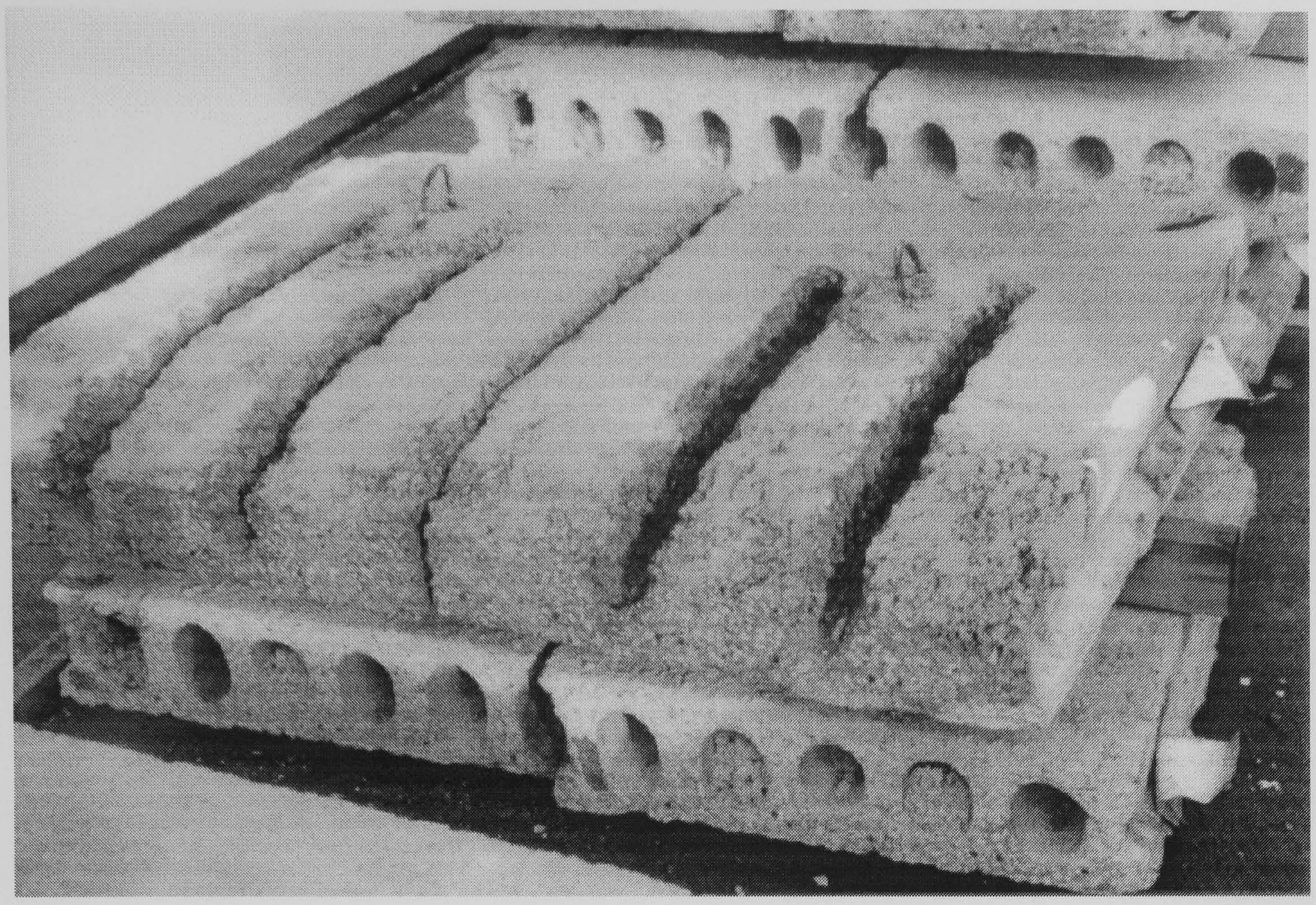

Fig. 2.1 General details of precast hollow cored floor units.

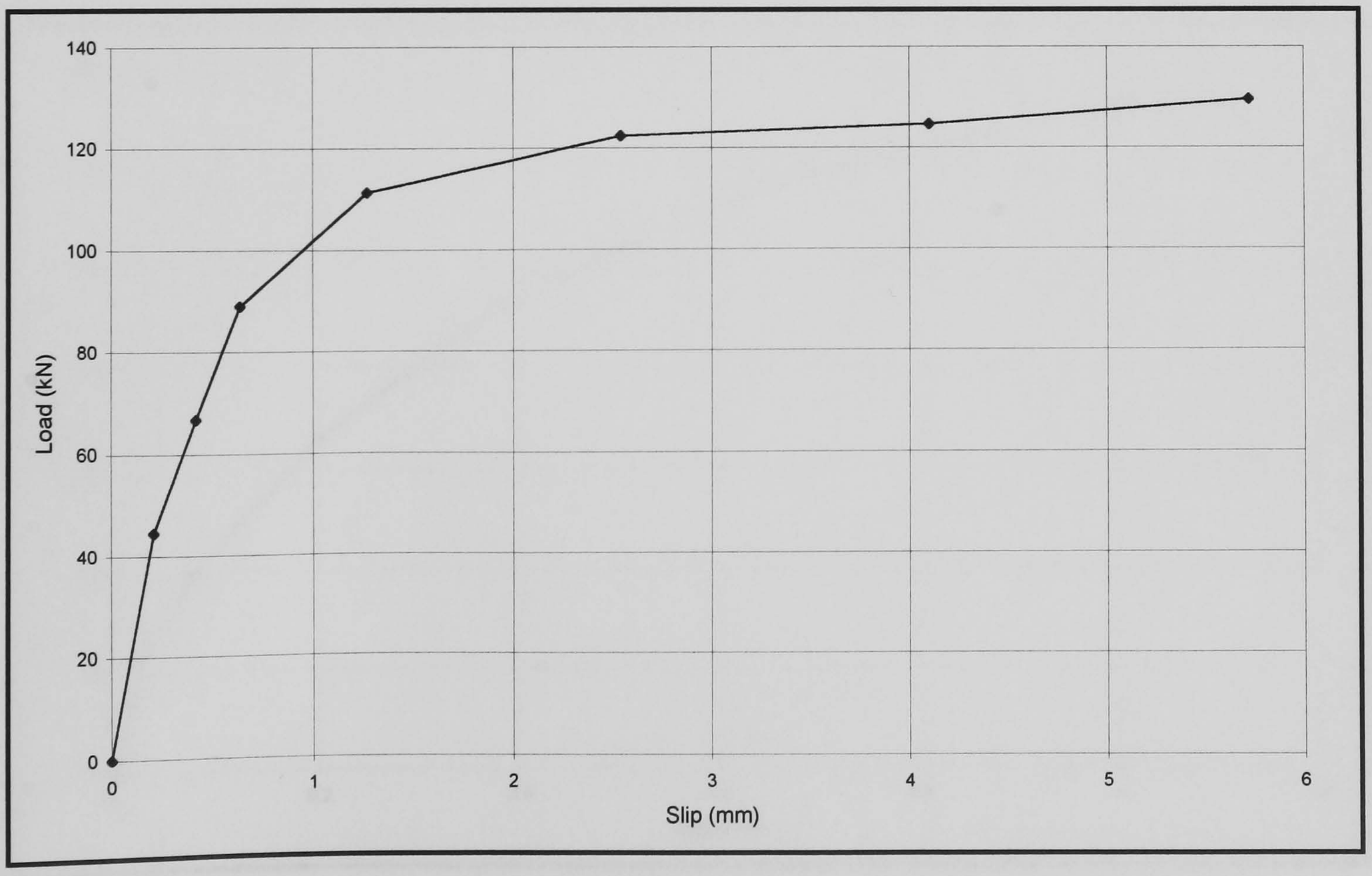

Fig. 2.2 Load-slip curve of 19mm headed stud in reinforced concrete slab
(Ollgaard *et al* ref. 8)

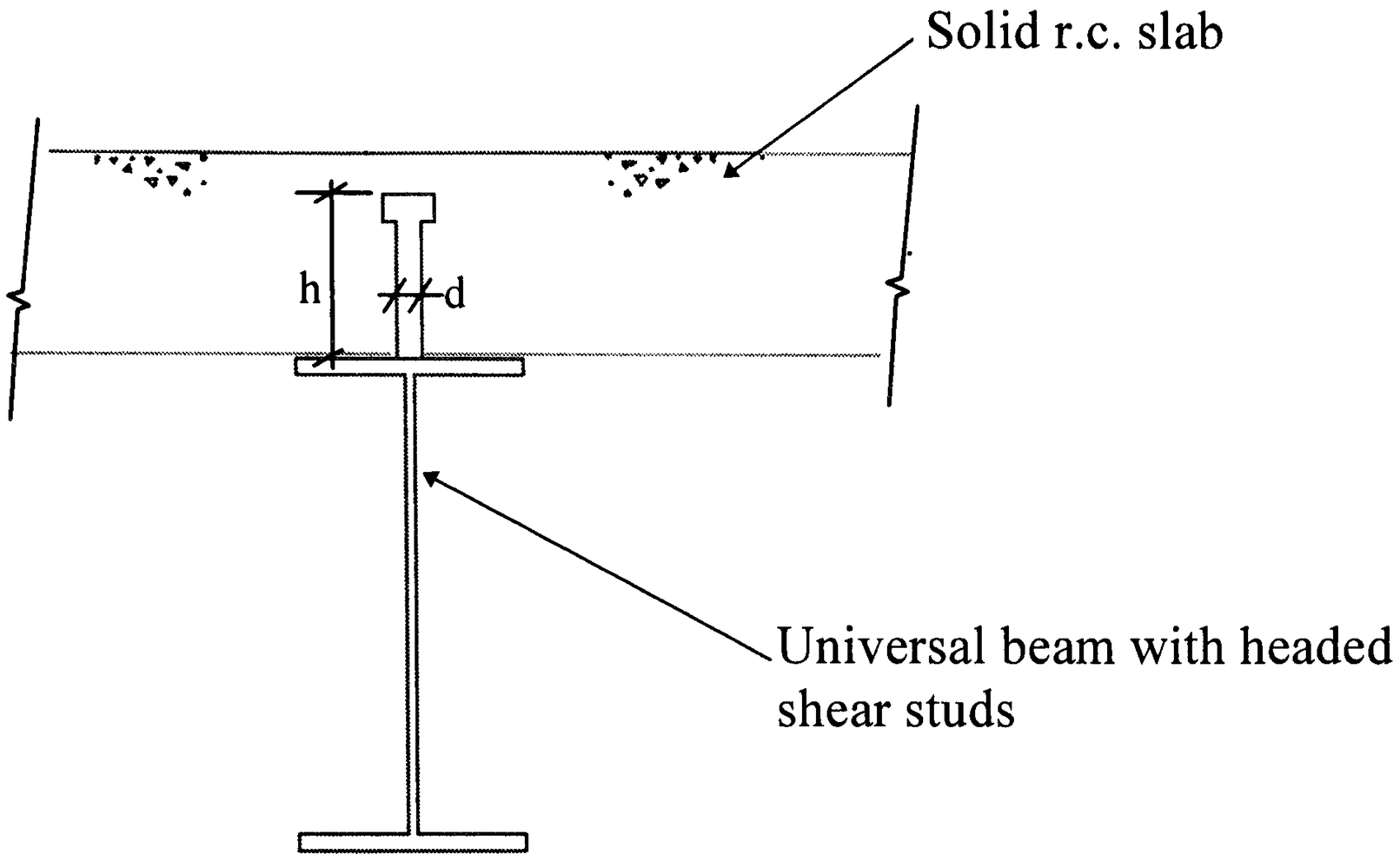

Fig. 2.3 Construction details for composite beam with solid r.c. slab

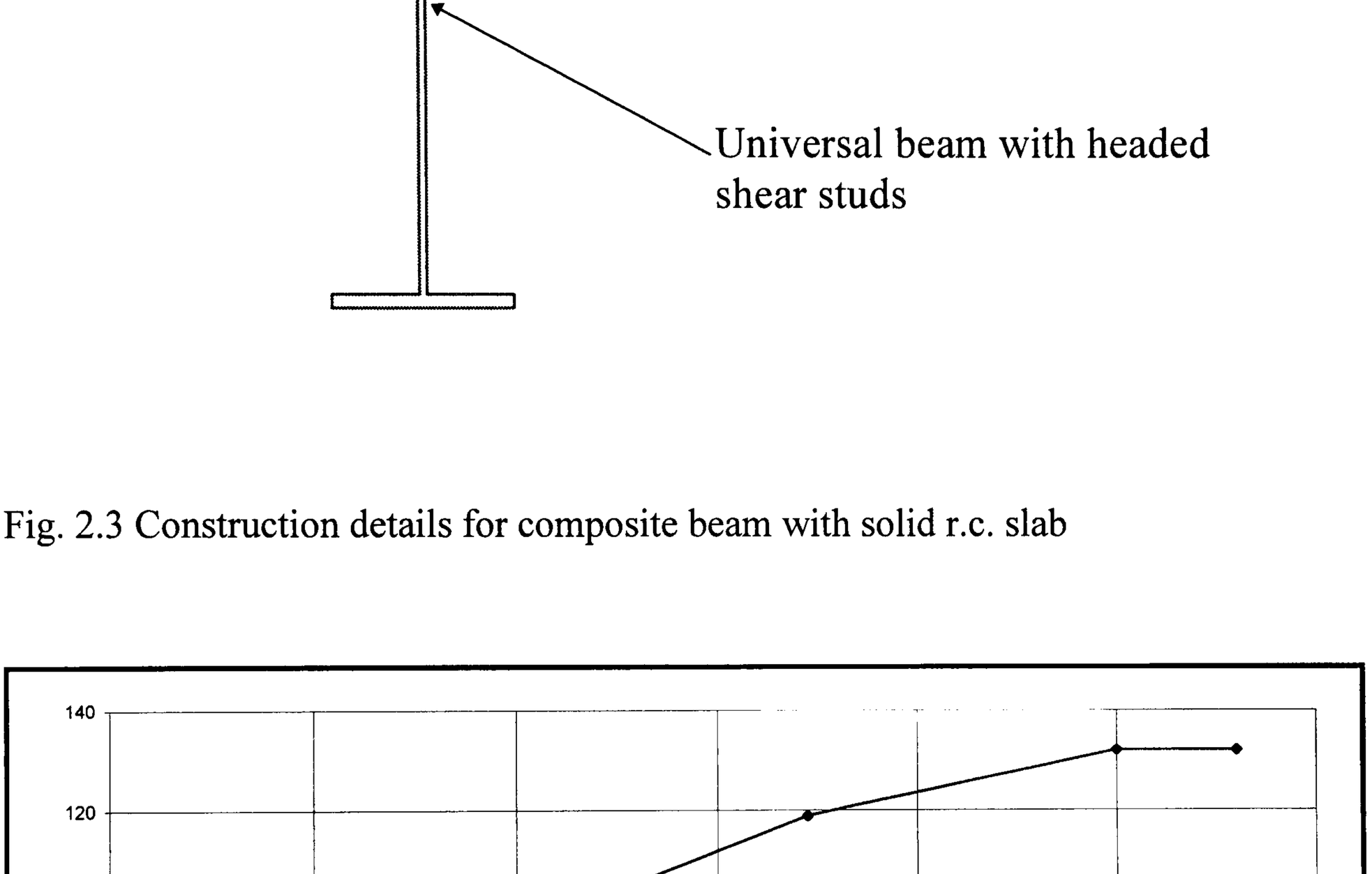

Fig. 2.4 Load-slip curve of 19mm headed stud in solid r.c. slab
(Chapman *et al* ref. 7)

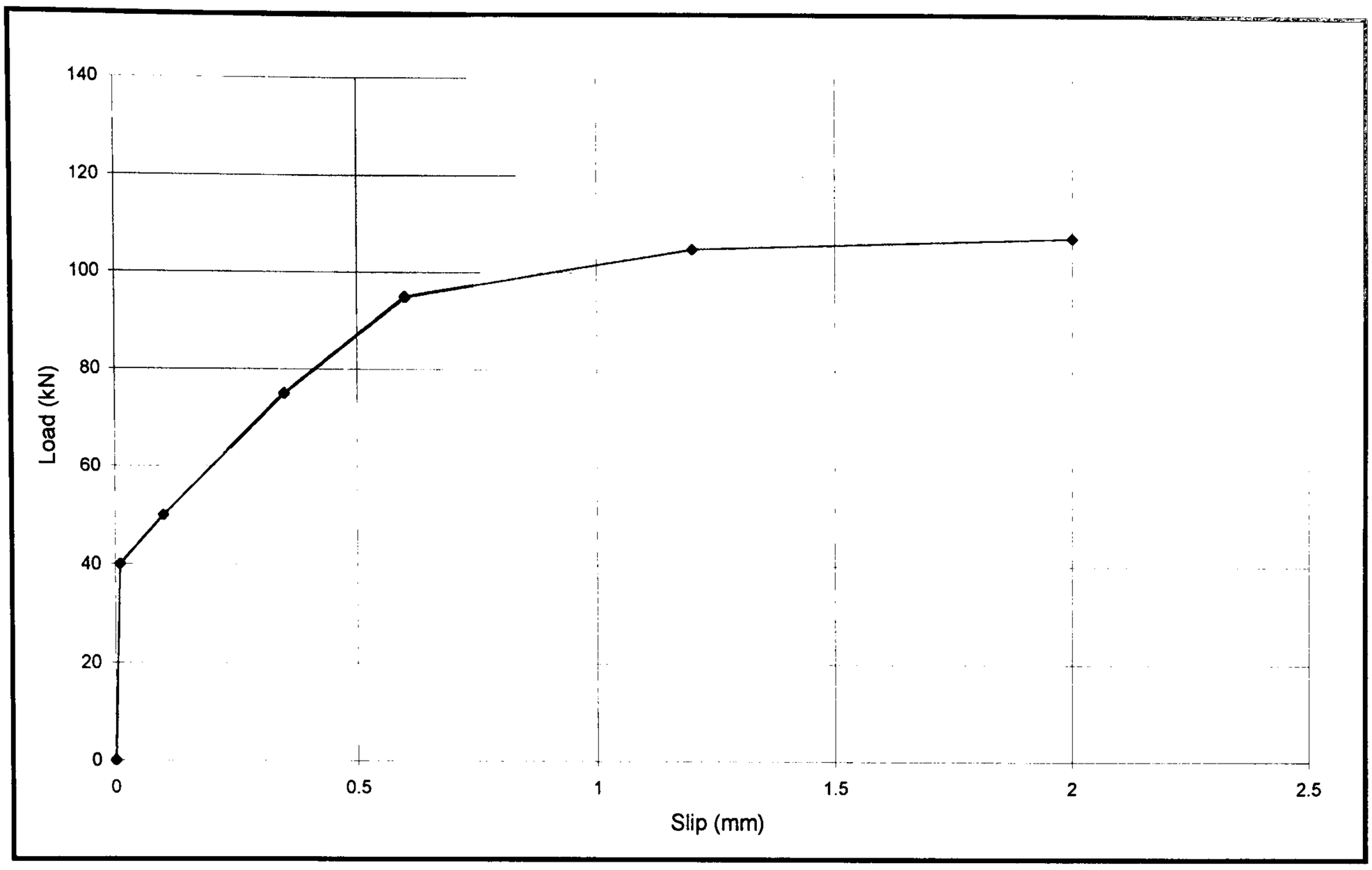

Fig. 2.5 Load-slip curve of 19mm headed stud in solid precast plank
(Moy *et al* ref. 19)

Chapter 3

Horizontal compression tests of hollow core slab

3.1 Introduction

In a composite beam with precast hollow core slabs, the precast and insitu concrete may only be considered monolithic when an adequate load transfer mechanism can be provided by interface bond and interaction with the transverse reinforcement. Thus, as well as the shear stud being able to resist the ultimate horizontal shear, the precast-insitu interface must also be designed to carry this force. The present state of knowledge on these mechanisms for this type of composite construction is limited. The main purpose of these tests was (a) to study the horizontal compressive strength of the slab when the hollow core units (hcu) form the compression flange of the composite beam and (b) to determine the effective breadth of the precast with insitu slab. This chapter reports on the experimental investigation of a series of five compressive slab tests, its setting up, instrumentation, material properties and the loading procedure.

A floor arrangement typical of current practice in steel / hcu structures with 8m span main beams and a 150mm deep hollow core slab spanning 6m is shown in Fig. 3.1. The beam size is calculated according to BS5950[1] and hence the neutral axis of the composite beam is determined by taking first moments of area of

transformed sections. In order to simplify the tests, the elastic strain in the slab experienced from flexural bending of the composite beam is replaced with the equivalent eccentric axial compression required to produce the same elastic strain in the slab, see Fig. 3.2. For the 150mm deep hcu, the compressive load is applied eccentrically 10mm above the centre line of slab, based on the theoretical calculation for the most common beam series used for this type of construction.

A compressive slab test may be considered as an economical way to study the compressive strength of the precast composite slab experience in bending. This simplified method permits the behaviour of the hcu slab to be investigated without the expense associated with full-scale bending tests.

3.2 Test arrangement

The test specimen was assembled from four 600mm wide, 150mm deep x 800mm long prestressed hcu's (supplied by Bison Floors Ltd.) and grade 43 steel 356 x 171 x 51 universal beam with a single row of shear connectors pre-welded at 150mm centres as shown on Fig. 3.3. 19mm diameter x 125mm height TRW-Nelson headed studs were used for all the tests, and were welded in the laboratory by using an automatic fusion welding process. The 600 mm slab width was chosen instead of the more common 1200 mm wide unit so that the effect of the edge joint was included in a test length of 1200 mm. The length of 800mm for the hcu was

chosen to suit the set up in the laboratory and is believed to be wide enough for the effective breadth for the slab. The characteristic cube strength for the precast concrete is taken as 50 N/mm^2. A gap of 65mm was left between the ends of slab, with the ends tapered for a distance of 235mm, and the top of the third core of each hcu left open for a length of 500mm to allow for placing of transverse reinforcement. The top cover to the transverse reinforcement was approximately 50mm as shown in Fig. 3.3. Insitu concrete was placed into the joints and compacted using 25mm diameter vibrating poker to form the composite slab.

Five tests were carried out according to the schedule in Table 3.1. The variable test parameters were (a) the strength of insitu concrete infill, and (b) the area of transverse reinforcement. The spacing of the headed stud and the depth of the hcu were kept constant. The spacing of the headed stud was not believed to be influential in the compression test. For the transverse reinforcement, T8, T12 and T16 were chosen. The tensile strength of the bars were believed to be in the range of concrete tensile splitting force experienced in the test and they were also commonly used on site . Specimen with pre-cracked longitudinal joint between the insitu infill and hcu was also tested to investigate the effect caused by shrinkage of the insitu infill.

The main structural components of the test rig consisted of the following (See Fig.3.4 & 3.5):

- A main reaction beam at each end of the composite slab where 2 no. of 1000 kN jacks necessary to produce compressive force through the slab were attached at one end.
- 2 no. of 1000 kN load cells are placed between the jacks and the specimen to record the reaction load.
- 2 no. steel RHS cross heads and 4 no. 40mm dia. Macalloy bars provided a self equilibrating reaction frame.
- A loading pack of 800mm width x full slab depth is placed between the jacks and the specimen to distribute the load uniformly across the width of the test slab.
- To minimize friction during test, the composite beam and the edge supporting beams are placed on roller bearings.

3.3 Instrumentation

Instrumentation comprised electrical resistance strain gauges (ERSG's) for measuring strains in the concrete slab, reinforcement and steel beam; linear voltage displacement potentiometers (POT's) for monitoring crack widths of the slab; and dial gauges (DG's) to detect movement of the specimen during the test for safety reasons. The set-up procedure of each instrument is described below:

Strains in the concrete slab, reinforcement and the steel beam were measured using two sets of ERSGs. One set was positioned in the middle of the test specimen with the other set near to the reaction ends to measure local effects due to the reaction rig. The strain in the concrete was measured by surface mounted gauge type PL-30-11 of a gauge length of 30mm. The strain gauge was of 120 ± 0.3 Ω resistance with a gauge factor of 2.12. The strain gauges on the concrete surface were used to measure stress in the insitu concrete, as a means of determining the effective width of the test slab. The positions of the concrete strain gauges are shown in Fig. 3.6.

The strain gauges used for the rebar and steel beam were of the type FLA-6-11 with a gauge length of 6mm. The gauge was of 120 ± 0.3Ω resistance with a gauge factor of 2.13. The strain gauges on the surface of the rebar were coated with epoxy to protect them from the concrete. The strain gauges were used to monitor the strain and yielding of the rebar and hence to deduce the tensile splitting force exerted during the compressive test. Strain gauges were positioned on the centre of the transverse reinforcement. Strain gauges were also placed on the top flange of the steel beam to measure the strain on the steel beam as a check on the position of the neutral axis of the slab throughout the test. The positions of the strain gauges are shown on Fig. 3.7.

The potentiometers (POT) were mounted on the surface of the test slab to monitor the crack width due to transverse splitting forces. The POT and the target were

bolted on the hcu so that crack widths between adjacent hcu can be measured, see Fig. 3.4. All the data were stored by the Orion Data Logging System and output to a spreadsheet after the test for analysis.

3.4 Loading procedure

Axial load is applied manually by a hydraulic pump simultaneously to the two jacks. Elastic tests were run before the test to failure to check the instrumentation and loading system. The load was applied at 50kN intervals with unloading cycles at about 200 to 300kN increments to observe the unloading stiffness. Loading was applied to the specimen until the failure mode was reached, i.e. excessive deformation of reinforcement and/or severe cracking was observed.

3.5 Material testing

3.5.1 Concrete testing

Insitu concrete infill between the hcu's was cast in the laboratory with the test slab in position. To monitor the insitu concrete strength, 6 no. cubes (100 x 100 x 100 mm) and 6 no. of cylinders (150 mm dia. x 300 mm long) were sampled and cured. These samples were tested at 7 days, test day and 28 days in accordance

with BS1881[2] using the Denison compression test machine. The compressive and tensile strength of the insitu concrete was derived from the compressive test and the Brazilian splitting test, respectively. The strength of all the test specimens is summarized in Tables 3.3 and 3.4.

3.5.2 Rebar testing

Tensile tests were conducted for a sample of rebars used in the slab tests. Tensile tests were conducted in the Zwick universal test machine under conditions defined by BSI standard. The tensile strength of the rebars is summarized in Tables 3.5 and 3.6.

3.6 Test results

The main purpose of these tests was to investigate the horizontal compressive strength of the combined insitu - precast slab, and hence determined the effective breadth of the compression flange. Test SPC1, SPC2 and SPC5 was designed to investigate the variation in transverse reinforcement ratio while SPC3 was designed to observe the influence in insitu concrete infill. Influence of the insitu / precast concrete bond was observed in Test SPC4. Applied load, concrete compressive strain and tensile strain of transverse reinforcement were monitored

throughout the test. Cracking and reduction in axial stiffness (i.e. increases in compressive strain) were observed at each load interval.

3.6.1 Test SPC1

The test results for SPC1 are shown in Table 3.2, and the load vs. concrete strain and load vs. reinforcement strain curves are shown in Fig. 3.8 & Fig. 3.9. In this test, 4 no. T16 bars were used as transverse reinforcement with insitu concrete cube strength of 25N/mm^2. The test proceeded in 50kN load intervals with unloading cycles at every 300kN intervals to observe the unloading stiffness.

The first crack in the composite slab appeared near the corner of the bearing plate at 700kN. Cracks developed at the insitu / precast interface at 947kN and the axial stiffness of the slab was greatly reduced. With further increase of applied load to 1160kN, more cracks began to form and opened up especially round the bearing area and travelled towards the centre of slab. Transverse cracks also developed along the joint between the hcu's. With crack propagation and further increased in compressive strain in concrete at 1167kN, test was terminated due to crushing failure of the insitu concrete. At maximum failure load of 1167kN, a compressive concrete strain of 1510με and a rebar tensile strain of 350με was recorded. No cracking was observed in the hcu's. The mode of failure was brittle and without sufficient prior warning. Fig. 3.10 shows the crack pattern of SPC1 at failure.

3.6.3 Test SPC2

From the test result of SPC1, the test failed in a brittle manner and would appear to be over-reinforced. Therefore, 4 no. T8 bars (equivalent to 25% of the transverse reinforcement used in SPC1) were used as transverse reinforcement in this test with insitu infill concrete grade C25 as in SPC1. Test SPC2 was designed to form a direct comparison with SPC1 to investigate the effect of the transverse reinforcement. Results are shown in Table 3.2. The load vs. concrete strain and load vs. reinforcement strain curves are shown in Fig. 3.11 and Fig. 3.12. Compressive load was applied to the specimen at 50kN increment with unloading at every 300kN intervals. First crack developed simultaneously at the insitu and precast interface and also in the transverse joint between the hcu's at 800kN, with fine cracks developing in the insitu concrete with further increase of load. At 1390kN the concrete continued to strain with no further increase in load and high strains were recorded by the rebar strain gauges, which indicated the rebars had yielded. The test was terminated due to excessive strain in the rebar and a reduction in the load. A maximum crack width of 2.0mm was observed at failure with some recovery noted during unloading. The crack pattern is shown in Fig. 3.13. At maximum failure load of 1396 kN, a compressive concrete strain of 1081με and rebar tensile strain of 2700με were recorded.

3.6.2 Test SPC3

The test arrangement for SPC3 consisted of 4 no. T8 bars as transverse reinforcement with insitu infill concrete cube strength of 32N/mm^2. A 40% increases in the insitu infill strength compared to Test SPC2. The test results are shown in Table 3.2. Load vs. concrete strain and load vs. reinforcement strain curves are shown in Fig. 3.14 & Fig. 3.15. First crack was found at the transverse joint between the hcu's at 750kN, with further cracking developing at the insitu / precast interface at 974kN. More cracks were developed between the interface and on the insitu concrete as the load increased to 1400kN, when the test was terminated due to excessive cracking. At maximum failure load of 1405kN, a compressive strain of concrete of 922με and rebar tensile strain of 3000με was recorded. A ductile failure mode is observed in this test with extensive yielding of the rebars.

3.6.4 Test SPC4

A pre-cracked joint between the insitu and precast was introduced to investigate the effect of shrinkage of insitu infill. A 2mm thick polythene sheet is laid on top of the precast slab with transverse reinforcement pierce through and cast between the insitu / precast interface. The test was designed to form a direct comparison

with SPC2. Results are shown in Table 3.2. The load vs. concrete strain and load vs. reinforcement strain curves are shown in Fig. 3.16 and Fig 3.17. Substantial strain was recorded in the reinforcement as soon as the loading began which had not been noticed in the previous tests. It was most probably due to the presence of the pre-cracked interface joint. The first crack appeared along the transverse joint between the hcu's at a much lower load of 250kN as compared to the previous tests. As the load increased to 700kN, a sudden increase in strain was noticed in the concrete strain gauges (CSG1) which coincided with a decrease in strain in the reinforcement strain gauge (RSG2). This was probably caused by slip between the insitu core and the precast slab or due to pull out of the reinforcement from the concrete. Crack width of 1mm were observed in the insitu infill. With a further increase of load to 950kN, more cracks developed up to 2mm wide. At maximum failure load of 1008kN, a compressive concrete strain of 670με and rebar tensile strain of 2600με were recorded. The mode of failure was due to yielding and slip on transverse reinforcements leading to splitting of the specimen.

3.6.5 Test SPC5

Test SPC5 was designed to form a direct comparison between SPC1 and SPC2, having a percentage of transverse reinforcement in the middle of the range. For this test, 4 no. T12 were used as transverse reinforcement (equivalent to 50% of transverse reinforcement used in SPC1) with insitu infill concrete cube strength of

25N/mm^2. Results are shown in Table 3.2. The load vs. concrete strain and load vs. reinforcement strain curves are shown in Fig. 3.18 and Fig. 3.19. First crack in the specimen was found longitudinally along the full length at a much higher load of 1050kN. More cracks were formed in the precast /insitu interface and between the hcu's as the load increased to 1250kN. As the load increased to 1350kN, random cracking was observed without further increase of load, the specimen failed suddenly without warning, see Fig. 3.20. Shear failure across the hcu's was also observed (Fig. 3.21). A brittle failure although not as sudden as Test SPC1 was observed. At maximum failure load of 1355kN, a compressive concrete strain of 1401με and rebar tensile strain of 992με was recorded.

3.7 Comparison of test results

The comparison of test results are given in this section. Full discussion of the results with theoretical comparison will be given in Chapter 8 . A comparison of these results with the numerical finite element studies will be given in Chapter 6.

3.7.1 Influence of transverse reinforcement

It is widely recognized that the most characteristic feature of the behaviour of a concrete structure is that associated with the fracture processes which such a

structure undergoes under increasing load. The processes take the form of extension and propagation of cracks in the direction of maximum principal stress. Crack extension and propagation occurs in order to relieve high tensile stress concentrations which develop under increasing load in the region of the crack tips. Transverse reinforcement is used to ensure a smooth transfer of the longitudinal force via the shear connectors into the slab and also as encroachment reinforcement against tensile splitting of the composite slab.

Tests SPC1, SPC2 and SPC5 were notionally identical except for the amount of transverse reinforcement, i.e. percentage of transverse reinforcement to area of concrete, ρ (A_s/A_c) = 0.45%, 0.11% and 0.25% respectively. Compressive load versus transverse reinforcement strains for test SPC1, SPC2, and SPC5 are shown in Fig. 3.22. The results indicated only the transverse reinforcement (ρ = 0.11%) of SPC2 is fully yielded (taken as 3100με in this work), whilst the steel strains of SPC1 and SPC5 were less than 1000με. Both SPC1 and SPC5 failed in a brittle manner without sufficient prior warning, and no yielding of reinforcement was evident in either case. This indicated that the slab did not fully benefit from the extra amount of reinforcement, and suggested that the slabs of SPC1 and SPC5 were in fact over-reinforced as the tensile splitting force was being restrained and could not be relieved by yielding of the reinforcement. The specimens continued to carry more load until the maximum compressive stress in the concrete was reached, leading to a complete and immediate loss of load-carrying capacity. On the other hand, SPC2 with less transverse reinforcement, failed in a ductile manner

with a maximum crack width of 2.0mm at failure. In this case, the failure mechanism indicated that the slab failed in tension, and that the specimen failed before the ultimate strength of the concrete in compression was attained. Such behaviour has been predicted by a numerical analysis which is given in the Chapter 6.

In contrast to the tests SPC1 and SPC5, the rate of cracking was reduced considerably in test SPC2 with less transverse reinforcement and crack sizes minimized by allowing the cracks to form in a controlled manner without causing rapid loss of strength. These results suggested that the transverse reinforcement should not only be provided to restrain the tensile splitting of the composite slab, but also to enable the tensile splitting to occur at a controlled rate so as not to cause a sudden loss of strength or stiffness of the composite slab.

3.7.2 Influence of insitu concrete strength

The test configurations of SPC2 and SPC3 were set up identically so as to investigate the influence of the insitu infill concrete cube strength. A concrete cube strength of 23.2 N/mm^2 was used for SPC2 whilst concrete cube strength of 32.7 N/mm^2 was used in SPC3. The results are shown in Table 3.2. From the result, it would appear that there are no significant increases in strength or stiffness of the slab with increased strength of insitu infill. Fig 3.23 shows the

comparison of compressive load versus concrete strain of SPC2 and SPC3. In both cases, the failure mode indicated that the slab failed in tension, and the ultimate strength of concrete in compression was not attained. As both tests were not failed in compression and the ultimate strength of concrete in compression was not attained, the strength of the insitu infill may not be significant. Although these results cannot be conclusive, within the parameters used in these tests, insitu infill concrete strength would not appear to be influential. However, the use of very high strength insitu concrete might introduce brittle failure and should be investigated further.

3.7.3 Influence of pre-cracked joint

SPC4 was introduced to investigated the effect of shrinkage of insitu infill on site by placing a polythene sheet between the insitu and precast. Comparison of load vs. reinforcement strains of SPC2 & SPC4 are shown in Fig. 3.24. High tensile strain in the transverse reinforcement was noted due to the presence of pre-cracked joint suggested the tensile splitting force was solely resisted by the transverse reinforcement. This suggested that the bond between insitu infill and precast units must have a large contribution to the tensile splitting resistance of the slab. Pre-cracking the joint between insitu infill and precast units did not lead to any early loss of stiffness to the compression slab. It would suggest the joint shrinkage would have not effect to the compressive resistance of the slab.

3.8 Conclusions

From the results of the horizontal compression tests, a number of observations regarding the precast composite slab behaviour have been made. The most significant finding was of the influence of the transverse reinforcement. Transverse reinforcement is essential for the composite slab and the percentage of reinforcement should be carefully determined to enable the relief of the tensile splitting force, by elongation of the reinforcement. Over-reinforcement would not be beneficial to the slab and would lead to brittle failure. Fig. 3.25 shows the relation between compressive concrete strain and tensile strain of transverse reinforcement and the percentage of transverse reinforcement. As indicated in Fig. 3.25, SPC1 and SPC5 with high percentages of transverse reinforcement showed high compressive concrete strain in the slab at failure, which led to top spalling and crushing of the concrete with very low tensile strain in the transverse reinforcement, i.e. brittle failure. While SPC2, SPC3 and SPC4 with a low percentage of reinforcement (0.11%) showed high tensile strain in the transverse reinforcement at failure with low compressive strain in concrete, i.e. ductile failure.

3.9 References

1. BS5950 Part 1 Code of practice for design in simple and continuous construction: hot rolled sections, British Standard: Structural Use of Steelwork in Building, British Standards Institution, London, 1990.

2. BS1881, (1983) Method for Determination of Compressive Strength and Tensile Splitting Strength, British Standards Institution, London.

TEST No.	HOLLOW CORE UNIT	SHEAR STUDS TYPE & SPACING	TRANVERSE REINFORCE-MENT	INSITU CONCRETE CUBE STRENGTH AT TEST DATE
SPC1	BISON 150mm HCU	TRW-NELSON 19mm x125mm @ 150 c/c	4 No. T16	25.1 N/mm^2
SPC2	BISON 150mm HCU	TRW-NELSON 19mm x125mm @ 150 c/c	4 No. T8	23.2 N/mm^2
SPC3	BISON 150mm HCU	TRW-NELSON 19mm x125mm @ 150 c/c	4 No. T8	32.7 N/ mm^2
SPC4	BISON 150mm HCU	TRW-NELSON 19mm x125mm @ 150 c/c	4 No. T8 Pre-cracked	26.7 N/mm^2
SPC5	BISON 150mm HCU	TRW-NELSON 19mm x125mm @ 150 c/c	4 No. T12	23.8 N/mm^2

Table 3.1 Test parameters for compression tests

TEST No.	MAX LOAD AT FAILURE	CONCRETE STRAIN AT MAX. LOAD	REINFORCEMENT STRAIN AT MAX. LOAD
SPC1	1166.84 kN	-1510 με	350 με
SPC2	1396.29kN	-1081 με	2700 με
SPC3	1405.42 kN	-922 με	3220 με
SPC4	1008.32kN	-670 με	2600 με
SPC5	1355.0kN	-1401 με	992 με

Table 3.2 Test results for compression test

Specimen	Compressive Strength (N/mm^2)								
	7 Days			Test Days			28 Days		
	1	2	Ave.	1	2	Ave.	1	2	Ave.
SPC1 (26 Days)	18.0	18.4	18.2	25.0	25.2	25.1	25.5	26.2	25.9
SPC2 (26 Days)	16.0	16.2	16.1	23.4	23.0	23.2	24.0	26.6	25.3
SPC3 (19 Days)	25.8	25.8	25.8	32.4	33.0	32.7	33.0	35.0	34.0
SPC4 (9 Days)	23.5	23.5	23.5	27.2	26.2	26.7	38.4	38.4	38.4
SPC5 (22 Days)	14.0	14.6	14.3	24.0	23.6	23.8	25.0	25.0	25.0

Table 3.3 Insitu concrete infill compressive strength

Specimen	Tensile Splitting Strength (N/mm^2)								
	7 Days			Test Days			28 Days		
	1	2	Ave.	1	2	Ave.	1	2	Ave.
SPC1 (26 Days)	1.92	1.75	1.84	2.32	2.52	2.42	2.35	2.43	2.39
SPC2 (26 Days)	1.41	1.44	1.42	1.85	2.06	1.96	2.06	2.04	2.05
SPC3 (19 Days)	2.33	2.33	2.33	3.08	3.03	3.06	3.14	3.11	3.12
SPC4 (9 Days)	2.0	2.0	2.0	2.08	2.29	2.15	2.59	2.88	2.63
SPC5 (22 Days)	1.49	1.42	1.46	1.98	2.22	2.1	2.59	2.26	2.43

Table 3.4 Insitu concrete infill tensile splitting strength

Rebar	Nominal Diameter (mm)	Specified Characteristic Strength (N/mm^2)	Specified Mass (Kg/m)	Specified Cross Section (mm^2)
T8	8.00	460.00	0.40	50.30
T12	12.00	460.00	0.89	113.10
T16	16.00	460.00	1.58	201.10

Table 3.5 Specified tensile strength of rebars

Rebar	Nominal Diameter (mm)	Measured Tensile Strength (N/mm^2)	Measured Mass (Kg/m)	Measured Cross Section (mm^2)
T8	7.99	660.00	0.39	50.10
T12	11.88	717.00	0.87	110.80
T16	15.85	634.00	1.55	197.20

Table 3.6 Measured tensile strength of rebars

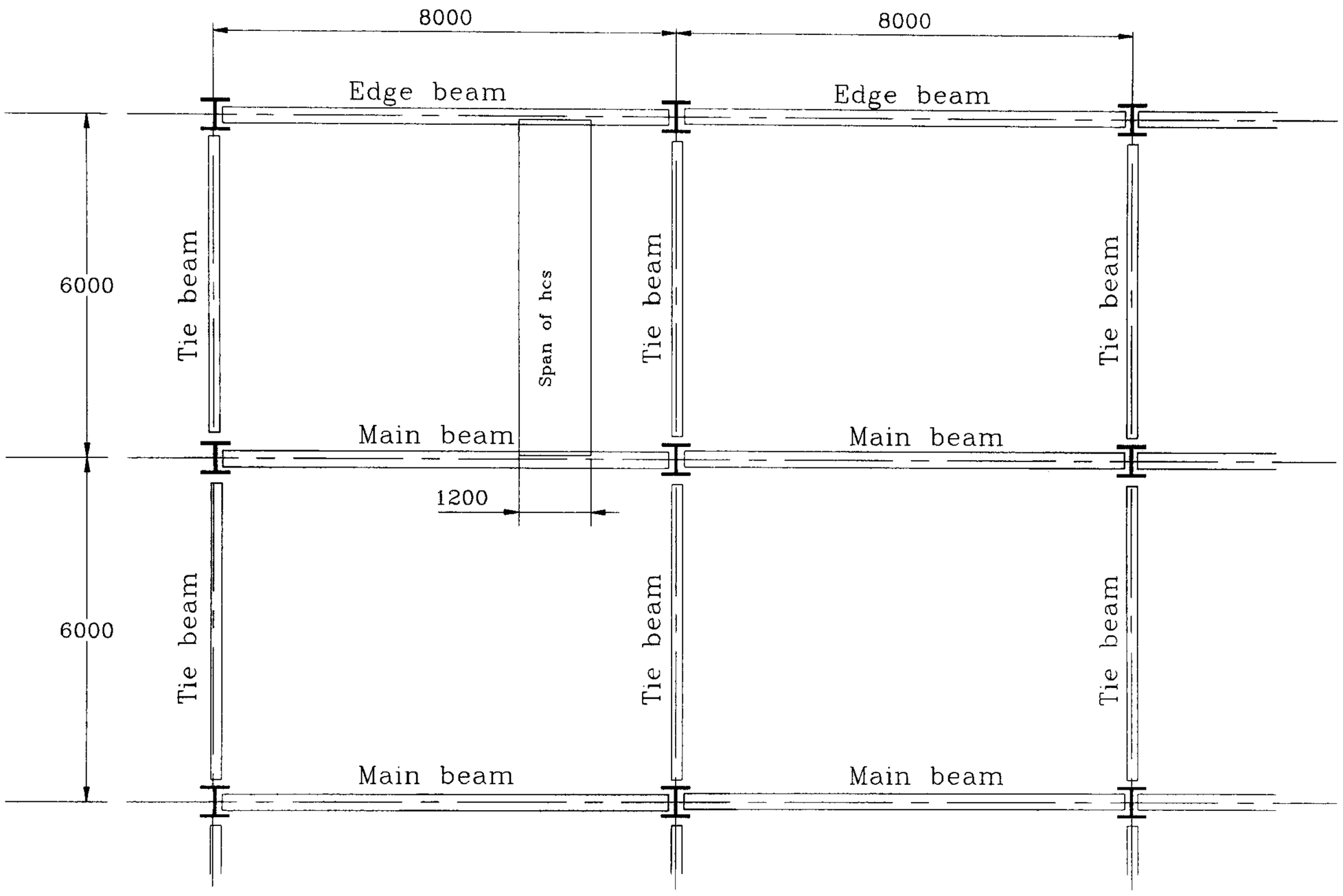

Fig 3.1 Typical floor arrangement of steel/hcu structures

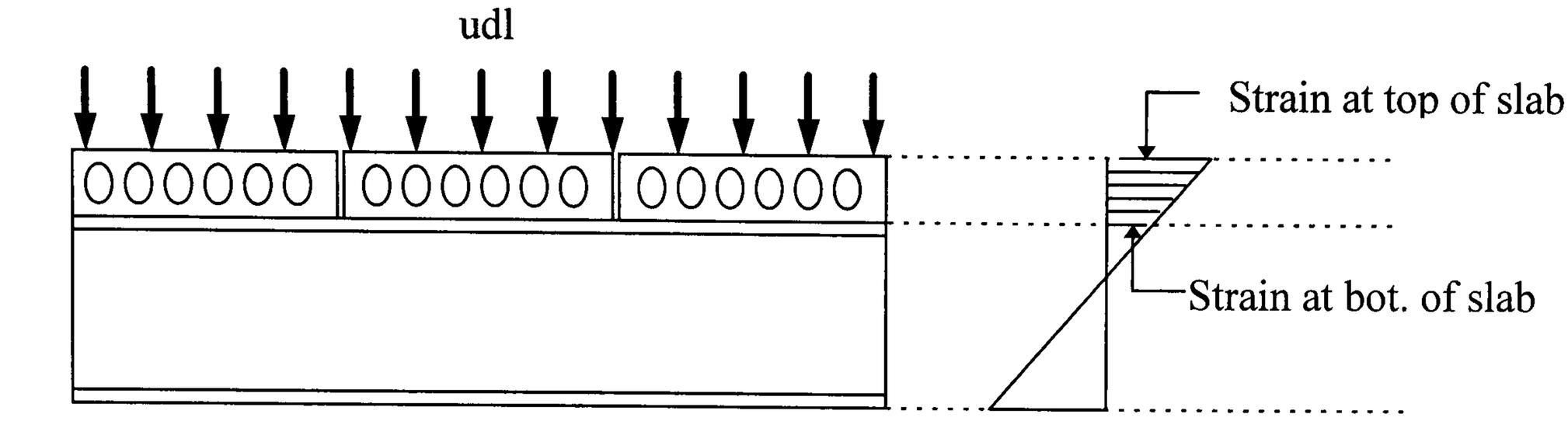

Strain produced from bending

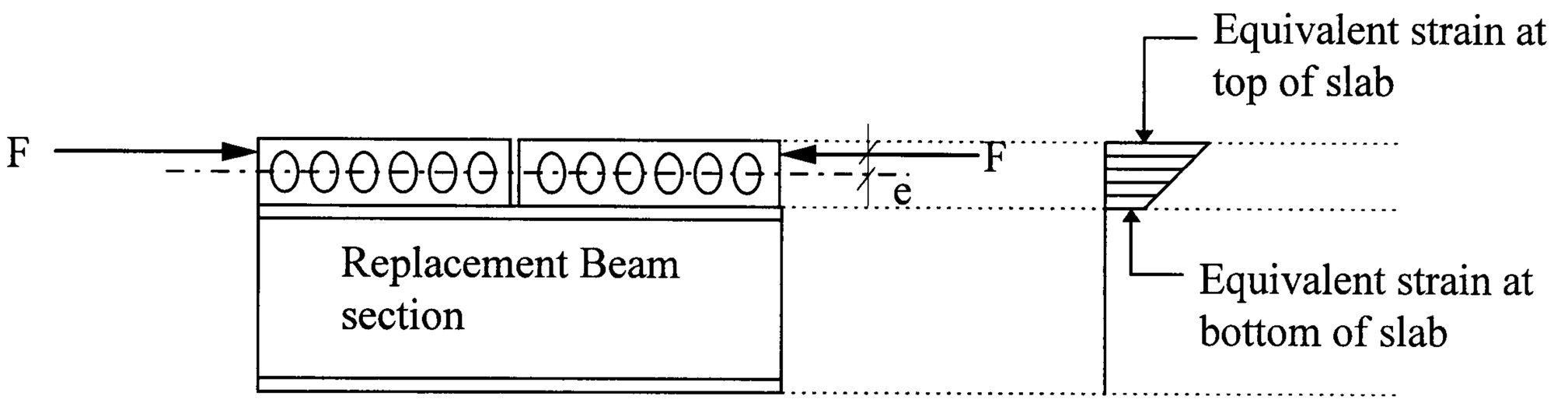

Equivalent strain produced from eccentric axial compression

Fig. 3.2 Elastic strain compatibility method

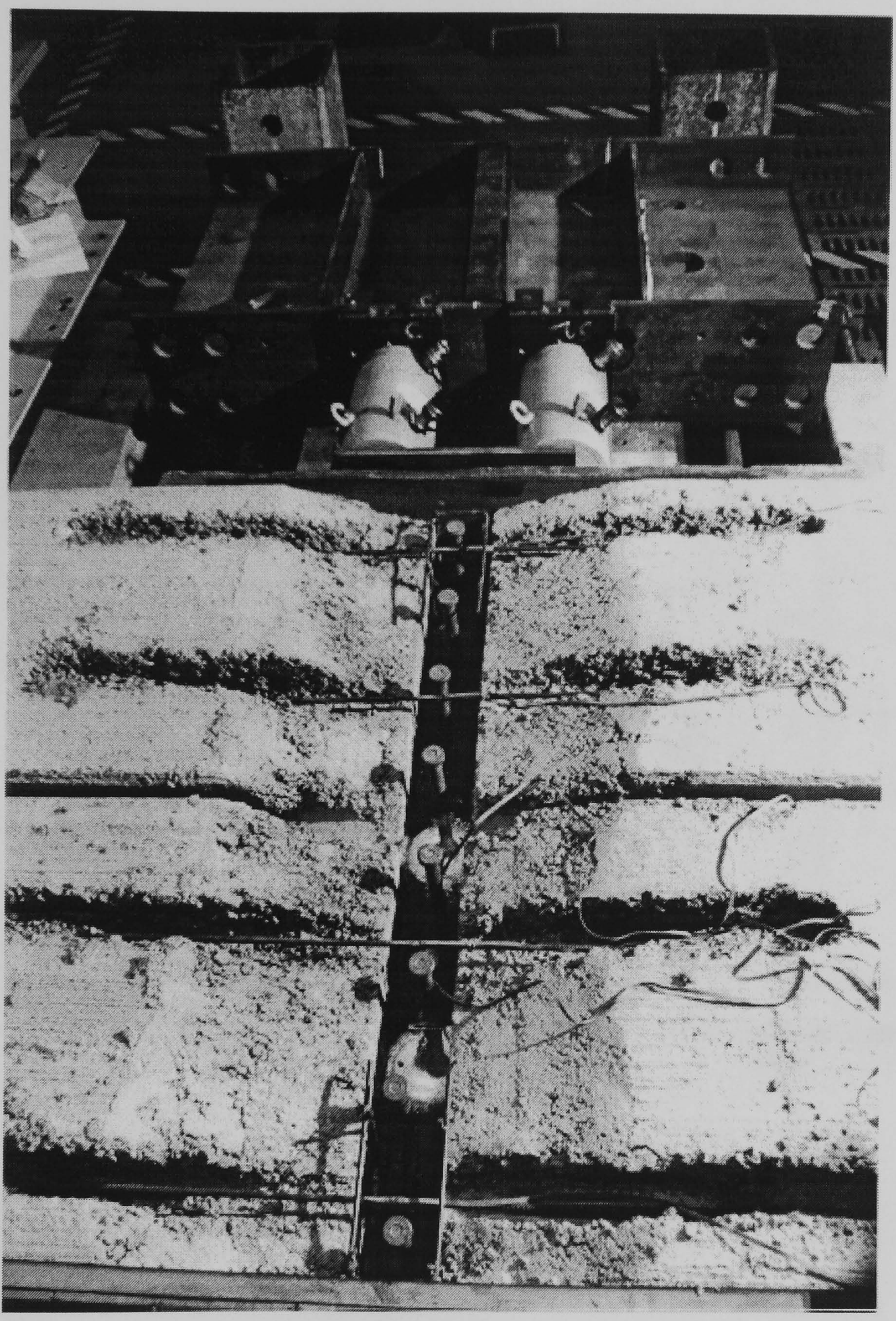

Fig. 3.3 General arrangement showing open cores and transverse reinforcement

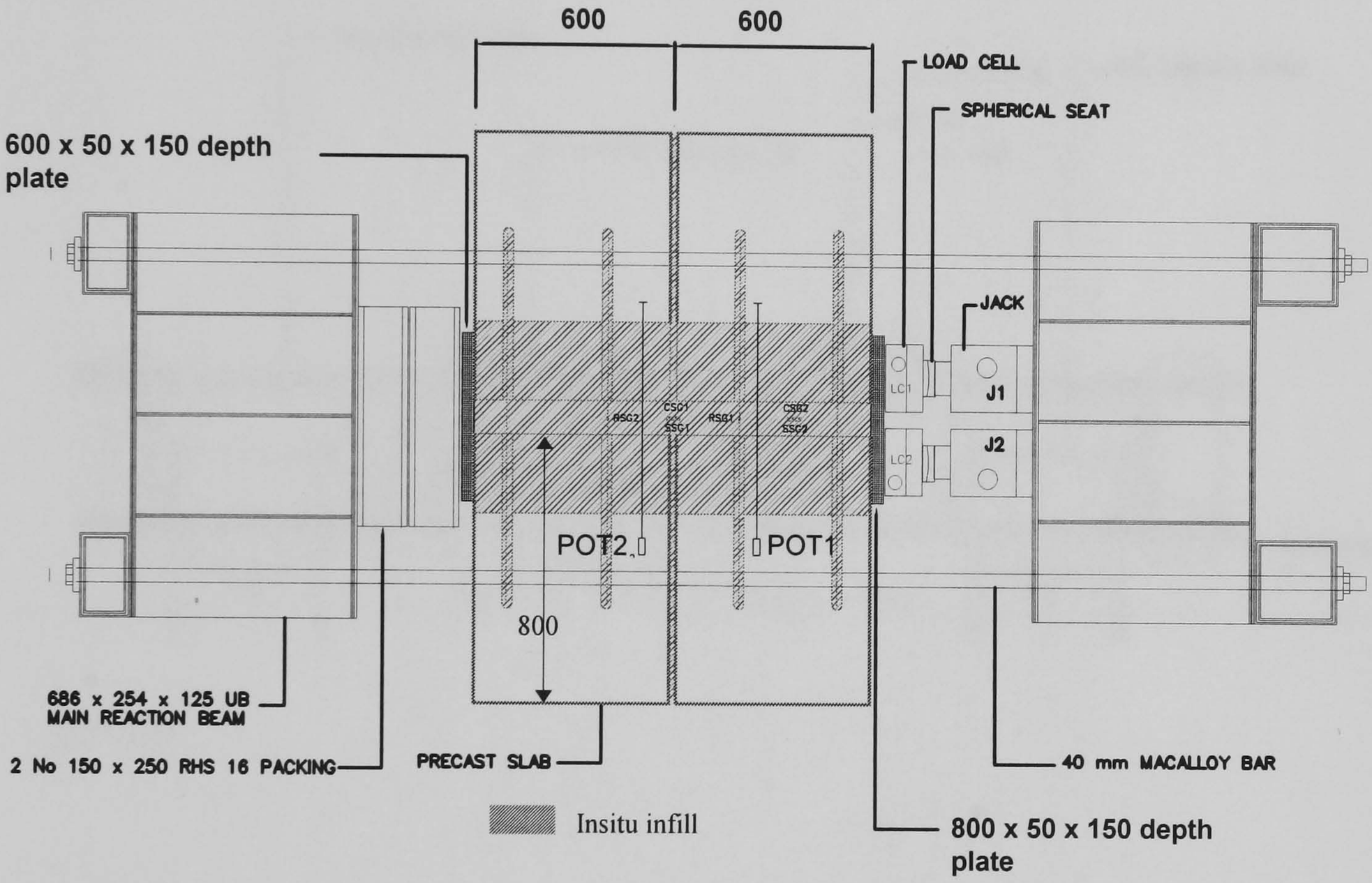

Fig. 3.4 General arrangement of compression test

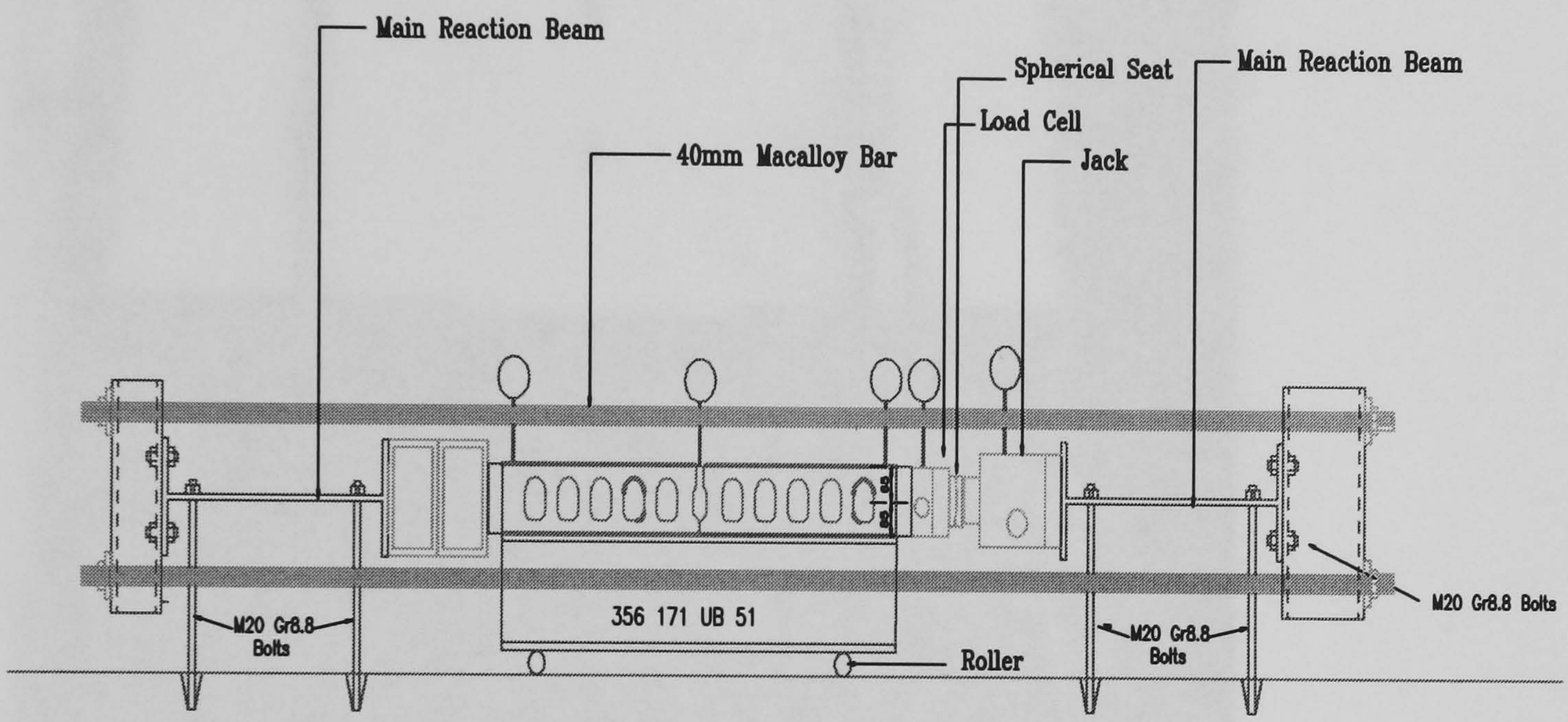

Fig. 3.5 Elevation of compression test arrangement

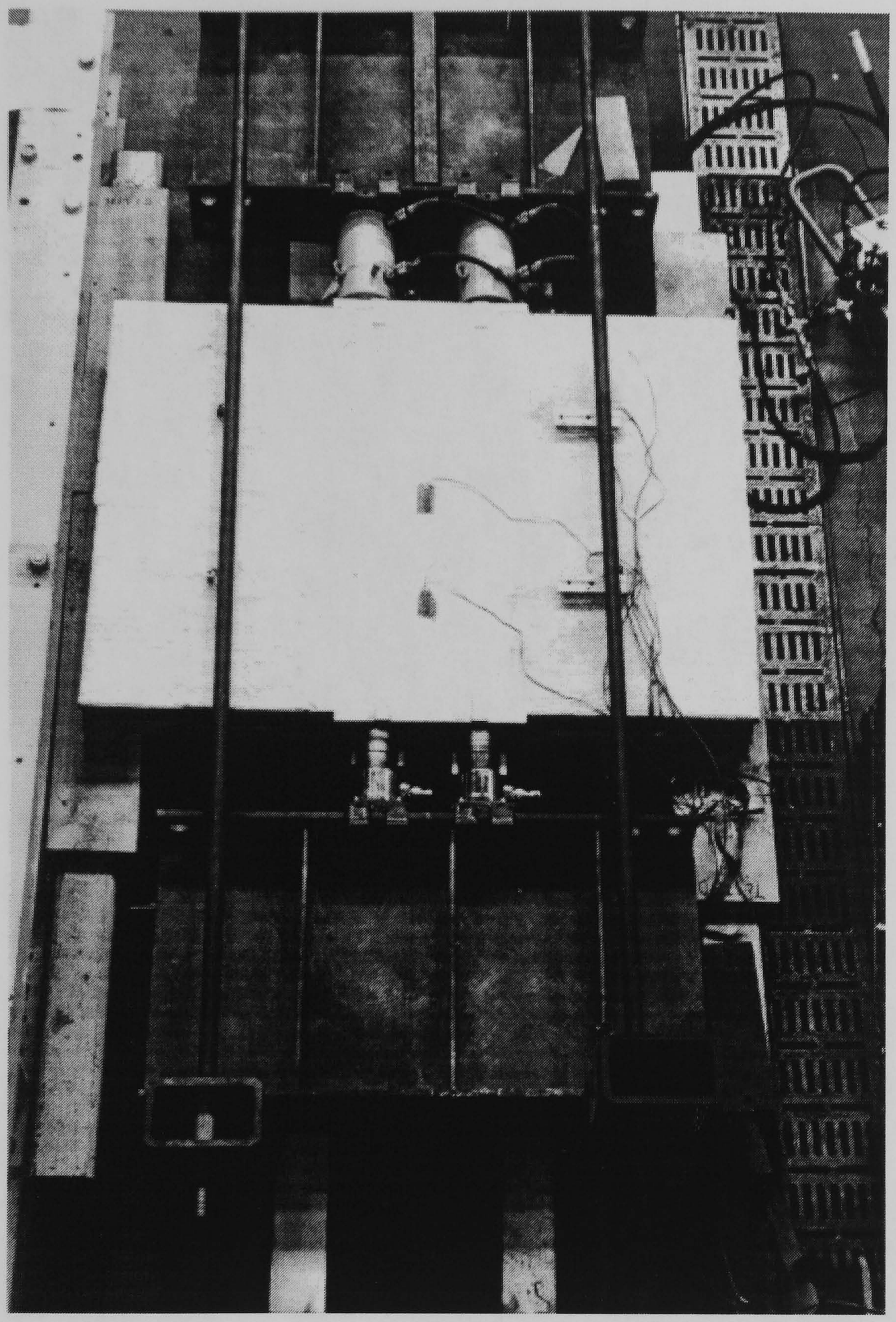

Fig. 3.6 General arrangement showing position of concrete strain gauges

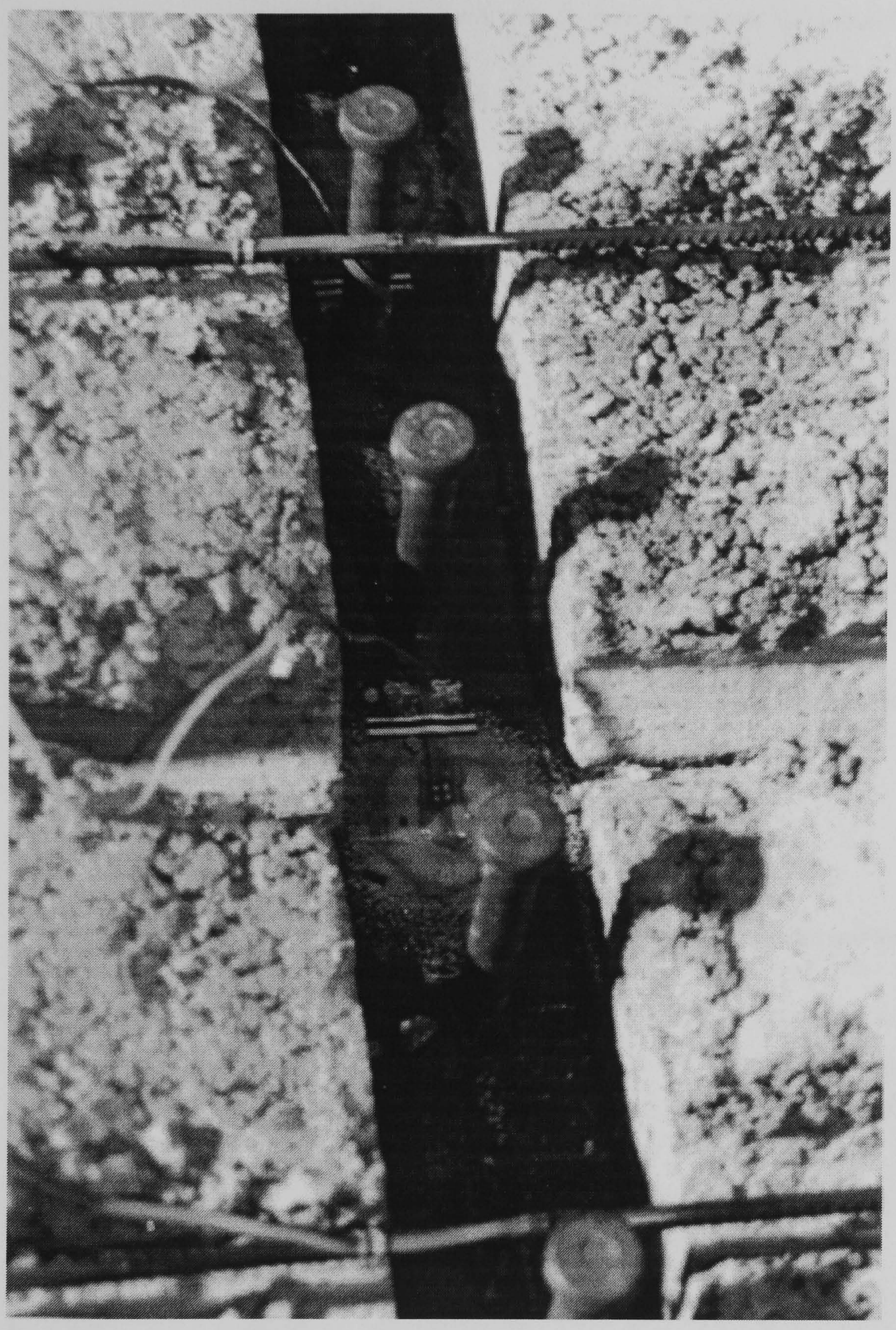

Fig. 3.7 Position of steel and rebar strain gauges in compression test

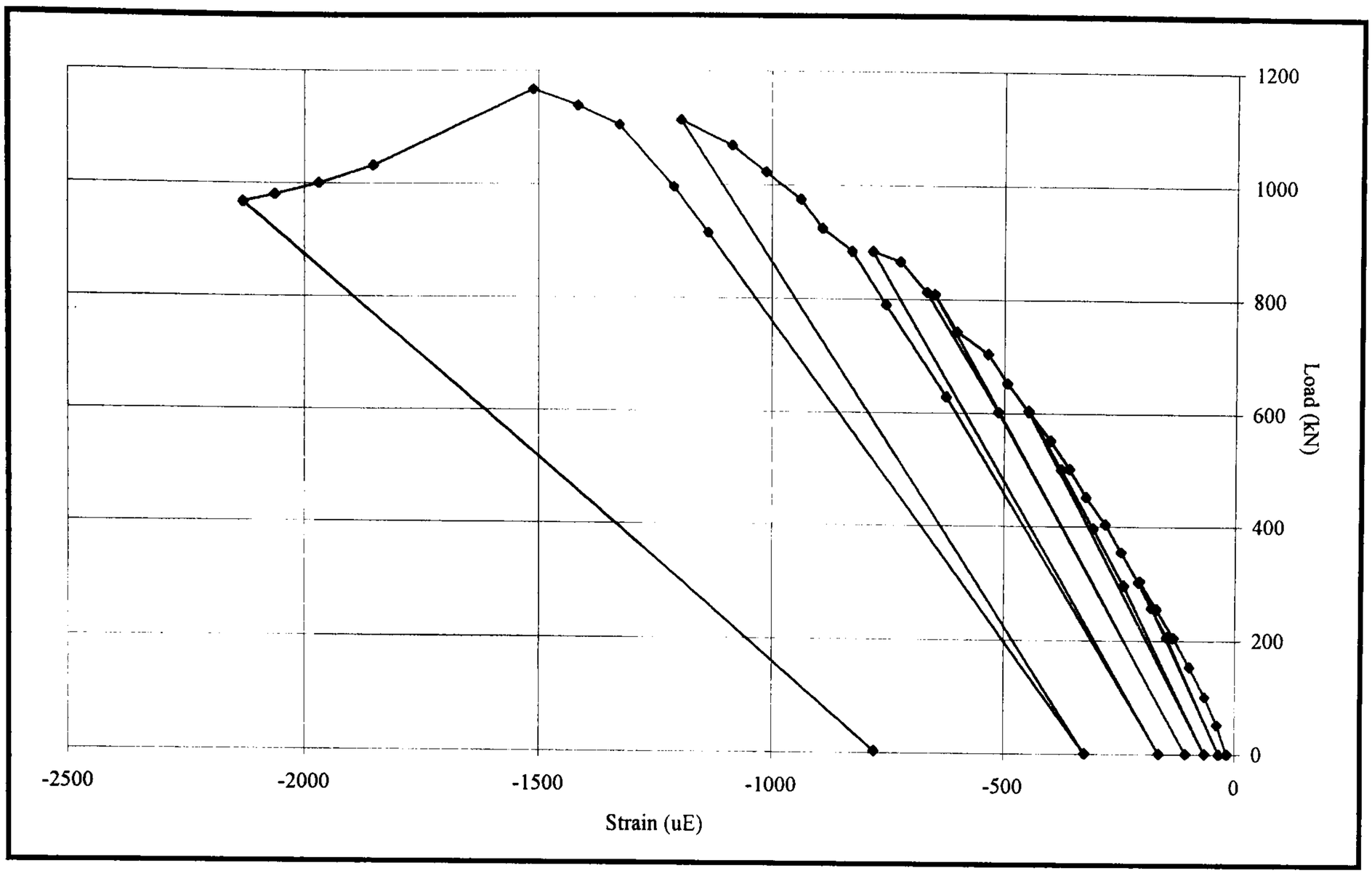

Fig. 3.8 Load vs. compressive concrete strain of SPC1

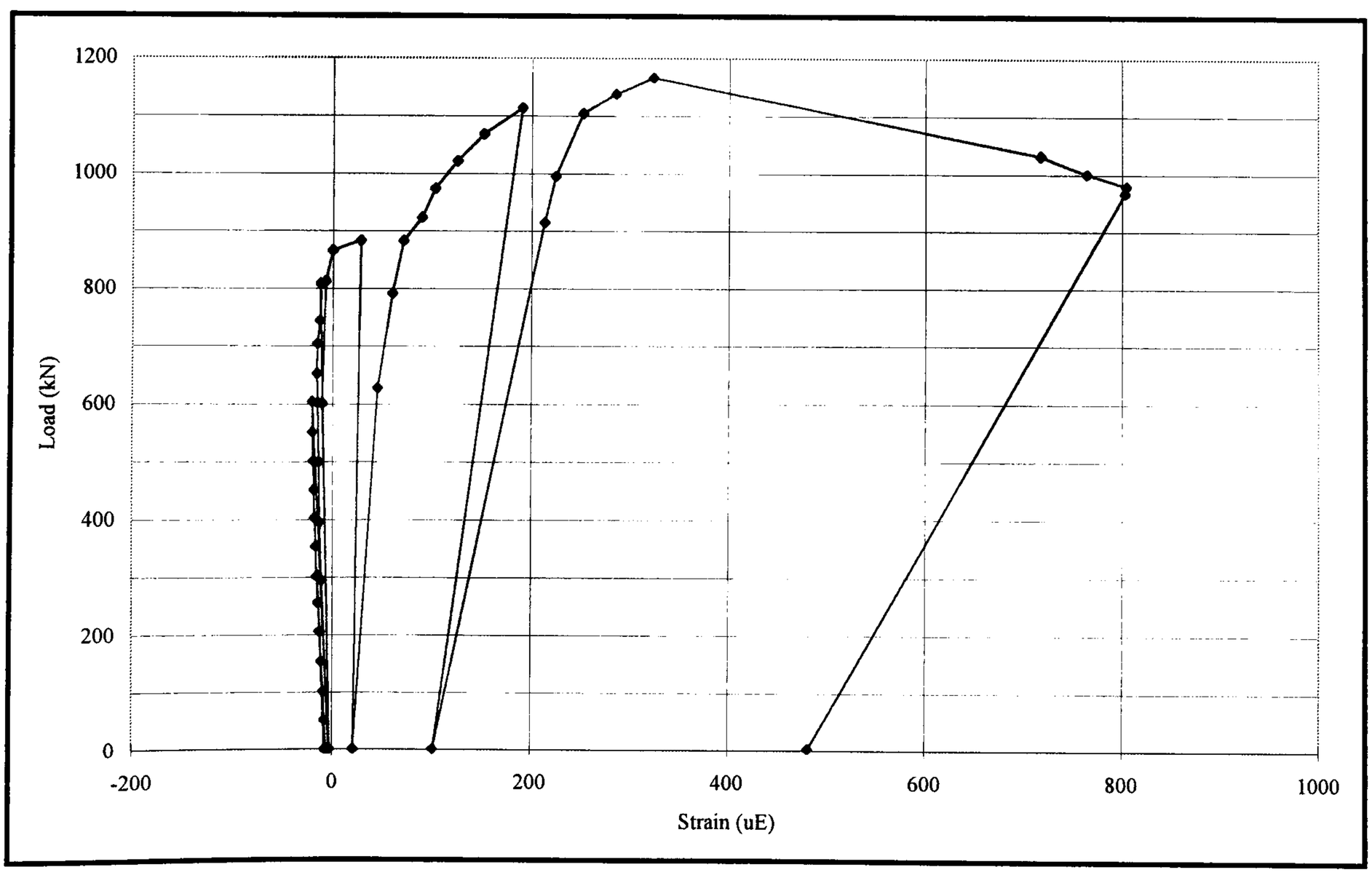

Fig. 3.9 Load vs. reinforcement strain of SPC1

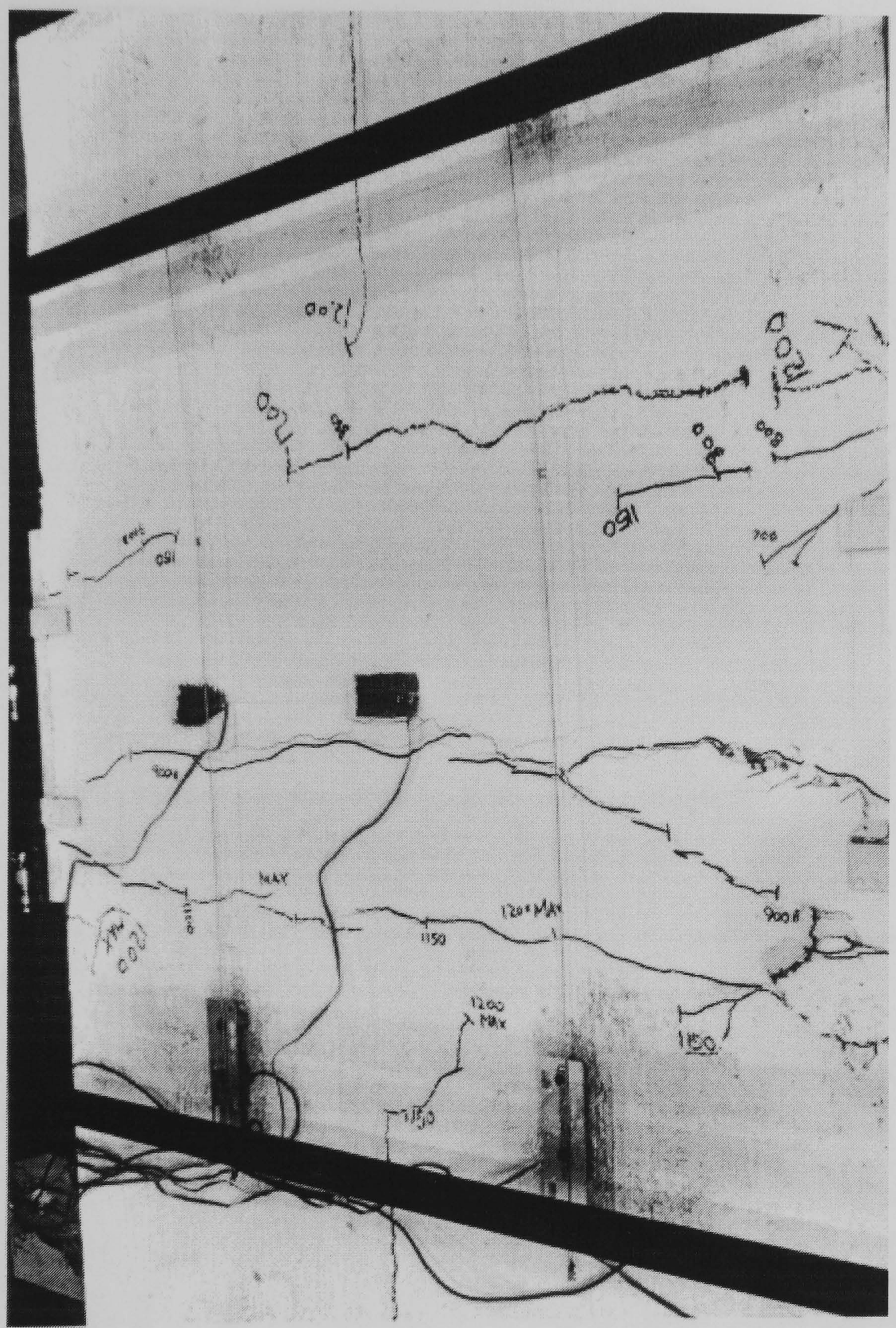

Fig. 3.10 Crack pattern of SPC1 at failure

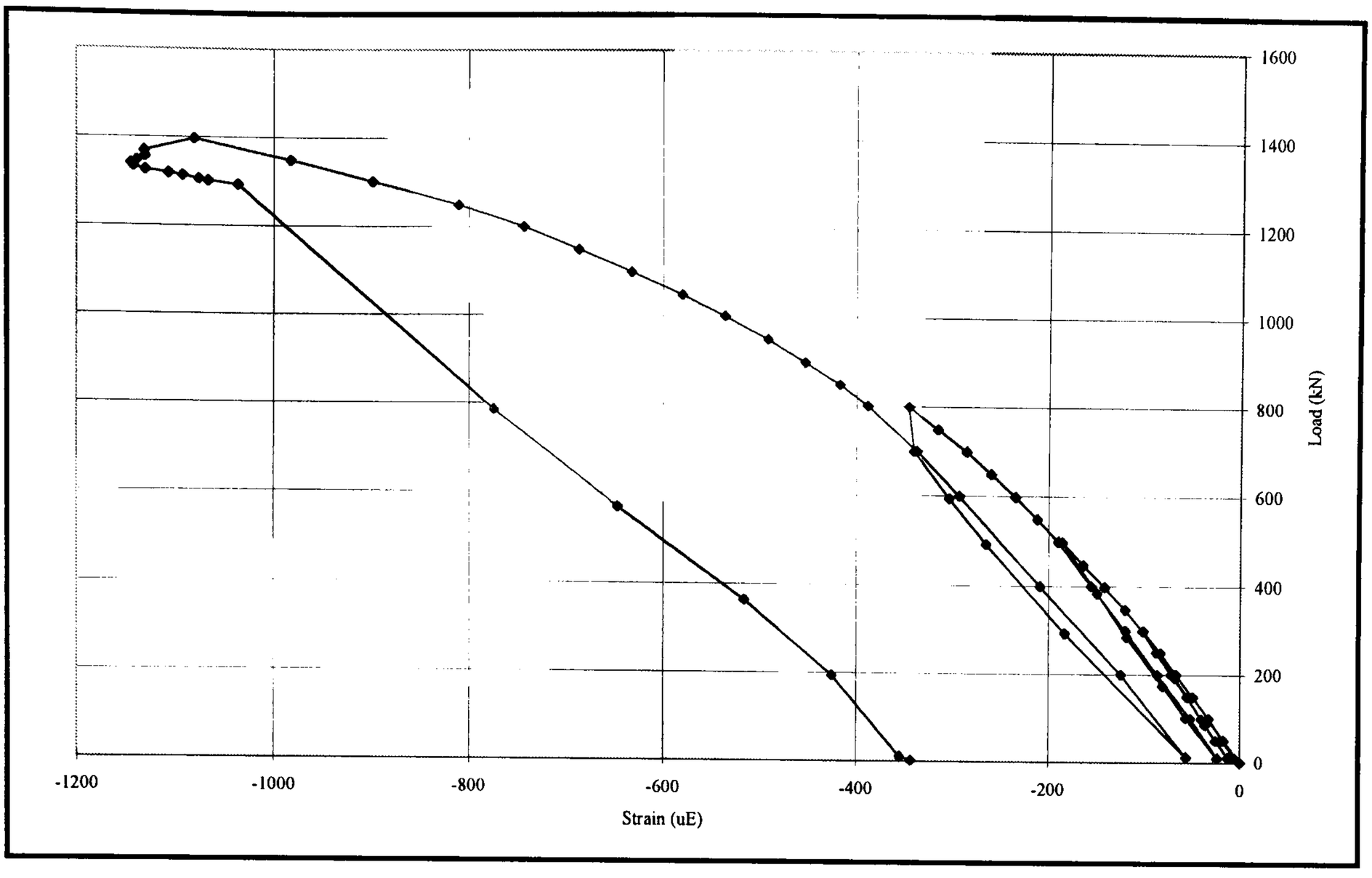

Fig. 3.11 Load vs. compressive concrete strain of SPC2

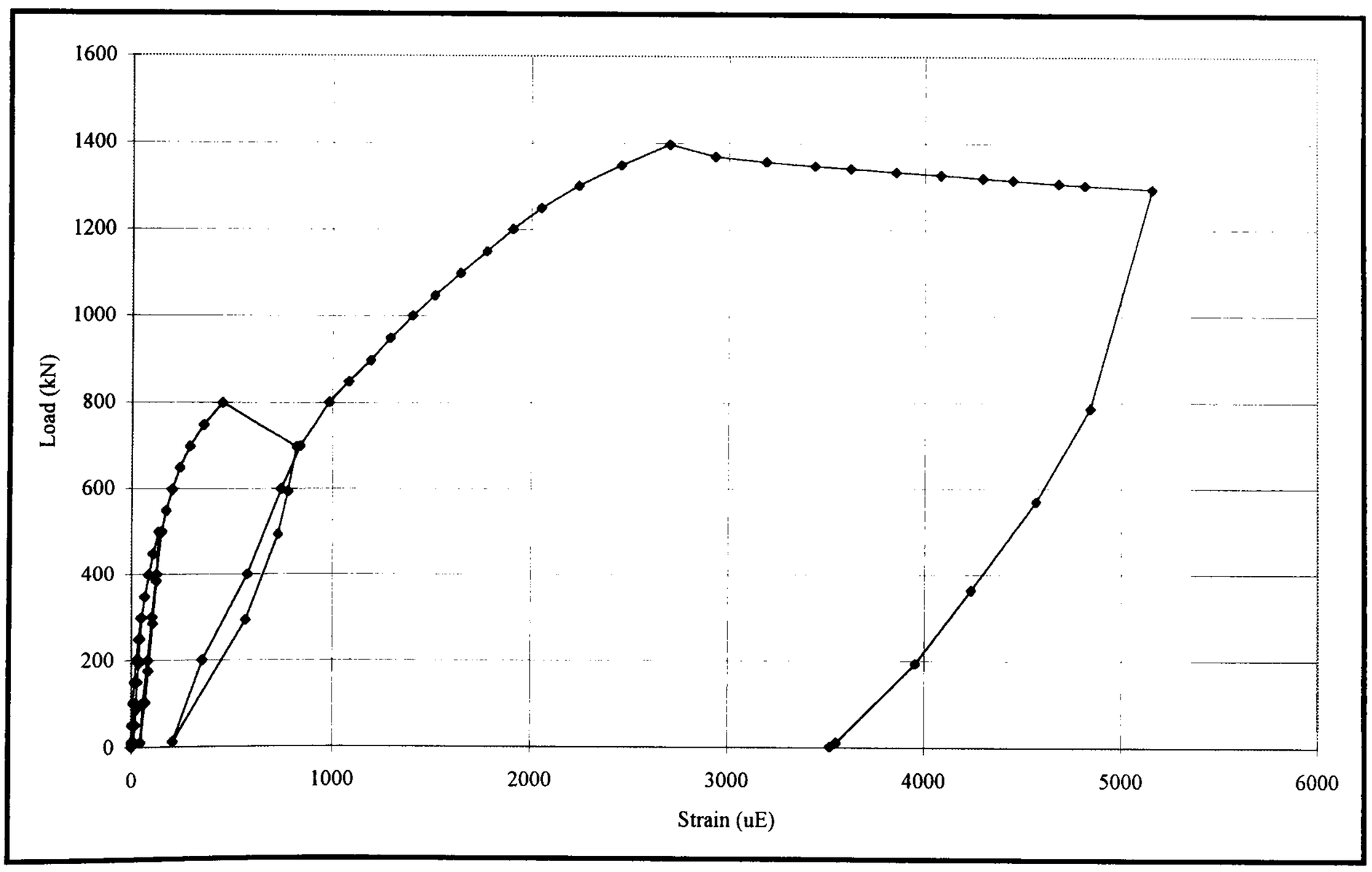

Fig. 3.12 Load vs. transverse reinforcement strain of SPC2

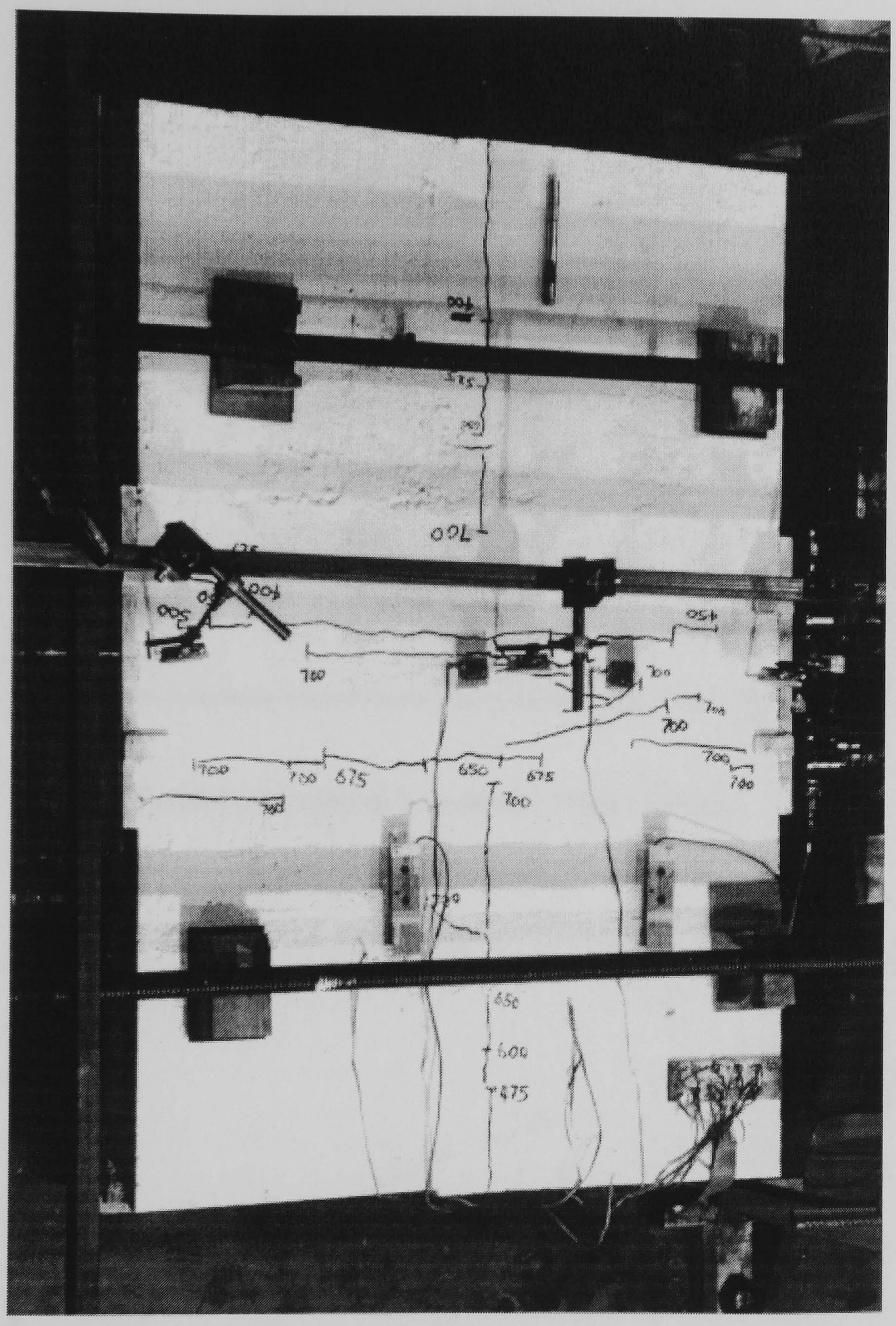

DIRECTION
OF LOAD

Fig. 3.13 Crack pattern of SPC2 at failure

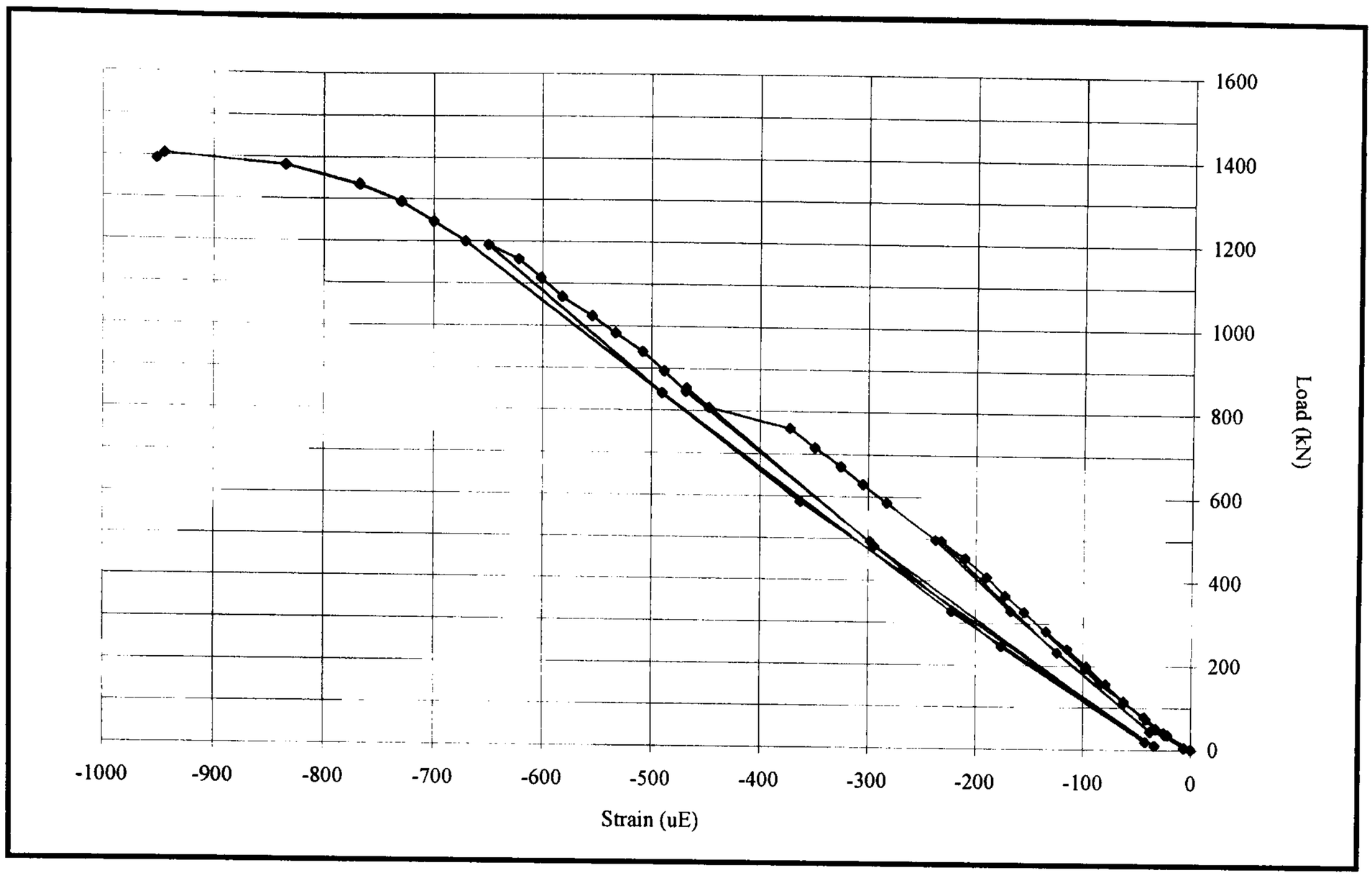

Fig. 3.14 Load vs. compressive concrete strain of SPC3

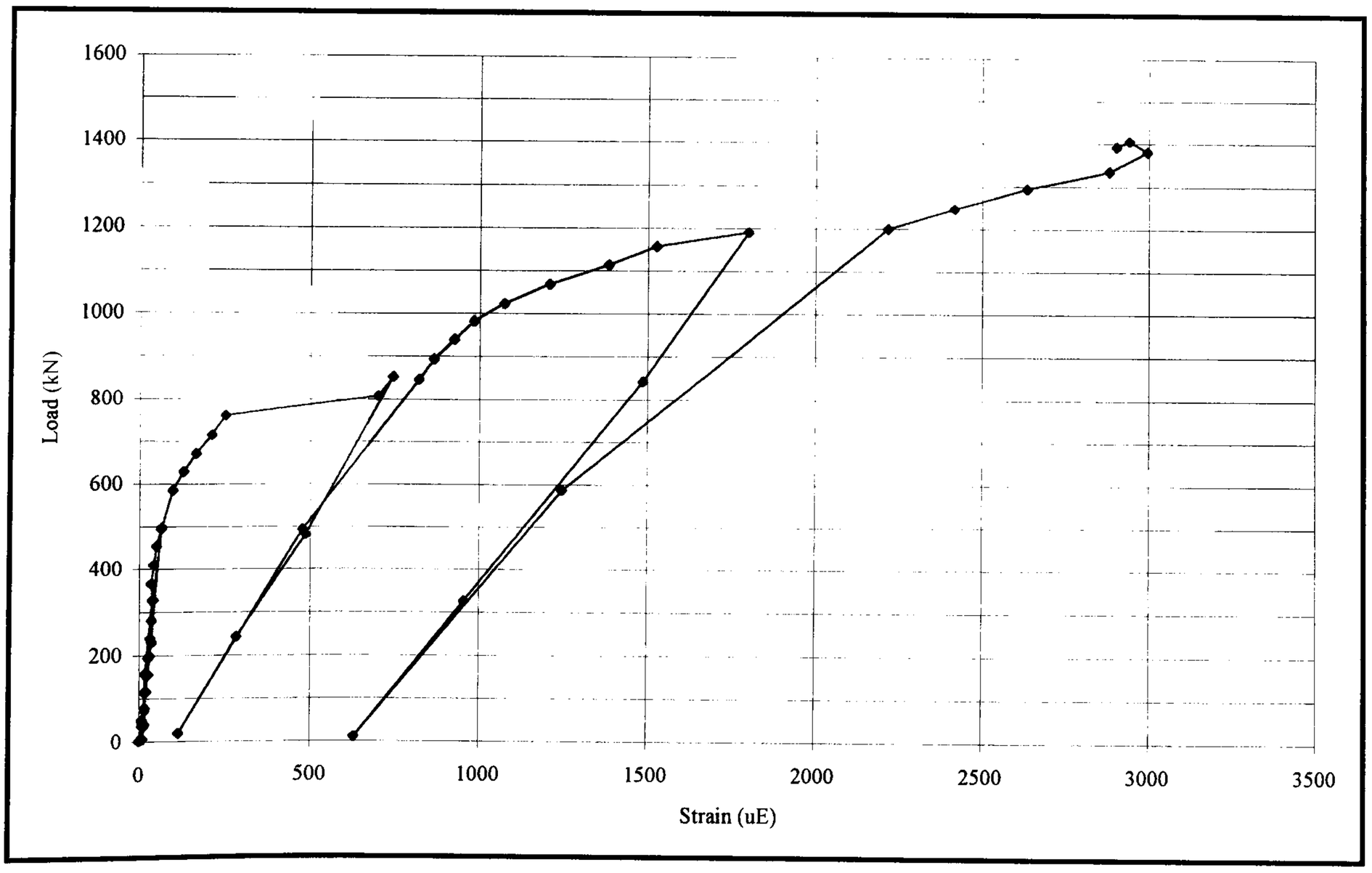

Fig. 3.15 Load vs. transverse reinforcement strain of SPC3

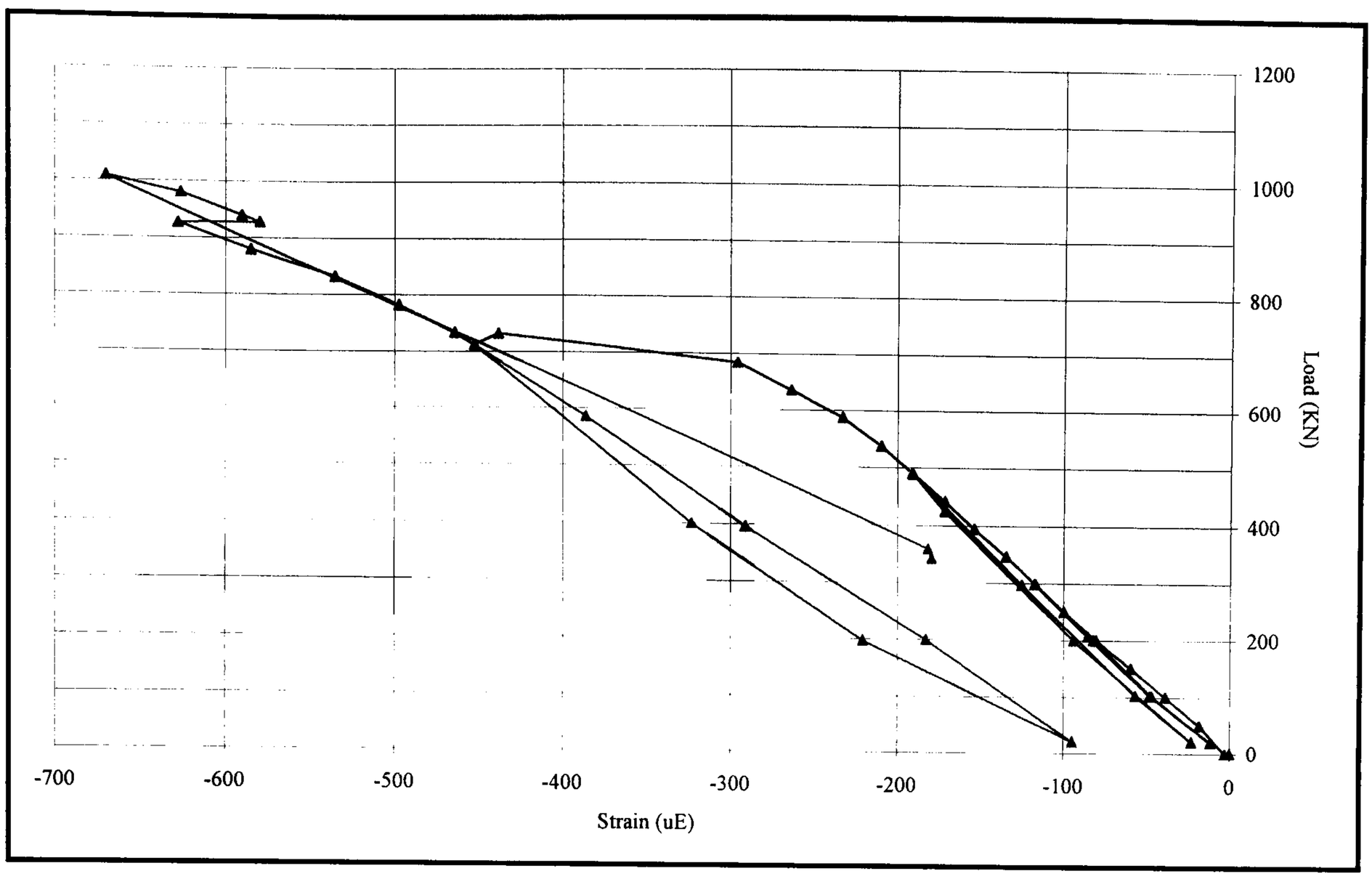

Fig. 3.16 Load vs. compressive concrete strain of SPC4

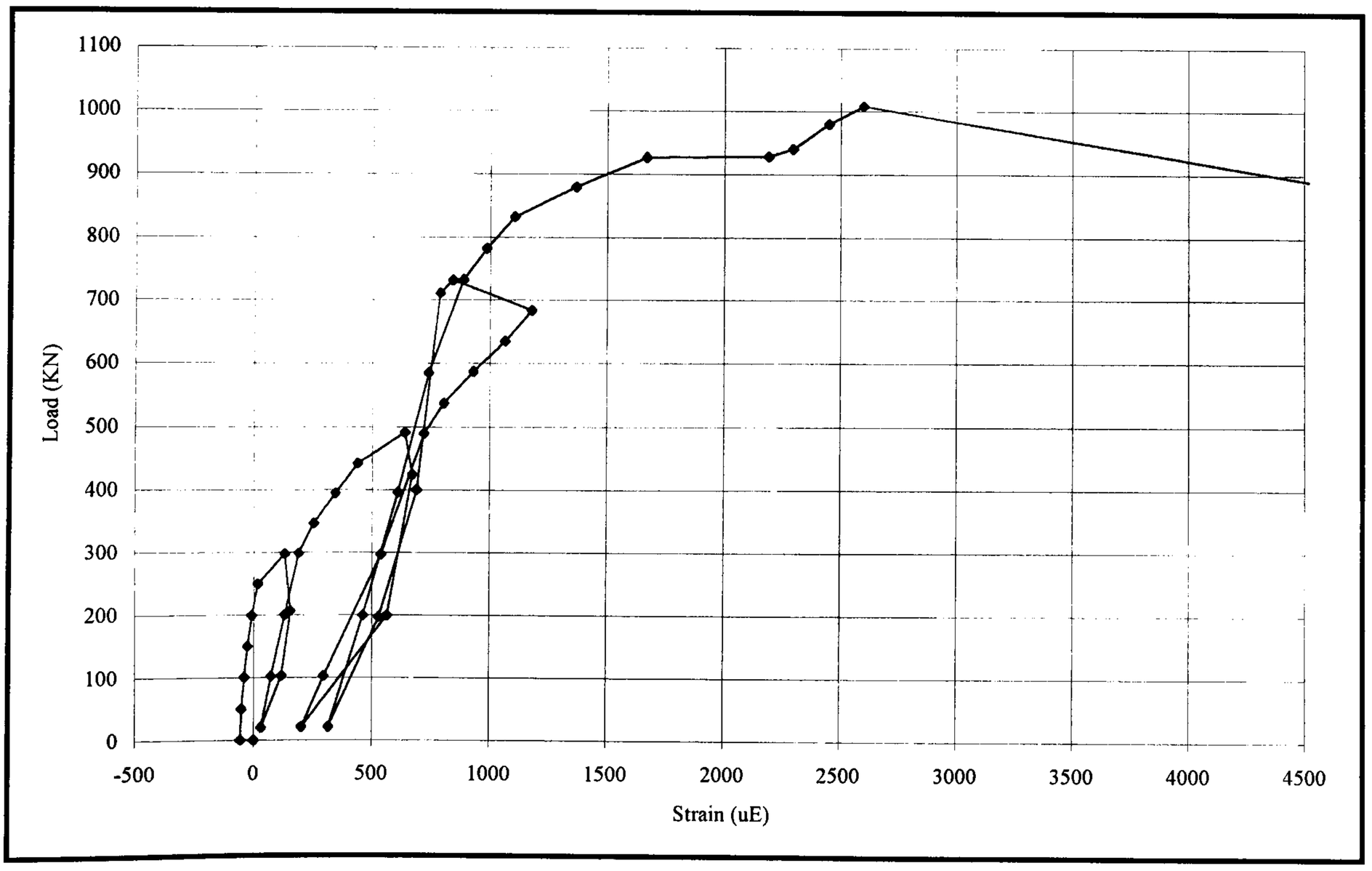

Fig. 3.17 Load vs. transverse reinforcement strain of SPC4

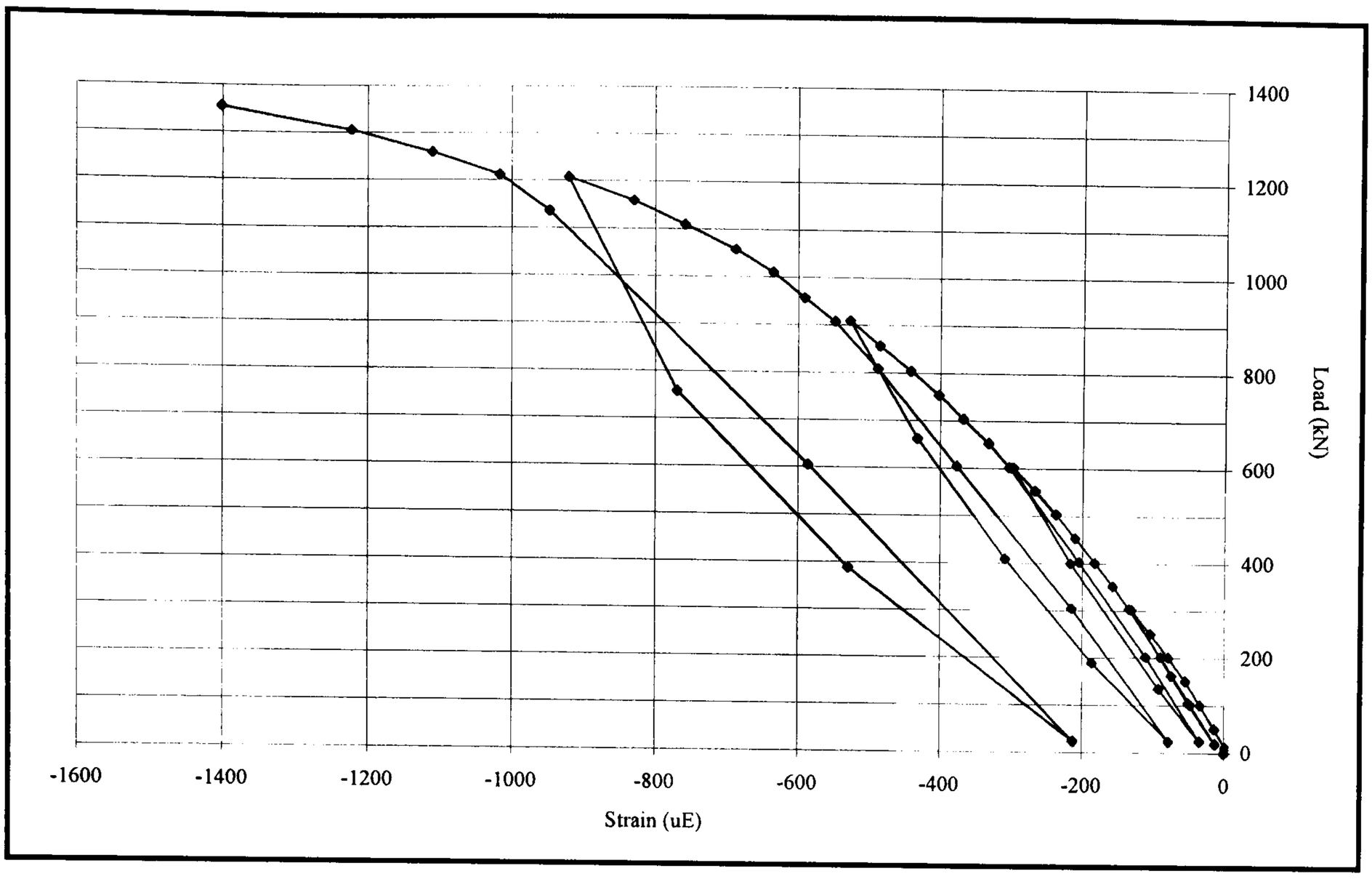

Fig. 3.18 Load vs. compressive concrete strain of SPC5

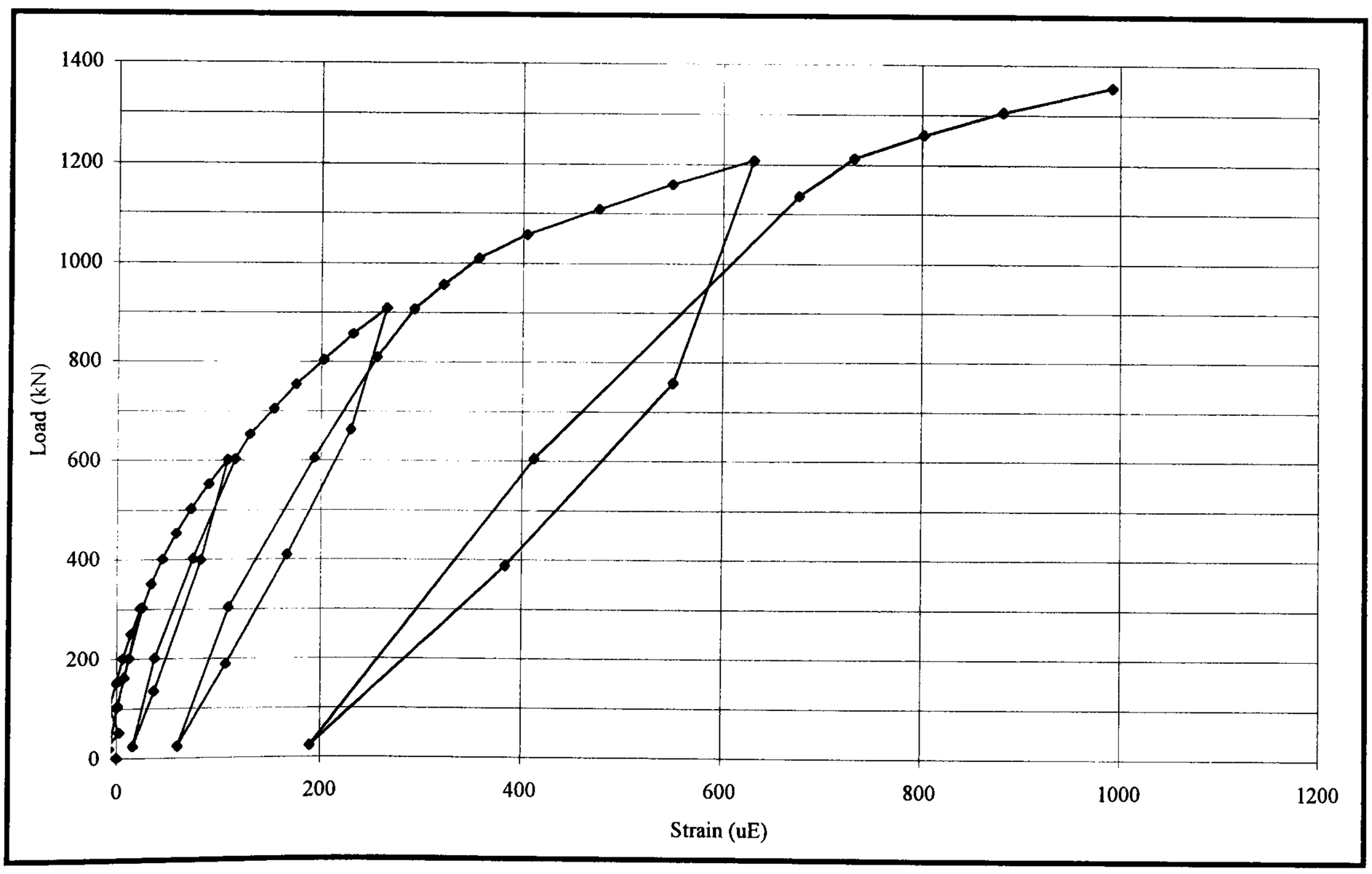

Fig. 3.19 Load vs. transverse reinforcement strain of SPC5

Fig. 3.20 Crack pattern of SPC5 at failure

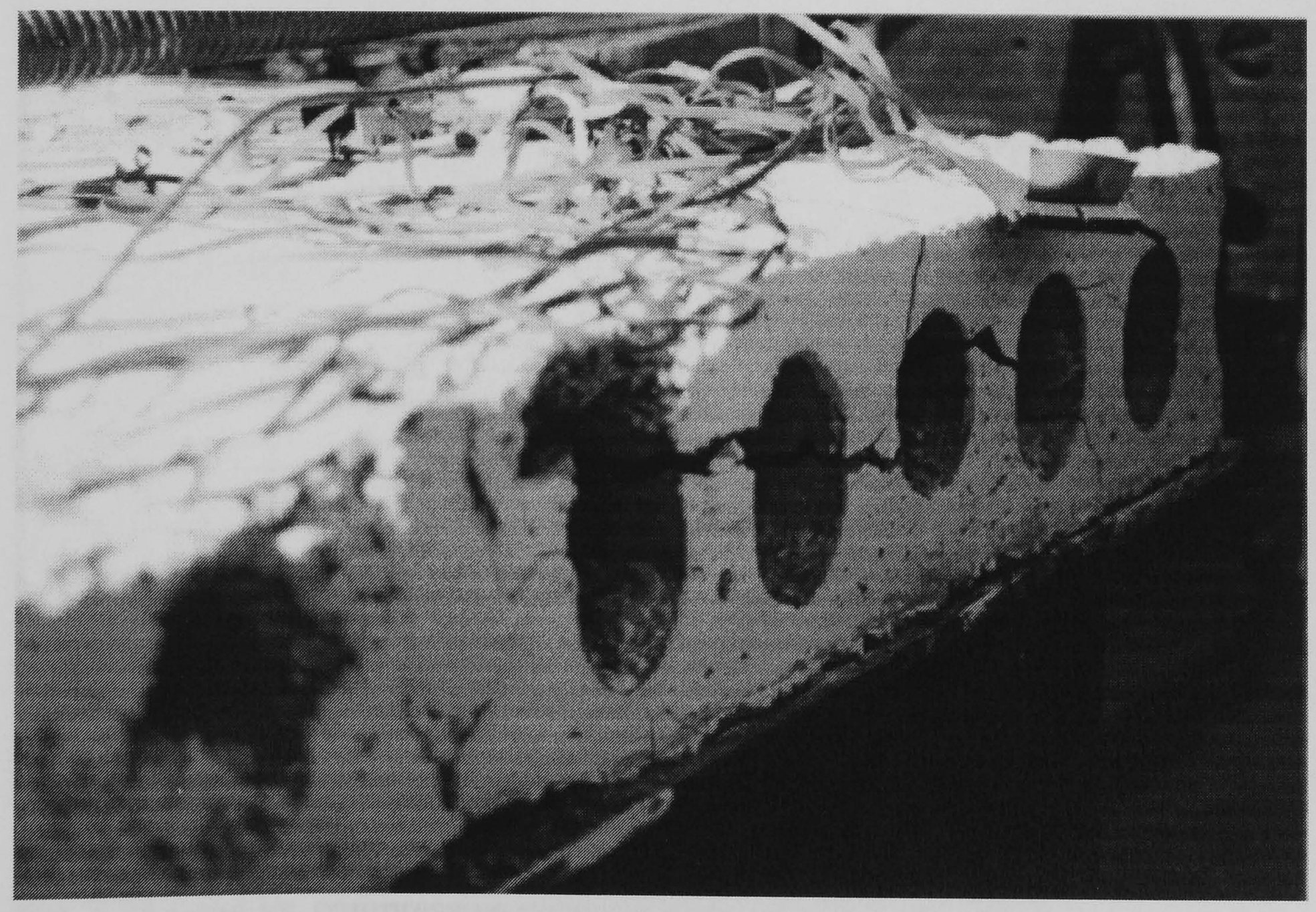

Fig. 3.21 Shear failure of hollowcore unit

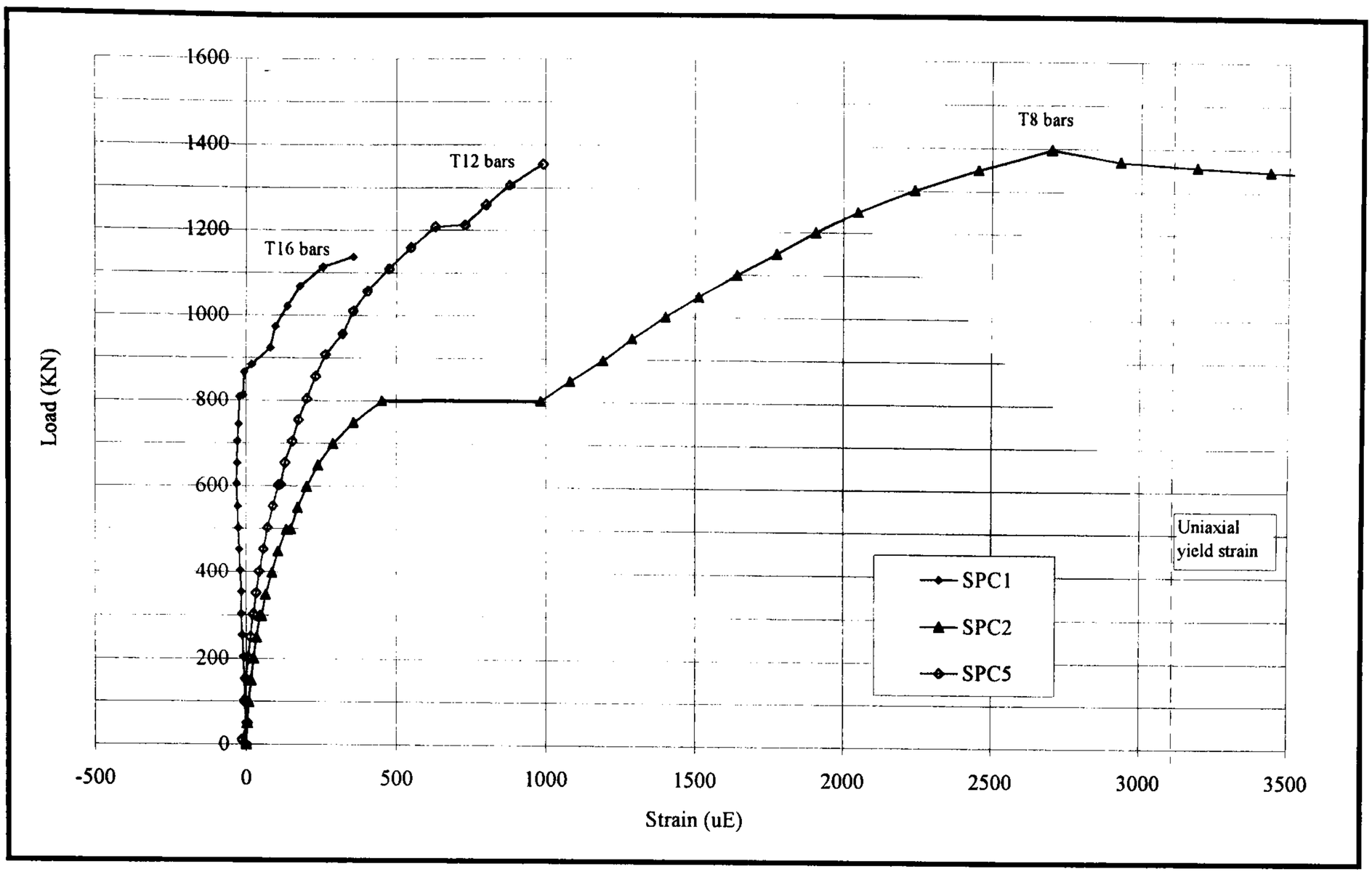

Fig. 3.22 Load vs. transverse reinforcement strain of SPC1, SPC2 and SPC5

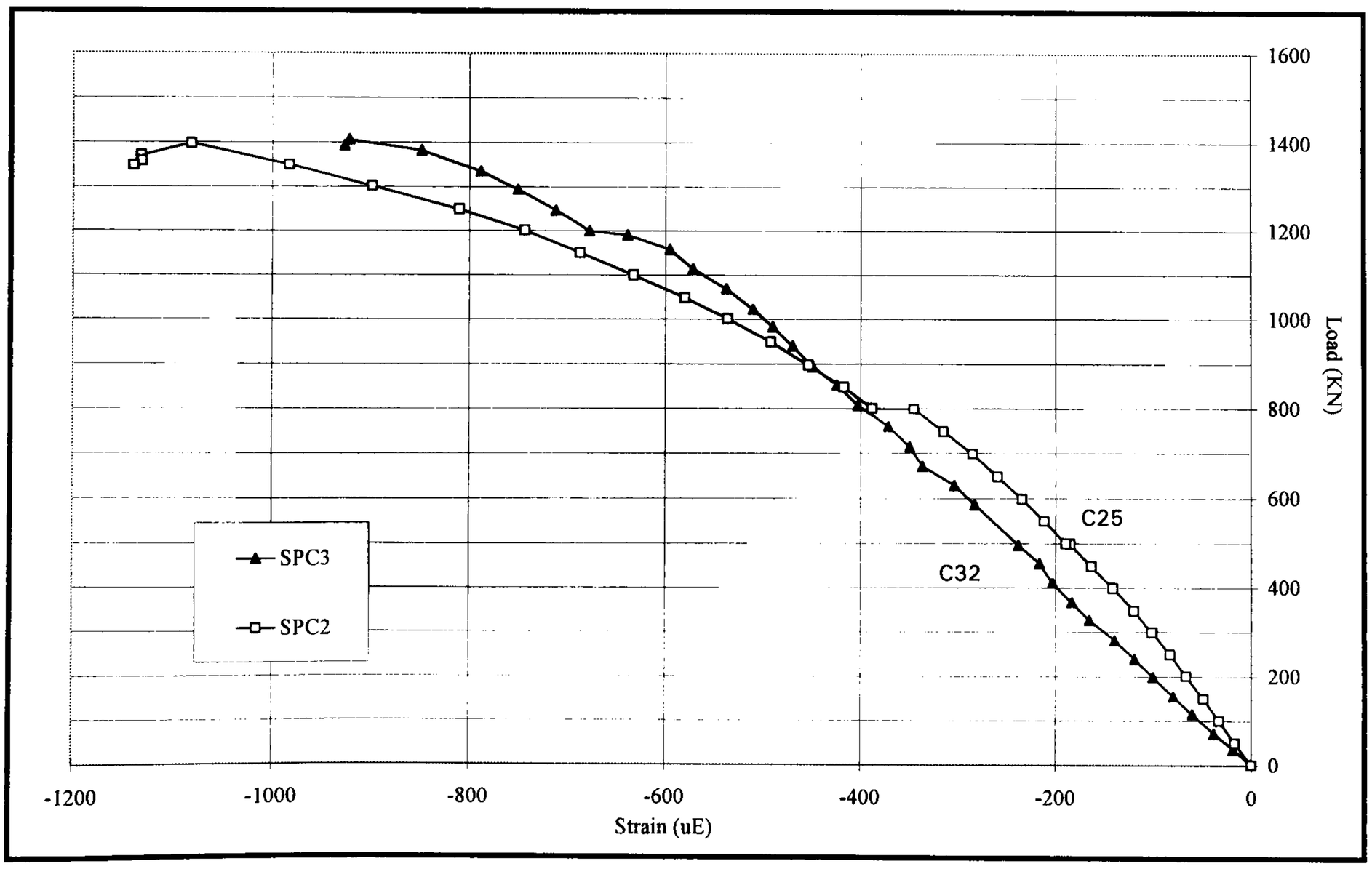

Fig. 3.23 Load vs. compressive concrete strain of SPC2 and SPC3

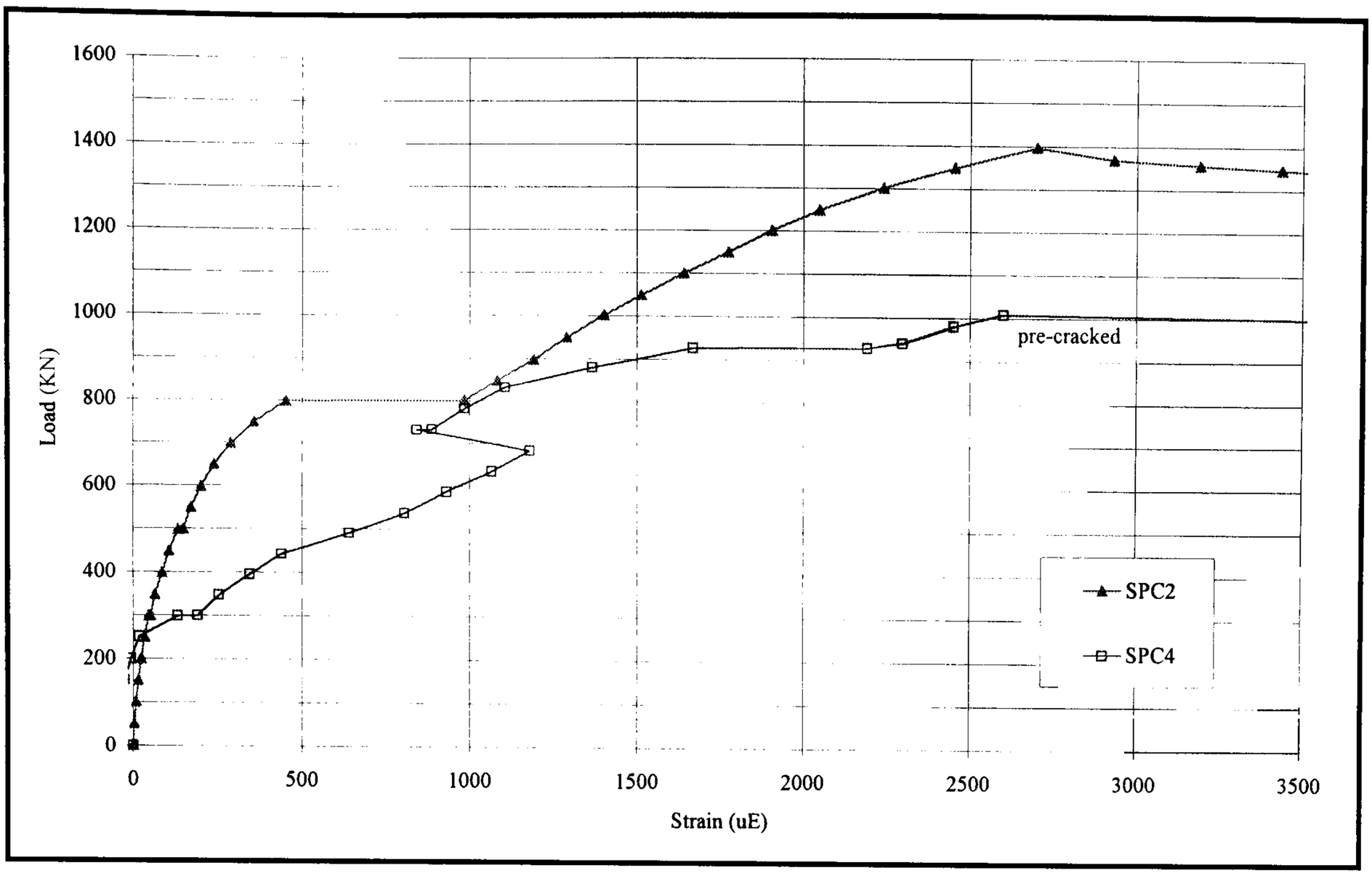

Fig. 3.24 Load vs. transverse reinforcement strain of SPC2 and SPC4

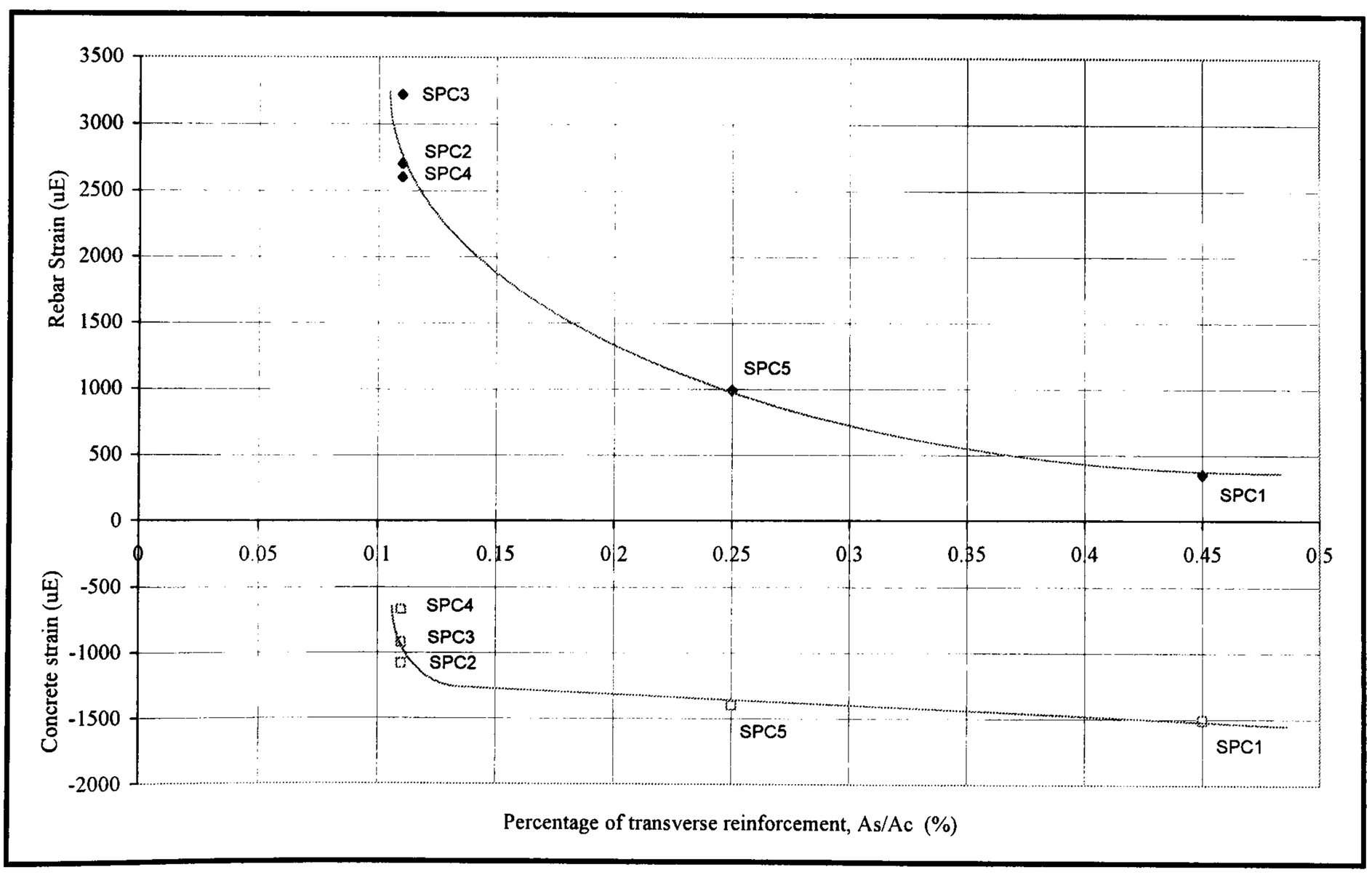

Fig. 3.25 Compressive concrete strain and tensile strain in transverse reinforcement at failure in relationship with percentage of transverse reinforcement

Chapter 4

Push Off Tests

4.1 Introduction

The longitudinal shear flow in a composite steel and concrete beam is transferred across the steel flange concrete slab interface by the mechanical action of the shear connectors. The ability of the shear connection to transfer longitudinal shear forces therefore depends on the strength of the shear connector, and also on the resistance of the concrete slab against longitudinal cracking induced by the high concentration of shear force. Previous researches, as described in Chapter 2, have not determined the strength of shear connection in this type of construction. The objective of this chapter is to describe such a mechanism, and to present the results of some full size push off tests using proprietary precast hollow core units (hcu).

4.2 Test arrangement

In a composite beam situation the floor slab tends to slide along the flange of the beam, and it is the function of the shear studs to prevent this slippage, as shown in

Fig. 4.1 and Fig. 4.2. The test used to replicate this action is shown in Fig. 4.3 and consists of four hcu's placed side by side, and on either side of a short steel universal beam (UB). The test provides a convenient way to study the behaviour of the shear connection without the expense of a full bending test. In all, ten tests were carried out using hcu's and two using solid reinforced concrete (r.c.) slabs, as shown in Table 4.1.

The standard push off test for solid reinforced concrete slabs described in BS5400[1] is not suitable for use in precast hcu composite construction for the following reasons:

1. The dimensions specified for the slab are too narrow and too short for precast composite construction.
2. The reinforcement used in the standard test is not appropriate since only transverse reinforcement is required for this type of composite construction. Unlike the solid r.c. slab, no longitudinal reinforcement is necessary.
3. For the standard test, two slabs of each specimen were cast either horizontally on consecutive days or vertically. Neither method is suitable for precast construction because of the need to avoid handling the assembly after construction of the precast / insitu joints.

The ten hollow core test specimens each consisted of either four 600 mm or two 1200mm wide x 150 mm deep x 800mm long prestressed hcu's (Supplied by Bison Floors Ltd.) connected to a grade 43 steel 356 x 171 x 51 UB with a single

row of pre-welded headed studs at 150 mm centres. See Figs. 4.4 and Fig. 4.5. The 600 mm slab width was chosen instead of the more common 1200 mm wide unit so that the effect of the edge joint was included in a test length of 1200 mm. The characteristic cube strength for the precast concrete is taken as 50 N/mm^2. Milled slots approximately 500 mm long were made in the second core from the edges of the units to allow placement of transverse reinforcement (the first core is not suitable due to small edge distances). The gap between the ends of the slabs was varied from 40 mm to 120 mm, according to the schedule of tests in Table 4.1. Six studs were used for each test, all studs were 19 mm diameter x 125 mm long 'TRW-Nelson Headed Studs' and were attached to the UB using an automatic fusion welding process. The top cover to the transverse reinforcement was approximately 50 mm. Insitu concrete was placed and compacted using a 25 mm diameter vibrating poker.

The two solid r.c. slab specimens consisted of a 150 mm deep slab reinforced using transverse reinforcement placed in the same positions as the transverse reinforcement in the milled slots in the hcu specimens, see Fig. 4.6. A small amount of longitudinal steels were used to complete the reinforcement cage. These tests are designed to test the apparatus and to compare the result with the standard test result from BS5950[(2)]. The test was also used to compare the reduction in shear capacity between a solid slab and a hollow core slab.

The main components of the test rig consisted of 2 no. 500kN hydraulic jacks bracketed onto the steel beam. A single manual pump was used for both jacks so that loading is applied simultaneously. Two no. 500kN electrical resistance load cells were placed between the jacks and specimen for direct measure of load. To improve distribution of load, a 500mm long spreader beam was placed between the load cells and the specimen so that the load was equally distributed along the slab edge, see Fig.4.7.

4.3 Instrumentation

Instrumentation consisted of ERSG's for measuring strain in the transverse reinforcement and POT's for monitoring steel/concrete interface slip. ESRG's were installed on the centre of two transverse reinforcement to measure the tensile strain in the transverse reinforcement. The strain gauges used for the rebar were of the type FLA-6-11 with a gauge length of 6mm. The gauge was of 120 ± 0.3Ω resistance and with gauge factor of 2.13. The strain gauges on the surface of the rebar were coated with epoxy to protect from the concrete. The strain gauges were used to monitor the strain and yielding of the transverse reinforcement. Four POT's were used as shown in Fig. 4.8 for monitoring the longitudinal slip during the test, two were placed onto the slab and the other two onto the edge of the top flange of steel beam. All values of slip reported are the mean of changes of the

POTs reading between the slab and the steel beam which eliminated any unbalancing effect on loading.

4.4 Testing procedure

The load was applied in 20kN intervals until excessive slip or failure was reached, studs shear off from steel beam or severe cracking was observed. In some cases, the load was released and re-applied at several load levels before failure. The load was usually released and recovered in two to three loading steps. All the data from the ERSGs, Load Cells and POTs were automatically recorded by the data logger and live plotting of load v slip and load v strain were output to the computer. Data were scanned initially at every load increments until the maximum load was reached, then the data were scanned with displacement until failure or excessive of slip. Crack widths and lengths were checked and observed and manually recorded at each load increments. After the test, specimen was dismantled to investigate the condition of the shear studs wherever possible.

4.5 Material testing

4.5.1 Concrete testing

Insitu concrete infill between the precast hcu or the r.c. slab was cast in the laboratory with the specimen in position. To monitor the insitu concrete strength, a numbers of cubes (100 x 100 x 100 mm) and cylinders (150 mm dia. x 300 mm long) were sampled and cured. These samples were tested in accordance with BS1881[3] using the Denison compression test machine. Compressive and tensile strength of the insitu concrete was derived from the compressive test and the Brazilian splitting test. The strength of all the test specimens is summarized in Table 4.2

4.5.2 Rebar testing

Tensile tests were carried out on a sample of rebars used in the tests using the Zwick universal test machine. The tensile strength of the size of rebar used in the push-of tests are summarized in Table 4.3 and Table 4.4.

4.6 Test results

The main objective of the push-off test was to determine the horizontal shear capacity of the shear connector for this type of construction. The variable test parameters were (a) the area of transverse reinforcement since it was most influential during the compression test, and (b) the gap of the insitu infill which proved influential from research conducted by Moy[8]. Load vs. slip curve was plotted for each test. The maximum shear capacity, slip at the shear interface and the initial shear stiffness are given in Table 4.5. Cracks in concrete and tensile strain in transverse reinforcement was observed throughout the test.

4.6.1 Test T8-25-40

This test was set up to investigate the influence of the gap width for the T8 series. A gap width of 40mm between the hcu was used for this test as it represented the minimum gap required for 10mm aggregate concrete (i.e. 10mm aggregate + 19mm headed studs + 10mm aggregate). Results are shown in Table 4.5. The load-slip curve is shown in Fig. 4.9. No cracks were observed for load up to 320kN. The first crack was found longitudinally along the specimen and also transversely between the joints as the applied load reached 330kN. Load reduction occurred as the applied load reached the maximum of 340kN (57kN per stud), with crack widths up to 1.0 mm as a high tensile strain was recorded in the transverse reinforcement. Slip at maximum load was just over 2.2 mm. The

applied load gradually reduced as the transverse reinforcement became fully yielded, until the load dropped sharply to 250kN with slip in excess of 10mm. Tensile cracks were observed after the maximum load was achieved. The test was terminated due to excessive cracking longitudinally along the specimen. Mode of failure is caused by yielding of transverse reinforcement and subsequently tensile splitting of the insitu infill concrete around the shear studs. Fig. 4.10 shows the crack pattern of T8-25-40 after the test.

4.6.2 Test T8-25-65

The gap width for this test was increased to 65mm as it represented the normal gap width associated with the steel beam used for the span. The load-slip curve is shown in Fig. 4.11. No slip was observed up to 180kN for the full specimen, or 30kN per stud. The first crack formed simultaneously along the slab and transversely across the joint as the load reached 380kN, indicating an improvement of shear capacity compared to the previous test. Maximum load of 420kN was reached with similar slip to T8-25-40. 23% increase of shear capacity was achieved with the gap width increased from 40mm to 65mm. High tensile strain was also recorded in transverse reinforcement as slip continued to increase. The load gradually reduced to a constant value of 275kN with a slip in excess of 30mm. Two studs were sheared off as the slip reached 35mm and 53mm. Mode of failure was due to excessive cracking in concrete. After the test was terminated,

the slab was taken apart to reveal that all studs were bent with two studs closest to the jacks sheared off completely during the final stage of the test. See Fig 4.12.

4.6.3 Test T8-25-65P

Pre-cracked longitudinal joints were introduced for this test to investigate the influence on the shear capacity. Fig. 4.13 shows the load-slip curve. The test result was expected to be lower than T8-25-65 due to the pre-cracked longitudinal joint as demonstrated in the compression test series. As for Test SPC4 of the compression test, tensile strain in the transverse reinforcement was recorded as soon as the load was applied. First crack was observed at the end of the specimen rather than in the transverse joint at a much lower load of 200kN as compared to all the previous tests. Rapid increase in strain was recorded in transverse reinforcement gauges as the maximum load of 320kN was reached, followed by a sudden loss of capacity as cracks developed in the insitu infill. The load reduced to 160kN with cracks developing longitudinally and transversely across the specimen. The test was terminated due to loss of capacity and excessive cracking. Fig. 4.14 shows the crack pattern of T8-25-65P after failure.

4.6.4 Test T8-25-65F

This test arrangement is similar to T8-25-65 apart from the 1200mm wide units used instead of the 600mm units to investigate the effect of not having a transverse joint. The load-slip curve is shown in Fig. 4.15 The behaviour of T8-25-65F is similar to T8-25-65 throughout the test with a slight increase in stud capacity. No slip was detected up to 250kN. At 350kN, strain of 285με in the transverse reinforcement was noted. First crack was observed at 420kN transversely across the precast units and longitudinally along the specimen suggested a slight improvement to T8-25-65. No further increases in load were possible as the load reached the maximum of 466kN (78kN per stud). Slip of 2.8mm was recorded at maximum load which was similar to the Test T8-25-65. Load reduced as the transverse reinforcement yielded with more cracks developing near the end of the specimen. Large strain was recorded in the transverse reinforcement, suggesting that the bars were fully yielded. No stud was sheared off during the test and the test was finally terminated with excessive cracking. Ductile behaviour was observed with no loss of stud. Slip at the elastic stage was less than 0.2mm, suggesting good serviceability performance. Crack pattern of T8-25-65F is shown in Fig. 4.16.

4.6.5 Test T8-25-120

This test was set up to ascertain the optimum gap width for the T8 series. A gap width of 120mm was used to represent the upper limit. The behaviour of T8-25-120 is very similar to T8-25-65 throughout the test. The load-slip curve is shown in Fig. 4.17. The first crack appeared both longitudinally and transversely as the specimen loaded to 400kN, suggesting a slight increase in stud capacity. With a rapid increase of tensile strain in the transverse reinforcement, load began to reduce after the maximum load of 440kN was recorded. Yield strains were recorded in all transverse reinforcement. The load was maintained at 360kN with a slip in excess of 20mm. Further load reductions were detected as two studs sheared off as slip reached 35mm and 58mm at the final stage of test. Fig. 4.18 shows the specimen at failure.

4.6.6 Test T16-25-65*

This test was set up to investigate the effect of increases in transverse reinforcement on the shear capacity of the stud. The load-slip curve is shown in Fig. 4.19. Early slip was noticed as soon as the load was applied. First crack formed along and across the slab when the applied load reached 330kN, continuous slip was observed with little increase in load. This test would appear to have failed prematurely as the expected shear capacity should be much higher.

Maximum load of 350kN was recorded. Release of tensile stresses in the transverse reinforcement was noticed as load began to reduce, suggesting a bond failure of transverse reinforcement. Maximum tensile strain in transverse reinforcement was 1460με before bond failure. Test was terminated due to splitting of concrete. This test was repeated as T16-25-65.

4.6.7 Test T16-25-65

Due to the unexpected premature failure of T16-25-65*, the test was repeated. The load-slip curve is shown in Fig. 4.20. Results of this test are shown in Table 4.5. In this test, small slips were recorded in the early stage of loading, reaching a value of 0.17mm at a load of 240kN. There was a full elastic recovery of slip when the load was released. First crack appeared transversely across the joint of hcu as load reached 440kN and continued toward the centre of the slab, see Fig. 4.21. At 520kN, cracks began to form longitudinally along the specimen. Maximum load was maintained with slip well in excess of 20mm and crack width of no more than 2.0mm. After the test was terminated and unloaded, crack width on the specimen recovered to no more than 1mm wide. At the maximum load of 540kN, tensile strain of 1200με in the transverse reinforcement was recorded, indicating the transverse reinforcement was not yielded. This test result suggests that increases in transverse reinforcement lead to an increased shear capacity.

4.6.8 Test T16-25-40F

The load-slip curve is shown in Fig. 4.22. T16-25-40F was introduced to investigate the effect of having a narrower gap for the T16 series. As shown in the T8 series, a reduction of gap width led to reduction in shear capacity. Tensile strain in the transverse reinforcement was first recorded as the applied load reached 100kN. First crack was observed near the end of the specimen as the applied load reached 480kN. No crack was noticed on the slab surface as the applied load reached 530kN and strain of 1000με was recorded in the transverse reinforcement. Rapid decrease in strain was observed in transverse reinforcement due to slippage, see Fig. 4.23, leading to sudden loss of capacity and cracks developed throughout the specimen. Fig. 4.24 shows the crack pattern of T16-25-40F at failure.

4.6.9 TestT25-25-40F

The test results obtained this far suggested that increases in transverse reinforcement led to increases in shear capacity. Therefore, a T25 series was suggested to investigate the effect of transverse reinforcement. The load-slip curve of T25-25-40F is shown in Fig. 4.25. First crack appeared at 510kN, which was much higher than all the previous tests, crack formed at the end of the specimen as shown in Fig. 4.26. At the applied load reached 580kN, slippage of the transverse

reinforcement was noticed leading to a reduction in strain in the transverse reinforcement. Further cracks developed on the surface of the slab as the transverse reinforcement relaxed. Rapid reduction of load was recorded. Mode of failure was due to bond failure of transverse reinforcement, leading to excessive cracking in the slab. Deformation of studs after the test is shown in Fig. 4.27.

4.6.10 Test T25-25-65

A gap width of 65mm was set up for this test to form a direct comparison with the test T25-25-40F. The load-slip curve of T25-25-65 is shown in Fig. 4.28. First crack was noticed at a load of 450kN with approximately 2.0mm of slip. The specimen was unloaded at 450kN and 500kN to observe the unloading stiffness, whilst the cracks closed during unloading. Large slip occurred with a very gradual increase in applied load. A maximum load of 605kN was reached with a slip of more than 15mm. The load reduced suddenly due to loss of two shear studs (one at 605kN and the other at 470kN). Failure of the shear studs was brittle and sudden. Results suggested high transverse reinforcement could lead to sudden failure of shear studs. A maximum shear capacity per stud of 101kN was recorded which was highest of all tests. Fig. 4.29 shows the crack pattern of T25-25-65 at failure.

4.6.11 Test T8-38-RC

Fig. 4.30 shows load-slip curve for the test. This test is set up to compare the behaviour of the precast hcu with the solid r.c. slab. The general behaviour of T8-38-RC is similar to T8-25-65 in the early stage of the test. No crack was observed as the load reached 300kN. First crack appeared longitudinally along the specimen as the applied load reached 380kN which was identical to T8-25-65. Cracks continued to develop along the specimen as the load reached the maximum of 440kN. High tensile strain was recorded in the transverse reinforcement gauges as the load began to reduce down to 380kN. The load was maintained at this level with continuous slip in excess of 20mm. The test was terminated due to opening of longitudinal cracks and shear failure of studs. Fig. 4.31 shows the crack pattern of T8-38-RC after the test terminated.

4.6.12 Test T16-25-RC

Fig. 4.32 shows load-slip curve for the test. The behaviour of T16-25-RC is similar to T16-25-65 throughout the test with a sight increase in stud capacity. First crack was observed at 330kN transversely across the specimen. The load continued to increase gradually to 582kN with a slip up to 20mm. Studs sheared off with a suddenly loss of strength as slip reached 23mm and 33mm. The test

finally terminated due to loss of studs. Failures of shear studs were sudden and without prior warning.

4.7 Discussion of test results

The idealized load-slip relationship for shear connectors is shown in Fig. 4.33. The shear connector in general should able to reach its maximum capacity at a slip of 2 to 3 mm and the drop off in load capacity at higher slips should not be excessive; a suggested criterion[4] is that the load capacity at 6mm slip is not less that 80% of the maximum value. It is suggested by the author that, the initial shear stiffness, K_i for the push off tests is measured by the gradient of the load-slip curve at 50% of the maximum shear capacity as the shear stud should still remain elastic.

The test results are presented in Table 4.5, and the full load vs. slip behaviour for the tests is shown in Fig. 4.34, whilst Fig. 4.35 is an enlargement of the same data to 2mm slip. Table 4.5 shows the maximum load per stud, Q_T; slip at 50% of maximum load; slip at maximum load and load at 6mm slip for each test. Percentage of load reduction at 6mm slip and the shear stiffness is also given. In all tests there was virtually no slip (less than 0.01 mm) until the first crack was observed in the transverse direction between adjacent hollow core units, as shown in Fig. 4.36. An increase in slip was coincident with crack widening, and an

increase in strain in the transverse reinforcement as shown in Fig. 4.37. Percentages of load reduction at 6 mm slip were less than 20% for all the tests except for T8-25-65P where the specimen was pre-cracked. The percentage reduction at 6mm slip for the T16 and T25 specimens is not truly representative as the maximum loads were achieved at a higher slip.

The rate of deterioration in shear stiffness, as defined by the gradient of the curves in Fig. 4.34 and Fig. 4.35, was much greater in the lightly reinforced specimens, i.e. T8 specimens, and the maximum load was attained at a smaller deformation, typically 2.0 to 3.0 mm slip. In contrast the maximum load was attained at about 20 mm slip in the heavily reinforced specimens - a slip which is greater than that recorded in previous researches on composite beams[5,6]. In these situations it was difficult to stabilise the applied loads and to know whether a maximum had indeed been reached. Yielding of the transverse reinforcement was accompanied by the development of some very large cracks, both longitudinally and transversely, and a gradual decrease in resistance. The failure mode was in contrast to the heavily reinforced specimens which failed suddenly due to shear fracturing of the studs, followed by a rapid decrease in resistance. Crack widths were much smaller at failure and the strains in the transverse reinforcement was less than 50% yield strain.

The behaviour of the shear studs may be related to the transverse confinement of the concrete at the stud, and to a certain extent the proximity of the transverse

reinforcement in preventing longitudinal cracks developing near the studs, although in these tests the maximum distance to any transverse reinforcement was less than 150 mm. The concrete bearing stress f_b on the shaft of the stud is determined over an effective height of 0.85 x height of the stud. This is to allow for bending of the stud assuming a rigid connection is made to the steel beam, see Fig. 4.38. If the load per stud is P, then $f_b = P/ 0.85hd$. When f_b exceeds the limiting bearing stress of 0.8 f_{cu} allowing for confined concrete, a transverse splitting force will result. Thus cracking may be anticipated when P = (0.8 x 25.0) x 0.85 x 125 x 19 $x10^{-3}$ = 40.4 kN per stud, or 40.4 x 6 no. studs = 242.4 kN for the test. This result is in good agreement with the observations made in the tests and is also shown in Fig. 4.35 to correspond approximately with the onset of non-linear load vs. slip behaviour. Prior to this the initial stiffness K_i of the connection was in the range $120 < K_i < 1200$ kN/mm/stud (see Table 4.5).

The results for all tests were fairly consistent with the predicted values apart from specimen T16-25-65*, where unexpected movement between the insitu concrete infill and the precast slabs was observed. It appeared that no interaction had been possible with the precast units and this lead to extensive bending of the studs prior to a ductile failure at a very low load. Poor compaction of the insitu concrete was partly to blame for the lack of interaction - which only serves to demonstrate the important of good workmanship where composite behaviour is assumed and may suggest this construction method could be sensitive to workmanship.

4.8 Comparison of test results

4.8.1. Effect of gap width.

The importance of the size of the gap involves the proximity of the precast-insitu infill interface in resisting the radial tensile forces around the stud, as shown in Fig. 4.39. It is believed that a breakdown in the bond between the insitu infill and the end of the hcu is responsible for increased compressive stresses in the infill which would otherwise be carried by the insitu and precast concrete together. The increased stress in the infill is ultimately the cause of failure, either directly by crushing or indirectly due to increased splitting forces. It is known that radial stresses decrease rapidly over a distance equal to 1.5 times the diameter of the dowel (or stud in this case)[7]. Thus a deterioration in the performance of the studs should be found when the gap is less than 4 x stud diameter = 76 mm.

Four tests were carried out with identical arrangements of T8 bars and C25 concrete, except for the gap widths of 40, 65 and 120 mm using precast units, and (effectively) infinity using a solid slab. The results show an increase in both shear capacity, Q_T and stiffness, K_i with increasing gap width, but an optimum value for gap is shown in Fig. 4.40 and Fig. 4.41 to be around 70 mm, i.e. the capacity hardly improves beyond this point. It is also recommended that the gap width should not be less than 30 mm for practical reasons of compacting concrete around the stud. Research work by Moy and Taylor[8] on composite beam tests using

square ended precast concrete planks found a reduction in shear stud capacity as the bearing length increased, and hence the gap width decreased.

4.8.2 Effect of transverse reinforcement

The transverse reinforcement enhances the in-plane shear resistance of the composite slab by crossing the precast-insitu infill interface. It is also required to control and limit the longitudinal splitting of the slab caused by transverse forces from individual shear connectors. If the transverse reinforcement is fully mobilised, as in the case of the T8 and T16 specimens, the shear capacity P_D due to the transverse reinforcement working as rigid dowels is given as $P_D = 0.6\ f_y\ A_s$, where $f_y = 460\ N/mm^2$. Thus for 4 no. T8 bars $P_D = 55.2$ kN, or 9.2 kN per stud, and for 4 no. T16 bars $P_D = 220.8$ kN, or 36.8 kN per stud. Thus the increase in shear capacity due to the T16 bars over the T8 bars should be approximately 27 kN per stud.

Three tests were carried out with identical arrangements of gap width (65 mm) and C25 concrete, except for the transverse reinforcement of 4 no. T8, T16 and T25 high tensile deformed bars. Although the test results indicated in Fig. 4.42 show an increase in shear capacity with increasing area of transverse reinforcement, the increase is not directly proportional to the increase in dowel shear described above. This suggests that the transverse reinforcement is unable to generate the

full dowel action force P_D due possibly to inadequate top cover and because the bars are embedded within the milled slots in the precast units rather than in solid concrete. The results suggest that for these particular parameters the maximum effective reinforcement is approximately 150 mm^2 per stud, or 0.66 % of concrete area. This amount of steel will provide an ultimate confinement pressure p = 3.1 N/mm^2, which because it is greater than the tensile splitting strength of the concrete (approx. 2.0 N/mm^2) ensures that the tensile forces in the concrete will be resisted by the transverse reinforcement.

The specimens with the larger areas of reinforcement (T16 and T25 bars) failed in a brittle manner by fracturing the shear connector, whilst the other specimen (T8 bars) failed in a ductile manner. Results in Chapter 3 giving the compressive resistance of composite slabs showed that the correct amount of transverse reinforcement should be provided to allow concrete tensile splitting to occur without a loss in load capacity, whilst over reinforcement (i.e. greater than 0.4% concrete area) led to concrete crushing failures without warning.

The push-off tests demonstrated that the specimen with T8 bars, and a confinement pressure, p = 0.51 N/mm^2, failed in combined compression and tension (ductile failure), while the specimens with larger transverse reinforcement (T16 and T25) failed in biaxial compression (brittle failure).

4.8.3 Effect of strength of insitu infill

The insitu concrete strength for the corresponding specimens T8-25-120 (hollow core) and T8-38-RC (solid) differed by 13.0 N/mm^2 (see Table 4.2), a variation large enough to permit a study of the effect of the concrete strength. The result showed no difference in strength, suggesting that if the average strength of the insitu and precast concrete was used in specimen T8-25-120, i.e. (24.5 + 50.0)/2 = 37.3 N/mm^2, the two test parameters and results would be identical. This finding is supported by two facts, as follows:

1. If the effective width of the composite slab is approximately 1.0 m, then the effective areas of insitu and precast concrete are roughly equal. In this area the applied strains and stresses were equal showing that the effective modulus of elasticity for the whole slab was approximately equal to the mean of Young's modulus for the two concrete.
2. a biaxial compressive strength greater than f_{cu} may be used in design because the insitu concrete is confined transversely by the transverse reinforcement and hcu's. A maximum value of 1.25 f_{cu} may be used [9].

It is therefore recommended that the effective strength and modulus of elasticity of the infill concrete is taken as the mean value of the insitu and precast concrete.

4.8.4 Effect of pre-cracked joint

The purpose of the pre-cracked joint was to investigate the effects due to shrinkage of the insitu infill. A polythene sheet was placed between the insitu and precast concrete to ensure no bonding between the insitu infill and hcu. Test results show early loss of shear capacity for the studs. Rapid yielding of the transverse reinforcement due to the loss of bonding at the insitu to precast concrete. A 20% reduction of the shear capacity is noted due to the loss of bonding. The test simulated the extreme effect of shrinkage as interlocking of aggregates after cracking would contribute to the shear capacity. The transverse reinforcement across the slab would also restrain the effect of shrinkage for this type of construction. Therefore, the effect to the stud strength due to actual shrinkage of the insitu infill will be minimal.

4.8.5 Effect of full width slab

The test results suggested a slight increase in shear capacity with full width hcu. This effect was mainly due to the elimination of the transverse joint in the push off test rather than any significant difference between the 600mm and 1200mm width hcu. Due to the relative short length of the hcu's used in the push off tests, there was a tendency for the transverse joint to open up, leading to initial cracking of the specimen. Although it is unlikely to occur in construction as the hcu's are much

longer in length and also restrained at the supports, it is important to compensate for the shear capacity when a transverse joint is present in the push off test.

4.9 Conclusions

The results of the push off tests suggest that the shear capacity of the stud for this type of construction was not only affected by the tensile capacity of the stud itself. It was also affected by the gap width, the amount of transverse reinforcement, the strength of the concrete and the presence of the longitudinal joint and transverse joint. From these push off tests results, parametric equations can be developed for calculation of the shear capacity. The detailed development of these equations is presented later in Chapter 8.

4.10 References

1. BS5400, Part 5 (1985), Steel, Concrete, and Composite Bridges, British Standards Institution, London.

2. BS5950, Part 3.1 (1990), Structural Use of Steelwork in Building, British Standards Institution, London.

3. BS1881, (1983), Method for Determination of Compressive Strength and Tensile Splitting Strength, British Standards Institution, London.

4. Johnson, R.P. and Anderson, D., 'Designers' Handbook to Eurocode 4: Part 1.1: Design of composite steel and concrete structures. Thomas Telford, London, 1993

5. Slutter, R.G. and Driscoll, G.C., 'Flexural strength of steel-concrete composite beams', *Journal of the Structural Division, Proceedings of American Society of Civil Engineers,* April, 1965, pp71-99.

6. Johnson, R.P. and Molenstra, N., 'Partial shear connection in composite beams for buildings', *Proceedings of Institution of Civil Engineers, Part 2,* Vol. 91, Dec., 1991, pp679-704.

7. Vintzeleon, E.N. and Tassios, T.P., 'Mathematical models for dowel action under monotonic and cyclic conditions', *Magazine of Concrete Research, Cement & Concrete Association,* 38, No.134, 1986, pp13-22.

8. Moy, S.S.J. and Tayler, C., 'The effect of precast concrete planks on shear connector strength', *Journal of Constructional Steel Research*, Vol. 36, No.3, 1996, pp201-213.

9. Kupfer, H., Hilsdorf, H. K. and Rusch, H., Behaviour of Concrete Under Biaxial Stress, *Journal of American Concrete Institute*, Vol. 66, No. 8, Aug., 1969, pp656-666.

Test reference	Type of floor slab	Gap width (mm)	Transverse reinforcement	Transverse reinforcement ratio (%)
T8-25-40	600 hcu	40	4 no. T8	0.11
T8-25-65	600 hcu	65	4 no. T8	0.11
T8-25-65P	1200 hcu	65	4 no. T8	0.11
T8-25-65F	1200 hcu	65	4 no. T8	0.11
T8-25-120	600 hcu	120	4 no. T8	0.11
T16-25-65*	600 hcu	65	4 no. T16	0.45
T16-25-65	600 hcu	65	4 no. T16	0.45
T16-25-65F	1200 hcu	65	4 no. T16	0.45
T25-25-40F	1200 hcu	40	4 no. T25	1.09
T25-25-65	600 hcu	65	4 no. T25	1.09
T8-38-RC	Solid rc	N/A	4 no. T8	0.11
T16-25-RC	Solid rc	N/A	4 no. T16	0.45

* Test repeated owing to experimental difficulties

P Joint pre-cracked with polythene.

Notation: T8-25-65 refers to 4 no. high tensile T8 tie bars, grade C25 infill concrete and 65 mm gap at the ends of the slabs. RC = solid rc slab.

Table 4.1 Schedule of push off tests

Test reference (Test Days)	Cube Strength* (N/mm^2)		Tensile Strength* (N/mm^2)	
	Test Days	28 Days	Test Days	28 Days
T8-25-40 (10 Days)	28.6	39.0	1.90	2.28
T8-25-65 (12 Days)	23.5	27.1	2.03	2.40
T8-25-65P (7 Days)	23.0	28.0	2.00	2.55
T8-25-65F (8 Days)	23.0	31.0	2.00	2.65
T8-25-120 (14 Days)	24.5	27.3	1.98	2.10
T16-25-65* (14 Days)	23.5	26.0	1.91	2.29
T16-25-65 (11 Days)	24.6	31.5	1.79	2.09
T16-25-40F (7 Days)	23.0	28.0	2.00	2.55
T25-25-40F (8 Days)	23.0	32.5	2.00	2.60
T25-25-65 (12 Days)	25.5	34.5	2.15	2.34
T8-38-RC (6 Days)	37.5	49.0	3.00	3.26
T16-25-RC (6 Days)	25.0	37.7	2.10	2.83

* Average of 2 samples

Table 4.2 Compressive and Tensile Splitting Strength for Insitu Concrete

Rebar Size	Nominal Diameter (mm)	Specified Characteristic Strength (N/mm^2)	Specified Mass (Kg/m)	Specified Cross Section (mm^2)
T8	8.00	460.00	0.40	50.30
T16	16.00	460.00	1.58	201.10
T25	25.00	425.00	3.85	490.90

Table 4.3 Specified tensile strength of rebars

Rebar	Actual Diameter (mm)	Measured Tensile Strength (N/mm^2)	Measured Mass (Kg/m)	Measured Cross Section (mm^2)
T8	7.99	660.00	0.39	50.10
T16	15.84	634.00	1.55	197.20
T25	24.75	643.00	3.78	481.10

Table 4.4 Measured tensile strength of rebars

Test reference	Shear capacity, Q_T (kN)	Slip at 50% of max. load (mm)	Slip at max. load (mm)	Load at 6 mm slip (kN)	Percentage of load reduction at 6mm slip (%)	Initial shear stiffness, K_i (kN/mm)
T8-25-40	56.5	0.22	2.27	49.0	13.3	128.4
T8-25-65	69.7	0.03	2.21	56.0	19.7	1161.7
T8-25-65P	54.3	0.10	1.14	27.0	50.3	271.5
T8-25-65F	78.0	0.13	2.79	64.3	17.6	300.0
T8-25-120	72.8	0.10	2.07	59.0	18.9	364.0
T16-25-65*	60.5	0.47	10.90	58.0	4.1	64.4
T16-25-65	89.1	0.23	17.04	86.1	3.4	193.7
T16-25-40F	88.4	0.28	17.66	80.5	8.9	157.9
T25-25-40F	97.1	0.27	10.60	91.5	5.8	179.8
T25-25-65	100.9	0.32	15.98	89.0	11.7	157.6
T8-38-RC	72.9	0.11	2.21	60.0	17.7	331.4
T16-25-RC	97.0	0.30	19.44	87.0	10.3	161.7

* Test repeated owing to experimental difficulties.
All shear loads and stiffness are given per stud

Table 4.5 Results of the push off tests

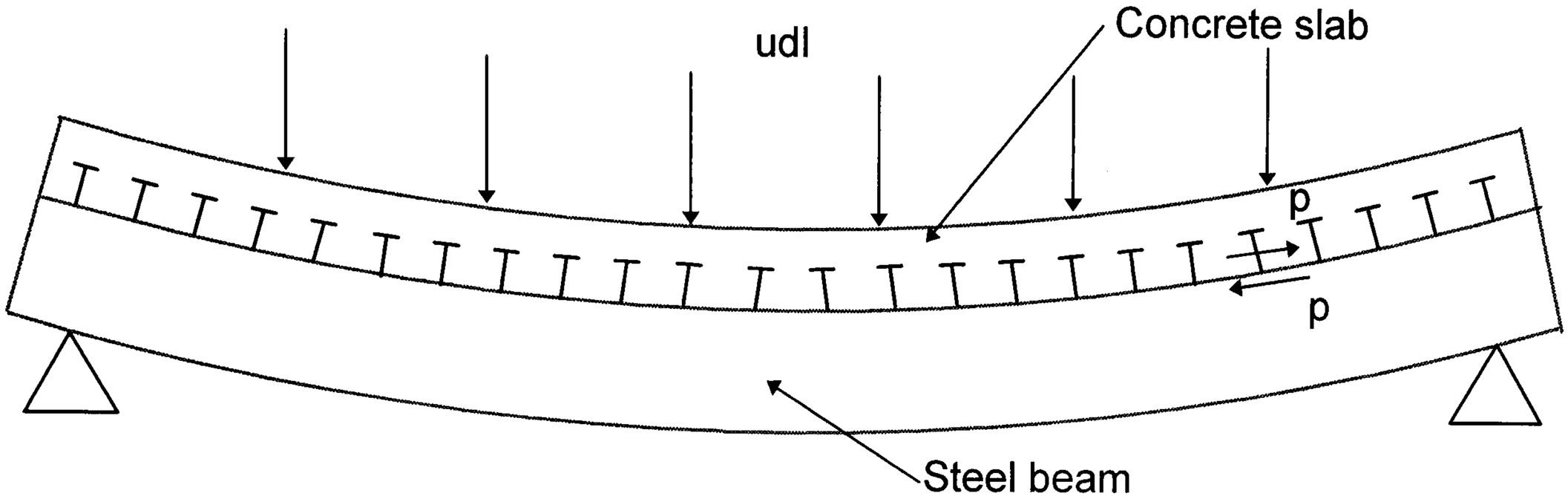

Fig. 4.1 Composite beam in flexure showing horizontal shear behaviour.

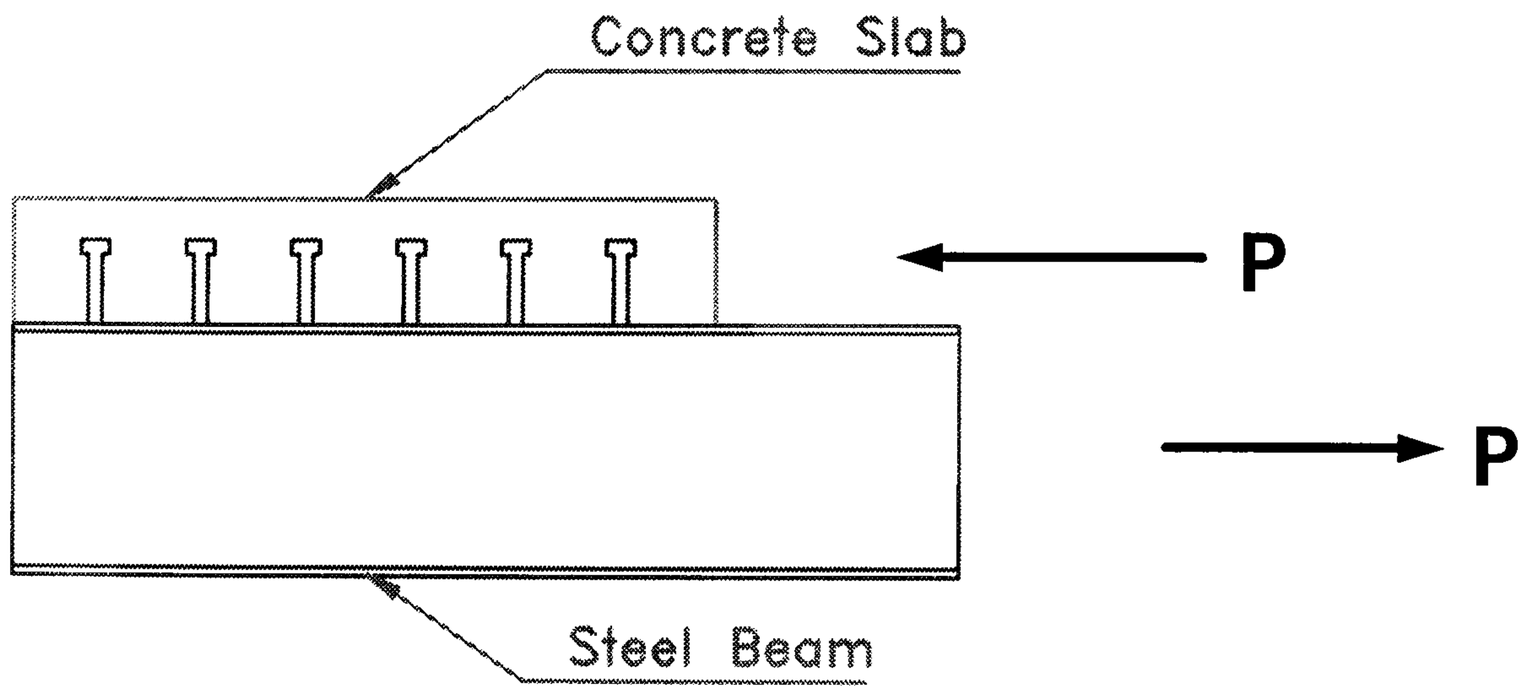

Fig. 4.2 Modelling of shear behaviour using push off tests.

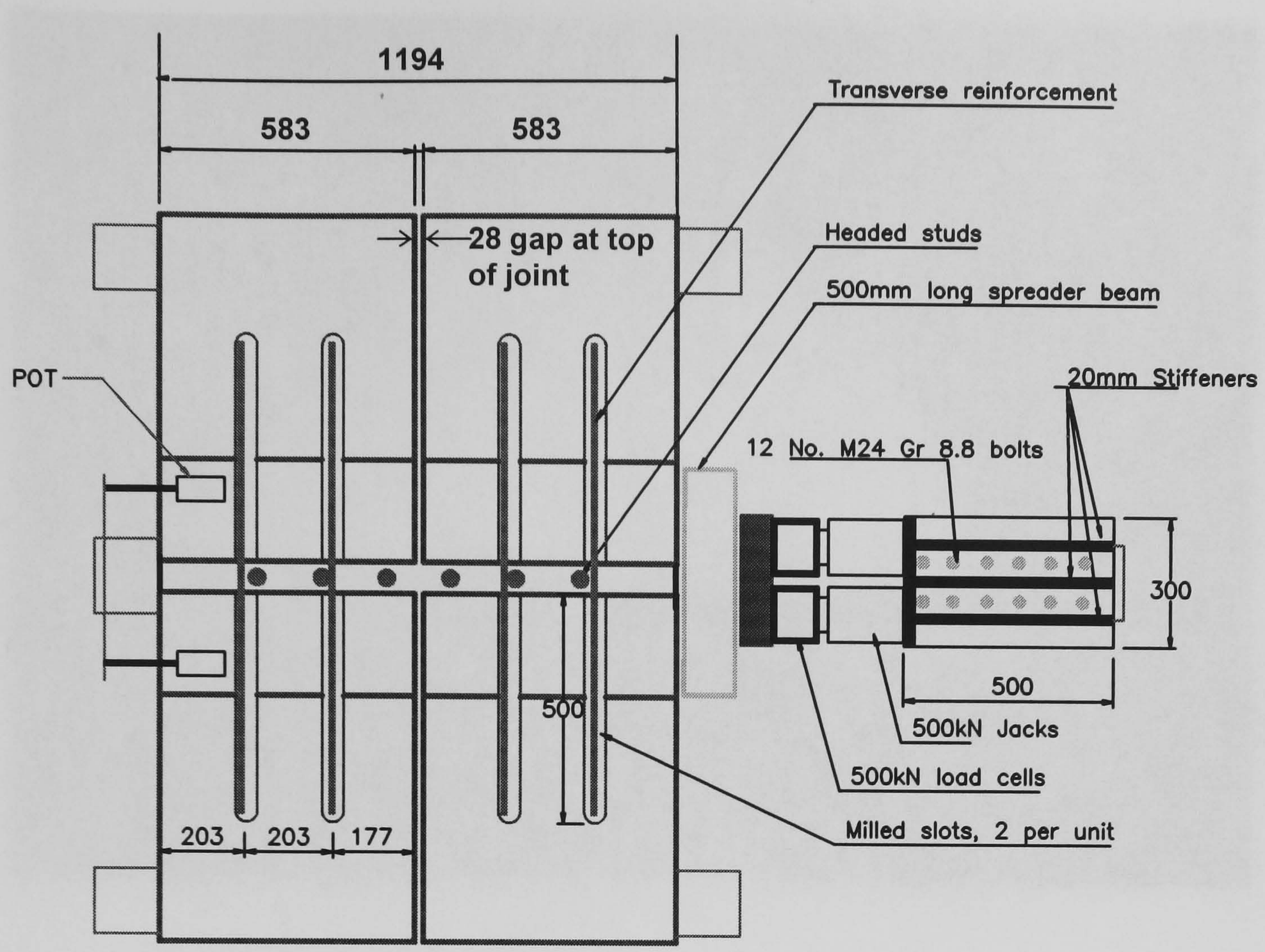

Fig. 4.3 General arrangement and instrumentation for push-off tests.

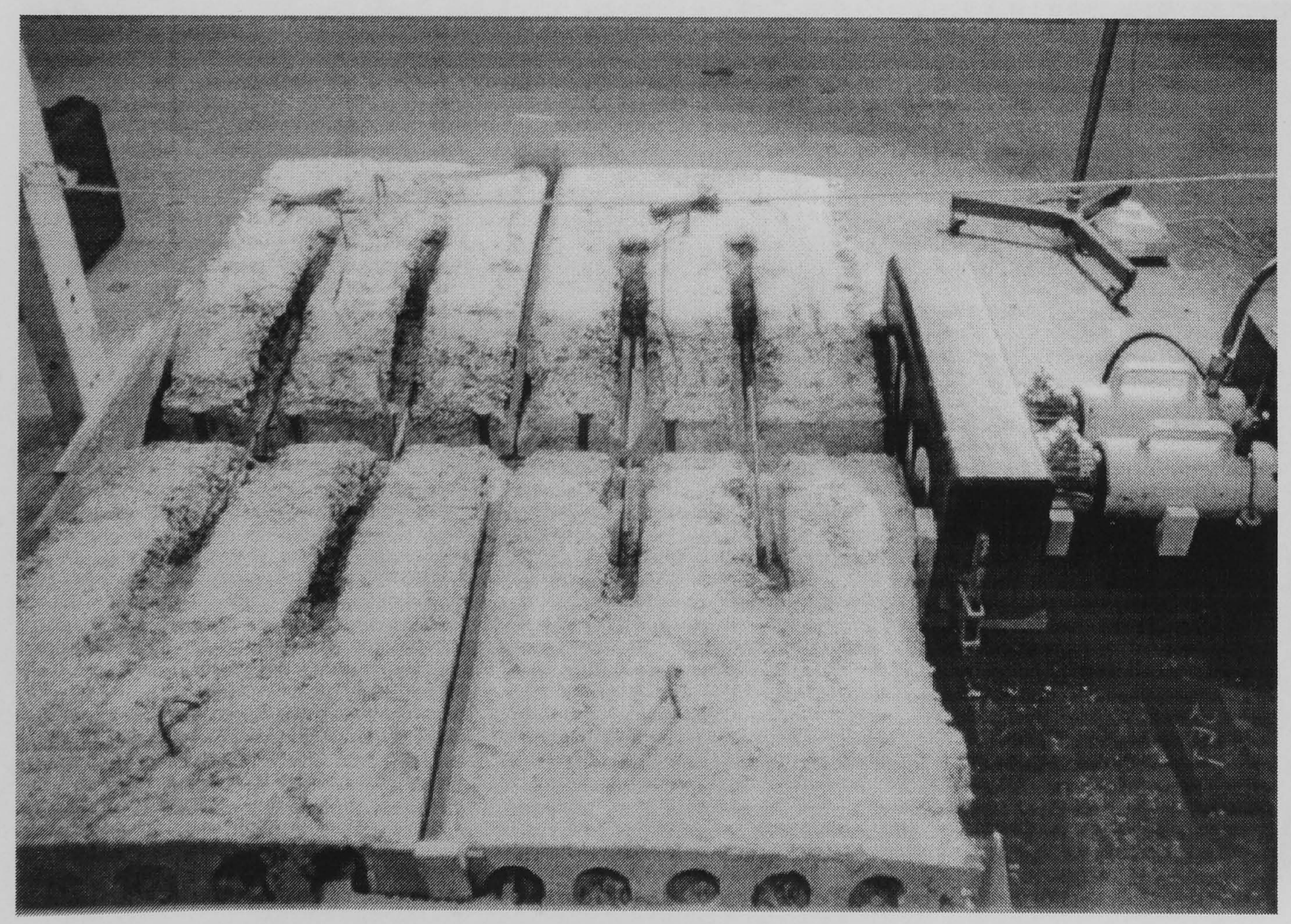

Fig. 4.4 Push-off test specimen before insitu infill concrete.

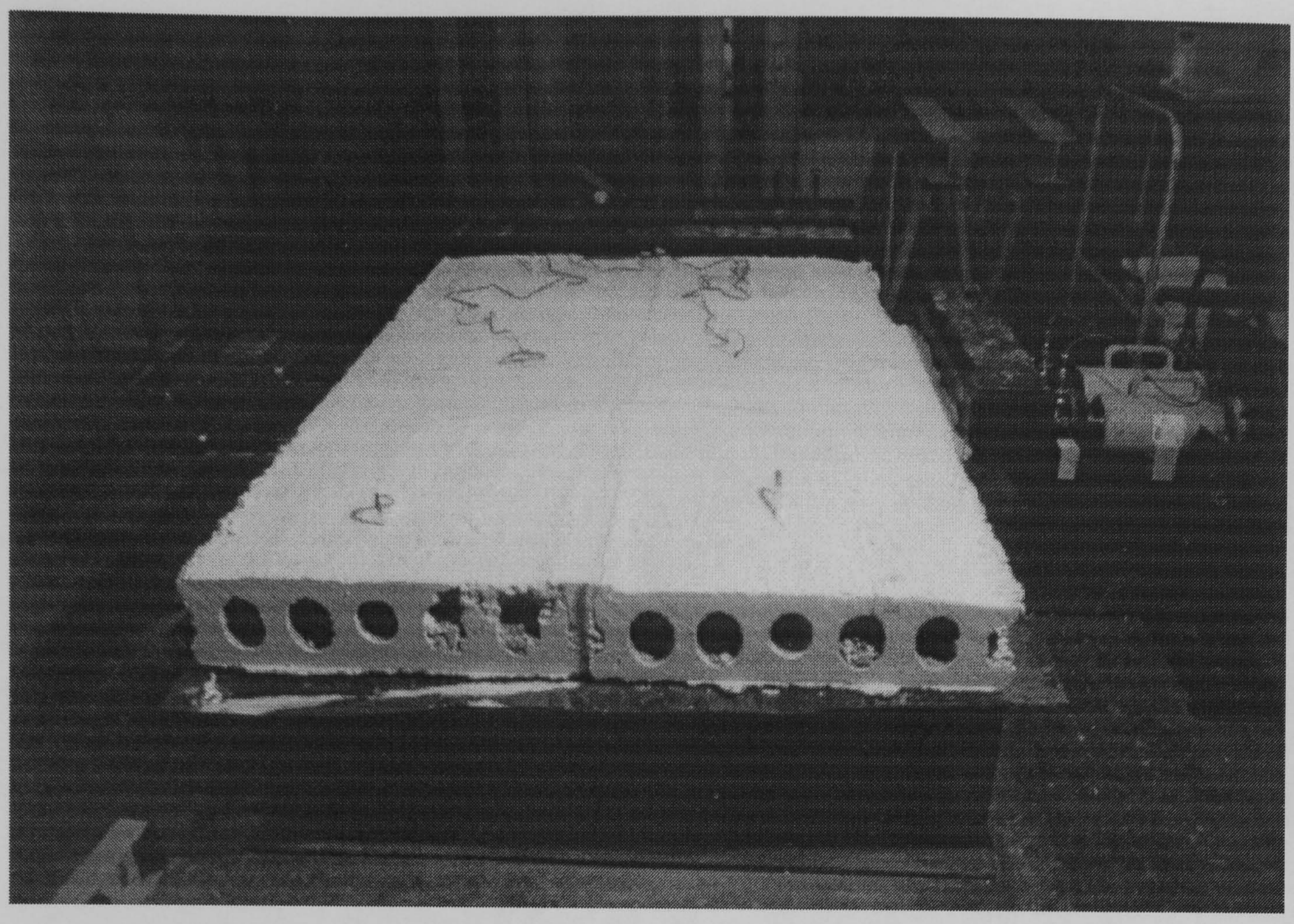

Fig 4.5 Push off test specimen after insitu infill is cast

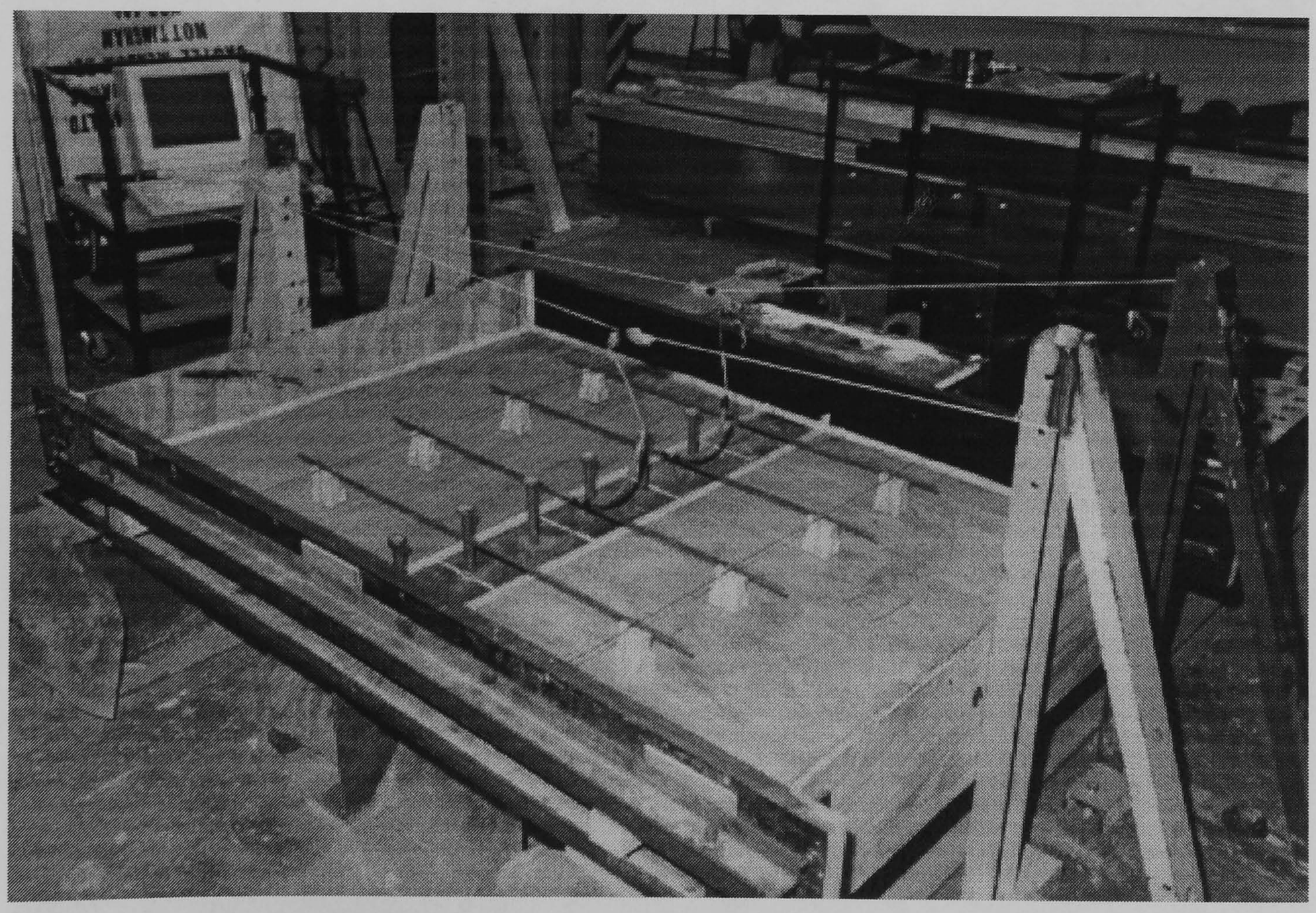

Fig 4.6 General arrangement of solid r.c. slab before concrete is poured

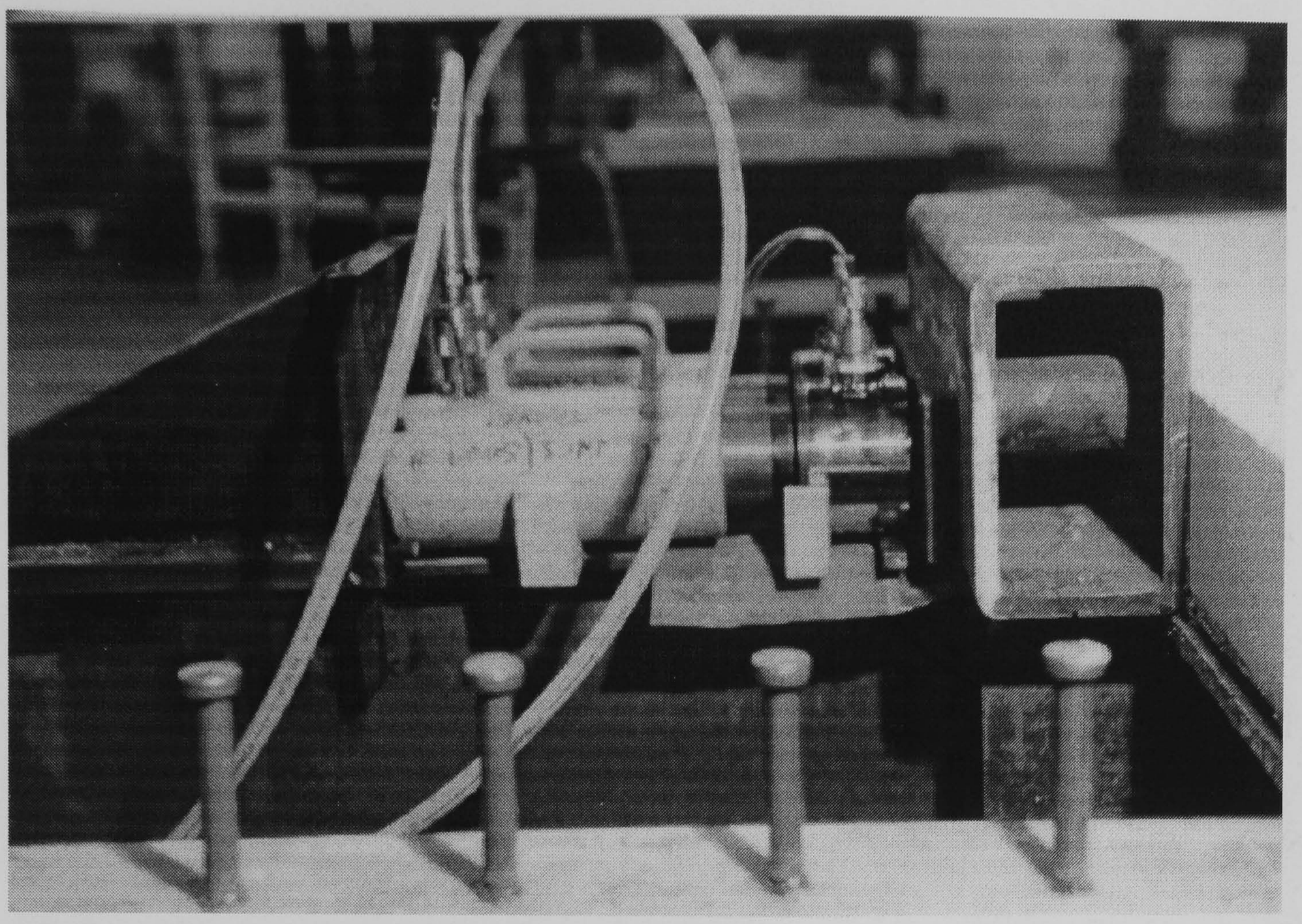

Fig. 4.7 Loading arrangement for the push off test.

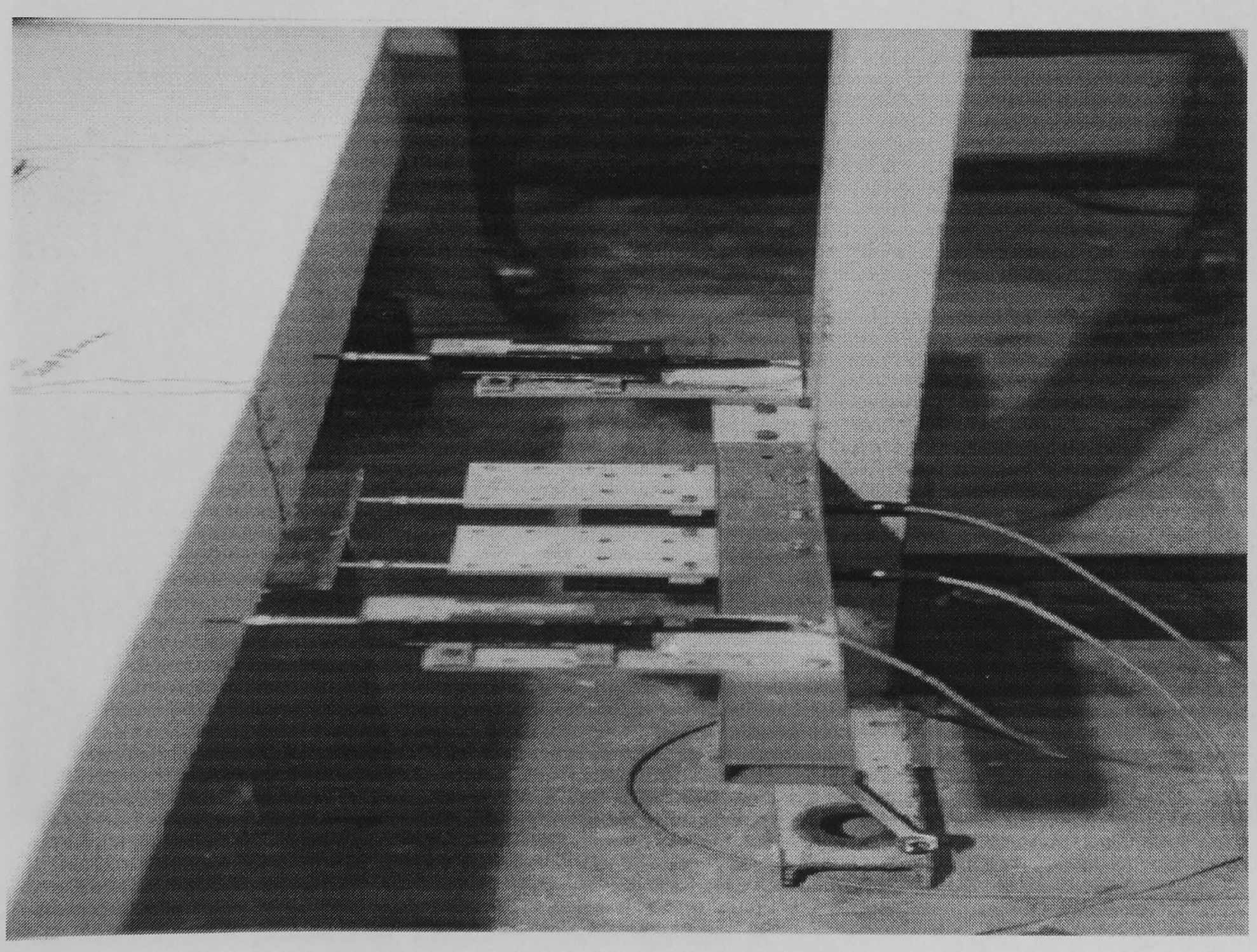

Fig. 4.8 Potentiometers for measuring end slips

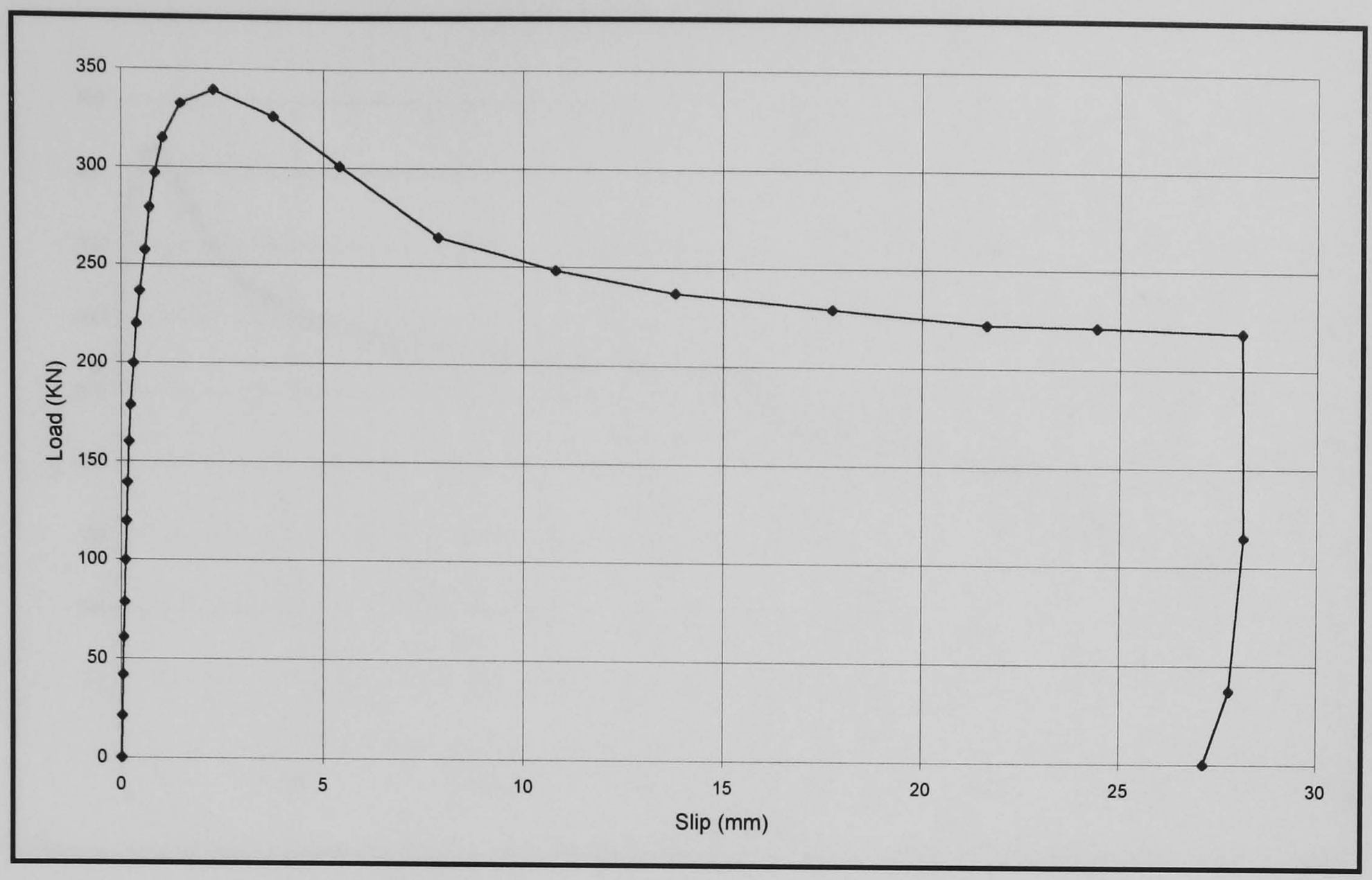

Fig. 4.9 Load vs. slip of push off test T8-25-40

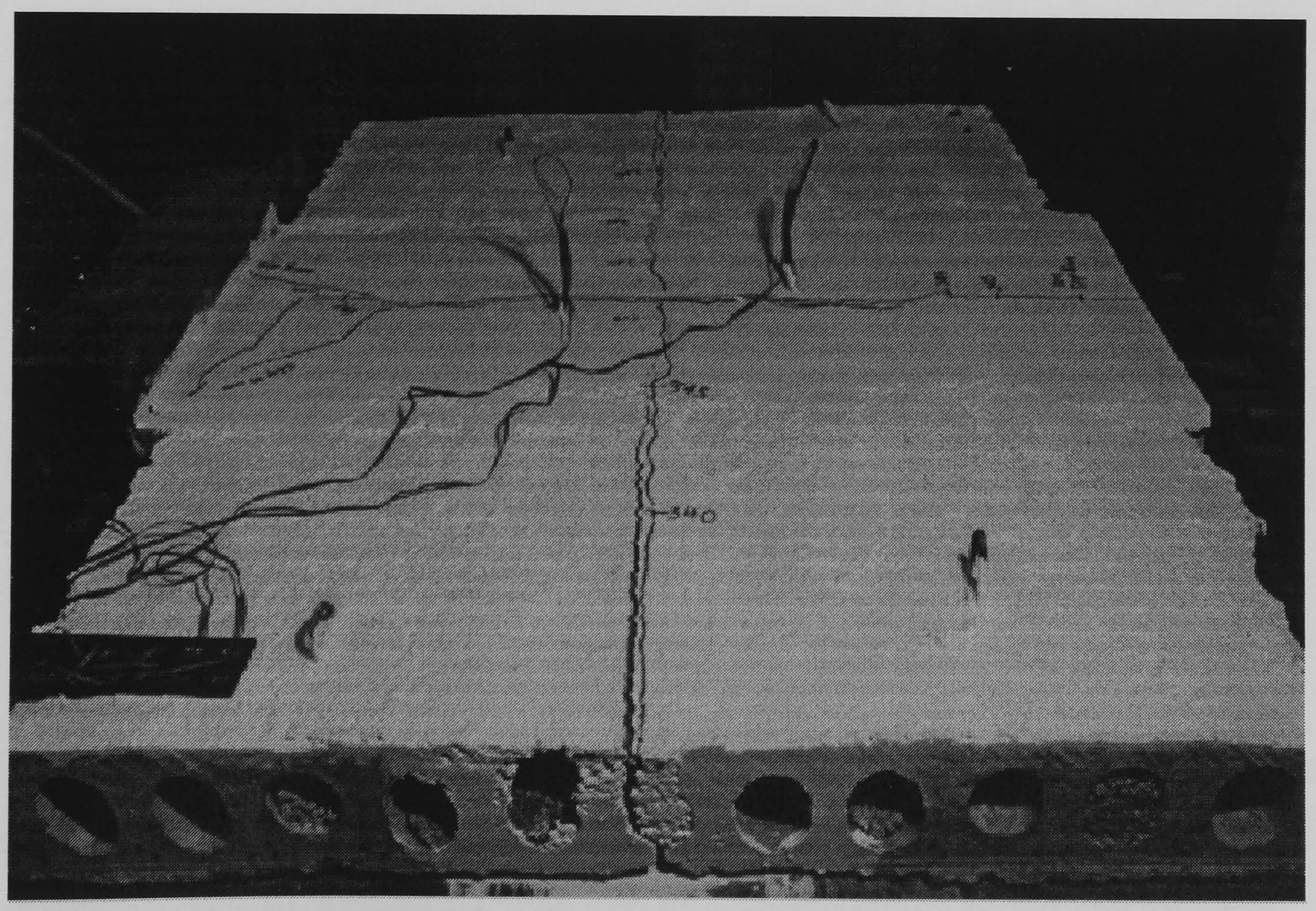

Fig. 4.10 Crack pattern of T8-25-40 after the test

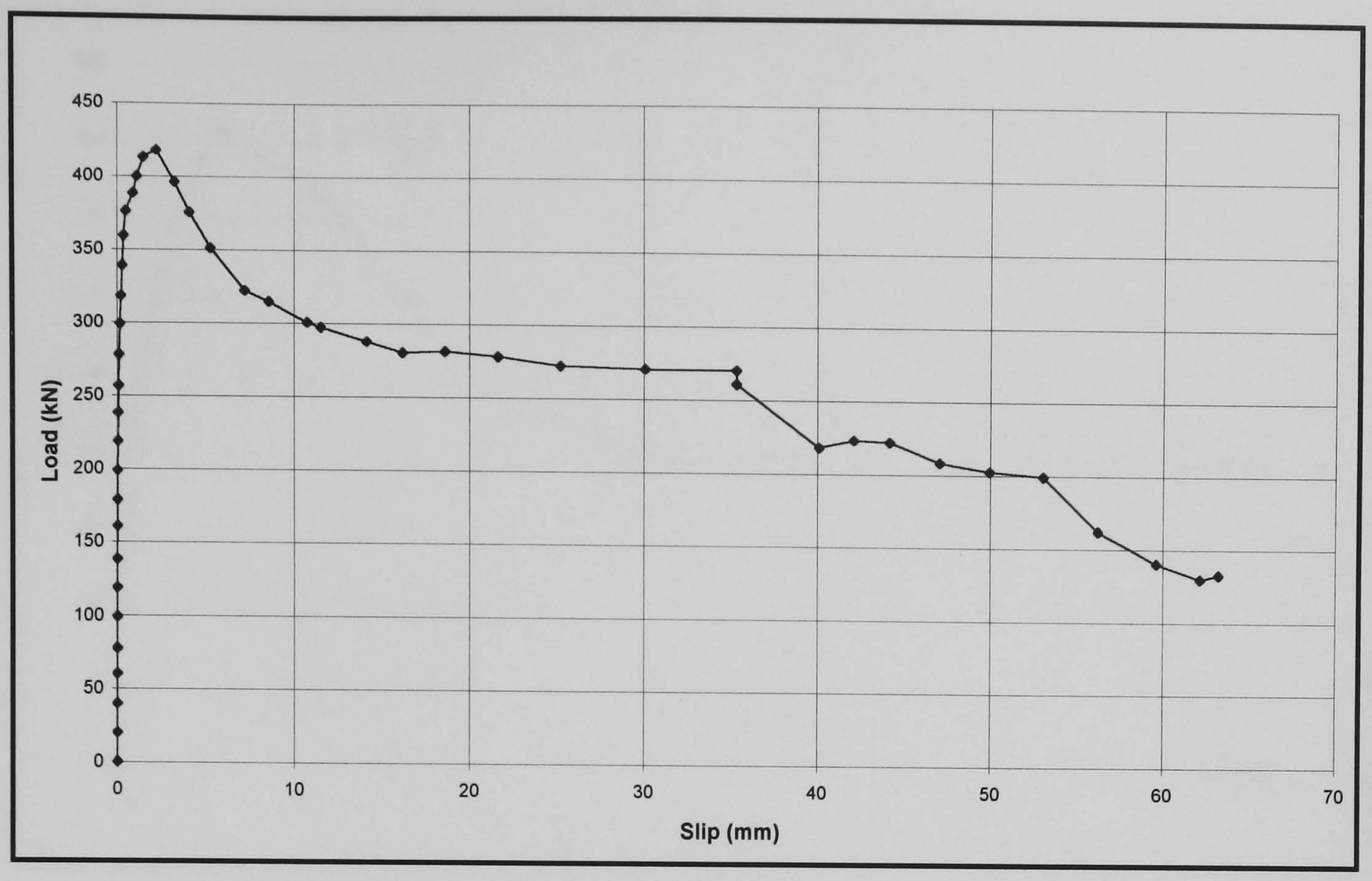

Fig. 4.11 Load vs. slip of push off test T8-25-65

Fig. 4.12 Shear studs for T8-25-65 after test terminated

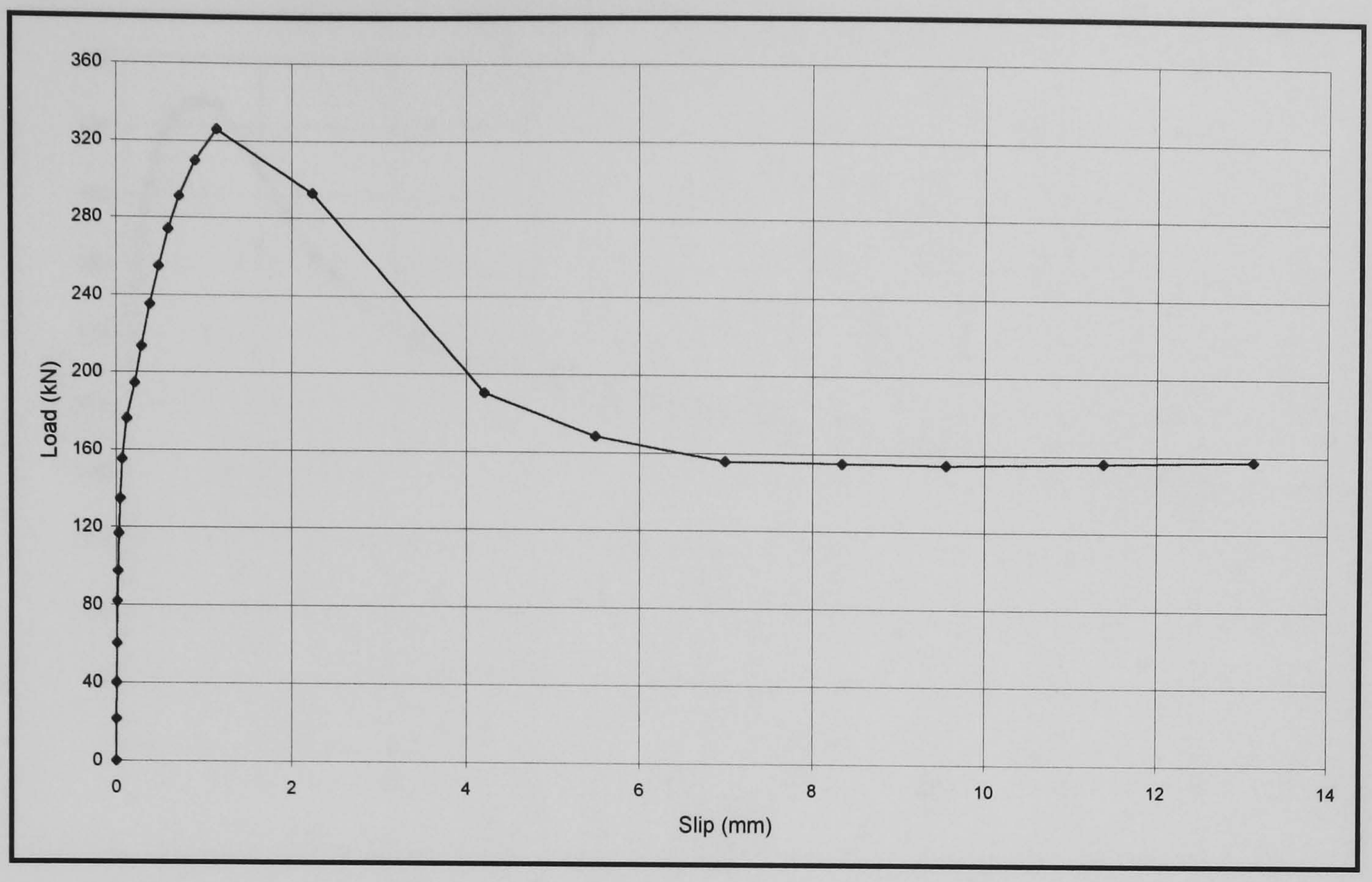

Fig. 4.13 Load vs. slip of push off test T8-25-65P

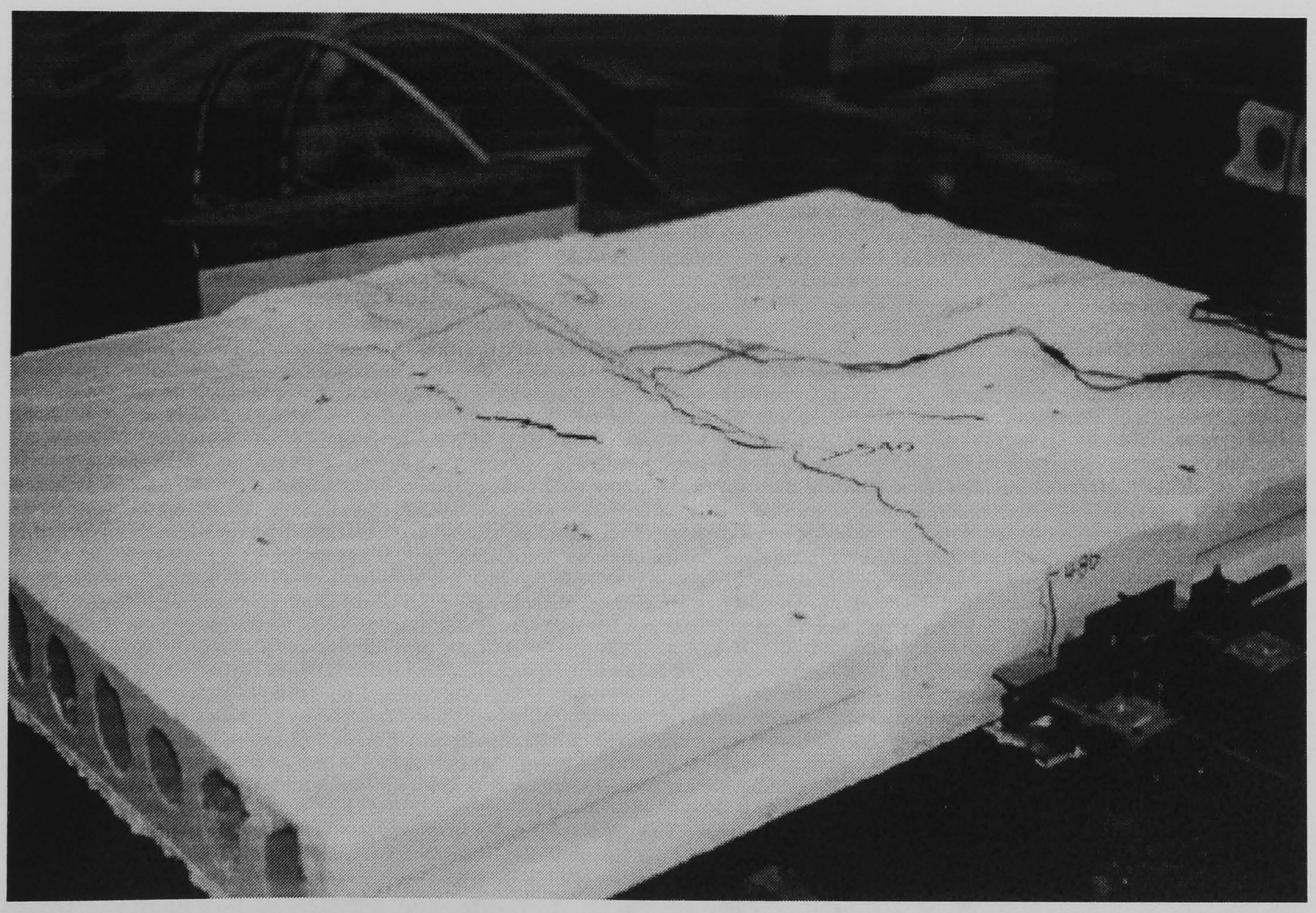

Fig. 4.14 Crack pattern of push off test T8-25-65P at failure

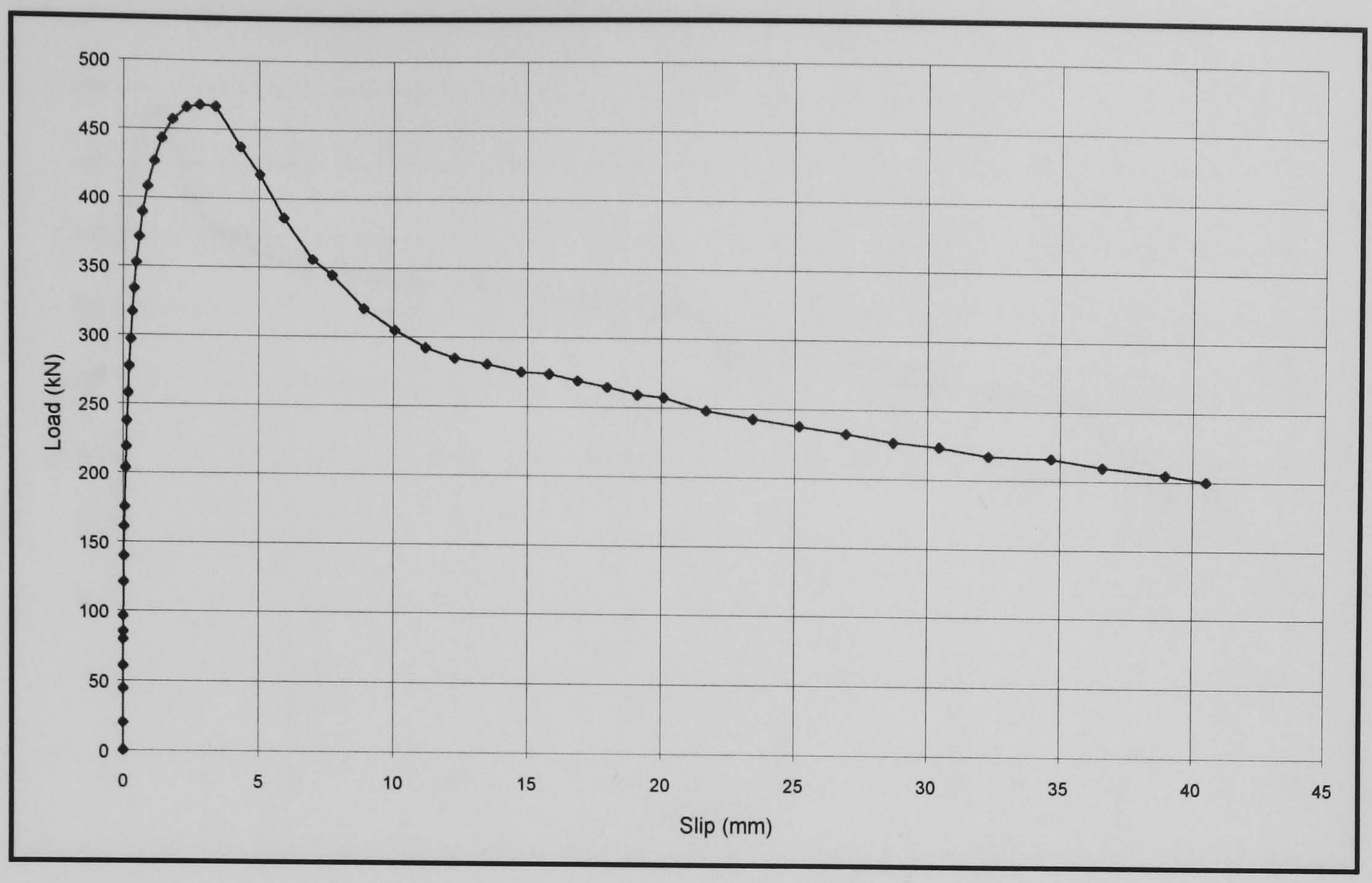

Fig. 4.15 Load vs. slip of push off test T8-25-65F

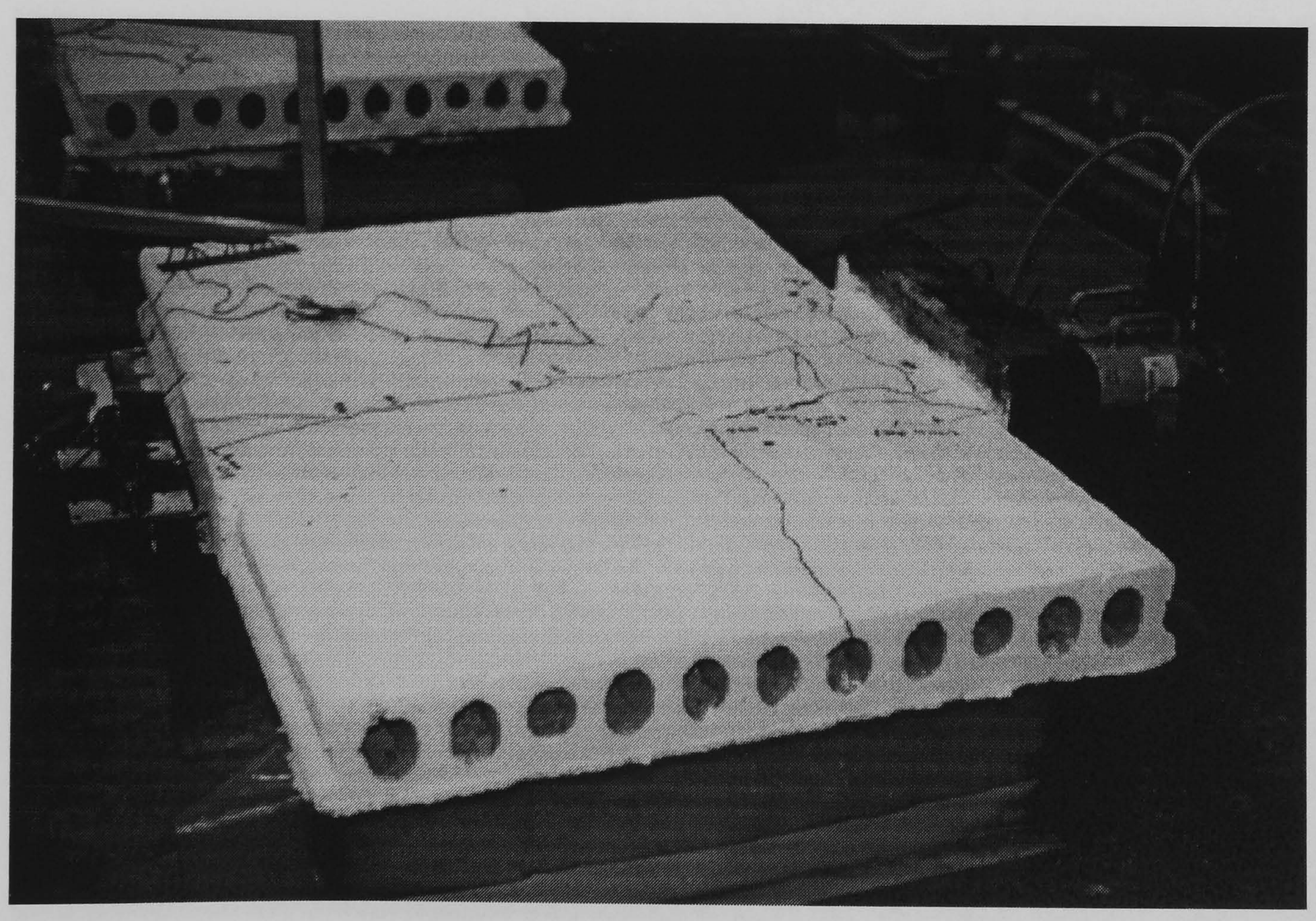

Fig. 4.16 Crack pattern of T8-25-65F after test terminated

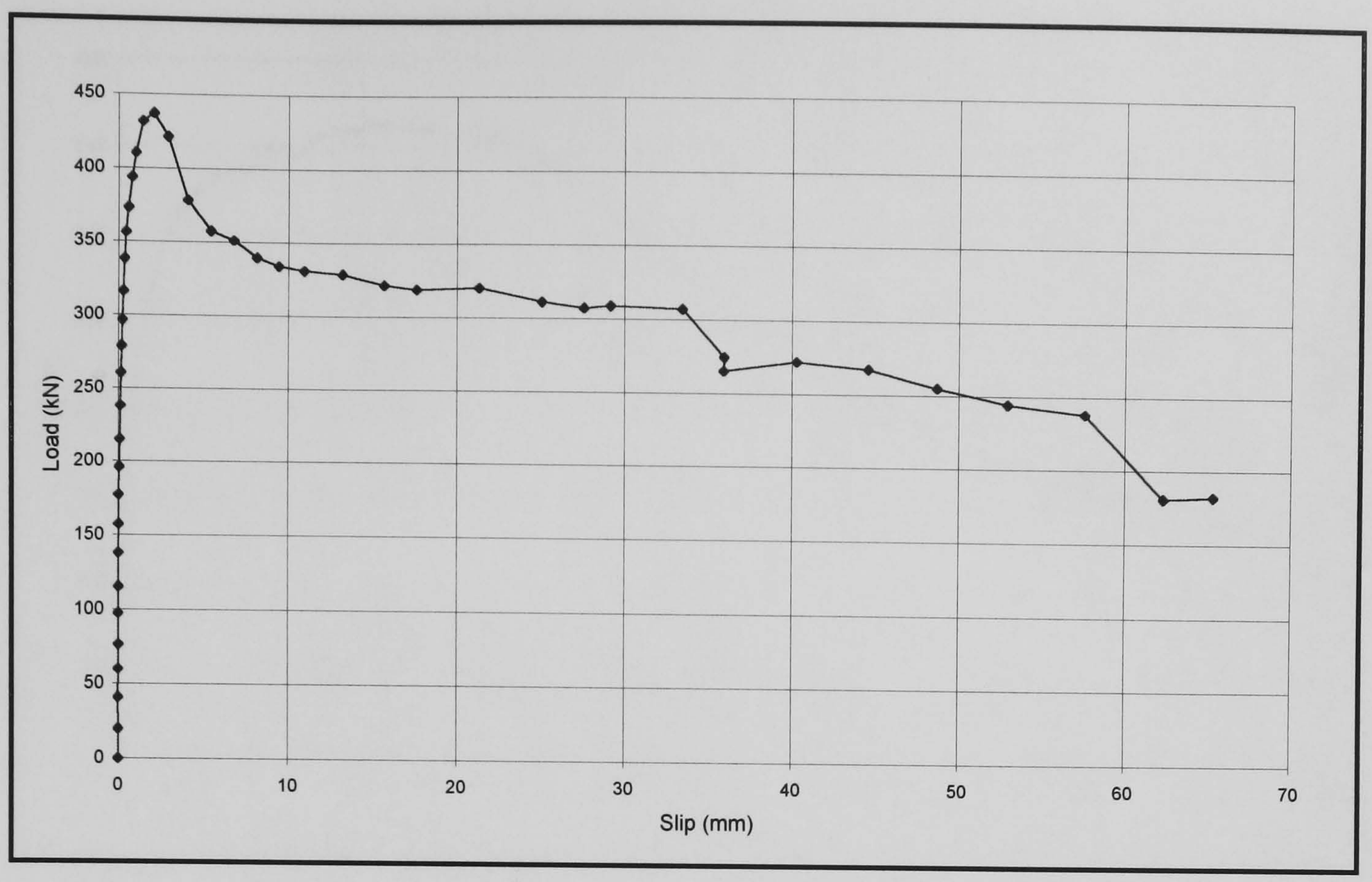

Fig. 4.17 Load vs. slip of push off test T8-25-120

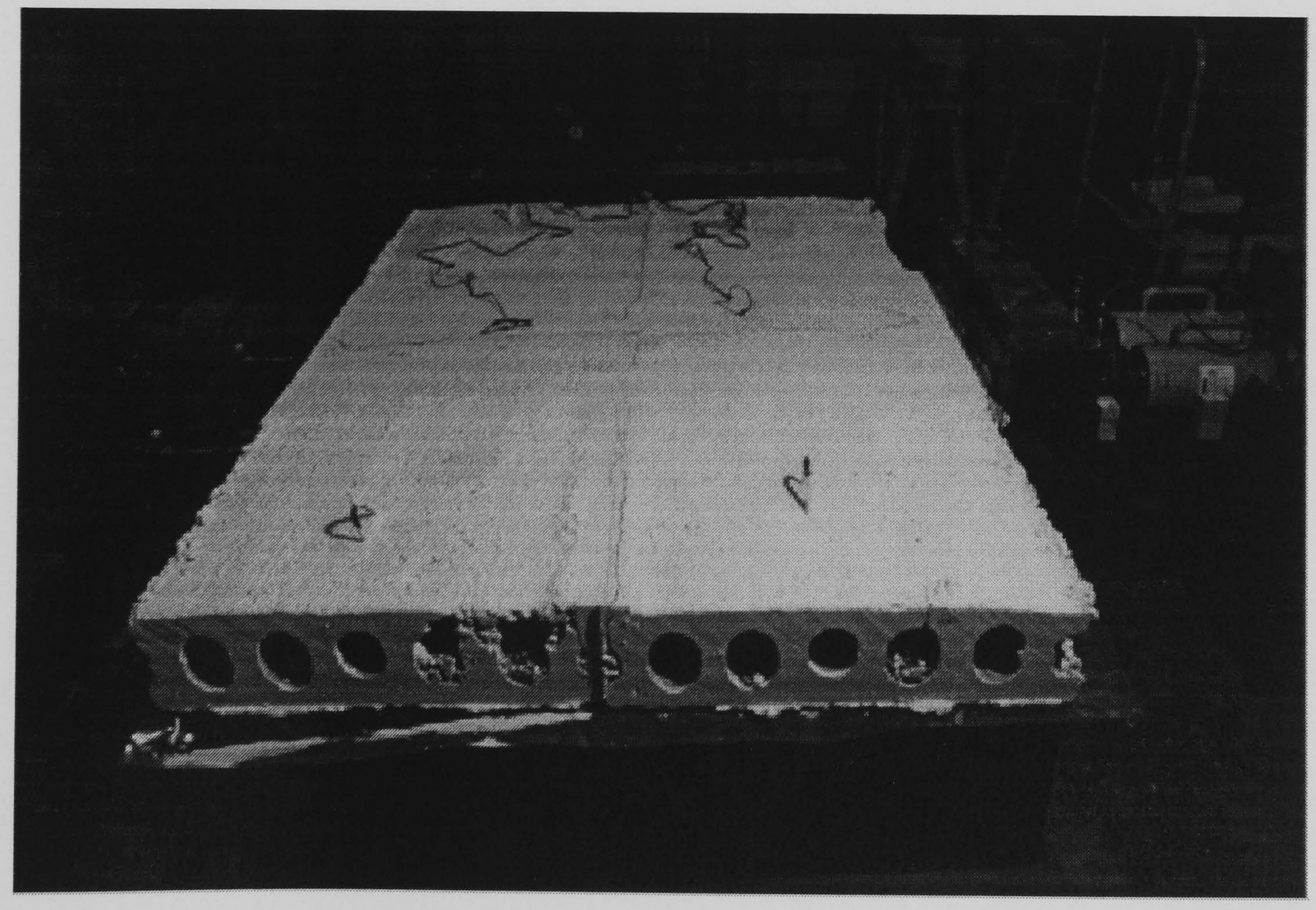

Fig 4.18 Push off test T8-25-120 at failure

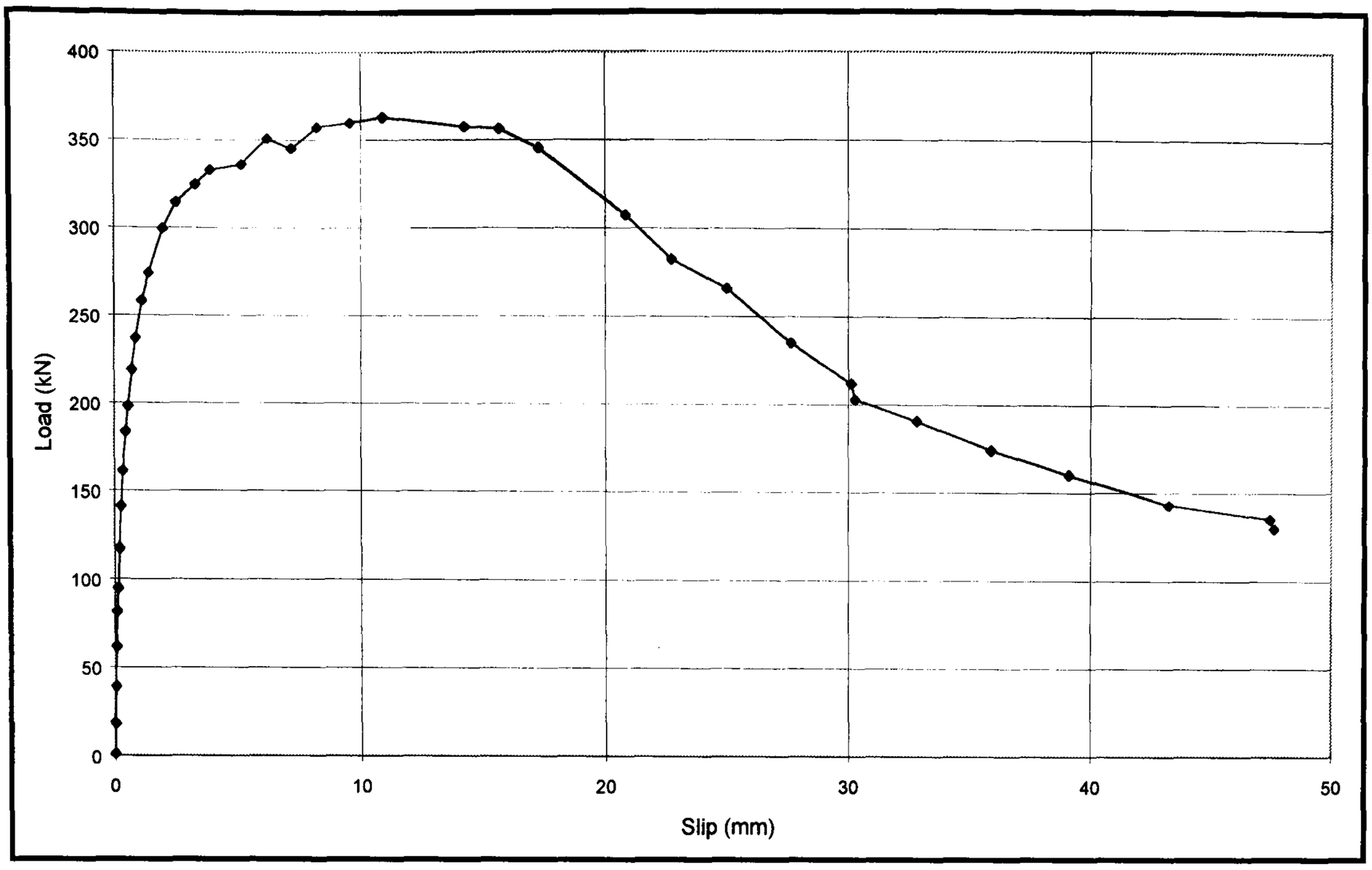

Fig. 4.19 Load vs. slip of push off test T16-25-65*

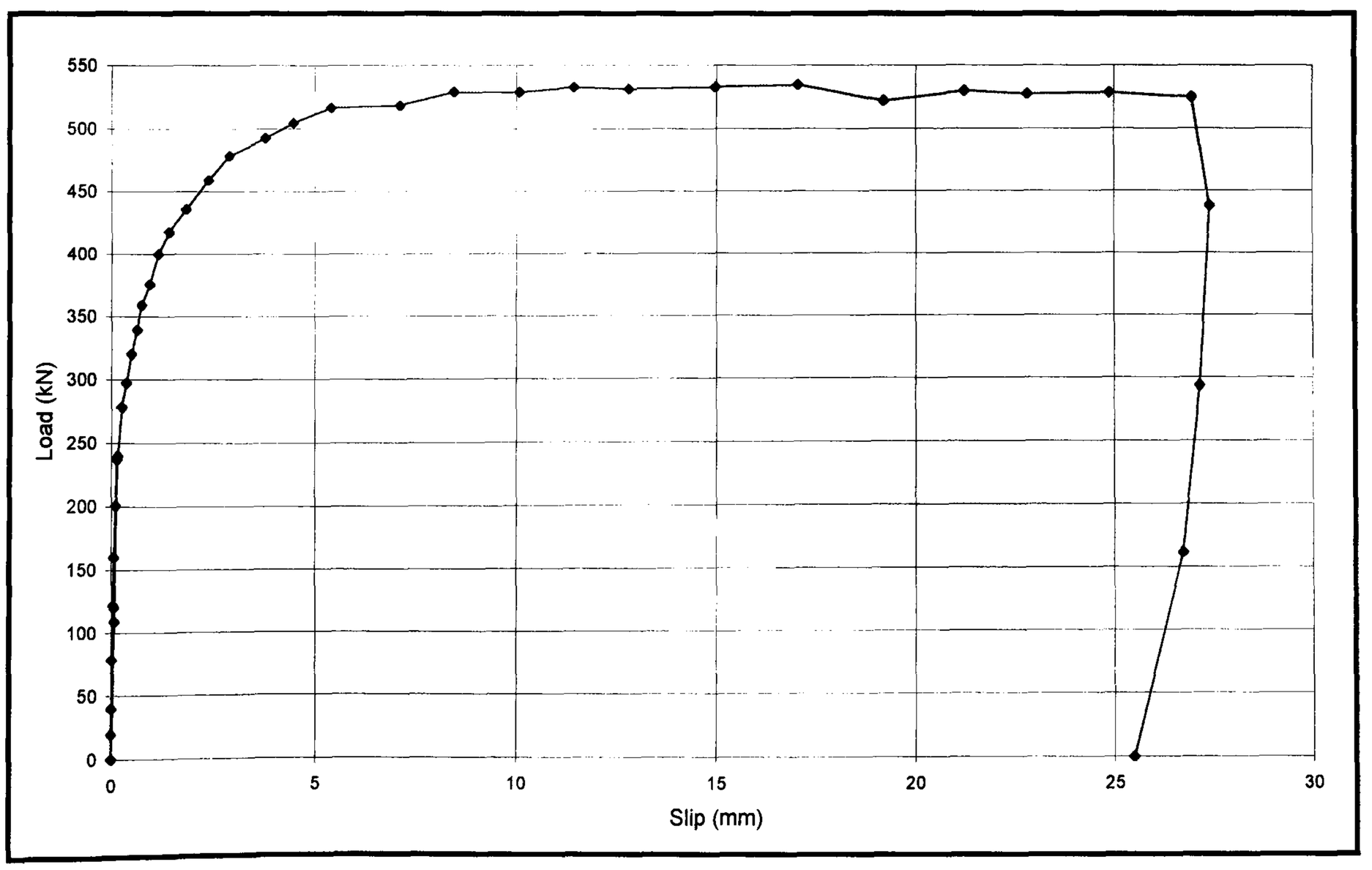

Fig. 4.20 Load vs. slip of push off test T16-25-65

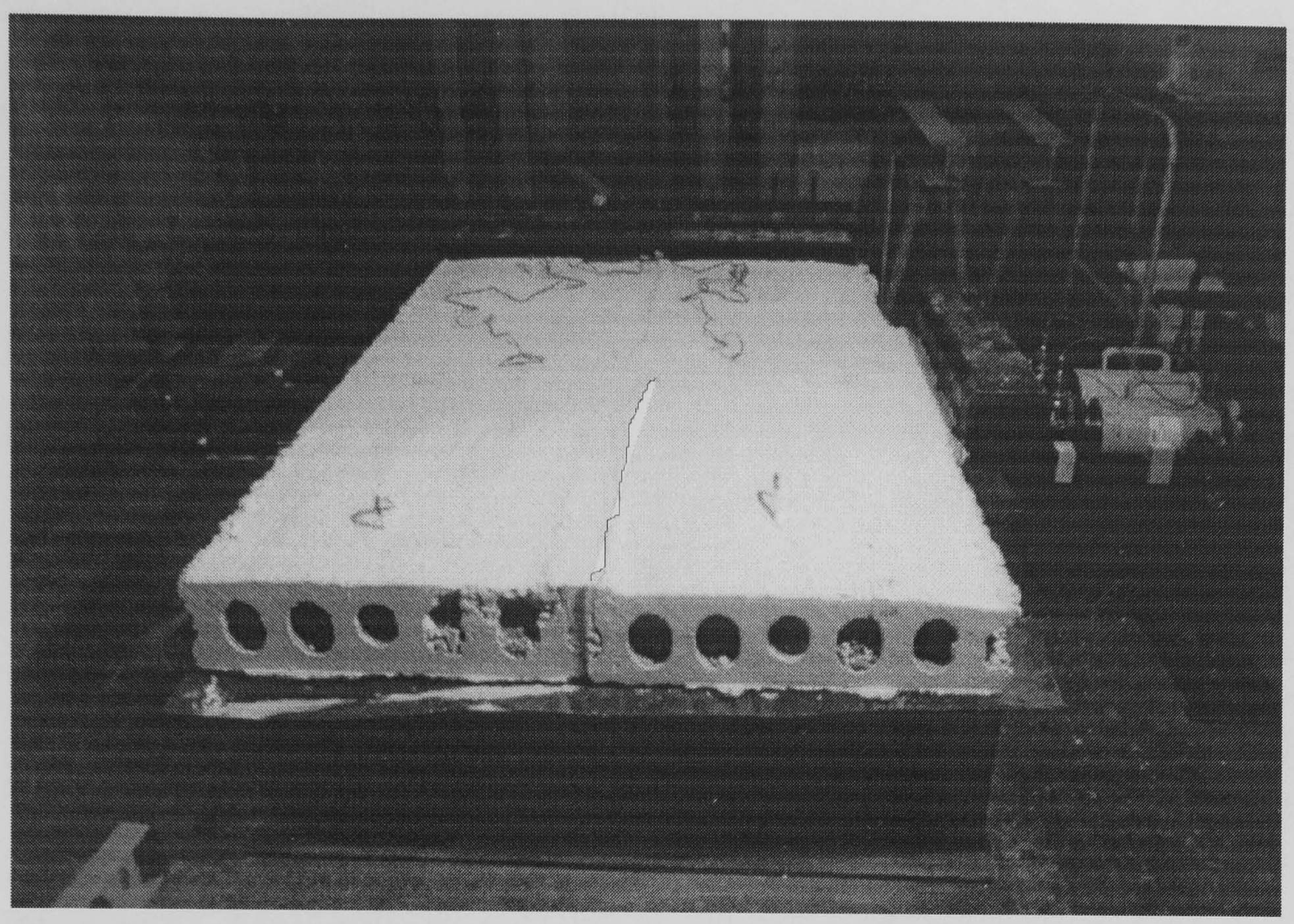

Fig. 4.21 Crack across the transverse joint of hollow core units in test T16-25-65

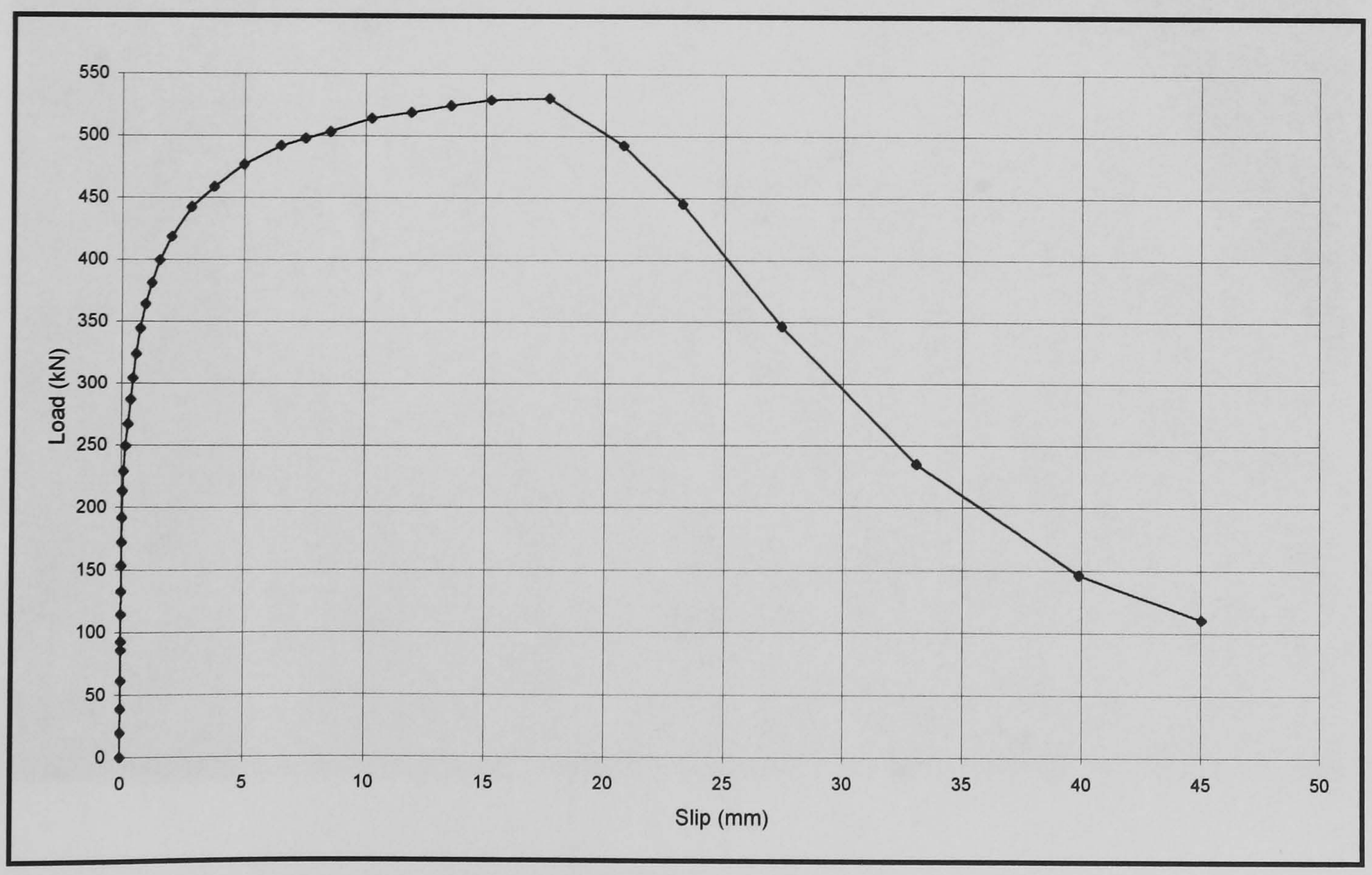

Fig. 4.22 Load vs. slip of push off test T16-25-40F

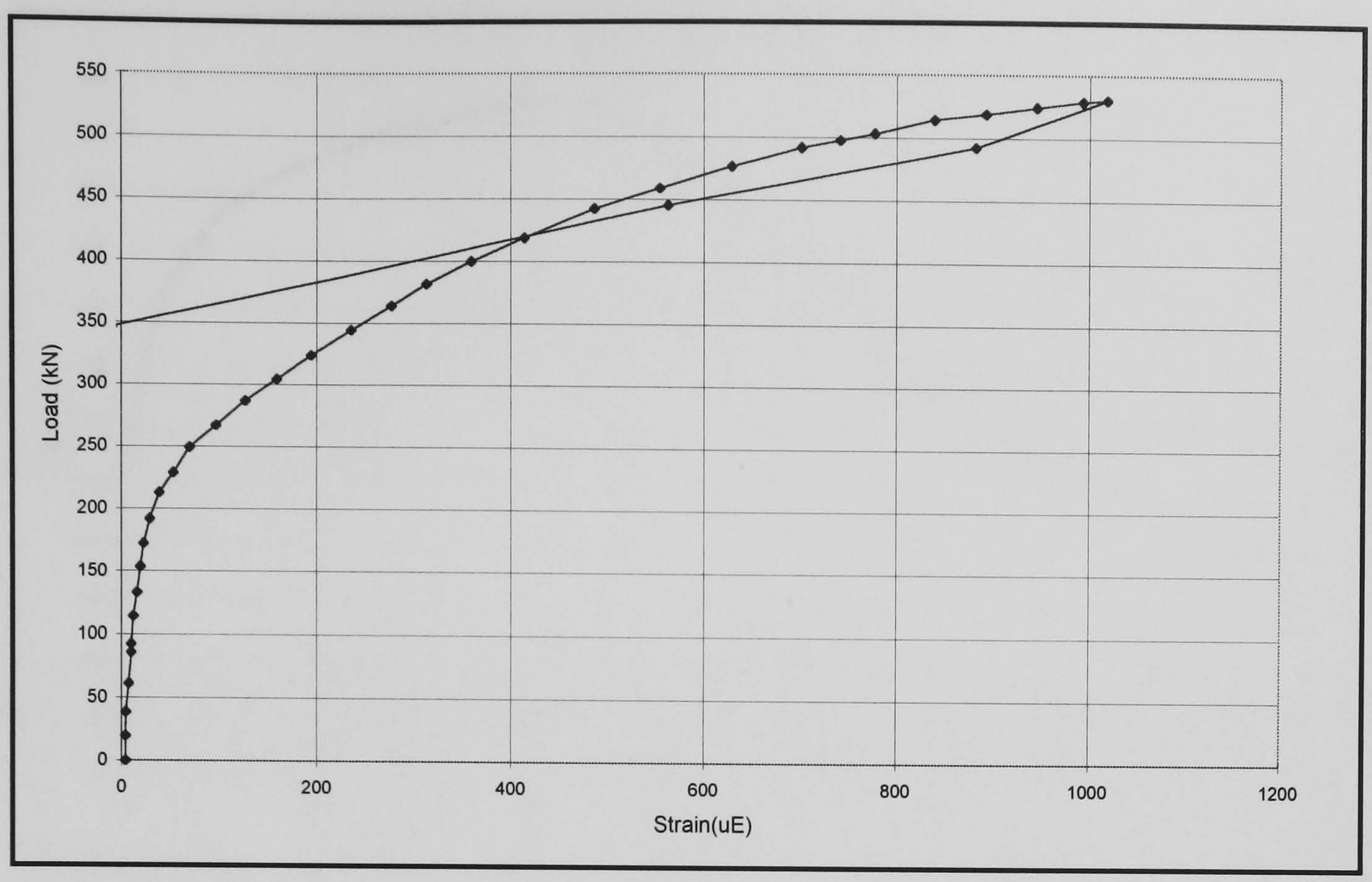

Fig. 4.23 Load vs. reinforcement strain of push off test T16-25-40F

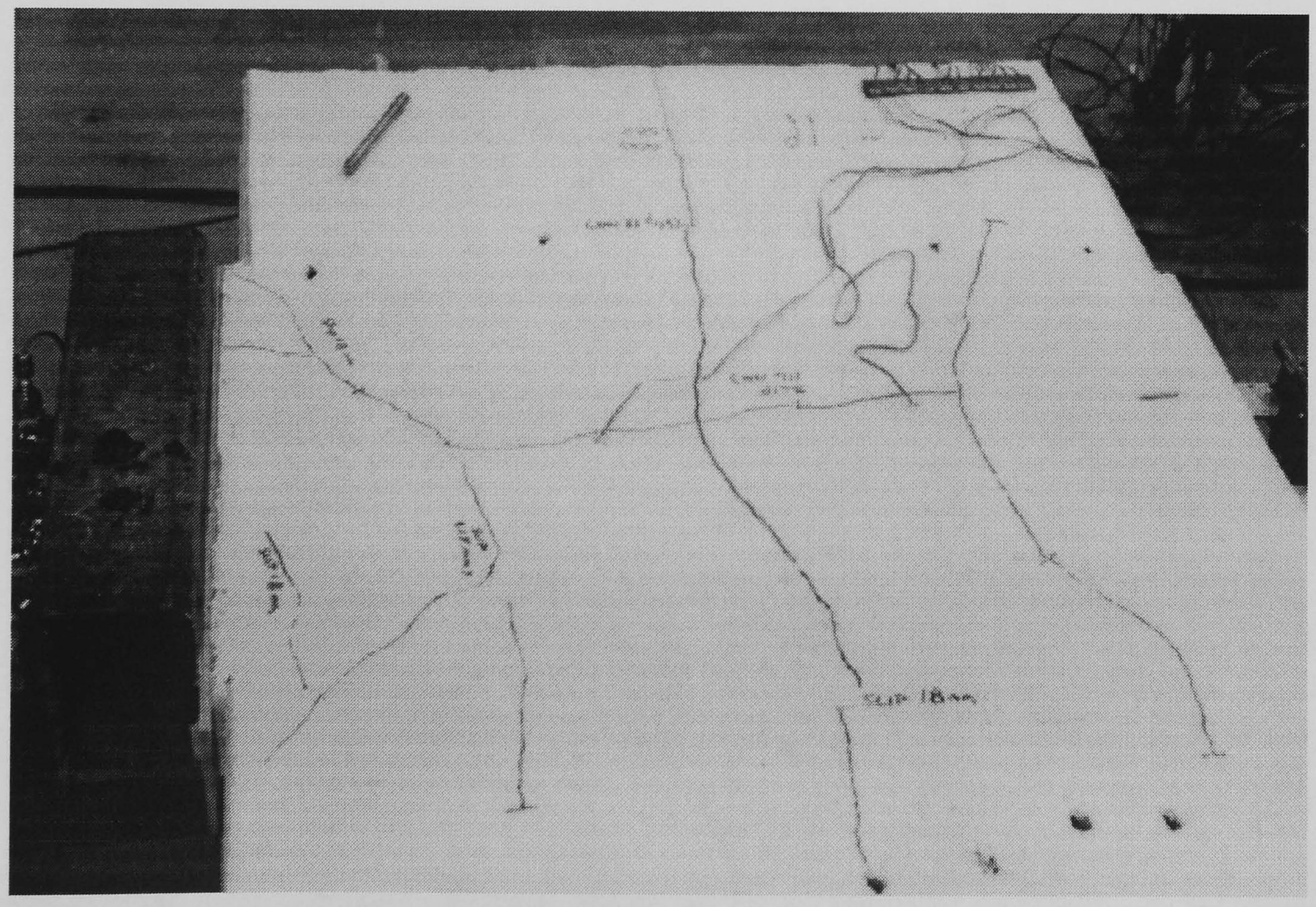

Fig 4.24 Push off test T16-25-40F at failure

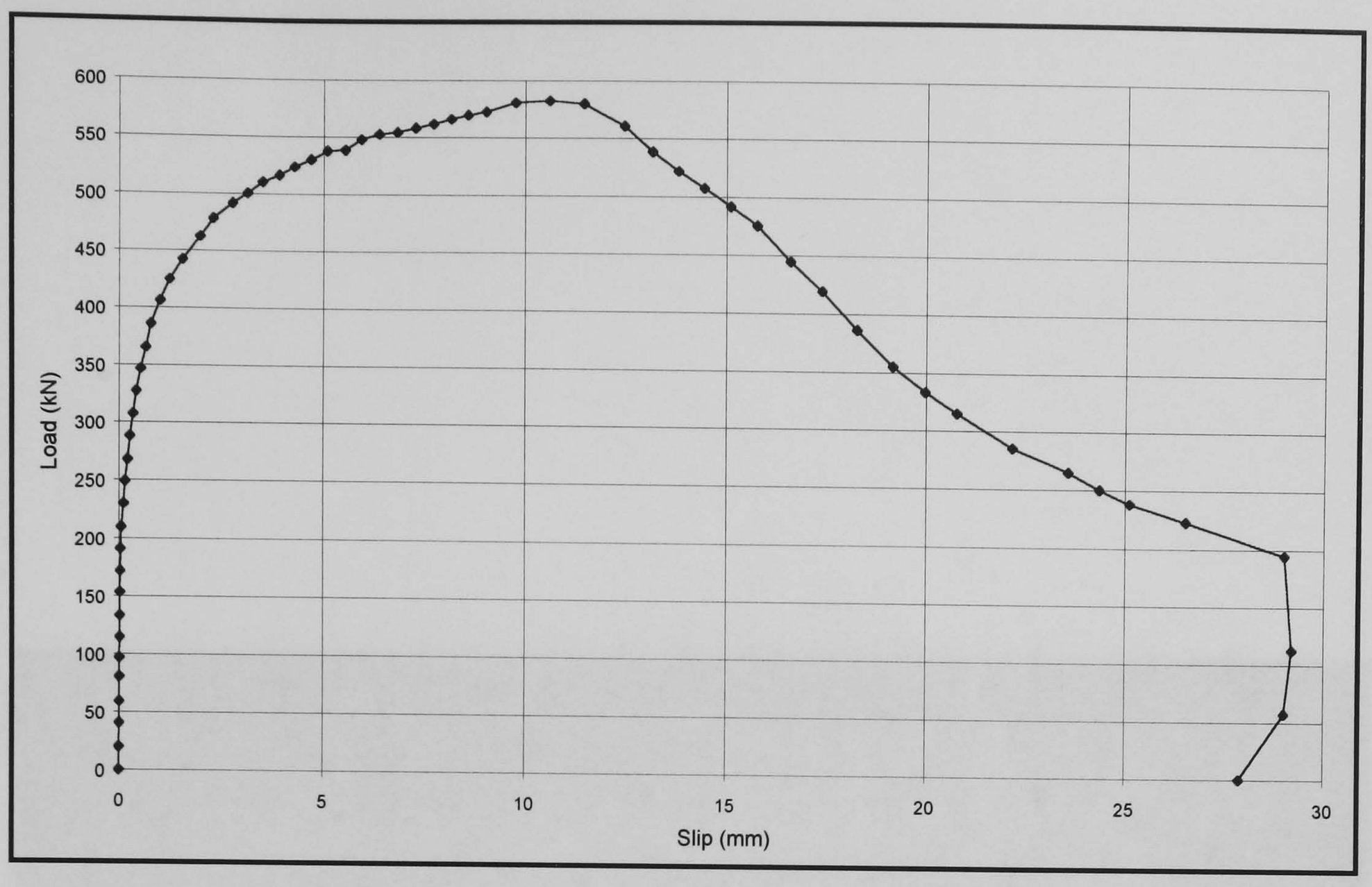

Fig. 4.25 Load vs. slip of push off test T25-25-40F

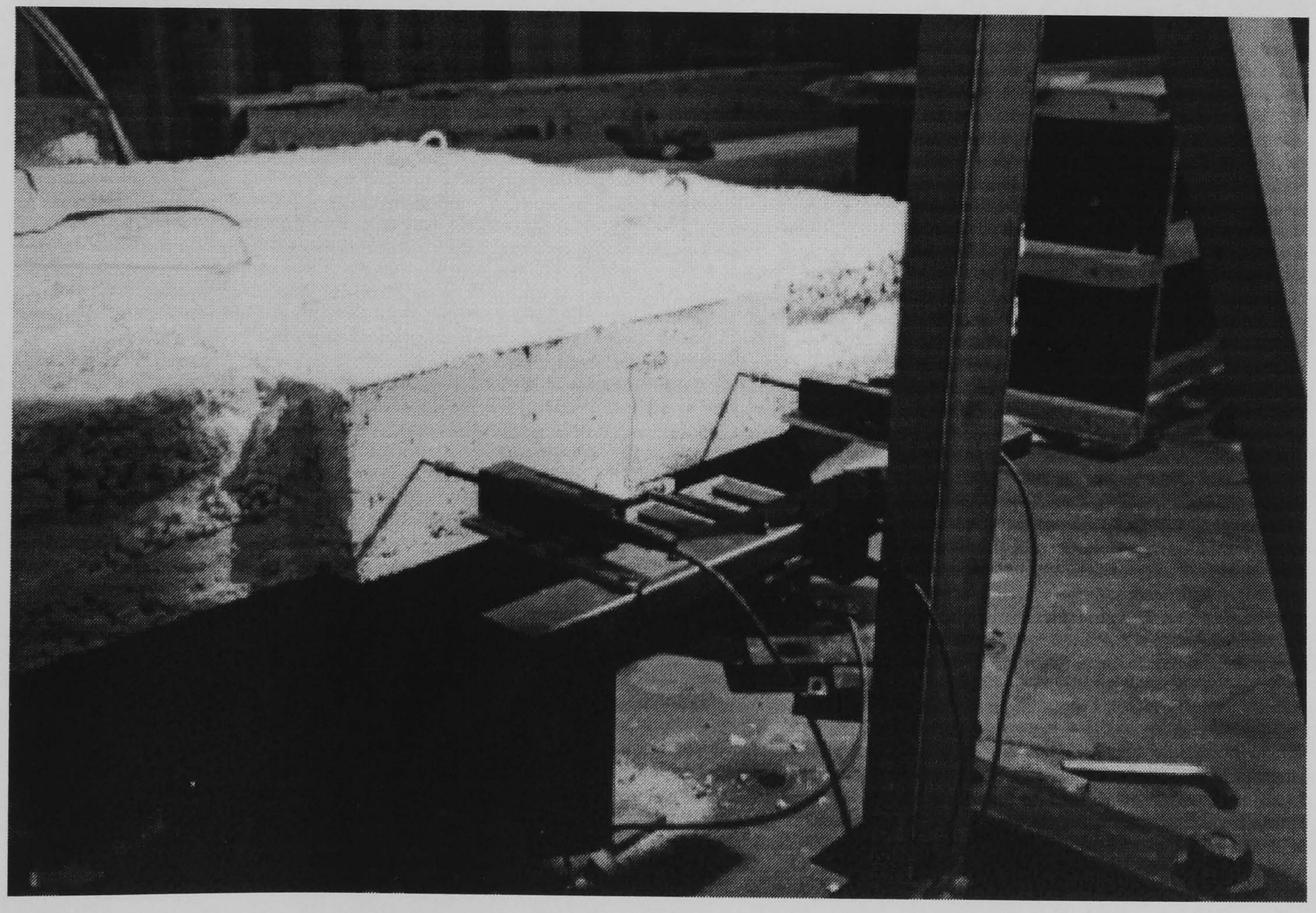

Fig. 4.26 First crack of T25-25-40F at end of slab

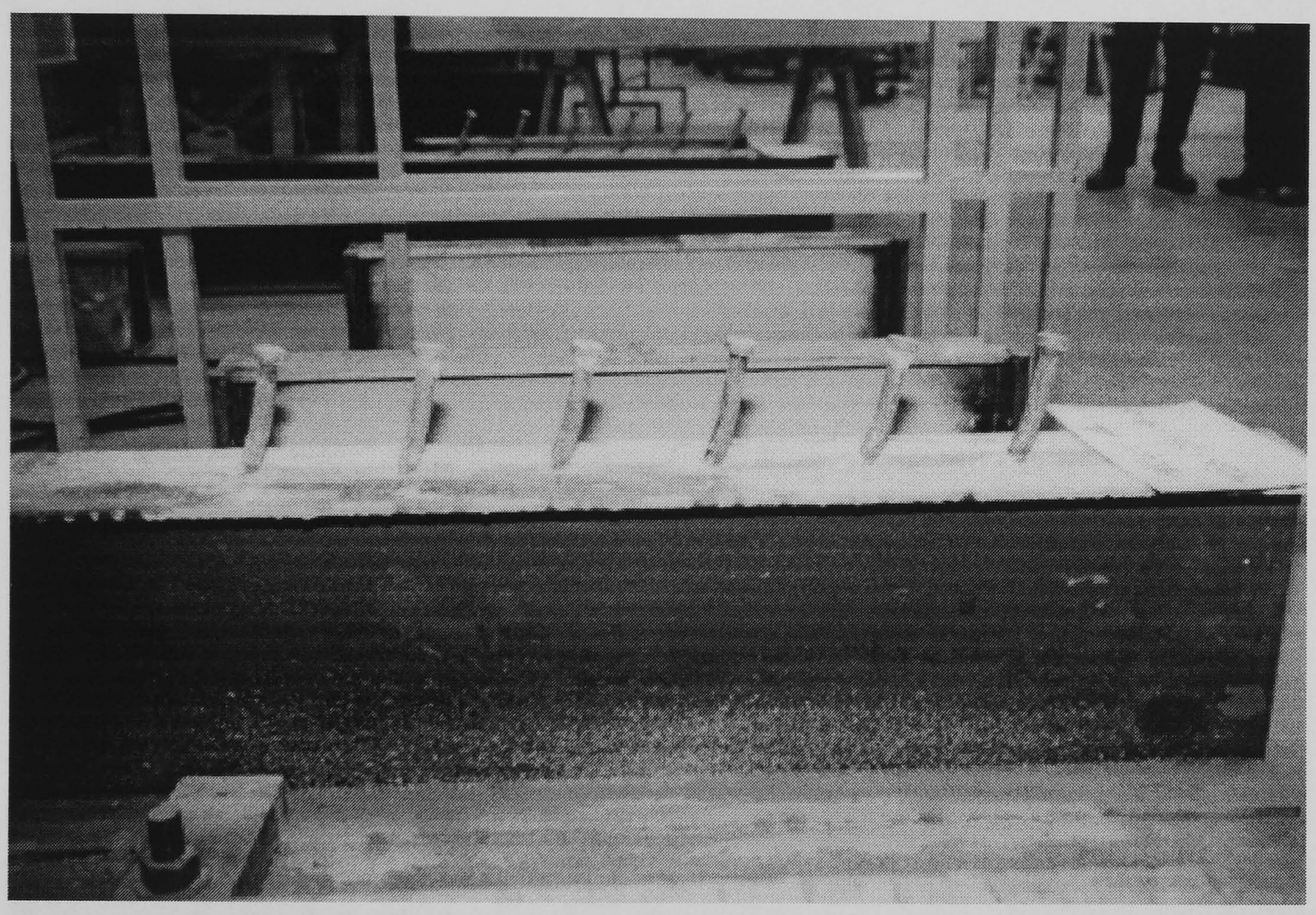

Fig. 4.27 Deformation of studs after the test of T25-25-40F

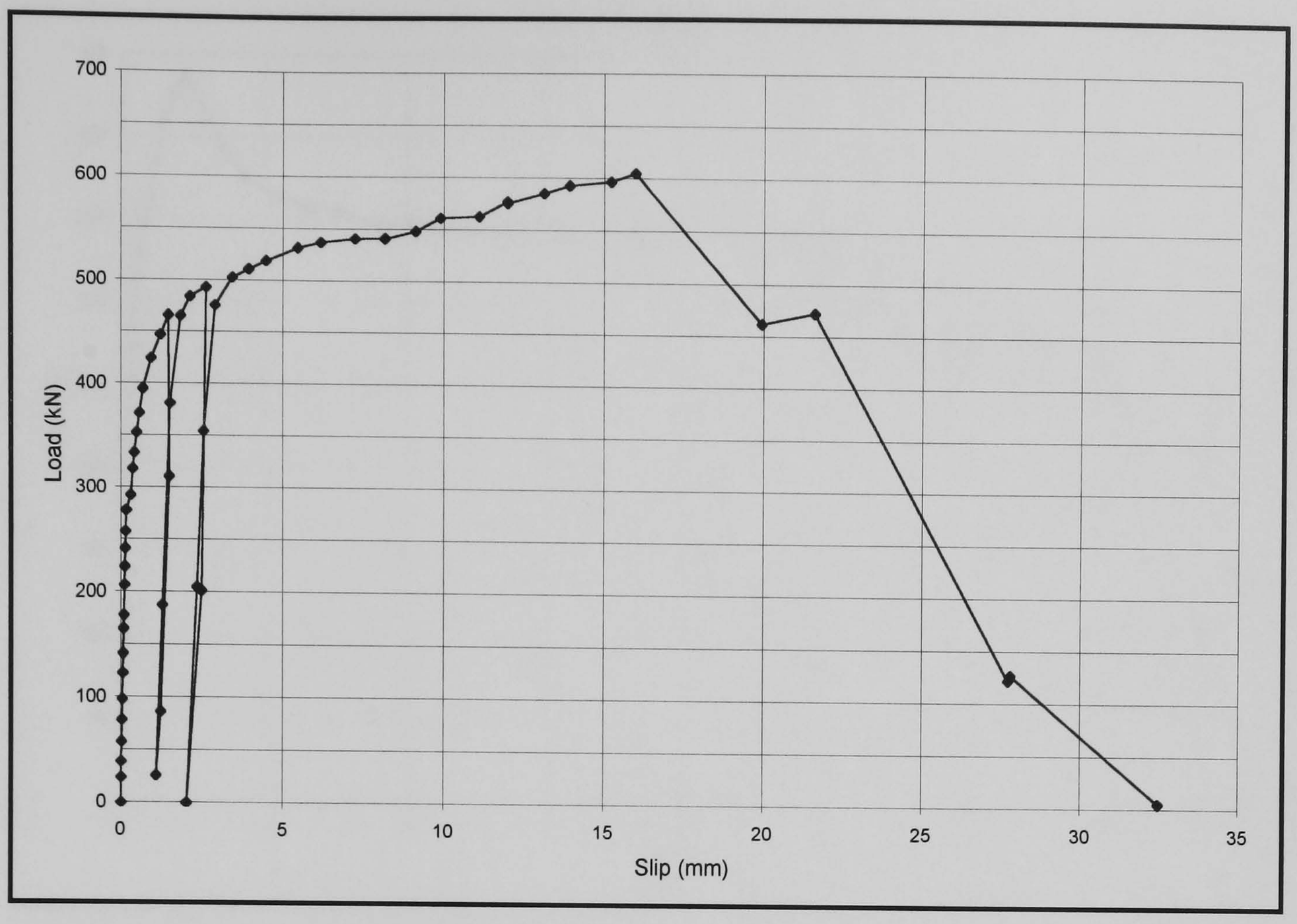

Fig. 4.28 Load vs. slip of push off test T25-25-65

Fig. 4.29 Crack pattern of T25-25-65 after test terminated

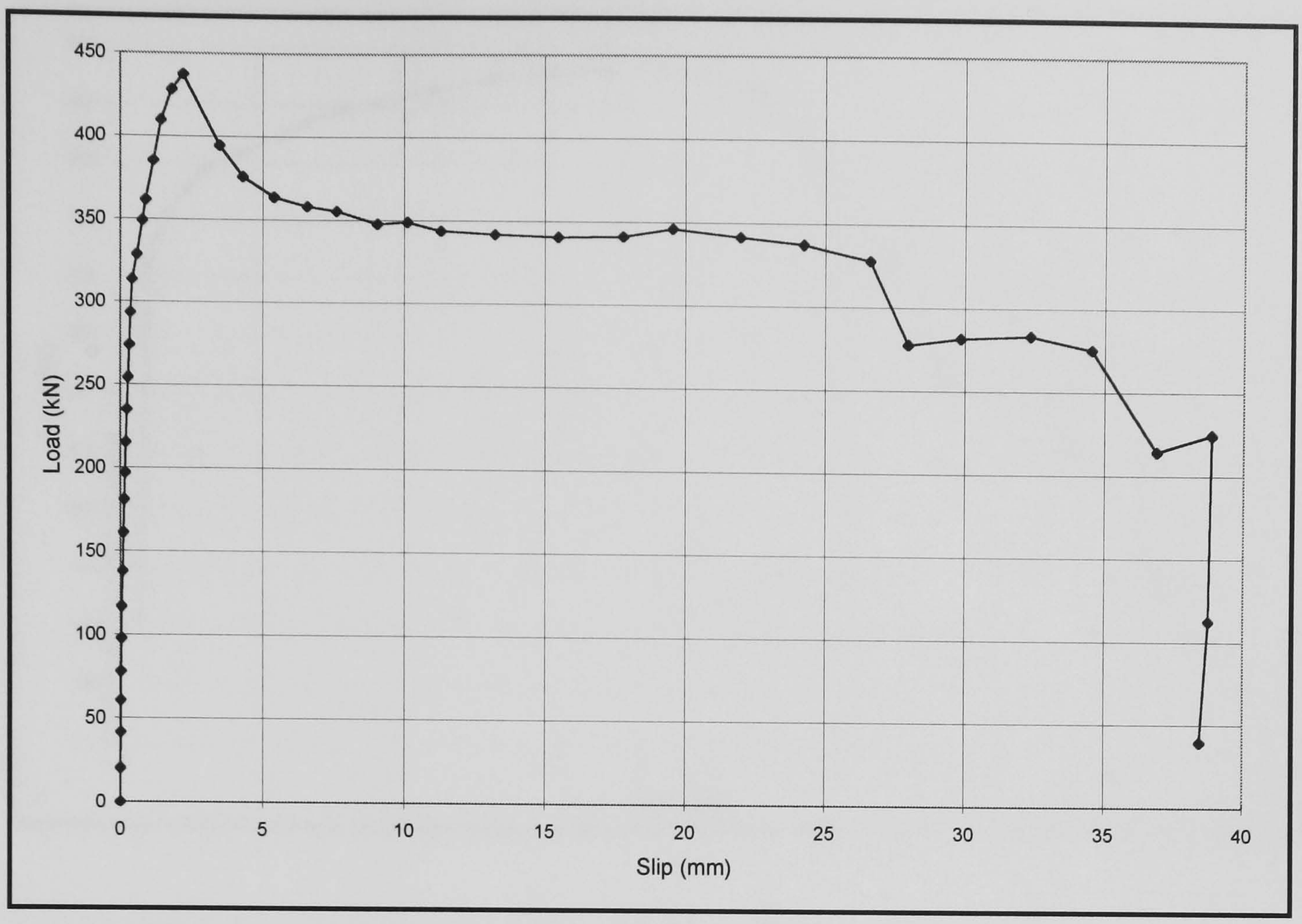

Fig. 4.30 Load vs. slip of push off test T8-38-RC

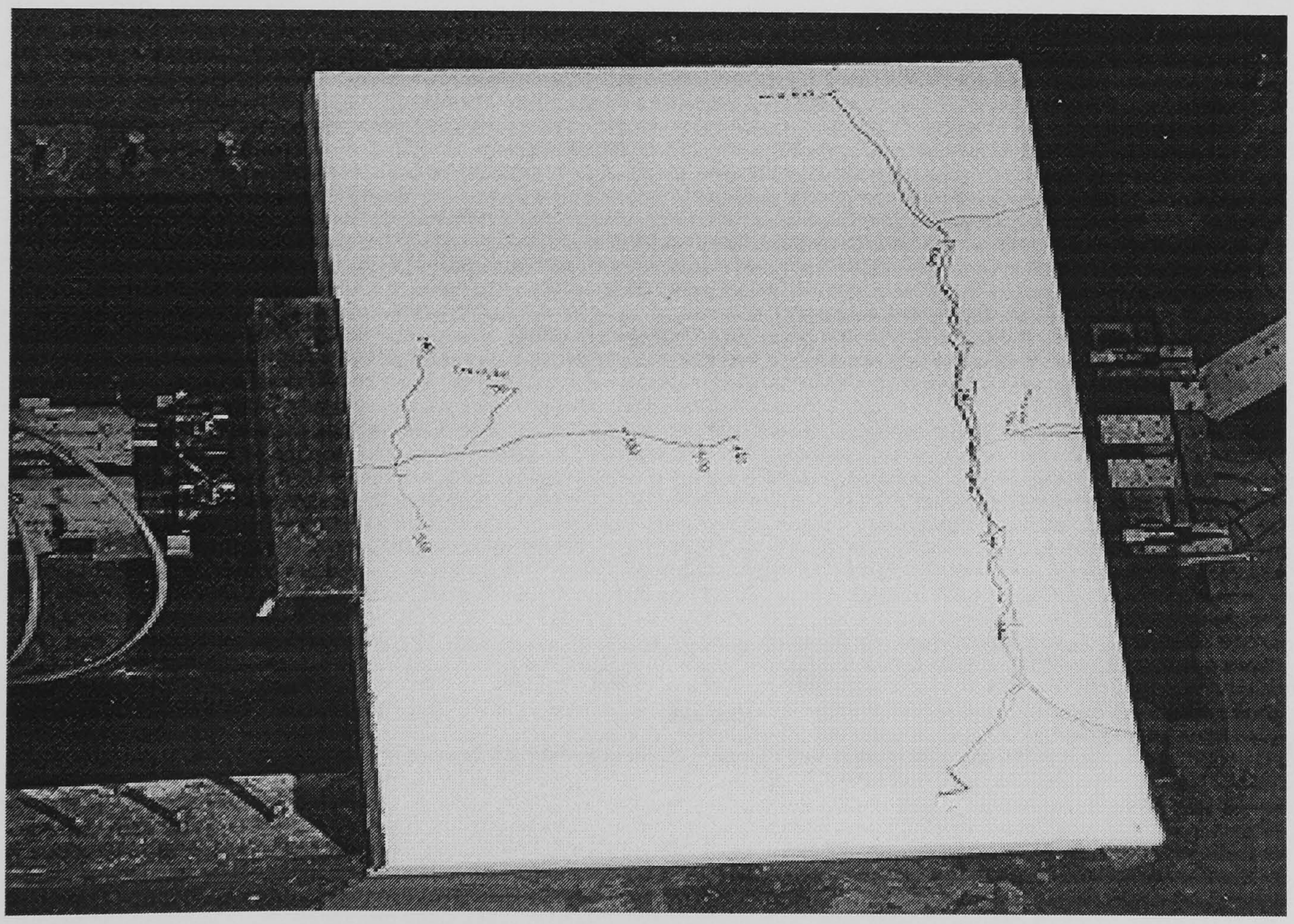

Fig. 4.31 Crack pattern of push off test T8-38-RC after the test terminated

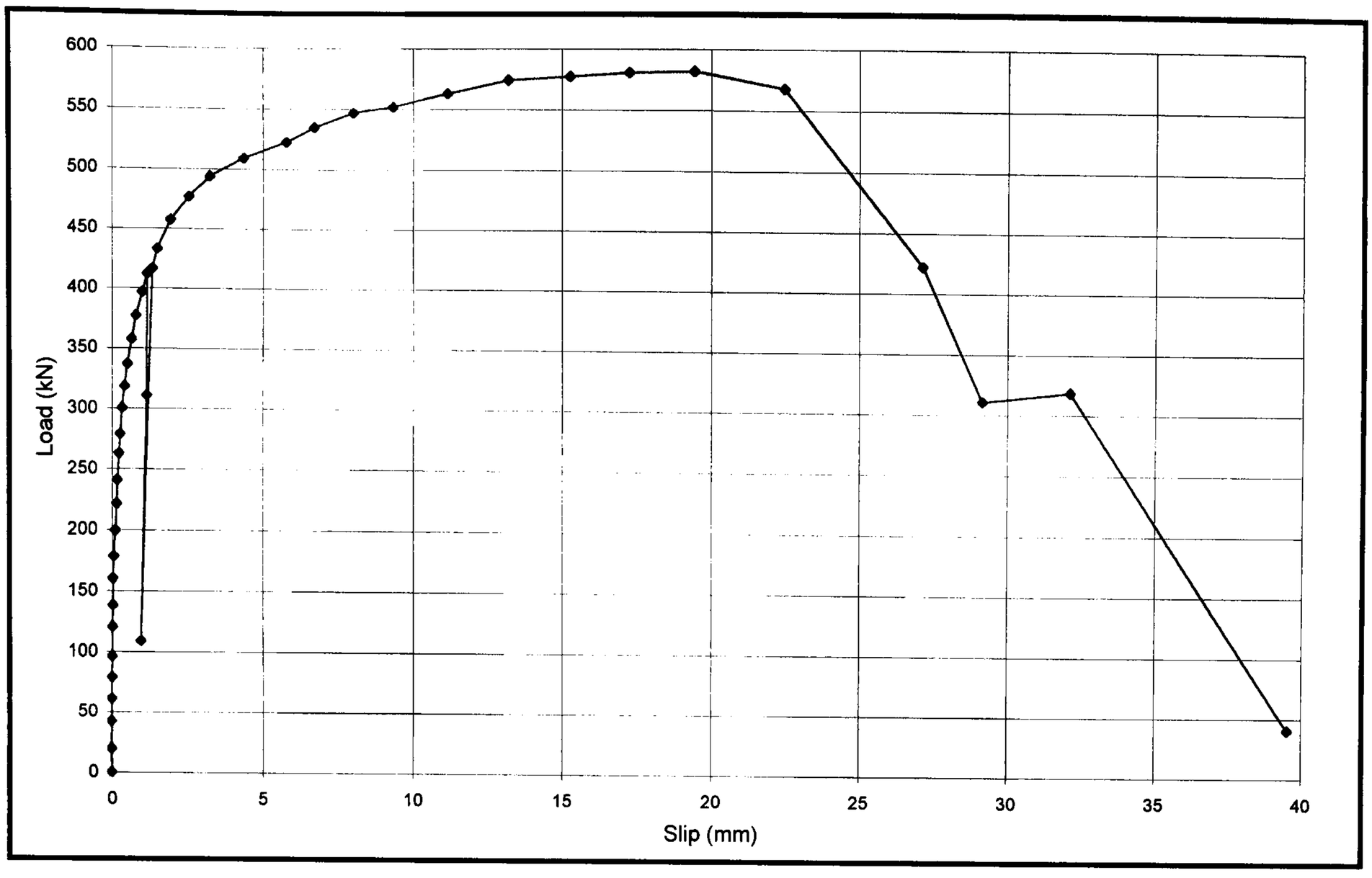

Fig. 4.32 Load vs. slip of push off test T16-25-RC

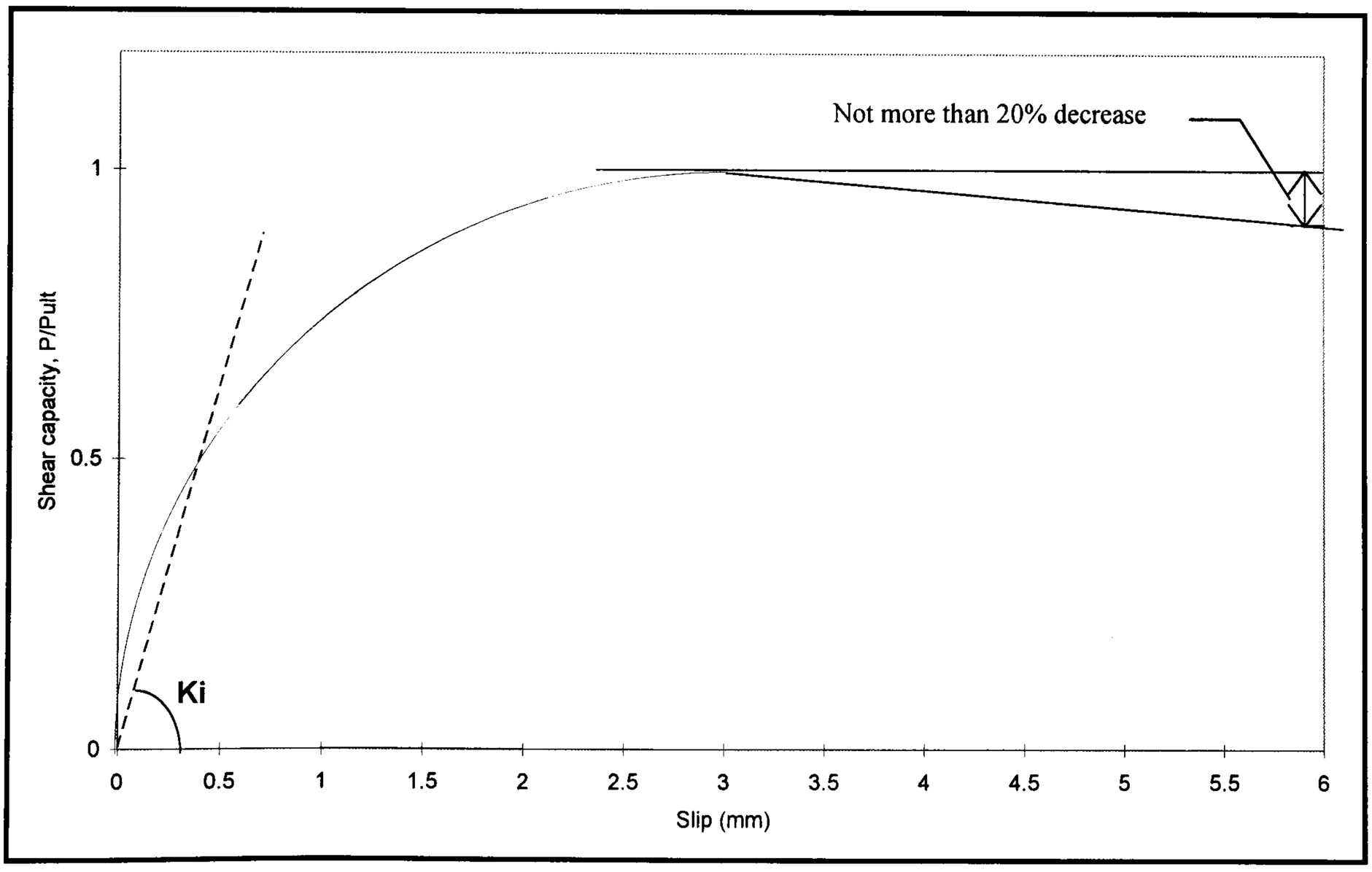

Fig. 4.33 Idealized load-slip relationship for shear connectors

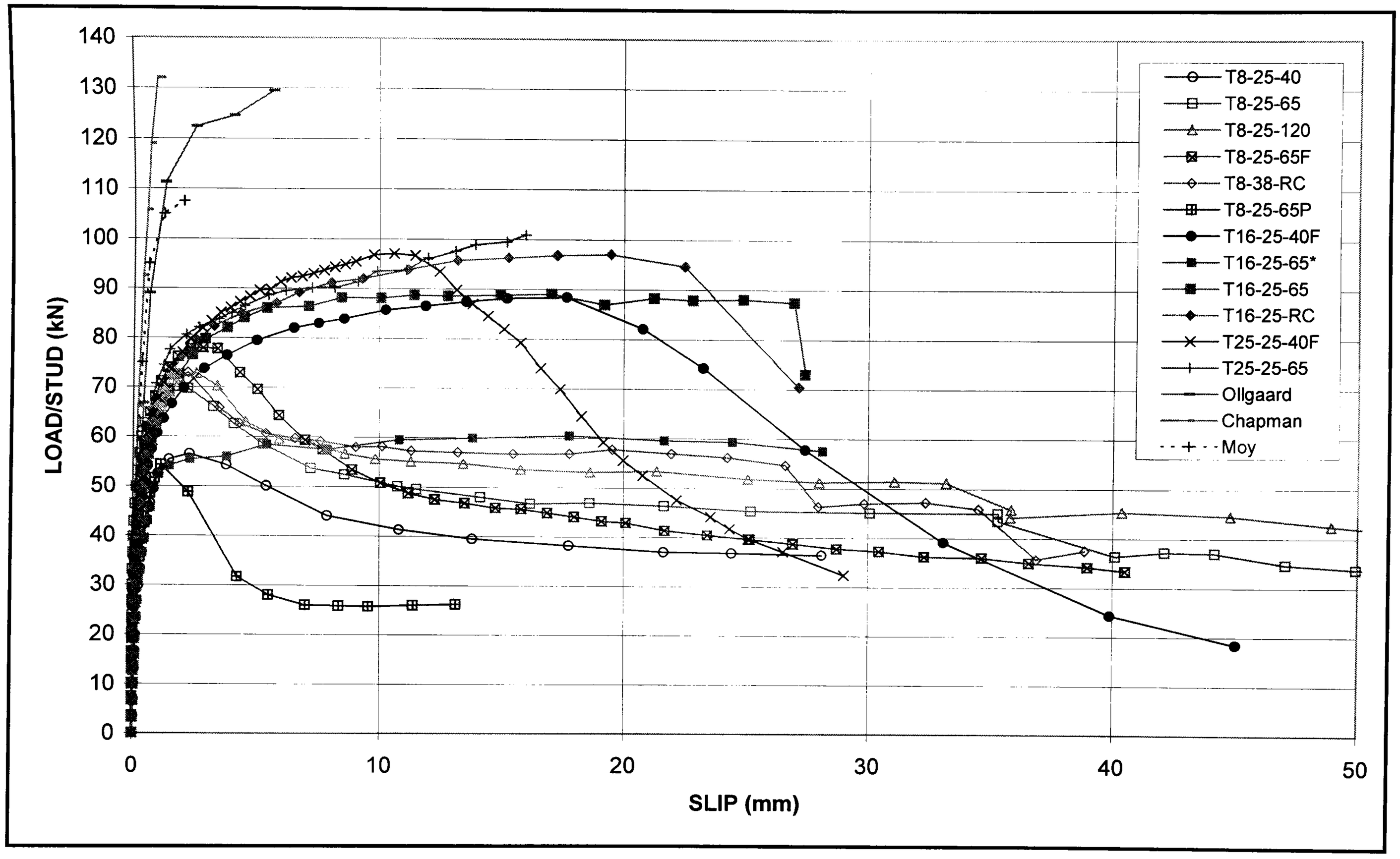

Fig. 4.34 Load / stud vs. deformation (slip) in all the tests upto 50mm slip or failure.

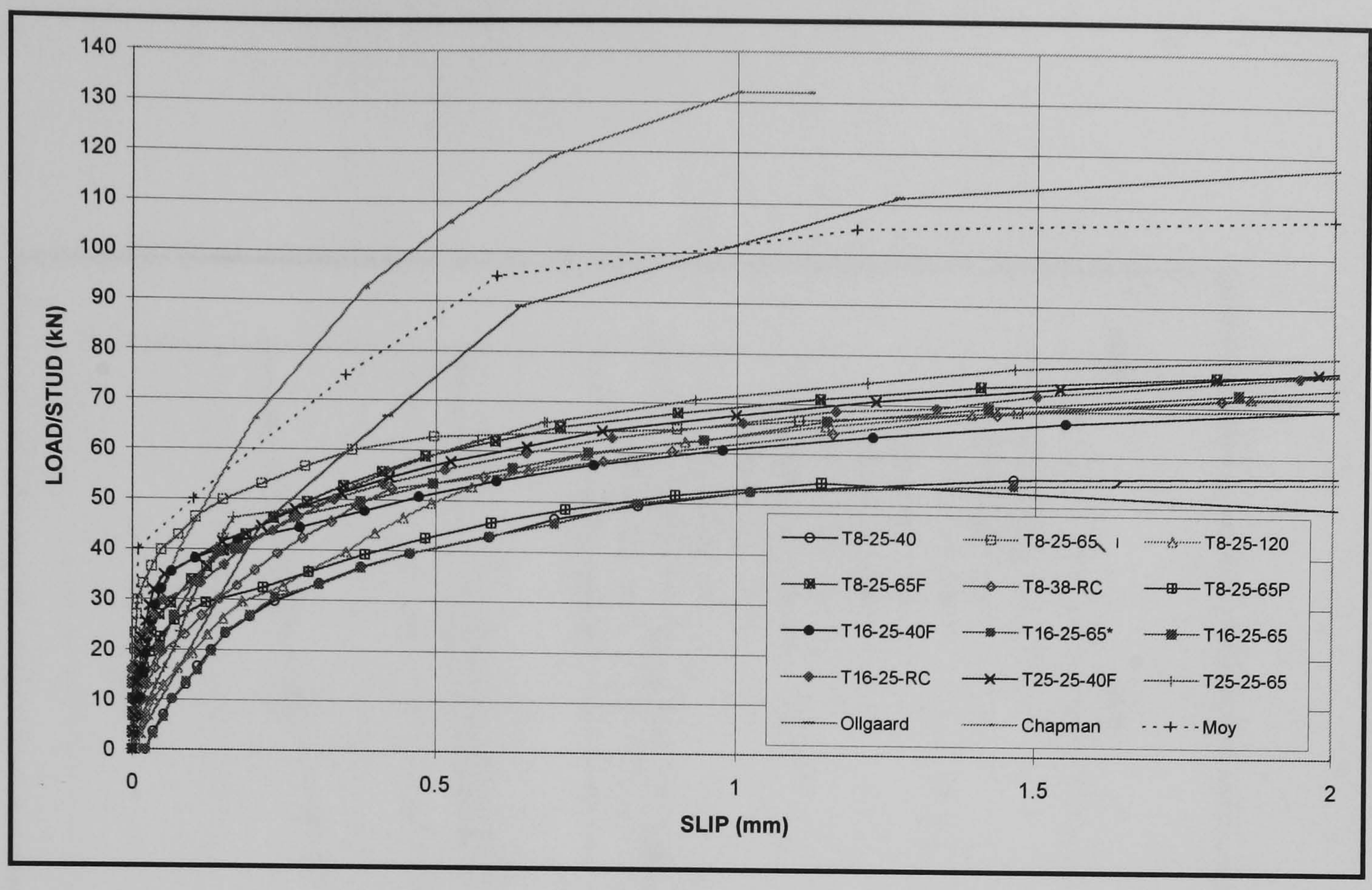

Fig. 4.35 Results of push-off tests for slip ≤ 2 mm

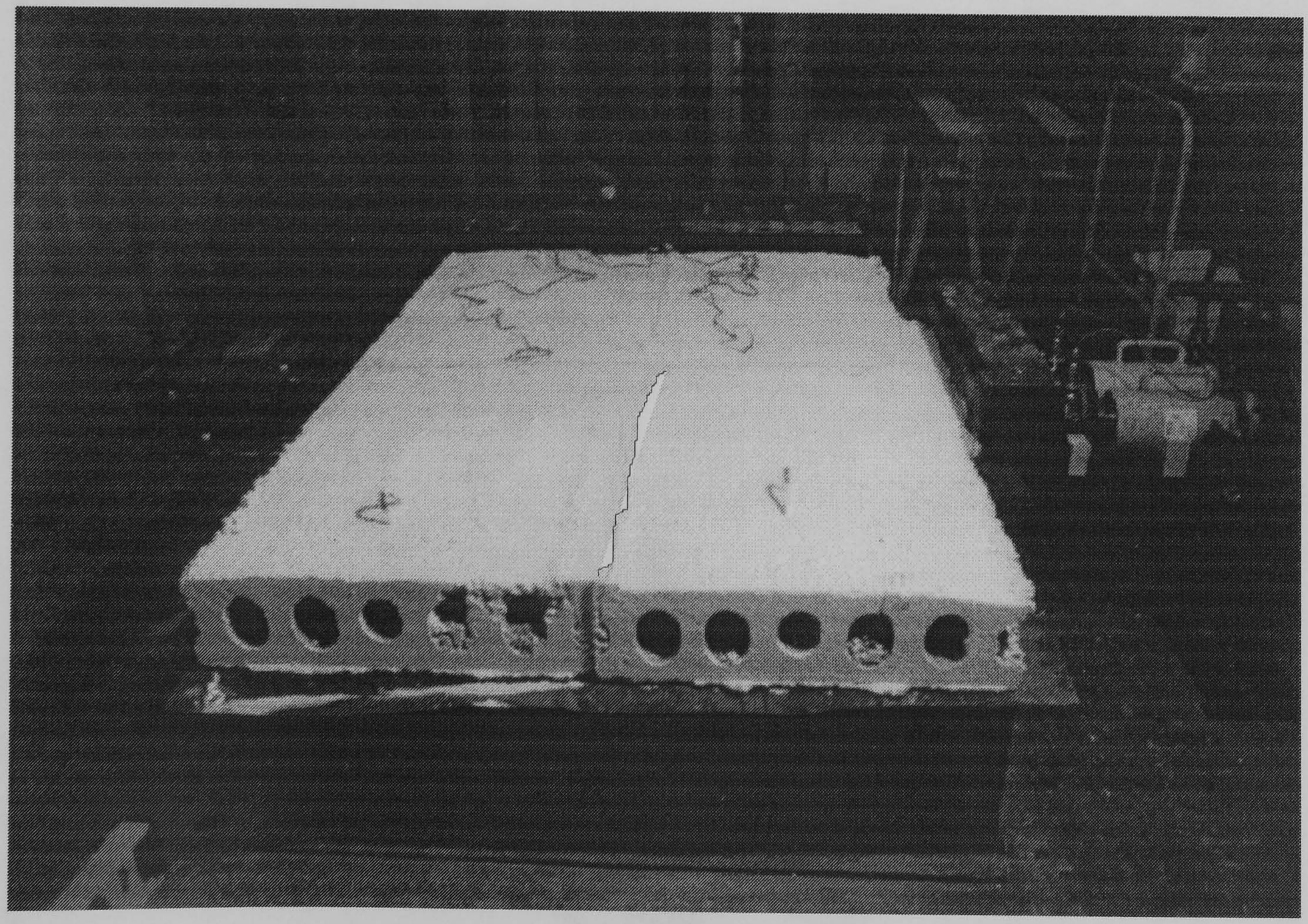

Fig. 4.36 Transverse cracking between the hollow core units

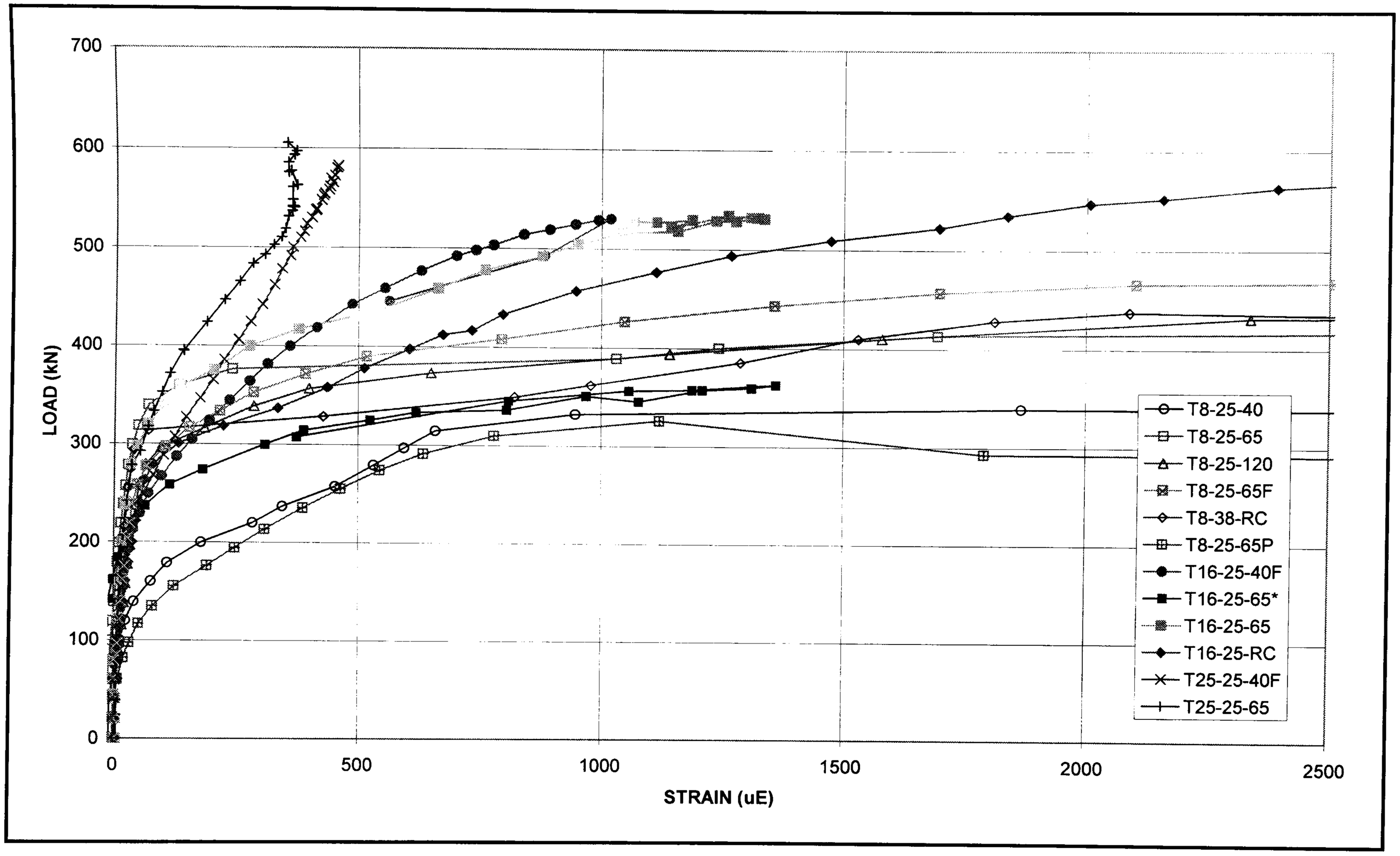

Fig. 4.37 Applied load vs. tie steel strains in all tests.

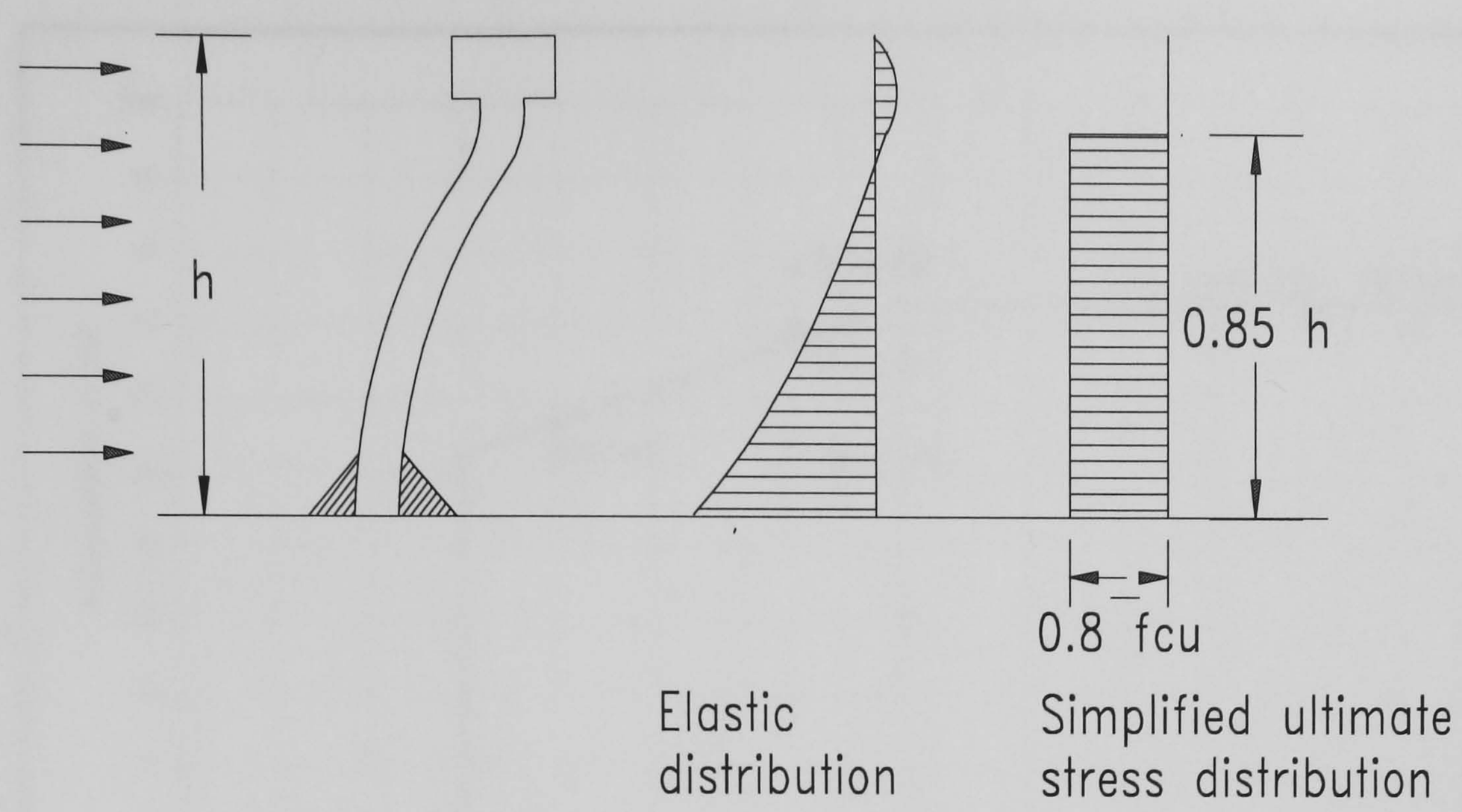

Fig. 4.38 Local stress distributions at headed studs

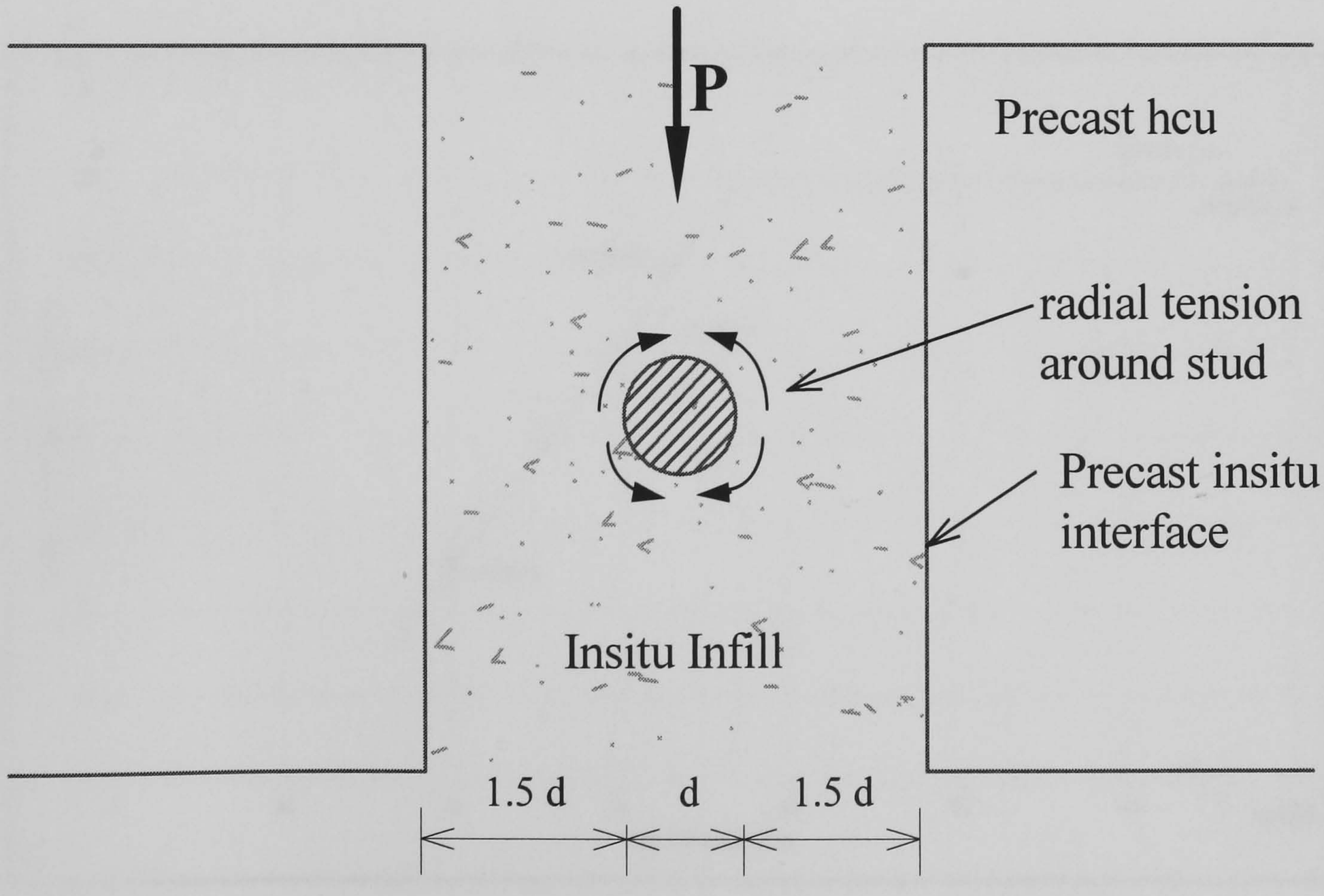

Fig. 4.39 Radial tension around shear studs.

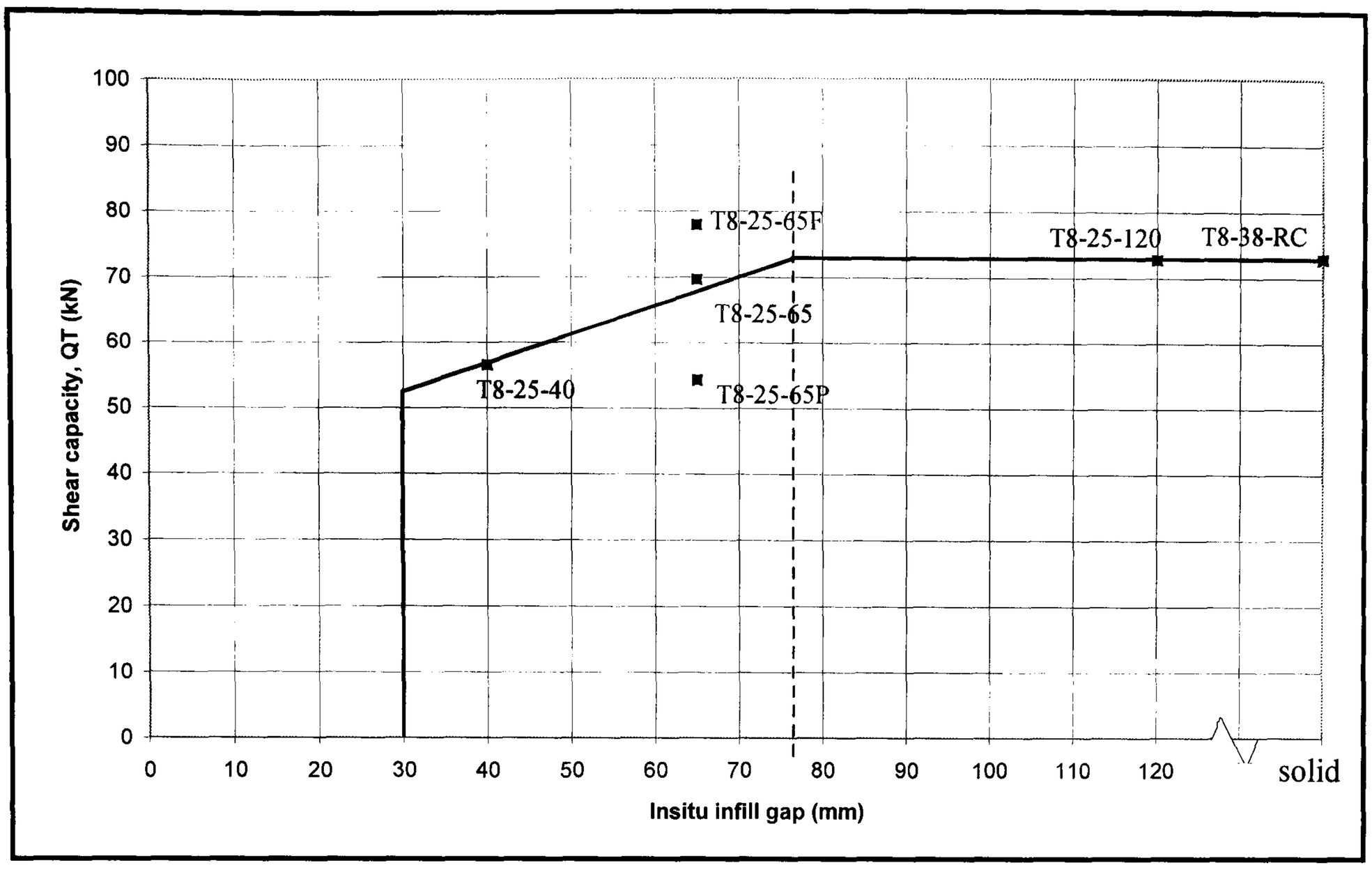

Fig.4.40 Shear capacity vs. insitu infill gap

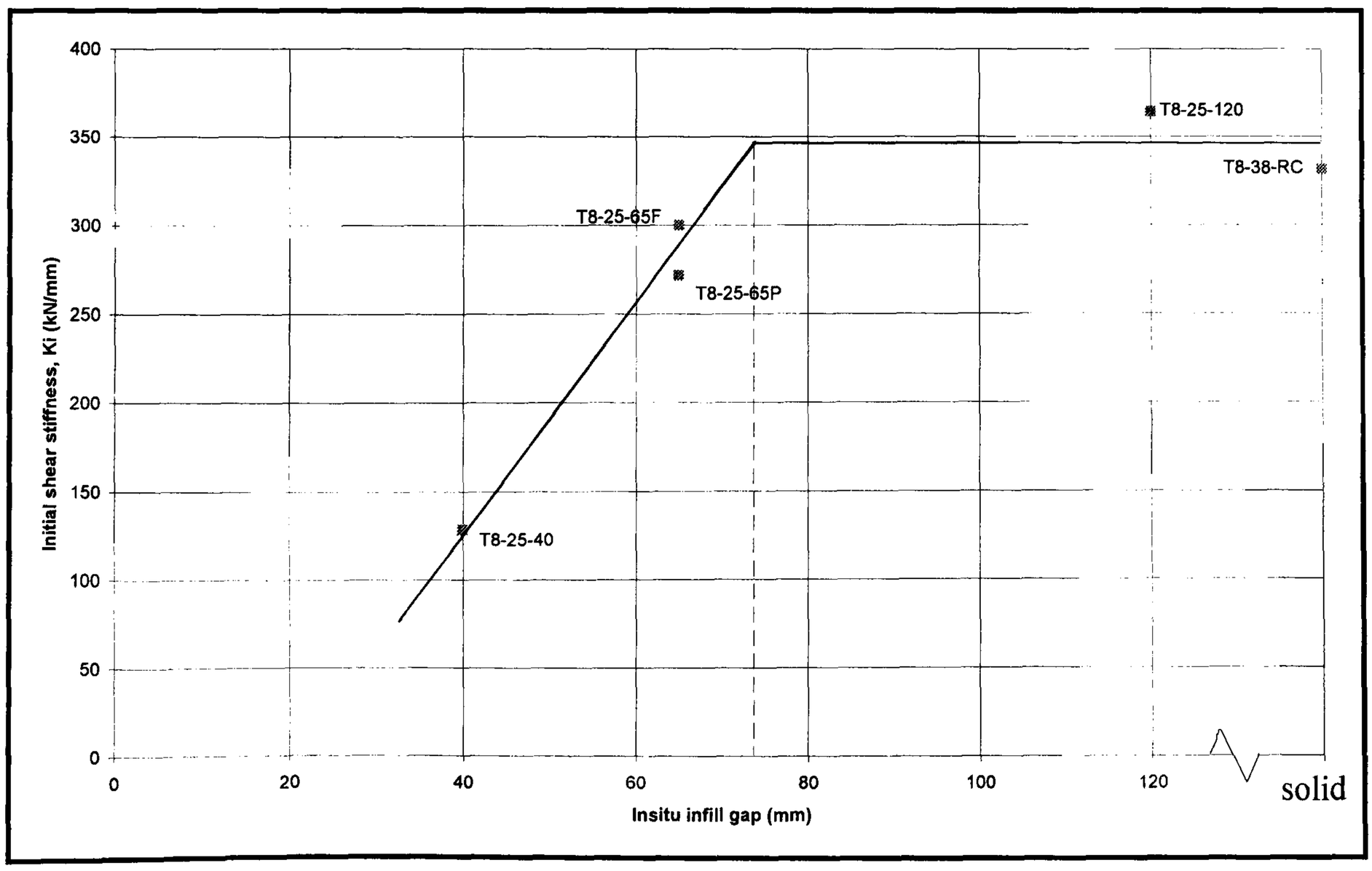

Fig. 4.41 Shear stiffness vs. insitu infill gap

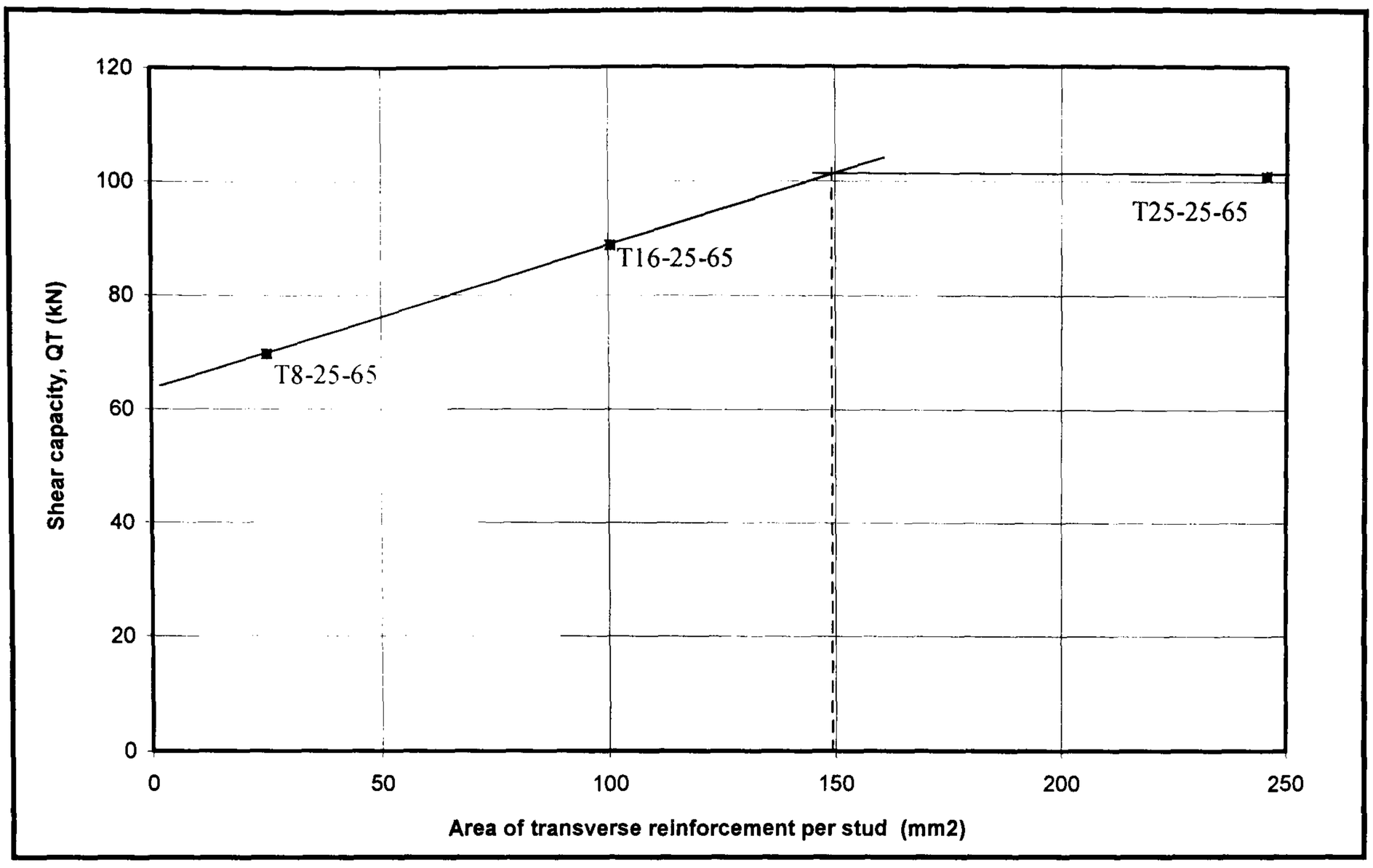

Fig.4.42 Shear capacity vs. area of transverse reinforcement per stud

Chapter 5

Composite Beam Tests

5.1 Introduction

The flexural behaviour of composite beams with hollow core units (hcu) is discussed in this chapter. Three full scale simply supported composite beams with variable parameters were tested to failure, so that the mode of flexural failure, and the enhanced strength and stiffness compared with non-composite bare steel beams could be investigated. In this chapter the test arrangement, instrumentation and materials are described and the test procedure is explained. The test results are presented in Section 5.7 and test results are compared in Section 5.8. The parameters for each test are set out on Table 5.1.

5.2 Test arrangement

The span of the beams was selected after giving due consideration to the testing facilities available in the laboratory and common spans for flooring in office accommodation. It was decided to use a 6.0m length of universal beam, with 150mm thick hcu giving a general floor area of 6.0m x 16.0m space free from

columns. The test specimens were assembled from ten 1200mm wide, 800mm long x 150mm deep prestressed hcu's with 235mm tapered end. (Supplied by Bison Floor Ltd.) and 356x171x51 universal beam (UB) with 19mm diameter x 125mm height TRW-Nelson headed studs pre-welded shear connectors at 150mm centres as shown on Fig. 5.1 & Fig. 5.2, giving 11 no. studs between support and load positions. The characteristic cube strength for the hcu's is taken as 50 N/mm^2. The specimens were simply supported over a span of 5.7 metres and loaded at two point loads spaced symmetrically at 1.5 metres from each end of support. All three specimens were similarly constructed, with the exception being the transverse reinforcement and insitu joint. Web stiffeners were used to eliminate local failure due to web buckling or flange yielding at the loading position. The slabs were placed directly on to the UB with a minimum bearing of 50 mm. The gap between the ends of the hcu's was carefully monitored during placing to ensure a 65 mm gap width was maintained throughout. The tops of four cores per hcu, i.e. 2^{nd}, 4^{th}, 8^{th} and 10^{th} core, were left open for a length of 500mm to allow the placing of transverse reinforcement giving an average bar spacing of 300 mm. Fig. 5.3 shows the specimen before the insitu infill was cast.

Following the horizontal compression tests (described in Chapter 3) and push off tests (described in Chapter 4), it was decided that transverse reinforcement of T8 and T16 bars should be used for the full scale tests. T16 bars were used in test CB1 to prevent tensile splitting and to confine the concrete slab from splitting failure, while T8 bars were used in test CB2 to allow tensile splitting to take place.

Insitu concrete with the design cube strength of 25 N/mm^2 was placed into the longitudinal and transverse joints and opened cores and compacted using a 25mm diameter vibrating poker to form the composite slab.

In addition, a full scale test (Test CB3) with debonded joints between the insitu and precast concrete was tested to observe the effect of a debonded insitu joint due to shrinkage. Two sheets of polythene were cast between the insitu concrete infill and the hcu to ensure a proper separation between the insitu infill and hcu, so that bonding and aggregates interlocking between the insitu infill and hcu could not be achieved, see Fig. 5.4. Transverse reinforcement of T8 bars was chosen for this test; identical to the arrangement of Test CB2.

After the bending test was terminated, the set up was re-arranged for the shear test. The arrangement is shown in Fig. 5.5. The shear test is carried out to monitor whether any increase of shear capacity results from composite action with the slab.

5.3 Test Rig

The rig was designed to sustain the worst load which would be applied at any stage of the test. The structural steelwork was designed in accordance with BS5950[1] using a partial safety factor of 3.0. Details of the test rig are shown in Fig. 5.6 and 5.7.

Four point bending was used so that bending stress can be monitored in the central region between the point loads while constant vertical shear can be monitored between the loading point and the support. Loads were applied manually by two hydraulic jacks, one at each loading position operated simultaneously by a single pump, to enable load to be applied to the specimen at each loading position. The use of hydraulic jacks with non-return valves permitted a relatively slow application of load and enabled equilibrium to be achieved quickly even when the load-deflection characteristic was falling. Point load is applied to 100x200x10 RHS steel stools pre-welded on to the steel beam and not directly to the slab so as to avoid loading directly through the hcu's which might result in local punching shear failure.

5.4 Instrumentation

In order to obtain the load, deflections, end slip, force in the tie bars and strain distribution of the steel section and concrete slab, a range of instrumentation was used to monitor the whole test procedure. These included strain gauges for the reinforcement and steel beam, potentiometers for end slip and for deflections. The instrumentation used is described in detail below.

5.4.1 Strain gauges

Strains in the transverse reinforcement, in the concrete and in the steel beam were measured using electrical resistance strain gauges (ERSGs). The gauges were 120±0.3Ω resistance and with gauge factor of 2.13. Strain gauges to monitor the stresses in the rebars were placed in the centre of the rebars. The position of the reinforcement gauges is shown in Fig. 5.8, where 4 are placed in the central region between the point loads and 4 are placed between the point load and supports. The strain gauges on the surface of the rebar were carefully coated with epoxy and checked before and after casting to ensure proper operation during the test.

Surface mounted strain gauges were used to monitor the compressive and tensile strain of the concrete in the test. Three sets of 20mm gauges consisted of a cruciform arrangement (i.e. one strain gauge measured compressive strain and the other measured tensile splitting strain) are placed on the central bending region of the specimen. The position of the concrete stain gauges is shown in Fig. 5.8.

The strain gauges on the surface of the steel beam were used to measure strains in the steel beam (and hence calculate the position of the neutral axis) and to monitor yielding of the beam. Two types of arrangement were used for the position of steel strain gauges. Three sets of gauges were placed on the steel beam to monitor the strain distribution of the steel beam during bending. The first type consisted of 5 strain gauges: one on the top flange of steel; one on the bottom flange of steel; one

on the centre of web and two 100mm above and below the centre of web. They were positioned to coincide with the position of the concrete strain gauges used to monitor the strain in the beam. The second arrangement consisted of a rosette strain gauge placed at the centre of the steel beam 325mm from the centre line of the loading position. It is used to monitor the principal shear strain in the shear test. The steel strain gauge positions are shown in Fig. 5.9.

5.4.2 Potentiometers

After the hollow core slabs were fully assembled on to the steel beam, instrumentation for measuring deflection and end slip was mounted on to the test specimen. Potentiometers (POT) were used to measured deflection of the specimen on the bottom flange of the beam at mid span and at the loading positions as shown in Fig. 5.9 and Fig. 5.10. Two sets of POTs were used to monitor end slip at both ends of the beam, the POTs were mounted on the end of the steel beam with purpose made bracket so that only end slip is measured. Any other effect such as end rotation is eliminated, see Fig. 5.11.

5.4.3 Data recording

All data from the strain gauges, potentiometers and load cells were collected electronically and stored by the Schlumberger data logger, which was set to a scanning rate of 40 channels per second. The data logger was linked to computer and operated by the proprietary software of Schlumberger Axis through Mircosoft Windows. The package allowed live plotting during a test so as to observe and monitor the important parameters as well as being used to control the test. After the test, all the recorded data were transferred to EXCEL for analysis. Cracks and crack widths were observed during the test at each load increment and recorded manually and photographically.

5.5 Testing procedure

Ready mixed concrete of grade C25 was used for all three tests; the actual test date is governed by the compressive cube strength of the insitu infill attaining an intended value of 25N/mm^2. Load was applied in increments of 20kN per jack until the maximum load. After the maximum load was reached, a deflection criterion was used to determine the loading increments. The specimen was unloaded and reloaded after reaching maximum load so as to ascertain the unloading stiffness. Test is terminated when excessive deflection and/or cracking was detected leading to reduction of load carrying capacity.

5.6 Material Testing

Nominal material strengths were used for the design of the composite beams. These strengths were expected to differ from the actual strengths of materials used in the specimen. Material properties of the steel members, reinforcement and concrete were all tested according to the relevant BSI standards. The results were then used in the computer modelling, described in Chapter 6, to predict the flexural capacity of the composite beam.

5.6.1 Concrete

Concreteing work was carried out inside the laboratory with the specimen in the test position. Ready mixed concrete with 10mm aggregates and slump of 50mm is used and samples were cast at the same time as the specimen to monitor the concrete strength. The cylinders (150mm dia. x 300mm long) and cubes (100 x 100 x 100mm) were cured in water at an average temperature of 20^0 C. The samples were tested at intervals until the required strength is reached, all tests were carried out using a Denison compression testing machine. The compressive strength was determined from the tests on the concrete cubes and the tensile splitting strength from cylinders. The compressive and tensile strengths for all the specimens are summarized in Table 5.2 and Table 5.3, respectively.

5.6.2 Steel coupons

Six tensile test coupons (see Fig. A.1 in Appendix A) were cut from the flanges and web of the beam (3 no. from top and bottom flange and 3 no. from the web) after each test was terminated. They were sampled from the area where the stresses had been very low, i.e. at the supports, and tested in a 200kN Zwick 1484 computer controlled universal test machine at a speed of 20mm/min[(2)]. The yield strength was defined as the stress producing 0.2% residual strain. The data and standard stress-strain curves are shown in Table A.1, Fig. A.2 and A.3 in the Appendix A. The average yield strength of the specimens is 334.5 N/mm^2 and the average Young's modulus is 196.1 kN/mm^2. Therefore, the uniaxial yield strain for the beam material is taken as 1706 με.

5.6.3. Rebars

Test lengths were cut from the 8mm and 16mm diameter high tensile deformed rebar from the material used in the bending test and tested in a Zwick universal test machine according to the BSI standard[(3)]. The test results are listed in Table A.2 in the Appendix A. The yield strength is defined as the stress producing 0.2% residual strain. The average value of the yield strength for T16 rebars is 585 N/mm^2 and 473.5 N/mm^2 for the T8 rebars. The average Young's modulus for the T16 and T8 rebars are 202 kN/mm^2 and 198.3 kN/mm^2 respectively. Therefore,

the uniaxial yield strain for T16 and T8 bars is taken as 2388 με and 2896 με, respectively.

5.7 Test results

5.7.1 General flexural behaviour of composite beam

For the composite beam, the elastic neutral axis is usually close to the interface between the steel and the concrete. As the moment acting on the composite section is increased, the bottom flange of the steel beam yields and the neutral axis moves towards the compression zone, causing tensile cracking at the underside of the slab. When the stress at the outer surface of the concrete slab reaches a maximum i.e. approx. 0.67 f_{cu} , spalling of the concrete begins and the ultimate strength of the section is then fully mobilized. As the curvature of the section is further increased, the load carried remain approximately constant and crushing of the slab might occur. Failure of the shear connectors may occur between yielding of the steel and crushing of the concrete slab; this would reduce the composite action and thus the load carrying capacity of the section.

5.7.2 End slippage

When the load is applied to the beam, there is a tendency for slip to occur between the slab and the beam to which the connector is attached. This is partly due to the deformation of the concrete surrounding the shear connector and partly due to bending of the shear connector. Observations show that no slip occurred at the serviceability load (i.e. 1.0 x dead load + 1.0 x imposed load)[1]. Slip is not uniform along the length of a beam, even when the external shear force is uniform. The largest slip tends to occur near the end of the beam and is generally also the region in which slip begins. From the observation of the bending tests, the effect of slip in the working range is unlikely to be sufficiently great to be considered in design. However, slip does have considerable influence on the development of the ultimate moment capacity.

5.7.3 Test CB1

The general arrangement is shown in Fig. 5.13. T16 rebars were used as transverse reinforcement. The testing of this specimen was delayed due to unforeseeable circumstance, such that, the compressive concrete strength of the insitu infill was 32.5N/mm^2.The applied load vs. vertical mid-span deflection relationship of the beam is given in Fig. 5.14. The test began with loads at 10kN increments so that the set up could be checked. The composite beam remained elastic up to 160kN,

with a mid-span deflection of 9.0 mm. First crack was observed as the applied load reached 240kN; at this point yielding in the bottom flange and cracking in the hcu occurred. The crack appeared at the rib of the hcu near to the loading position, see Fig. 5.15. Yielding in the bottom flange of the steel section was monitored by the ERSG mounted on the steel section and the applied load vs. strain curve is shown in Fig. 5.16. The specimen was unloaded once the steel section attained first yield to monitor the unloading stiffness. A full recovery of load was observed. As the load was further increased, yielding of the steel section and cracking in the underside of the hcu extended to the full length of the slab, with a gradual reduction in stiffness. At the load reached 330kN, a sudden fracture of shear studs were observed leading to rapid reduction of load. The applied load never recovered and remained at the lower plateau with further deflection. The test was terminated with deflection in excess of 50mm. The condition of the beam after the maximum load was reached is shown in Fig. 5.17.

No surface crushing of the concrete slab was observed and the strain recorded in the concrete (i.e. 900με) indicated that the ultimate crushing stress (i.e. approx. 0.67 f_{cu}) was not reached. The applied load vs. concrete surface strain curve is shown in Fig. 5.18. Yielding or bond failure was not detected on any transverse reinforcement. Stresses developed in the rebars were less than 20% of the yield stresses, suggesting the transverse bars were not fully mobilised. The applied load vs. strain in the transverse reinforcement is shown in Fig. 5.19.

The cracking near the rib of the hcu is a consequence of yielding of the bottom flange of the steel section. This causes the neutral axis to move towards the compression zone, allowing tensile force to develop in the hcu. The strain distribution for test CB1 is shown in Fig. 5.20.

One of the most important factors in composite construction is the horizontal slip at the steel to concrete interface. A very small amount of slip, i.e. 0.5mm was observed until the failure of the shear studs, after that large slips occurred as the interaction between the steel and concrete was reduced, leading to reduction in capacity of the beam. The applied load vs. end slip is shown in Fig. 5.21.

After the bending test was completed, the test rig was re-arranged for the shear test. The shear test showed the shear force was carried mainly by the web of the steel section as expected and did not benefit from the composite section. The maximum shear strain of 750με was recorded at yield. The applied load vs. maximum principal shear strain is shown in Fig. 5.22.

After both the flexural bending test and vertical shear test were performed, the test specimen was carefully dismantled, it was found that 10 shear studs on one side of the beam between the loading point and the support were completely sheared off. This will account for the sudden reduction in capacity of the beam. Fig. 5.23 shows the steel beam after dismantling.

5.7.4 Test CB2

The setup of Test CB2 was identical to Test CB1 except that T8 transverse rebars were used instead of T16 rebars and, the compressive concrete strength was 25N/mm^2. The applied load vs. vertical mid-span deflection behaviour of the beam is indicated in Fig. 5.24. The deformation was linear up to 170kN, the design serviceability loading. (i.e. 1.0 dead load + 1.0 imposed load). The beam was unloaded to monitor the unloading stiffness; full recovery of load was observed. Hair line cracks developed at the rib of the hcu near the loading position as the applied load reached 230kN. Yielding of the bottom flange of the steel beam was recorded as before. The applied load vs. strain in the bottom flange is shown in Fig. 5.25. The reason for the crack in the rib of the hcu is the same as in Test CB1. Reductions in stiffness continued with yielding in the steel section and extended cracking in the hcu. A maximum load plateau was reached at 315kN with continuous deflection.

Yielding of the transverse reinforcement was observed as the load reached the maximum. This continued until longitudinal cracking appeared on the surface of the slab leading to rapid straining of the transverse reinforcement. Fig. 5.26 shows the applied load vs. strain of the transverse reinforcement. Tensile splitting of the concrete slab occurred due to yielding of the transverse bars, causing concrete failure around the shear studs and a gradual reduction in load carrying capacity to a lower plateau of 245kN. The load remained constant with continuous deflection

in excess of 60mm at mid span. The test was terminated when no further increase in load capacity was possible.

Concrete cracking is observed at the surface as maximum stresses was reached and indicated in the applied load vs. concrete surface strain curve in Fig. 5.27. No fracture of the headed stud was recorded in this test as failure of the steel concrete interface was governed by the crushing of the concrete around the headed studs. An end slip of 2.5mm is recorded at the maximum load, indicating that a large slip is not required before maximum bending capacity is achieved. Fig. 5.28 shows the load slip curve of Test CB2 and the strain distribution of the test CB2 is shown in Fig. 5.29.

5.7.5 Test CB3

The applied load vs. vertical mid-span deflection curve for this beam is given in Fig. 5.30. The main characteristic difference noticed from the introduction of the pre-cracked joint was the position of the neutral axis from the start of the test, which was located in the web of the steel section about 20mm below the steel concrete interface. The position of the neutral axis may be determined from the strain distributions shown in Fig. 5.31. Although deformation remained linear up to 100kN, the position of the neutral axis moved from 20mm to 58mm below the steel concrete interface which suggested a reduction of the effective concrete

section. As soon as the loading commenced, fine cracks appeared immediately along the pre-cracked joints and a reduction of initial stiffness of 25% was noticed as compared to the Test CB2. A high value of strain was recorded on the surface of the concrete at the applied load of only 100kN, Fig. 5.32 shows the applied load vs. concrete surface strain. High strains in excess of 1000με were also recorded in the transverse reinforcement at this stage. The applied load v strain curve of the transverse reinforcement is shown in Fig.5.33. The specimen was unloaded to observe the unloading stiffness. Gradual reductions in stiffness continued until crushing on the top surface of the slab near the load point began as the applied load reached 230kN. The load reached a maximum with continuous crushing of the slab, yielding of the bottom flange of the steel beam was also detected. Applied load vs. strain of the steel bottom flange is shown in Fig. 5.34. Cracks extended around the loading points and longitudinally along the slab, see Fig. 5.35. Transverse reinforcement was also fully yielded at this stage leading to further tensile splitting of the slab. Crushing of concrete was observed in the mid-span region of the beam.

A slip of 3mm was recorded at the maximum load with no fracture of any of the studs throughout the test. Fig. 5.36 shows the applied load vs. slip curve of the Test CB3. The maximum load of 230kN was maintained with deflections well in excess of 50mm as a ductile mode of failure was observed. A crack in the transverse joint between the hcu's was noticed in the later stage of the test but no crack in the rib of the hcu was detected, see Fig. 5.37. After the test was

terminated, the specimen was carefully dismantled. It was found that all shear connectors were intact with only slight deflections noticed.

5.8 Comparison of test results

5.8.1 Moment deflection characteristic

The results of the full scale flexural bending tests are given in Table 5.4 with moment vs. deflection curves shown in Fig. 5.38. The moment deflection curve of the bare steel UB obtained from finite element analysis is included for comparison. Increased moment capacity M_R and flexural stiffness of the composite beams compared to the bare steel UB is apparent. The sudden reduction in strength in Test CB1 was due to fracture of the shear studs at one end of the beam. The reduction in strength in Test CB2 was due to yielding of the transverse reinforcement which led to failure of concrete around the studs. A gradual reduction of strength is noted compare to the sudden loss of strength which happened in Test CB1. In both cases, maximum M_R had been attained, based on the theoretical calculations of the composite beam described in Chapter 8. The span/deflection ratio when this occurred was about 175:1 and 150:1 for Test CB1 and Test CB2, respectively, i.e. much less than the allowable limit of 360:1 used in the limit state design[1]. The stiffness of the pre-cracked specimen CB3 was approximately 75% of that in the former tests, and the moment capacity was

approximate 69% of the Test CB2, indicating a reduction in both stiffness and load carrying capacity when the bonded insitu / precast joint is destroyed.

5.8.2 Interface slip

The load-end slip relationships for all three tests are shown in Table 5.4 and in Fig. 5.39 and Fig. 5.40. Very little slip was observed in Test CB1 until fracture of the shear connectors occurred, indicating the brittle mode of failure. At the post-fracture condition, a large slip occurred leading to rapid loss of stiffness. The slip measured at the maximum load was less than 0.4mm. By comparison, a much higher slip was recorded for both test CB2 and CB3 at maximum load, Slips of 2.6mm and 5.9mm were noted at maximum load for test CB2 and CB3, respectively. It is also interesting to note that the slip increased much more rapidly in test CB3 than test CB2, especially at the lower loads. (e.g. At 100kN, by a factor of 10)

5.8.3. Rebars and concrete strains

The applied load vs. strain curves of the transverse reinforcement of all three tests are shown in Fig. 5.41. In Test CB1, the area of transverse reinforcement was equivalent to 0.45% of the concrete area. With the high percentage of transverse

reinforcement, the concrete splitting force was heavily restrained around the studs leading to fracture of the studs and a sudden reduction in load carrying capacity of the composite beam. T8 rebars were used in both test CB2 and CB3, equivalent to a percentage of 0.11% of the concrete area. In Test CB3, where a pre-cracked joint was introduced, no bonding or aggregate interlocking was allowed between the insitu / precast concrete interface, strain in transverse reinforcement was noticed as soon as the load was applied whereas a small amount of strain was recorded in test CB2 until the load reached 230kN, which is after failure of bond strength and aggregate interlocking. This shows that the bonding between the insitu / precast joint greatly contributes to the initial stiffness of the beam.

The applied load vs. longitudinal concrete surface strain relationships for all three tests are shown in Fig. 5.42. The strain for tests CB1 and CB2 is relatively similar, with concrete strain in test CB2 reaching a maximum value at the maximum load. Maximum strain in the concrete is not achieved in test CB1. The gradient of the load-strain curve for CB1 and CB2 is almost identical, with that of CB1 being slightly greater. This is possibly due to the increase in strength of insitu concrete of CB1. The gradient of test CB3 is in contrast lower than both CB1 and CB2. The result suggested a reduction of the effective concrete slab width for CB3 and the importance of the precast insitu joint to the composite slab.

5.8.4 Position of neutral axis

The positions of the neutral axis for all specimens are shown in Fig. 5.43 to Fig. 5.45. All the beams exhibited generally similar behaviour except test CB3, where the neutral axis moved upward as the bottom flange of the steel section began to yield. In contrast, neutral axis of test CB3 moved downward as soon as the load was applied and was located in the web throughout the test.

In Test CB1, the neutral axis remained at approximately 25mm above the steel concrete interface at maximum load until the sudden loss of shear studs leading to loss of interaction, and hence the sudden movement in the position of the neutral axis. In Test CB2, again the loss of interaction between the steel and concrete led to the neutral axis moving into the steel web. With the pre-cracked joint introduced in Test CB3, the position of the neutral axis was in the web of the steel section at the beginning of the test as shown in Fig. 5.45. It suggested that the effective breadth of the concrete section was greatly reduced compared with the test CB2, due to the introduction of the pre-cracked joint. The neutral axis moved further downward to the web as the pre-cracked joint opened up. The neutral axis remained at the position of 70mm below the interface until the maximum stress in the concrete was reached causing the neutral axis to move further down to the steel section. At failure, the position of the neutral axis was approximately 85mm below the interface.

5.9 Conclusions

Three full scale bending tests were carried out and the experimental behaviour of each test is fully described in this chapter. Two modes of failure were observed: (a) Sudden failure due to loss of shear studs and (b) Tensile failure of concrete due to yielding of the transverse reinforcement. The former is associated with beams having a high percentage of transverse reinforcement. The residual moment capacity of all the beams was at least 40% above the moment capacity of the bare steel beam. A beam with a pre-cracked insitu / precast concrete joint was tested and the result showed a reduction in both the stiffness and the moment capacity. The results of these tests were used to validate the finite element beam model described in Chapter 6.

5.10 References

1. BS5950, Part 1 (1990) Structural Use of Steelwork in Building, British Standards Institution, London.

2. BS EN 10002-1, Part 1 (1990) Tensile Testing of Metallic Material, British Standards Institution, London.

3. BS 4449 (1988) Carbon Steel Bars for the reinforcement of Concrete, British Standards Institution, London.

Test Ref.	Hollow Core Unit	Insitu Concrete Strength	Transverse Reinforcement	Percentage of area of steel, A_s/A_c
CB1	Bison 150mm hcu	32 N/mm2	T16 at 300 mm c/c	0.45%
CB2	Bison 150mm hcu	25 N/mm2	T8 at 300 mm c/c	0.11%
CB3	Bison 150mm hcu	28 N/ mm2	T8 at 300 mm c/c (Pre-cracked)	0.11%

Table 5.1 Test parameters for composite beam tests

Test Ref. (Test date)	Compressive Strength (N/mm²)								
	7 Days			Test Days			28 Days		
	1	2	Ave.	1	2	Ave.	1	2	Ave.
CB1 (8 Days)	30.6	30.8	30.7	31.0	33.0	32.5	43.0	44.0	43.5
CB2 (8 Days)	25.4	25.5	25.5	25.6	25.5	25.5	34.5	35.5	35.0
CB3 (7 Days)	27.5	28.5	28.0	27.5	28.5	28.0	36.5	38.5	37.5

Table 5.2 Insitu concrete infill compressive strength

Test Ref. (Test date)	Tensile Splitting Strength (N/mm²)								
	7 Days			Test Days			28 Days		
	1	2	Ave.	1	2	Ave.	1	2	Ave.
CB1 (8 Days)	2.65	2.75	2.70	2.75	2.85	2.80	3.00	3.10	3.05
CB2 (8 Days)	2.15	2.25	2.20	2.20	2.30	2.25	2.65	2.55	2.60
CB3 (7 Days)	2.30	2.20	2.25	2.30	2.20	2.25	2.85	2.75	2.80

Table 5.3 Insitu concrete infill tensile splitting strength

Test Reference	At first yield				At maximum load			
	Moment (kNm)	Mid-span Deflection (mm)	Stiffness, M_y/δ (kNm/mm)	End slip (mm)	Moment (kNm)	Mid-span Deflection (mm)	M_y/δ (kNm/mm)	End slip (mm)
CB1	372.8	16.07	23.2	0.2	497.3	31.9	15.6	0.4
CB2	355.8	15.83	22.5	0.6	474.0	36.4	13.0	2.6
CB3	311.8	20.3	15.4	2.3	361.5	50.1	7.2	5.9
Bare Steel (ABAQUS)	193.8	25.11	7.7	N/A	244.2	51.4	4.8	N/A

Table 5.4 Flexural bending test results

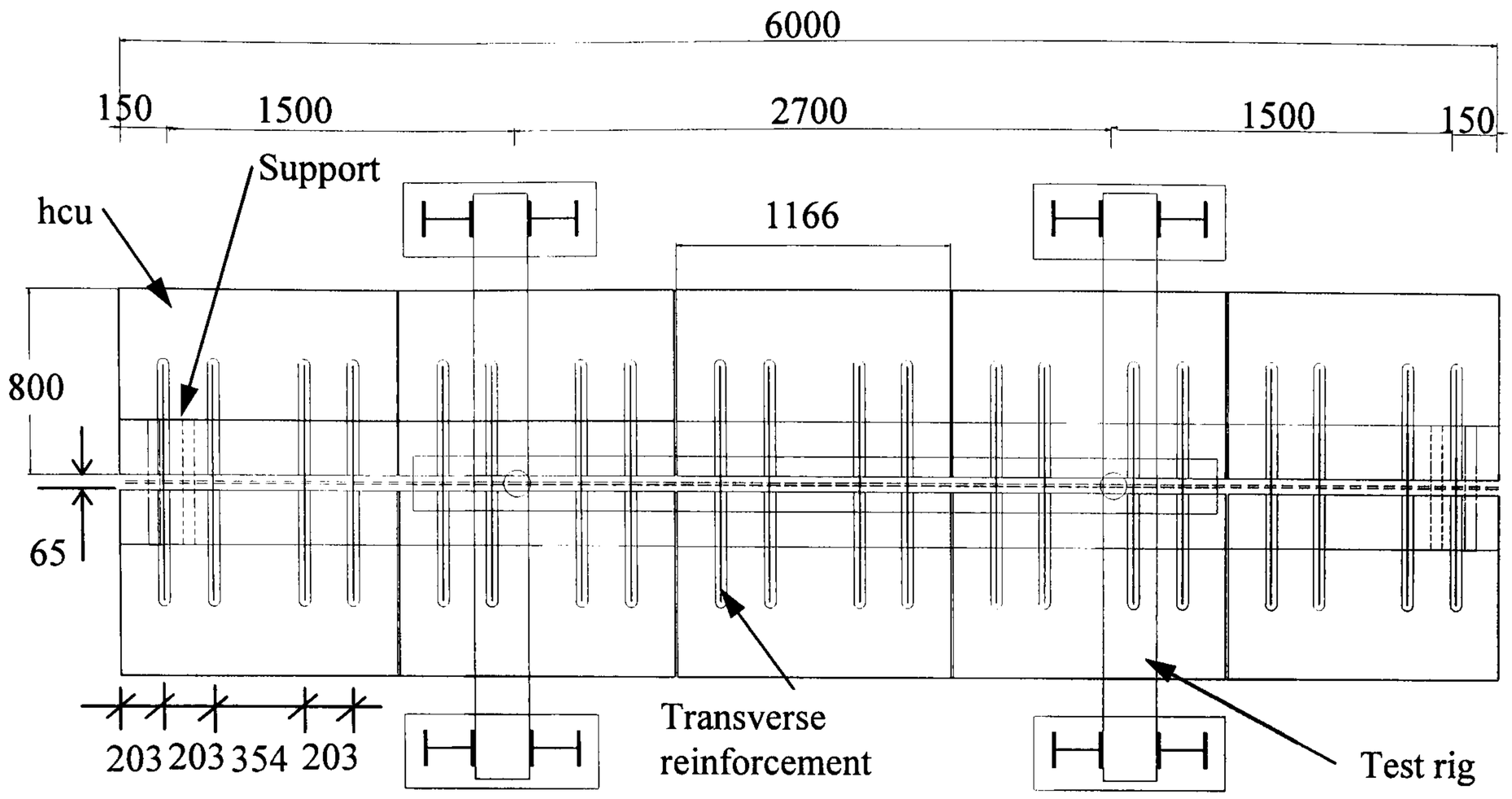

Fig. 5.1 Plan view of the beam test

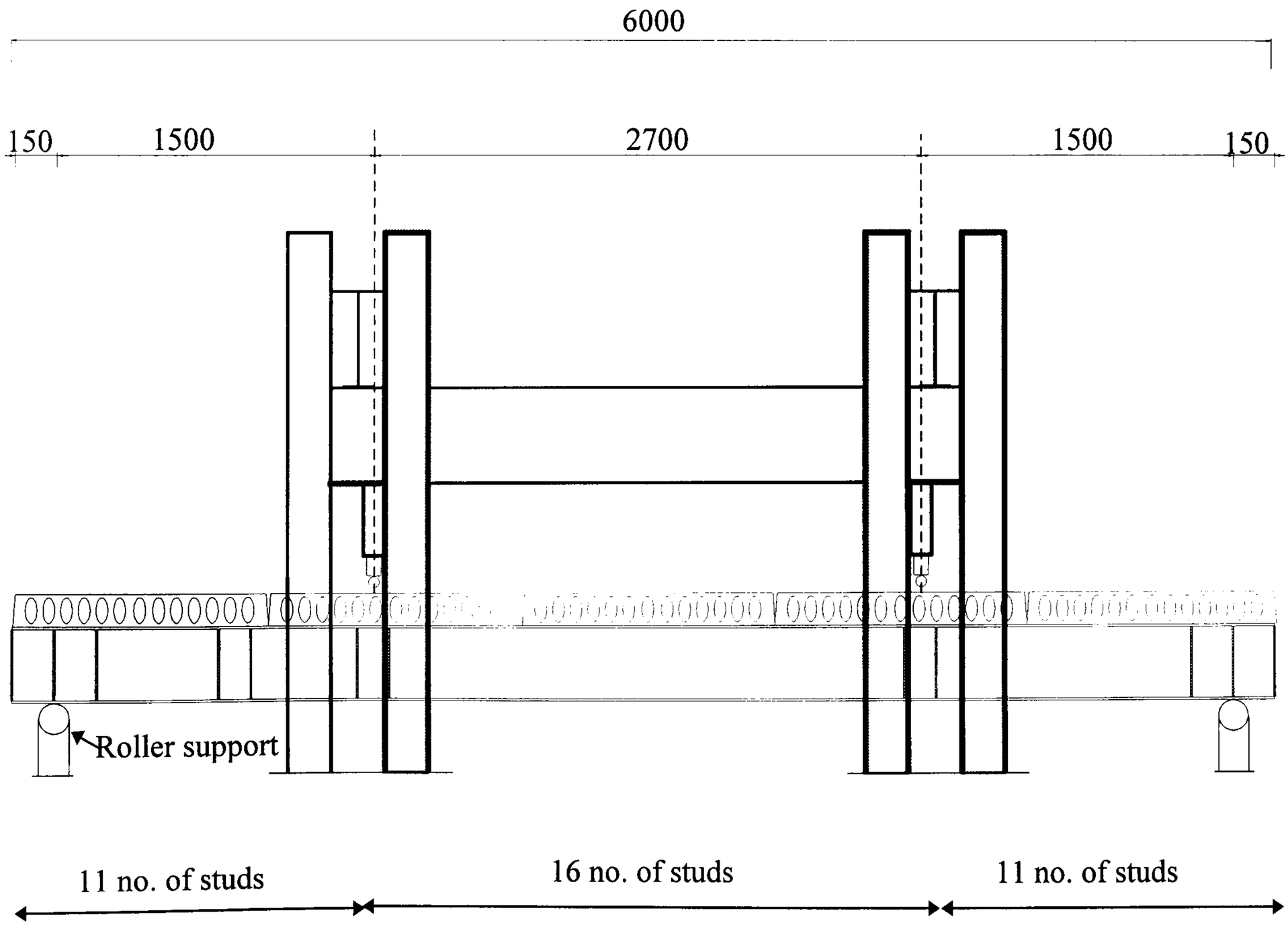

Fig. 5.2 Elevation view of beam test

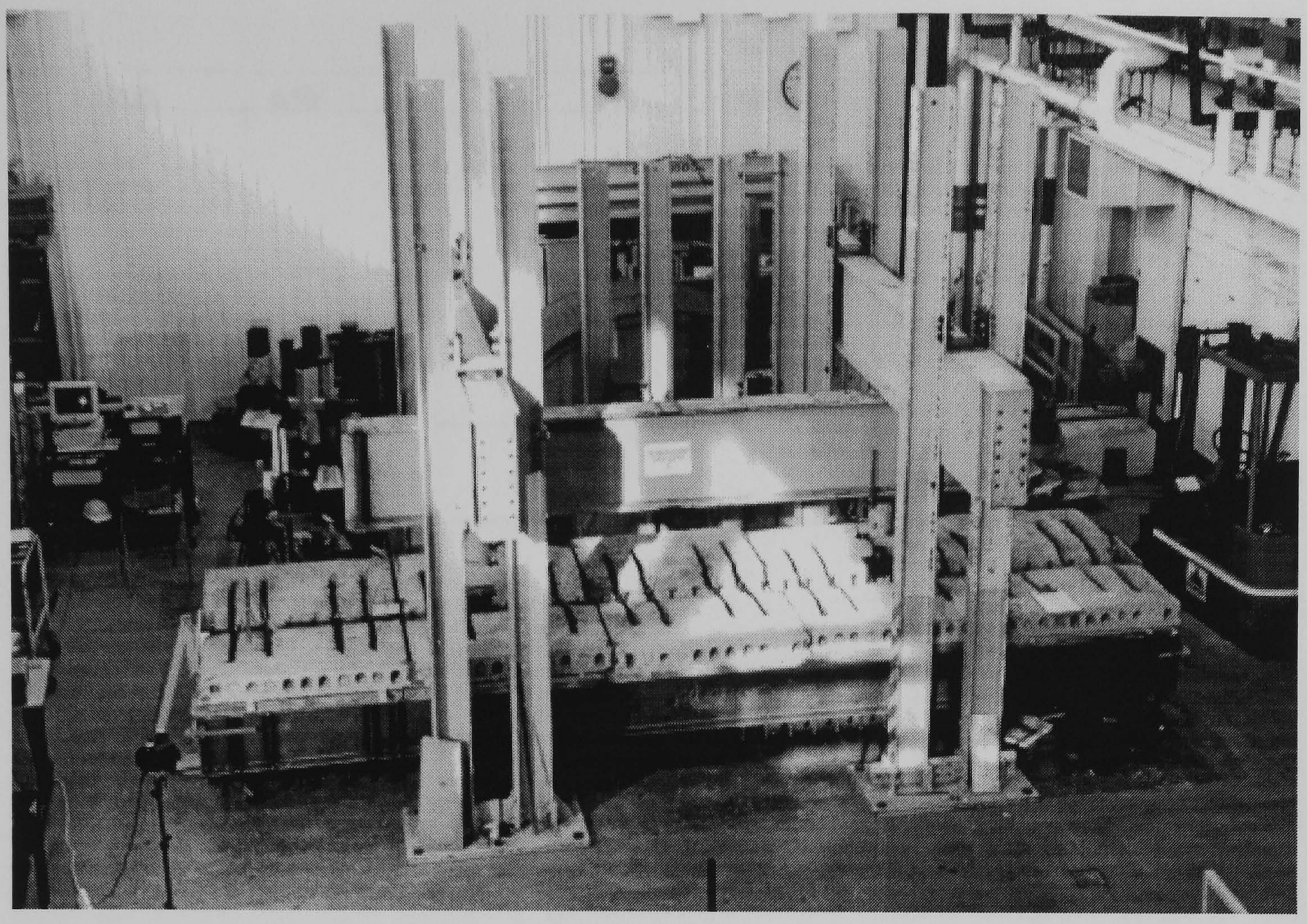

Fig.5.3 Test specimen before insitu infill cast

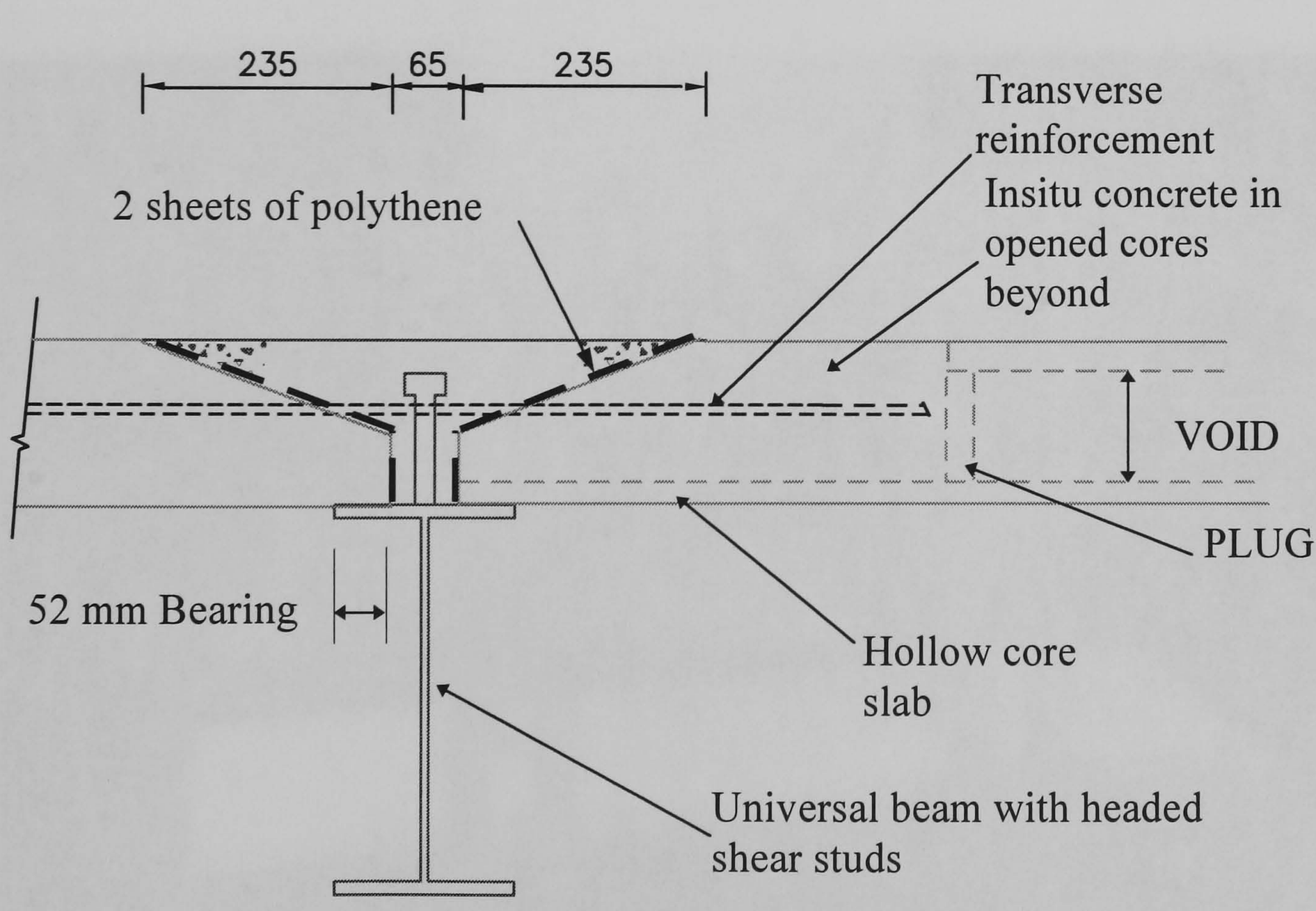

Fig. 5.4 Composite beam with debonded insitu joint

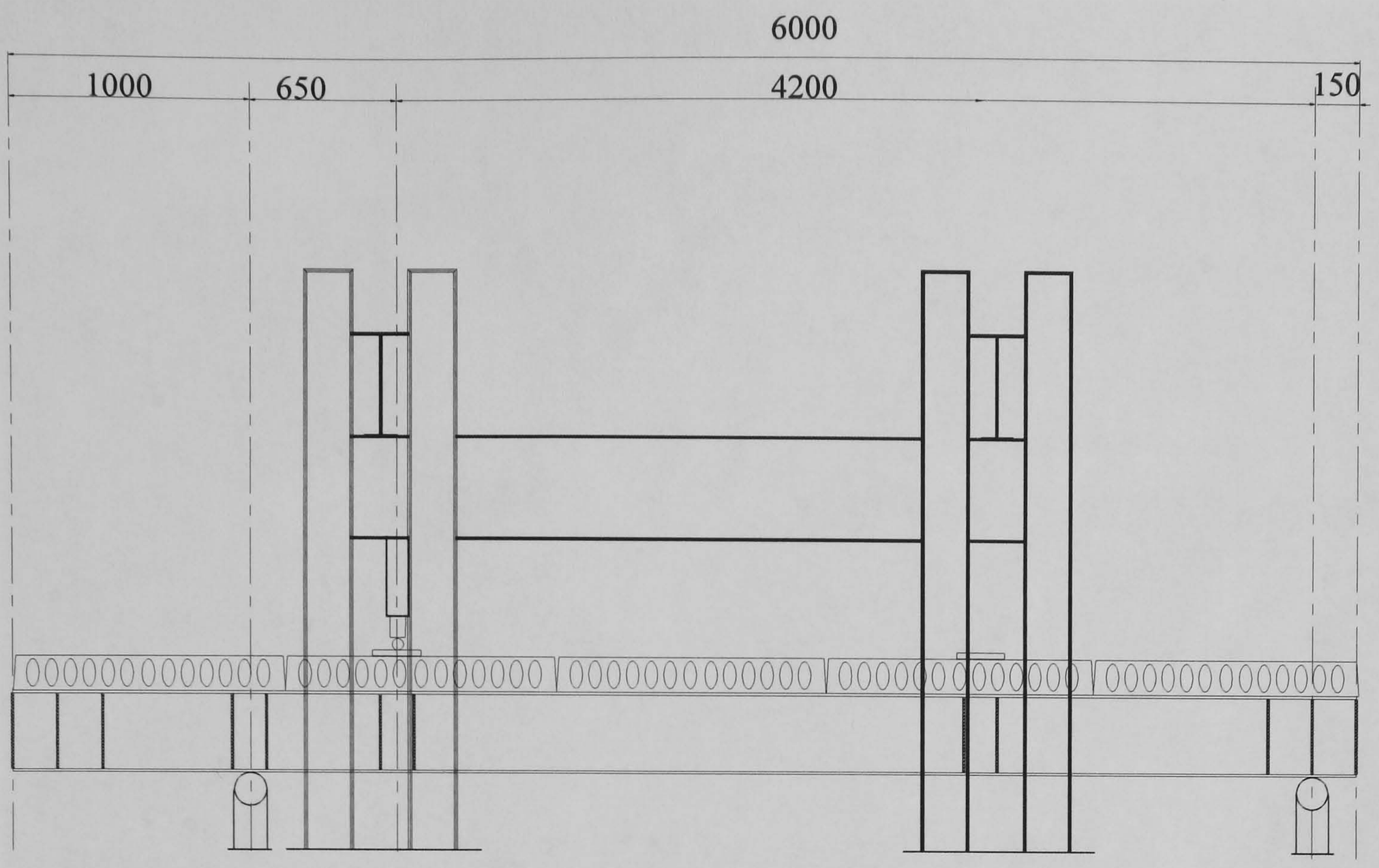

Fig. 5.5 General arrangement of shear test

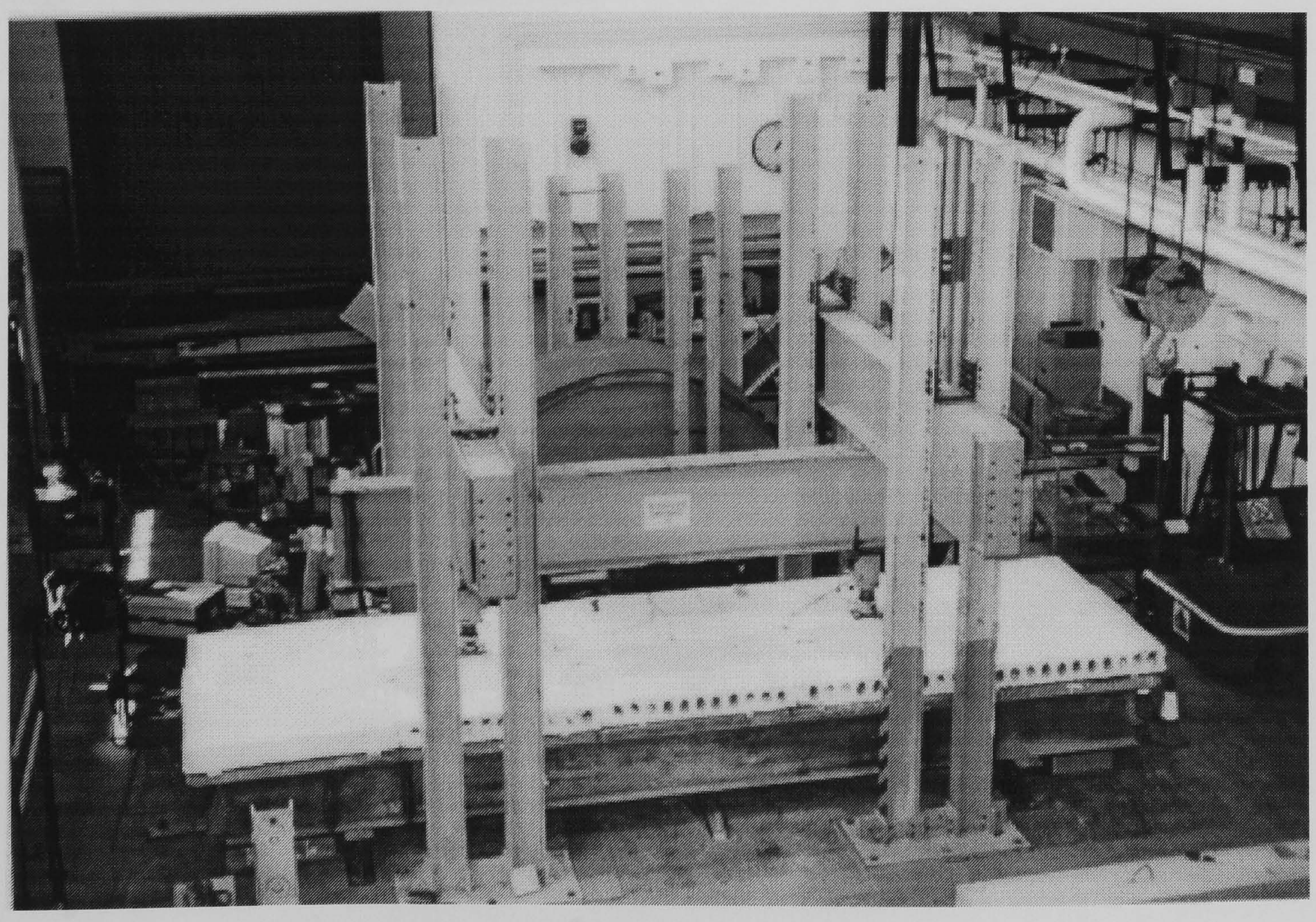

Fig. 5.6 Details of test rig

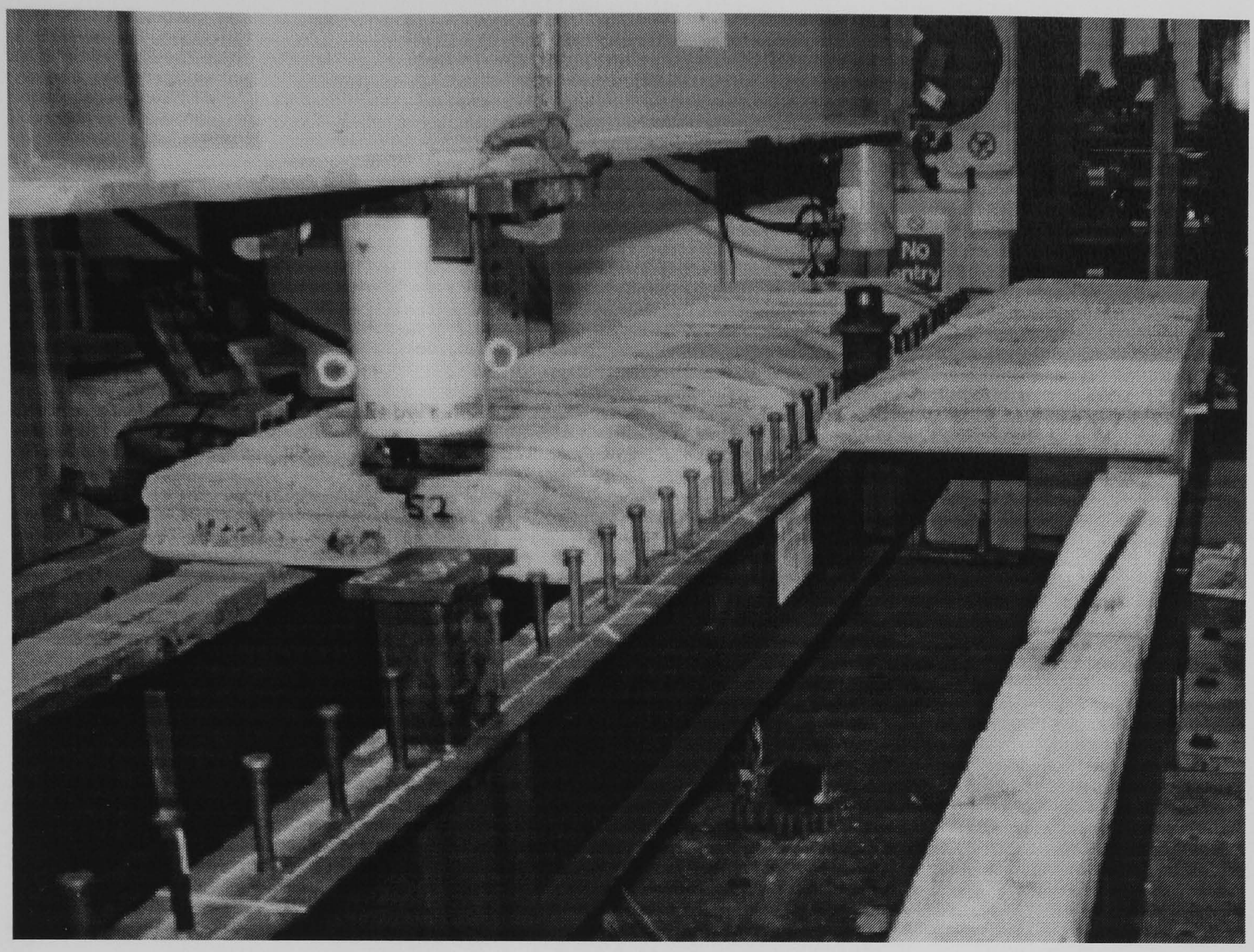

Fig. 5.7 Details of loading arrangement

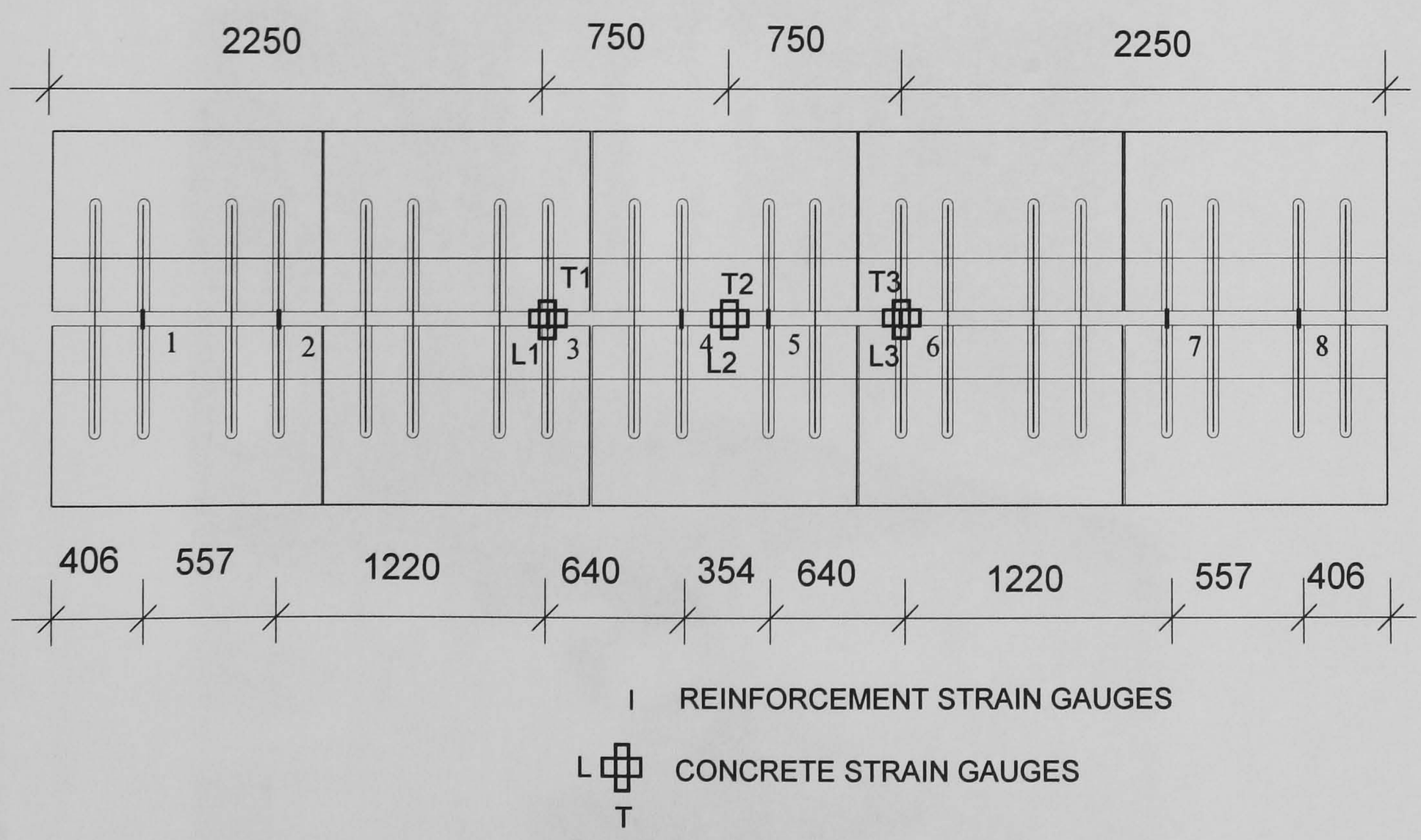

Fig. 5.8 Positions of concrete and transverse reinforcement gauges

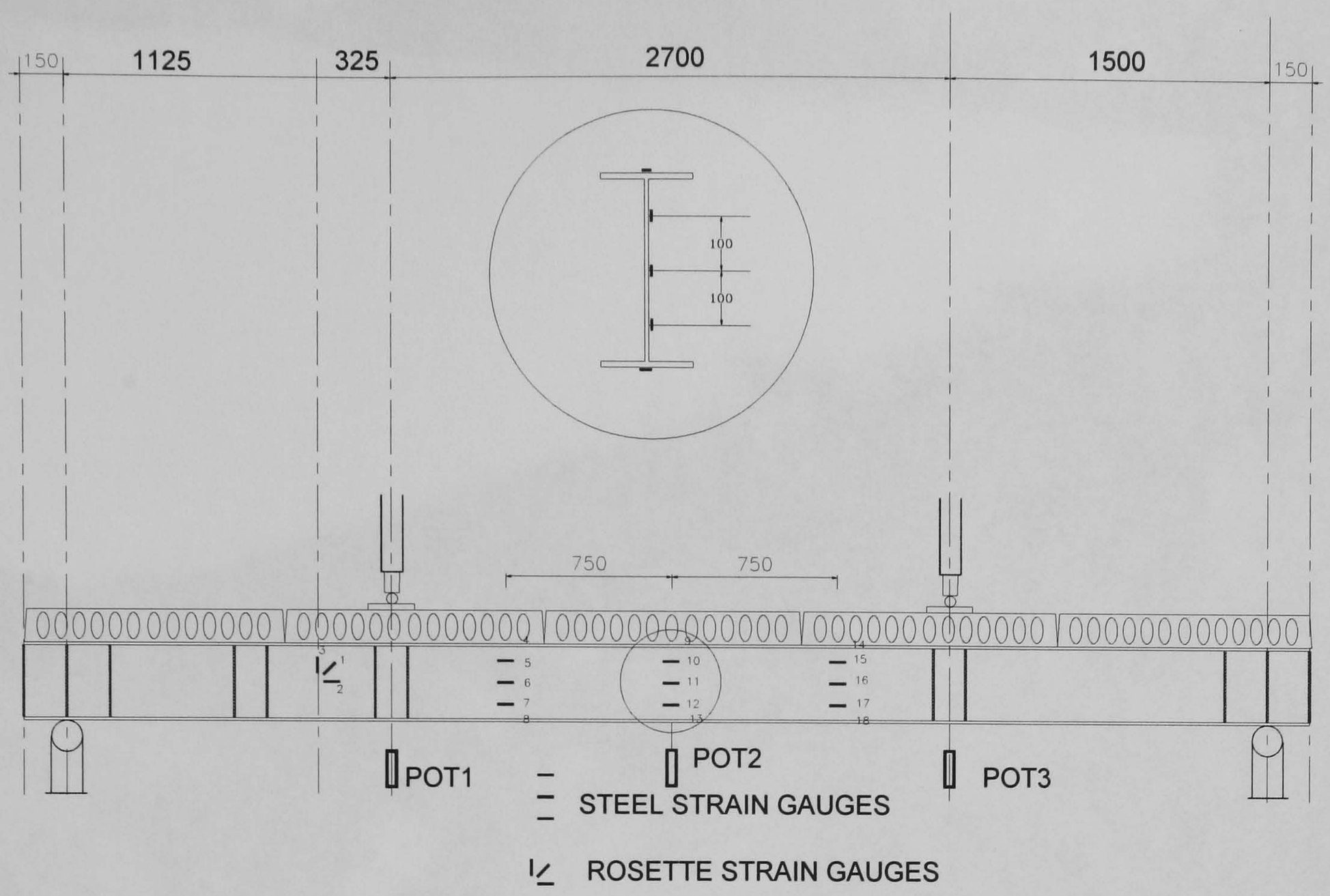

Fig. 5.9 Positions of strain gauges and potentiometers on steel

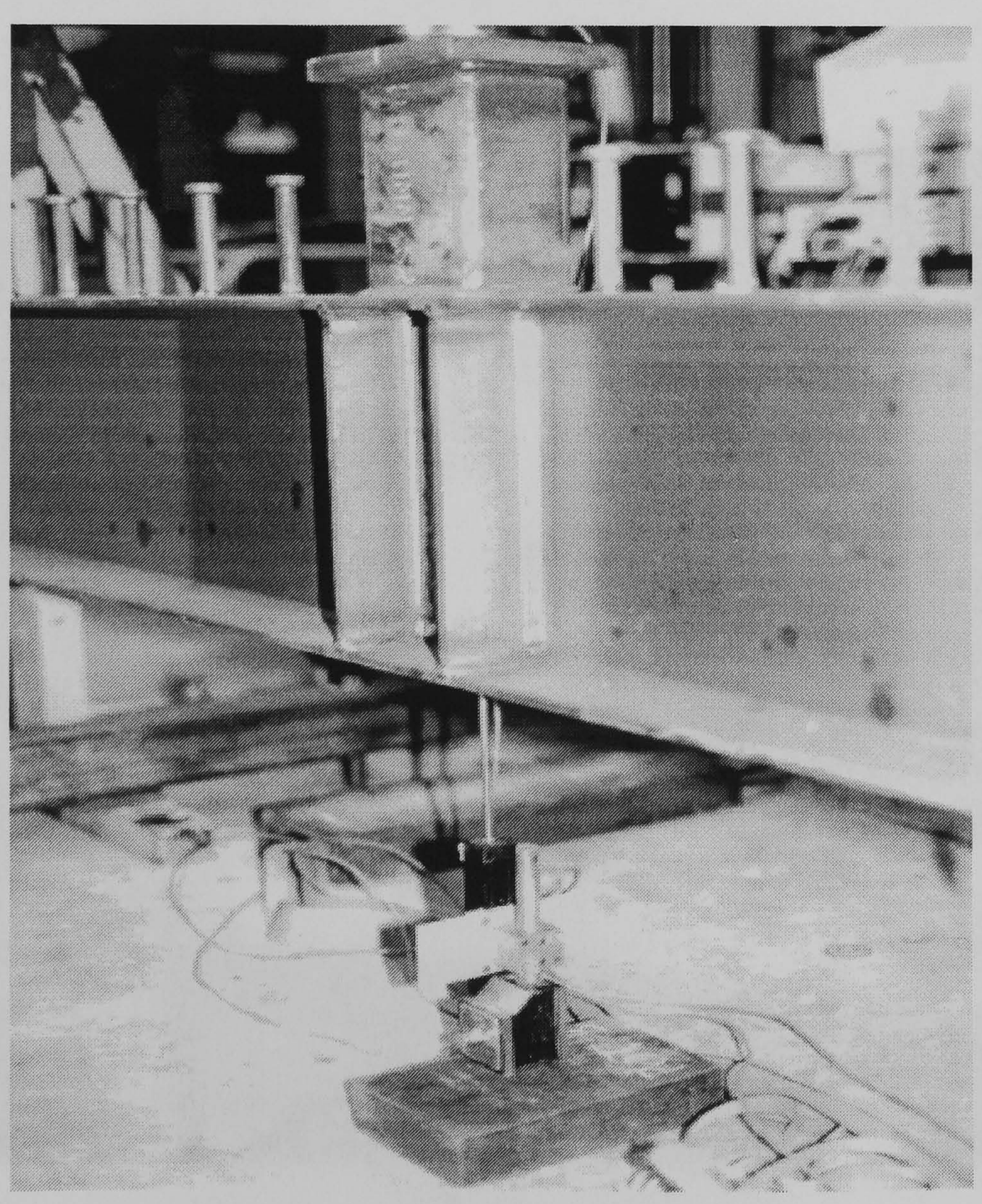

Fig. 5.10 Potentiometer used for measuring deflection

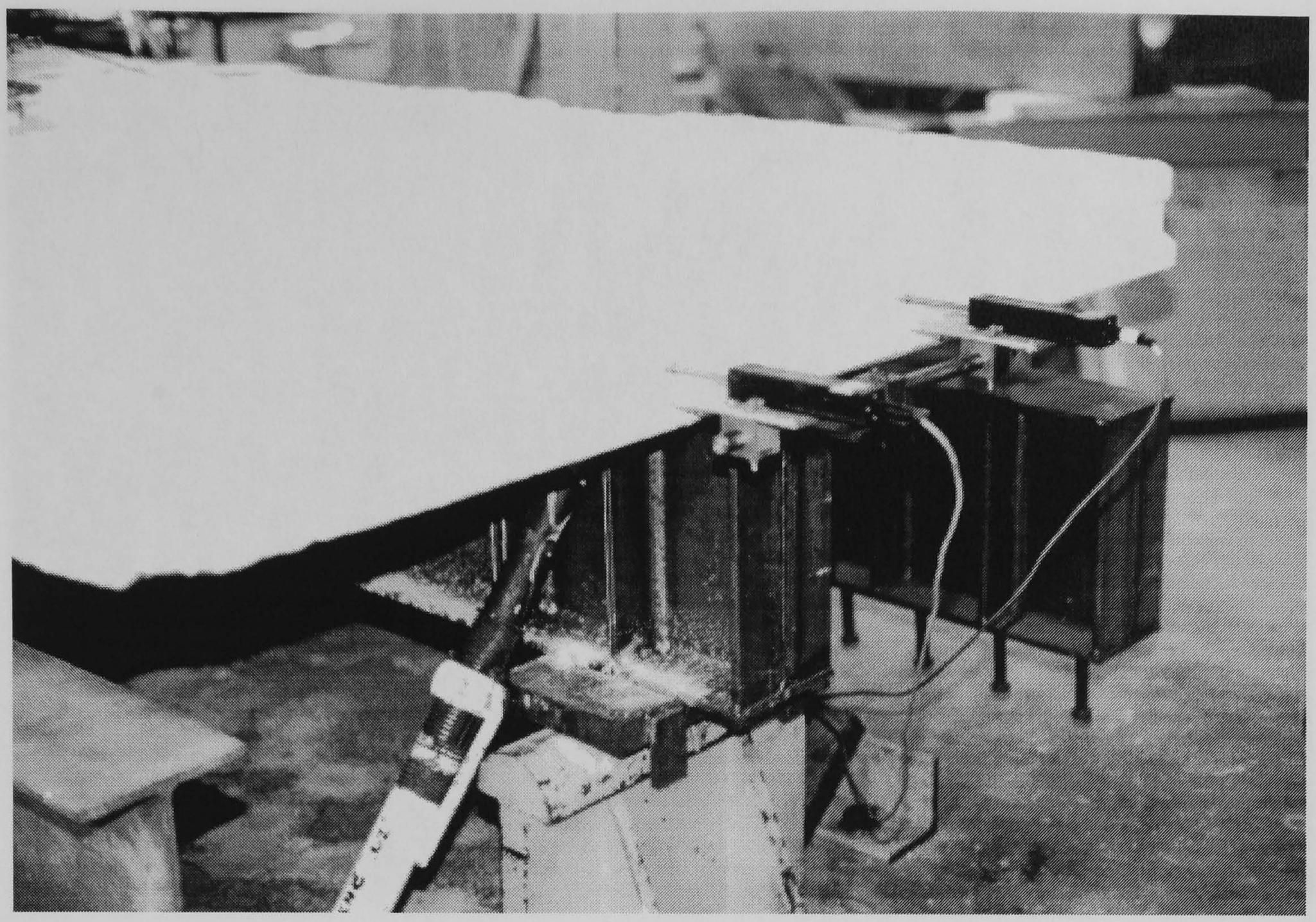

Fig.5.11 Potentiometers used for measuring end slip

Fig.5.12 Data logger and computer link system used for the beam tests

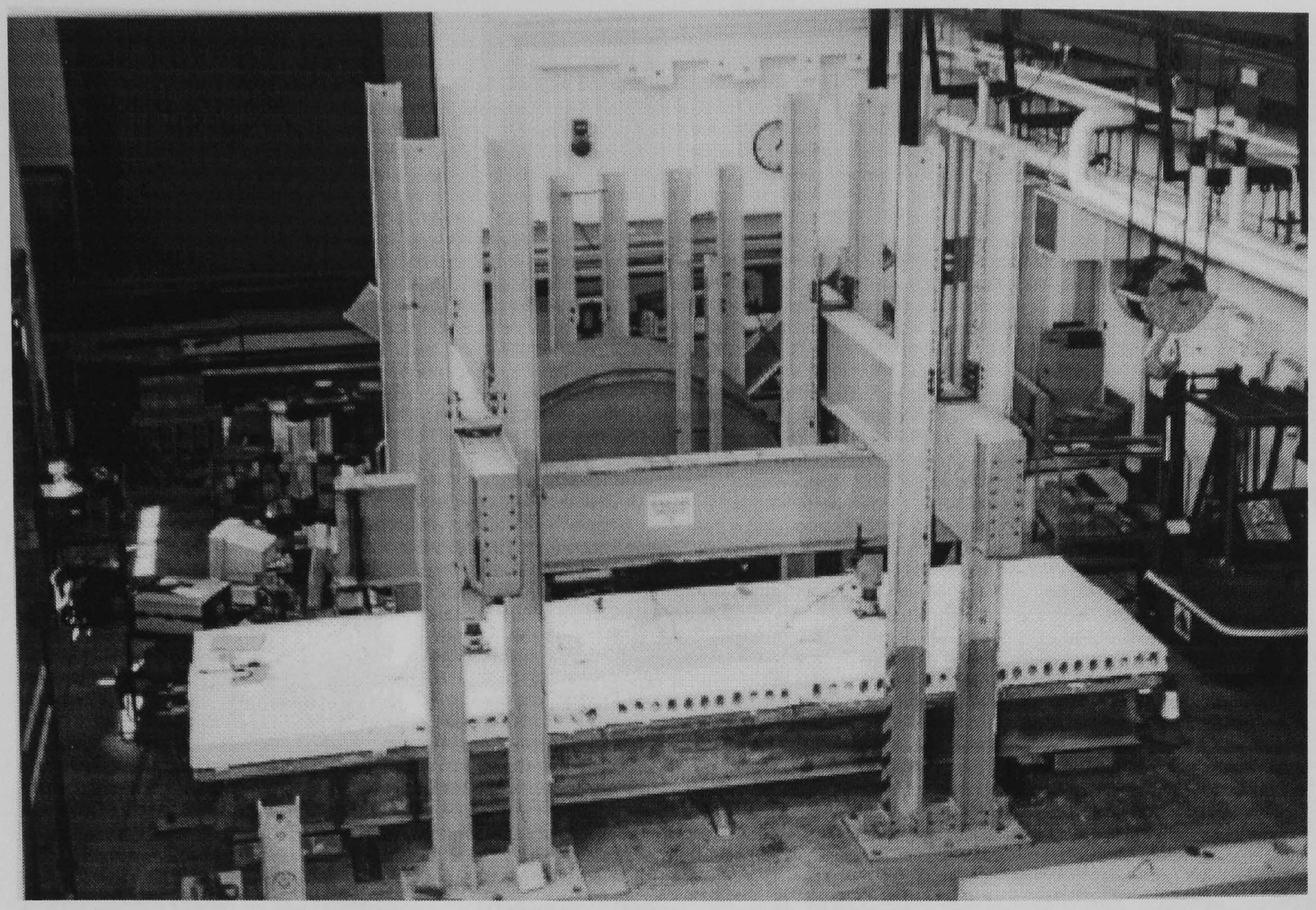

Fig. 5.13 General arrangement of Test CB1

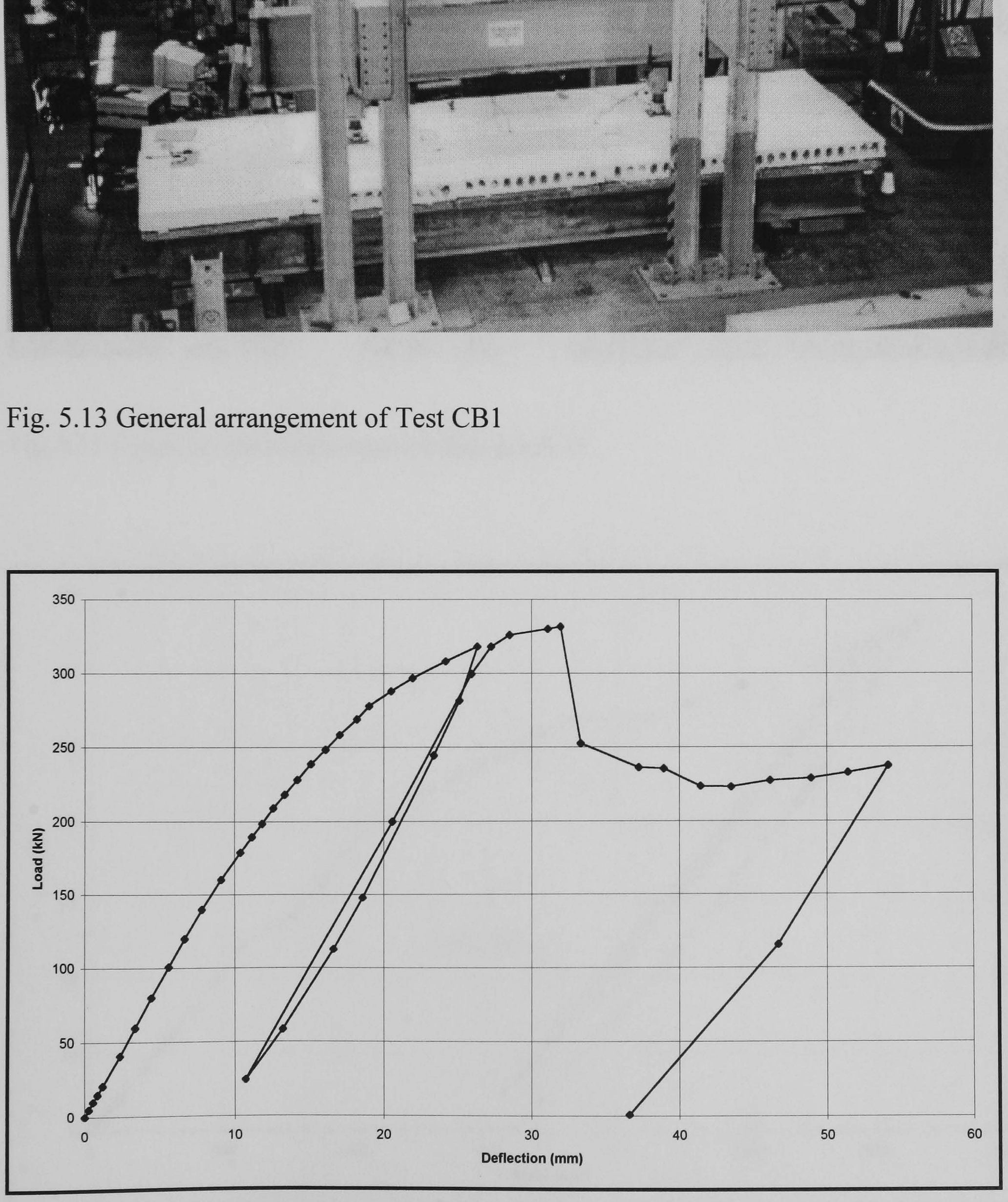

Fig. 5.14 Applied load vs. mid-span vertical deflection curve of Test CB1

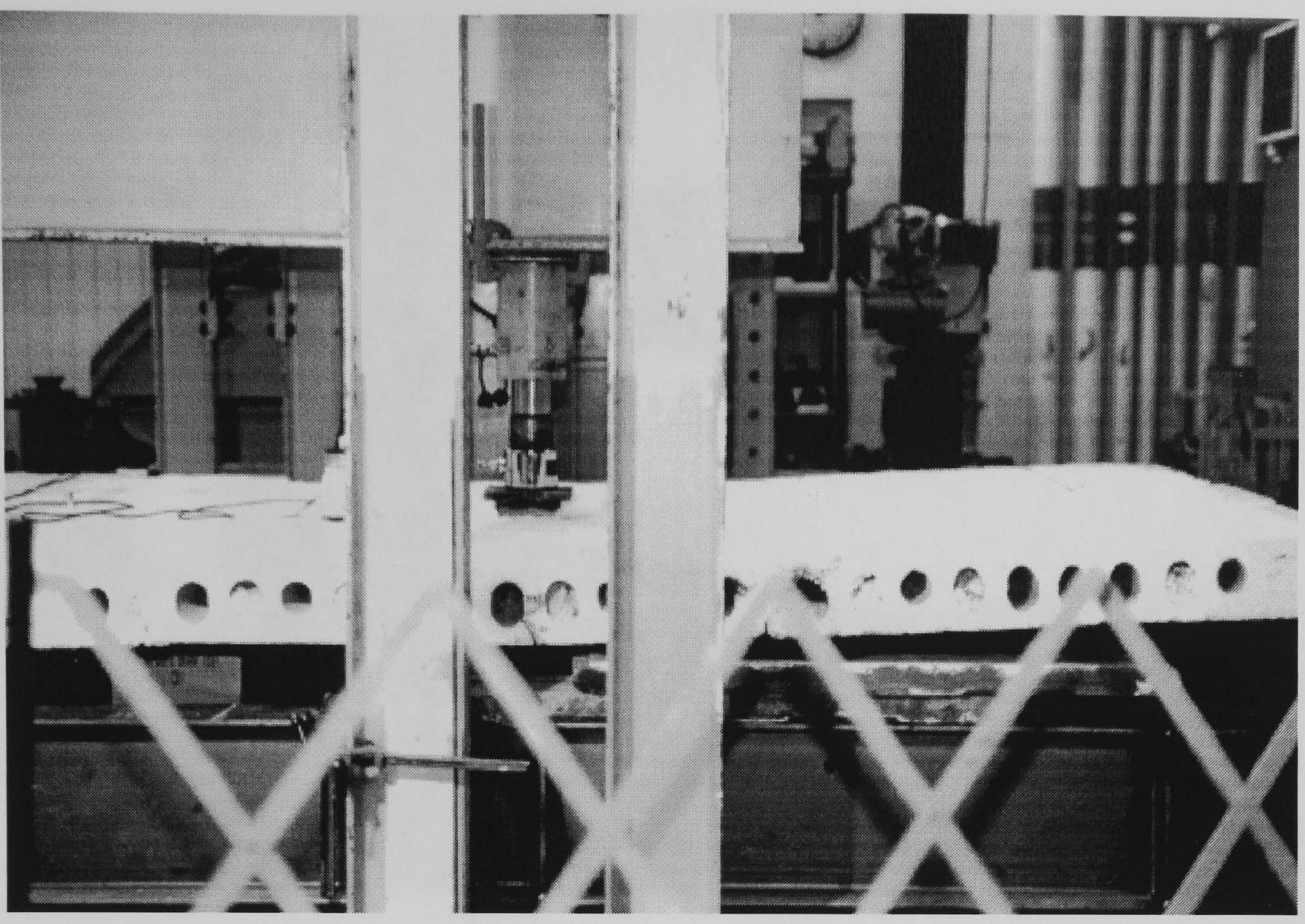

Fig.5.15 Crack at ribs of hcu near loading position

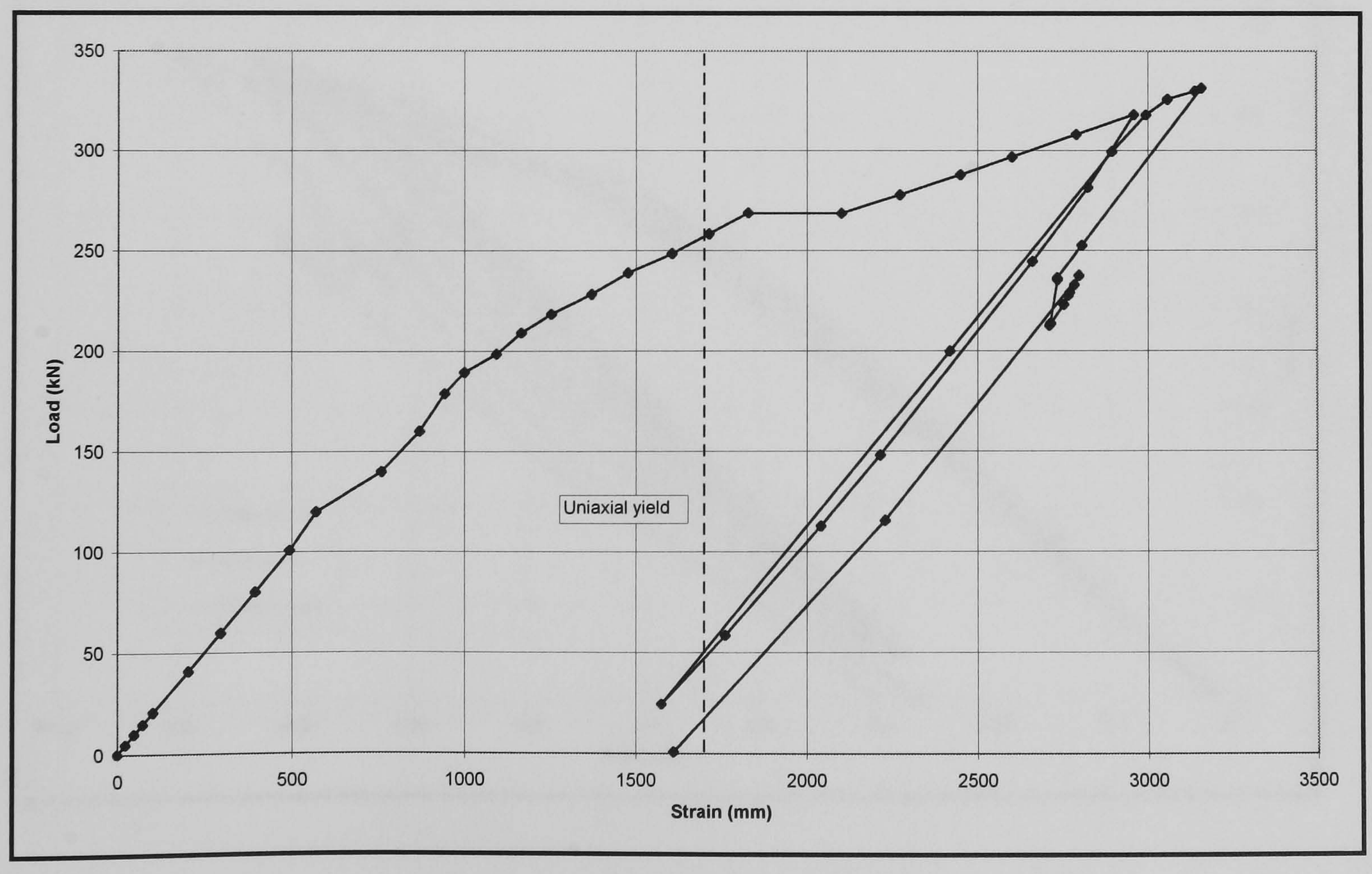

Fig.5.16 Applied load vs. strain in steel bottom flange at mid span of Test CB1

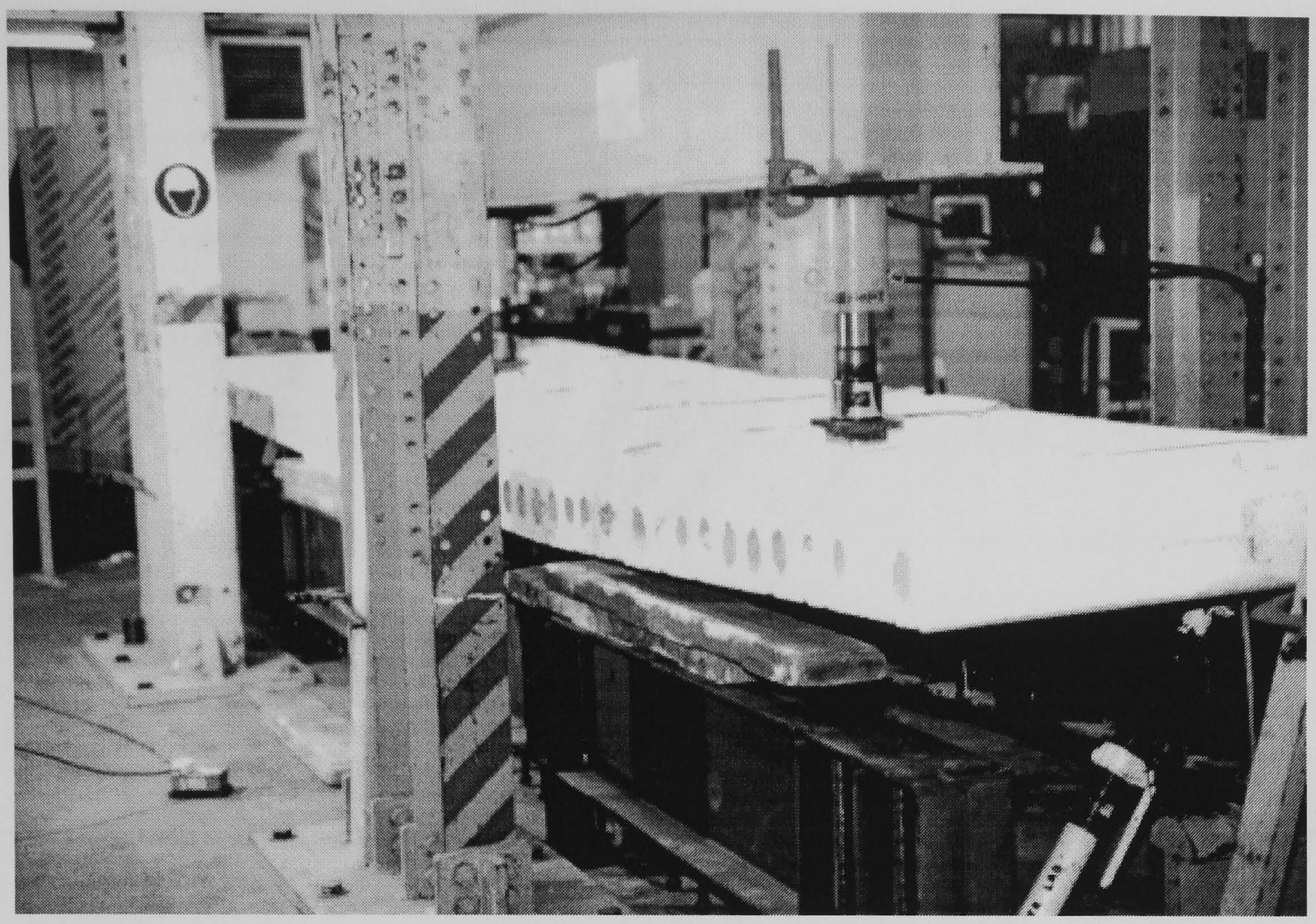

Fig.5.17 Deflection at end of beam at maximum load

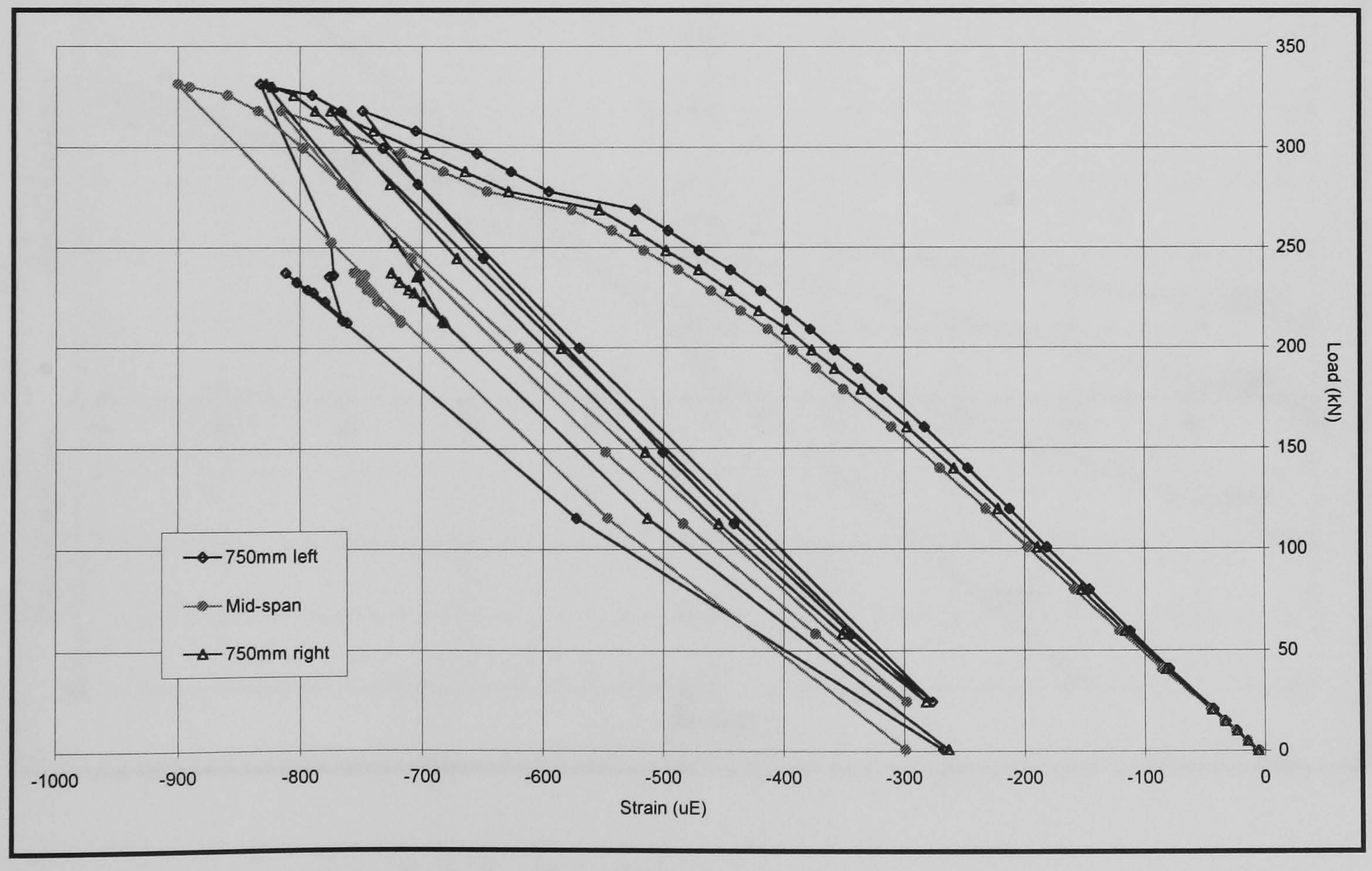

Fig.5.18 Applied load vs. concrete surface strain of Test CB1

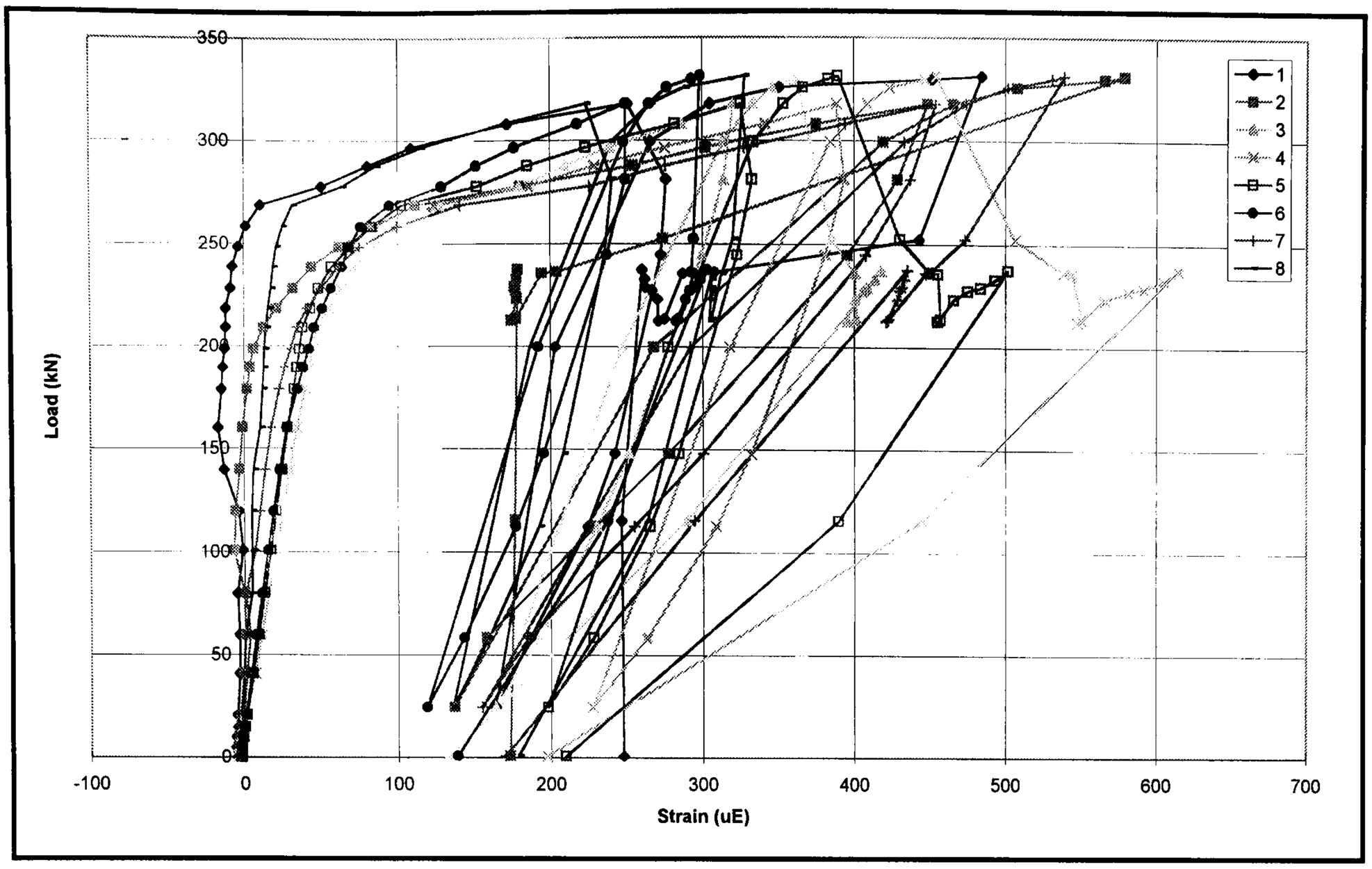

Fig. 5.19 Applied load vs. strain of transverse reinforcement of Test CB1

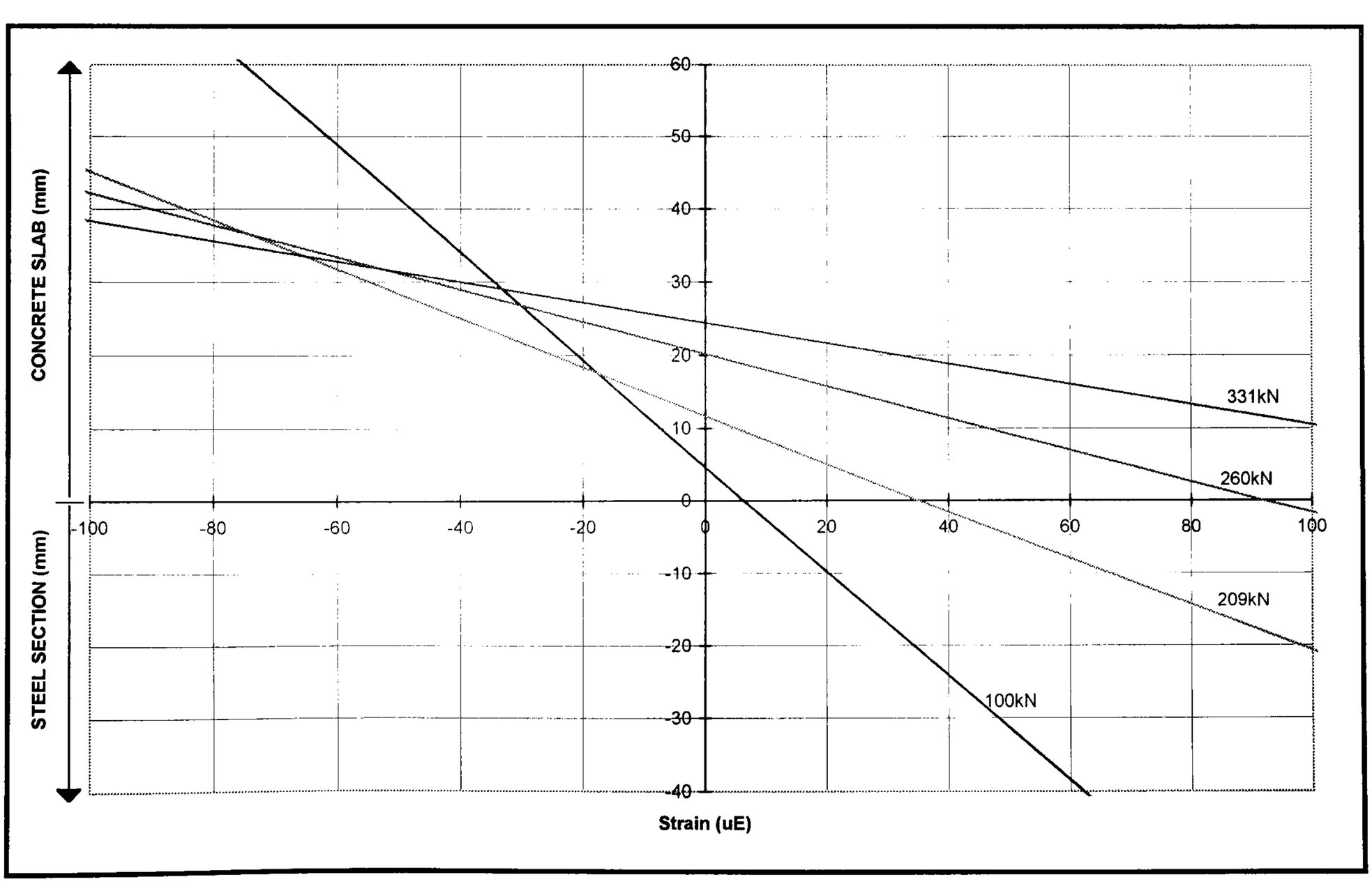

Fig. 5.20 Strain distributions for Test CB1

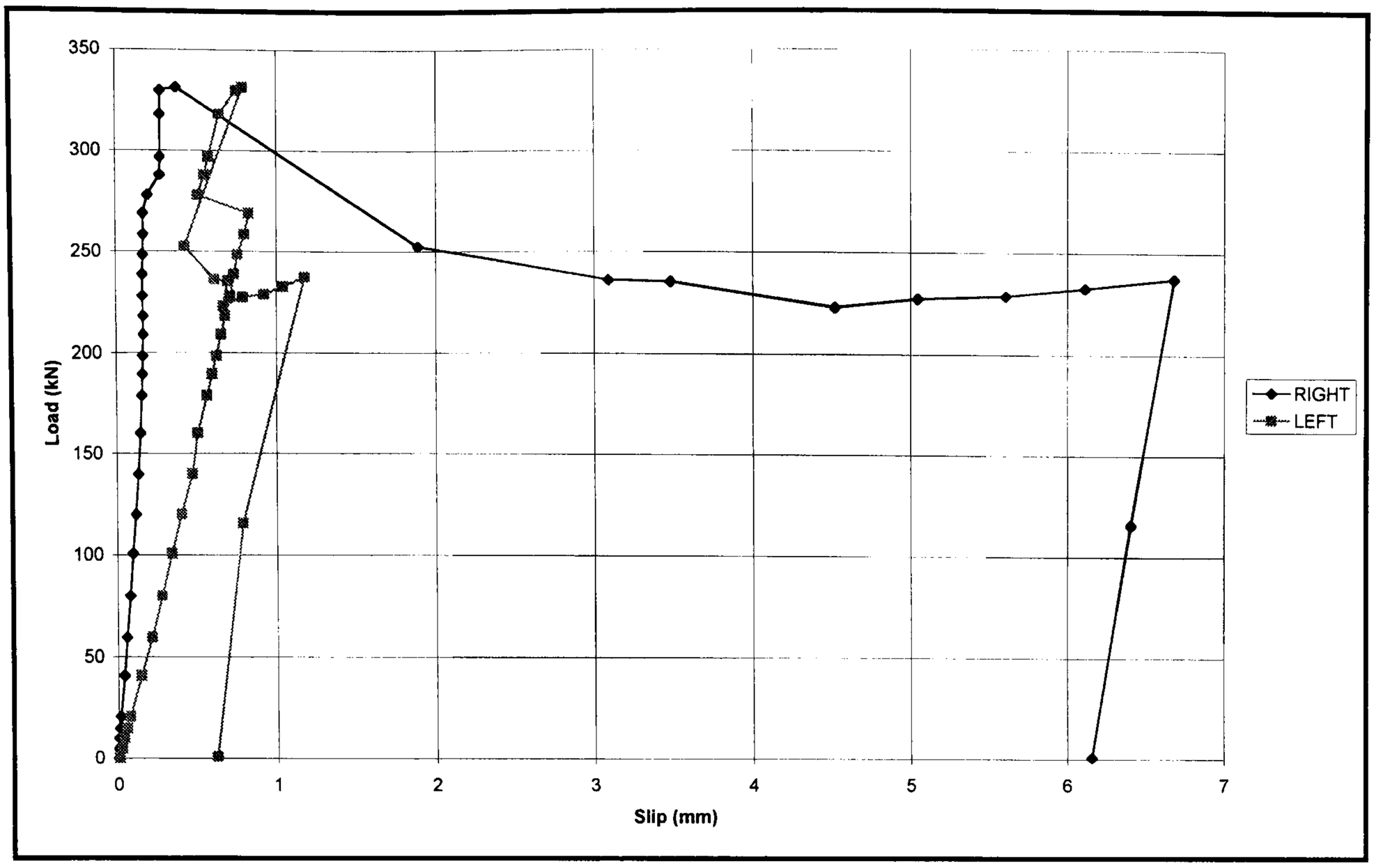

Fig.5.21 Applied load vs. end slip of Test CB1

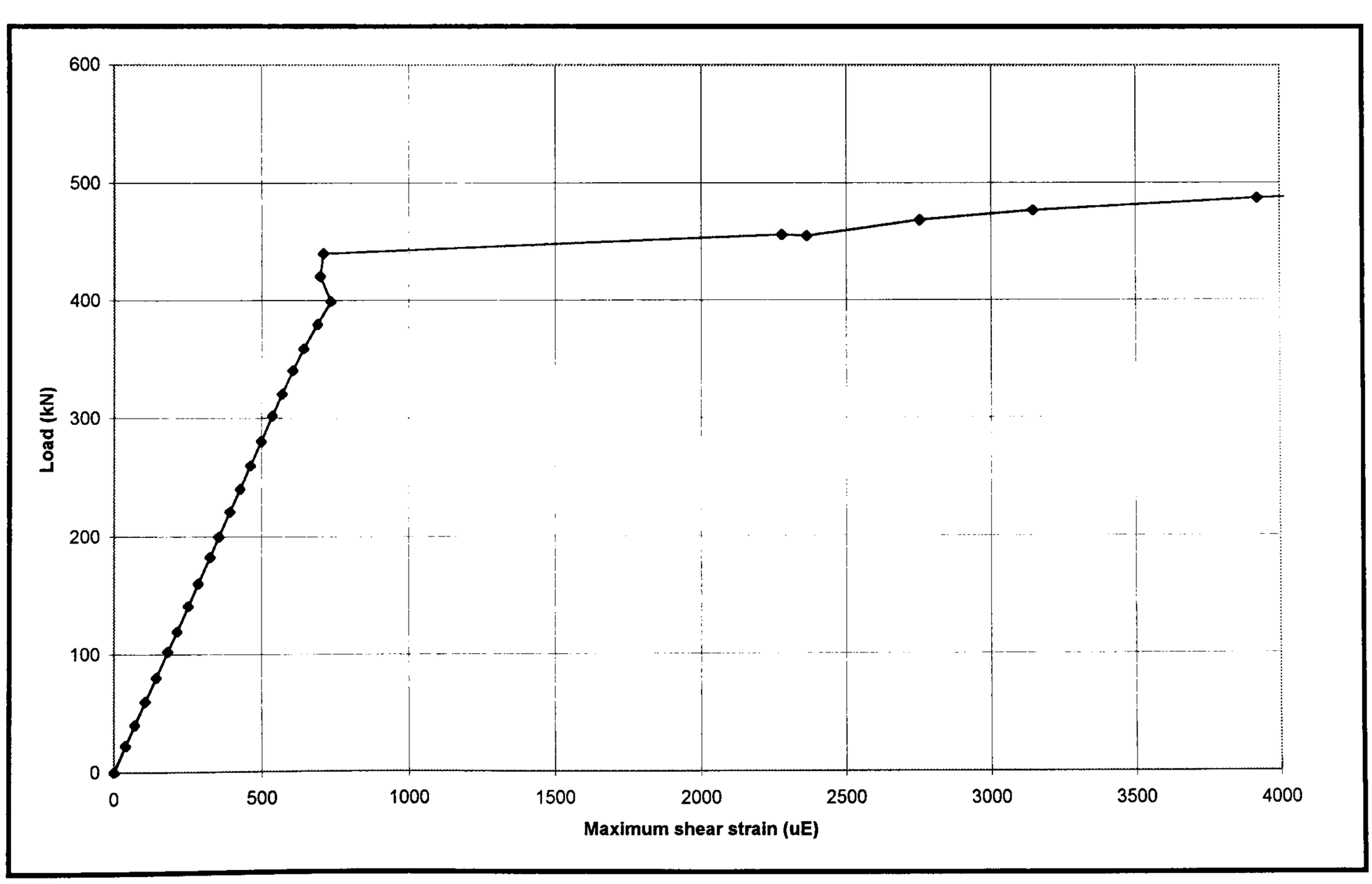

Fig. 5.22 Applied load vs. maximum shear strain of Test CB1

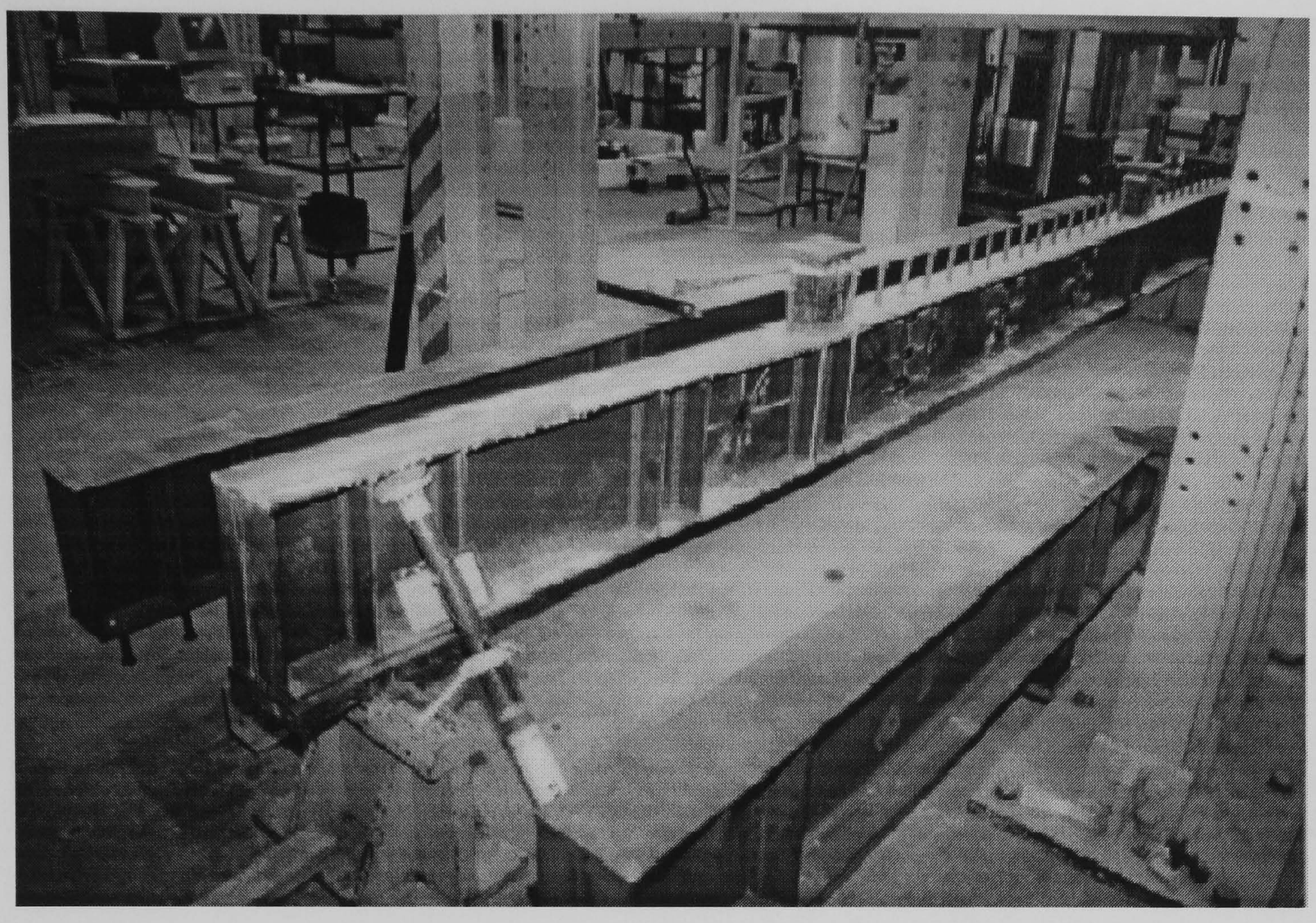

Fig. 5.23 Steel beam after slabs dismantled

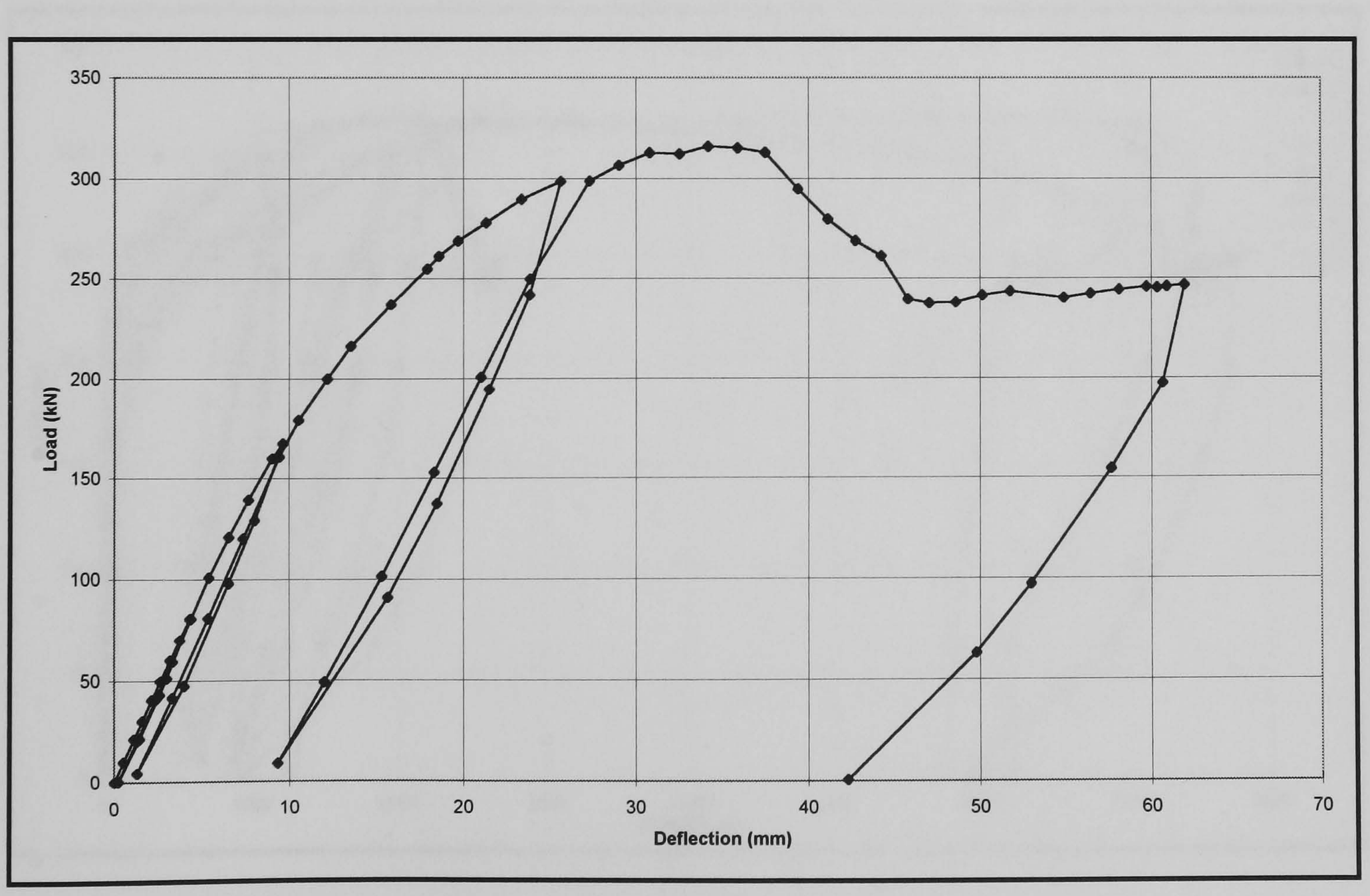

Fig. 5.24 Applied load vs. vertical mid-span deflection of Test CB2

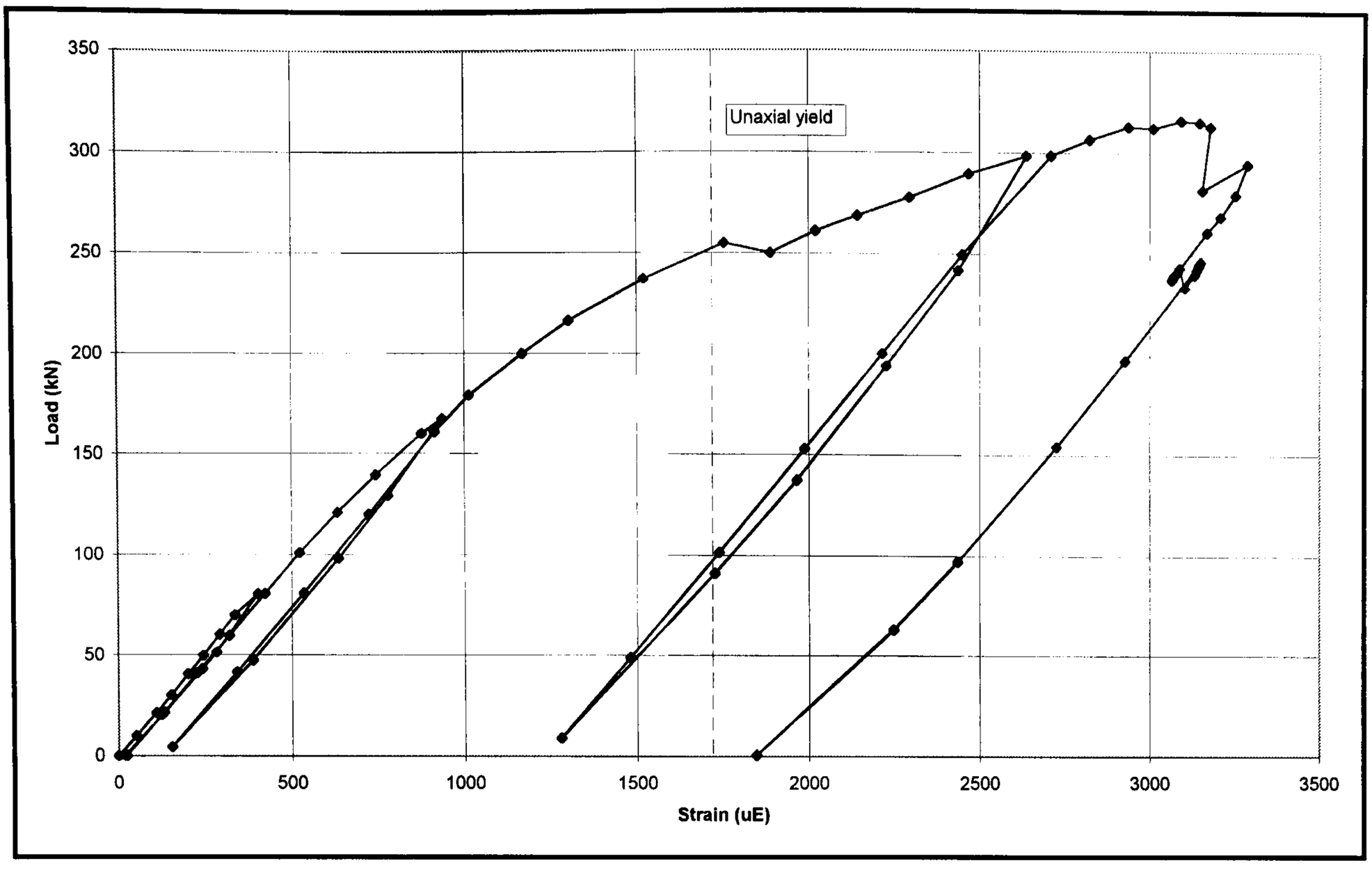

Fig. 5.25 Applied load vs. strain of steel bottom flange at mid span of Test CB2

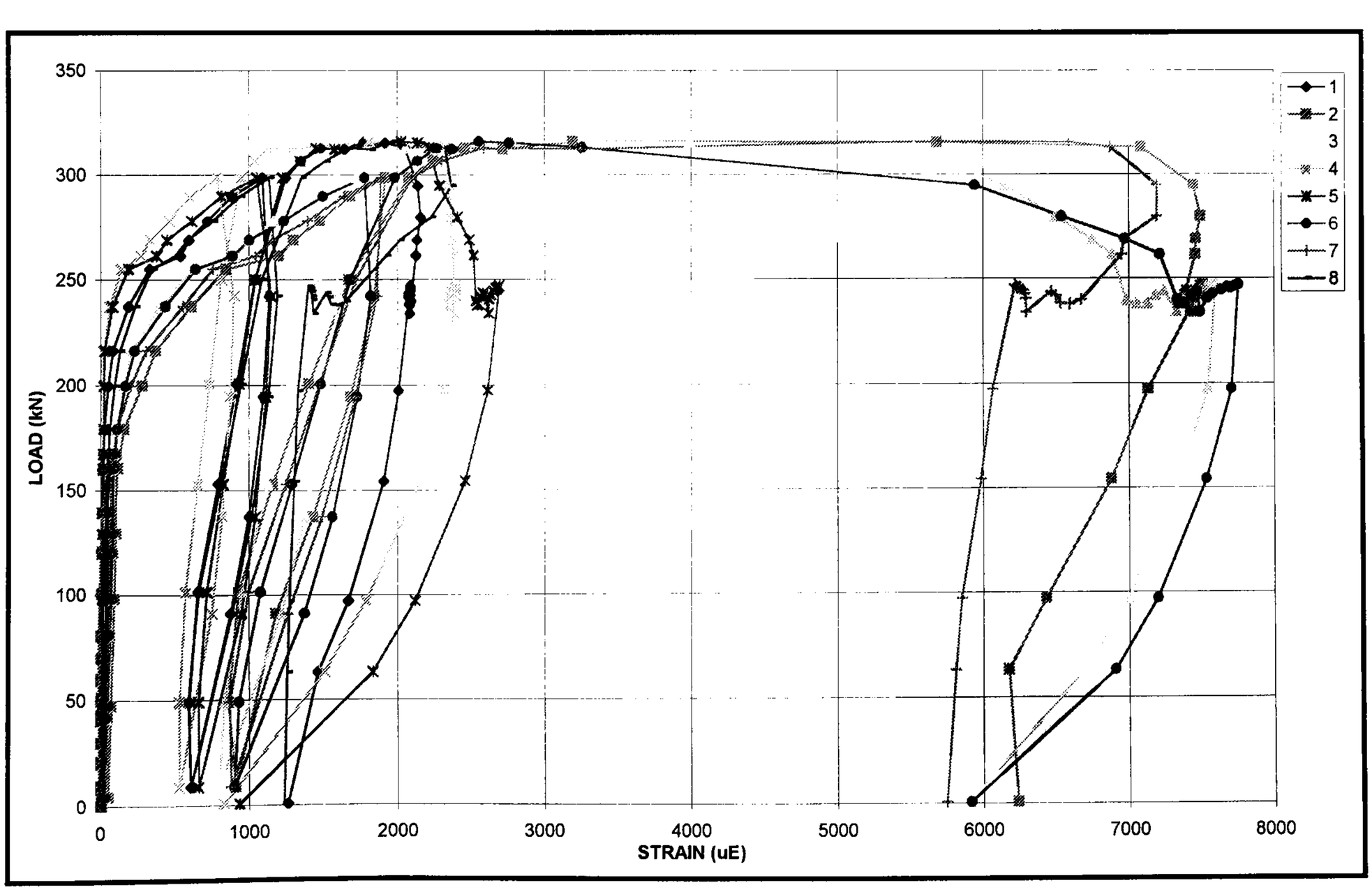

Fig. 5.26 Applied load vs. transverse reinforcement strain of Test CB2

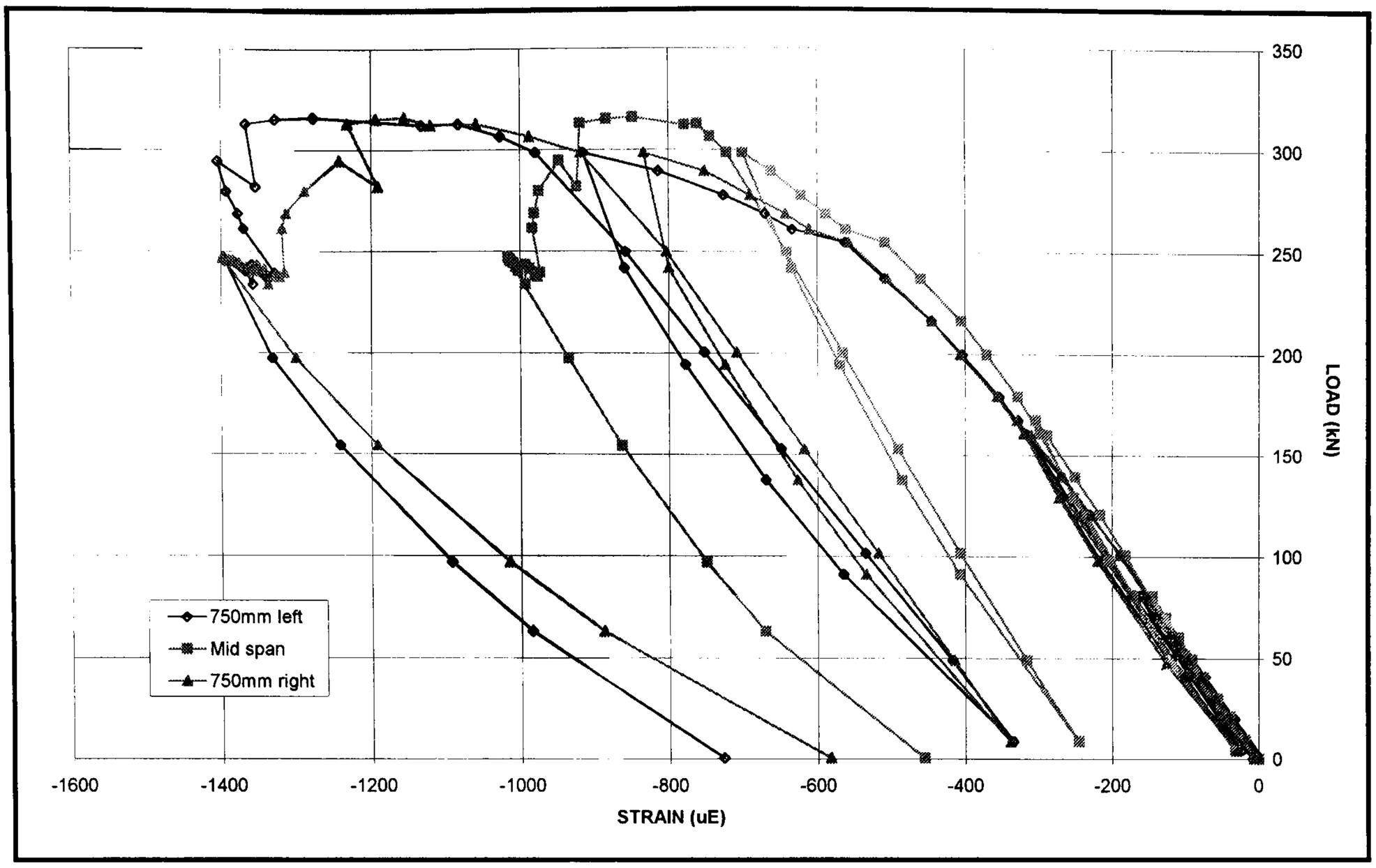

Fig. 5.27 Applied load vs. concrete surface strain of Test CB2

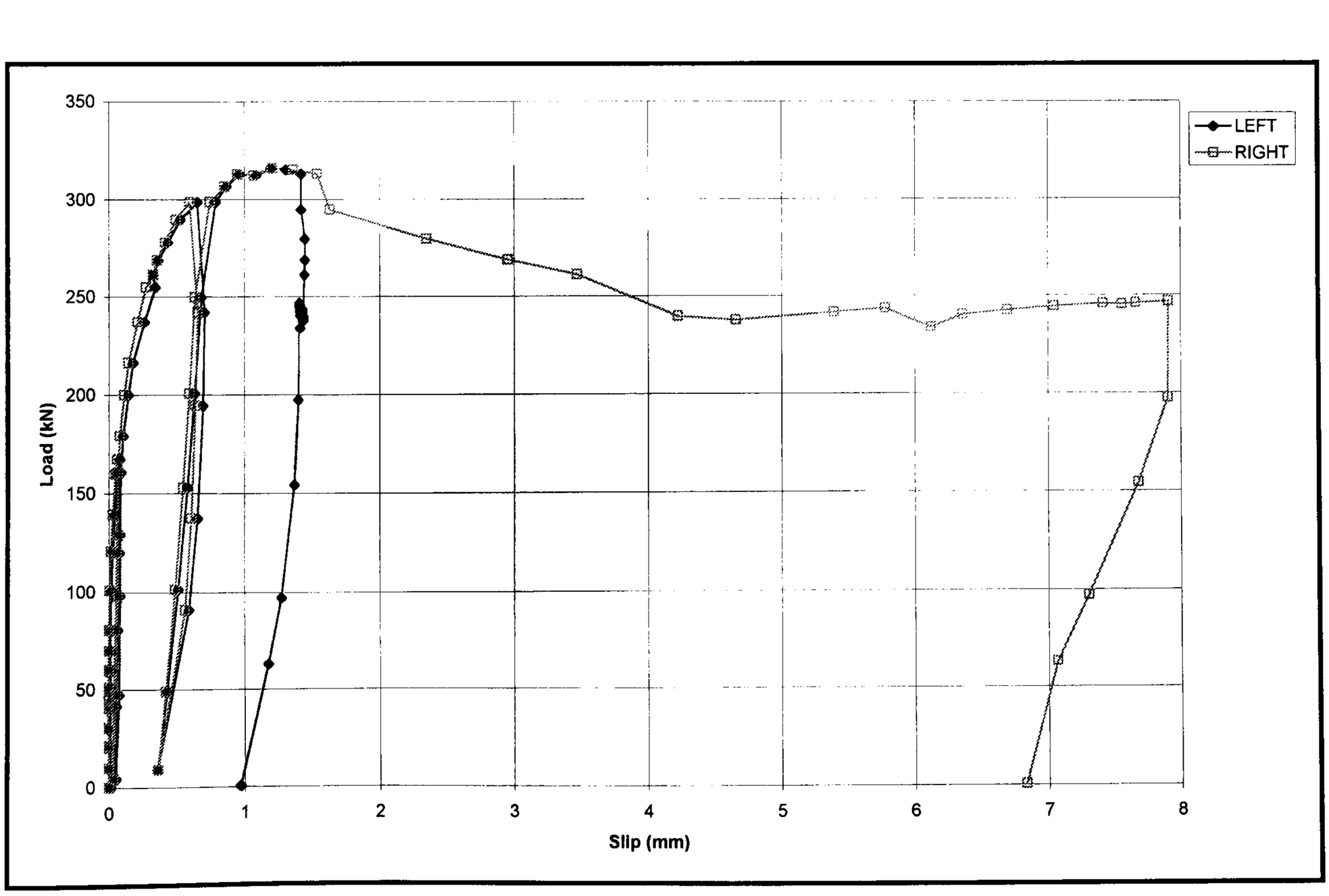

Fig. 5.28 Applied load vs. end slip of Test CB2

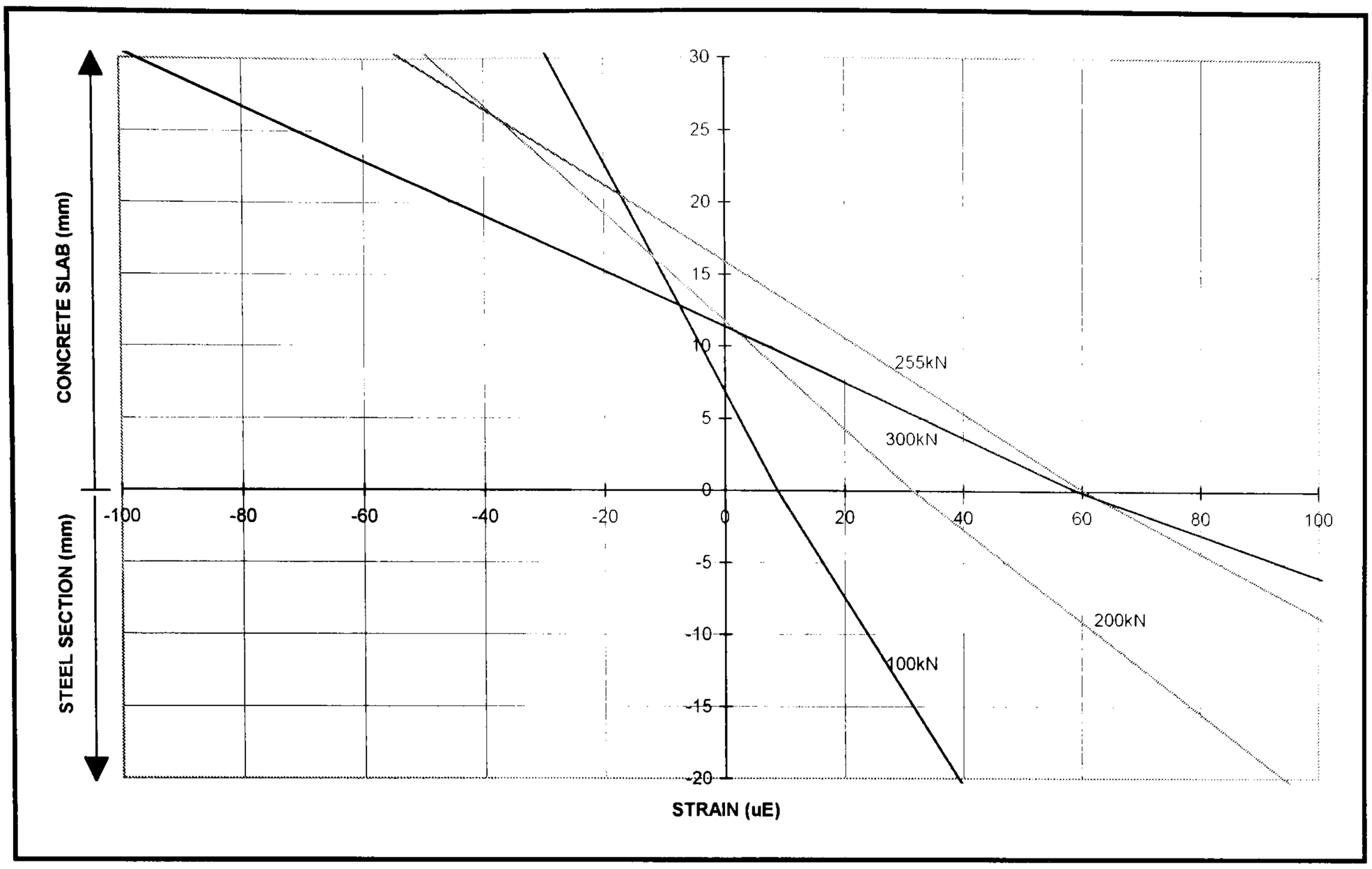

Fig. 5.29 Strain distribution of Test CB2

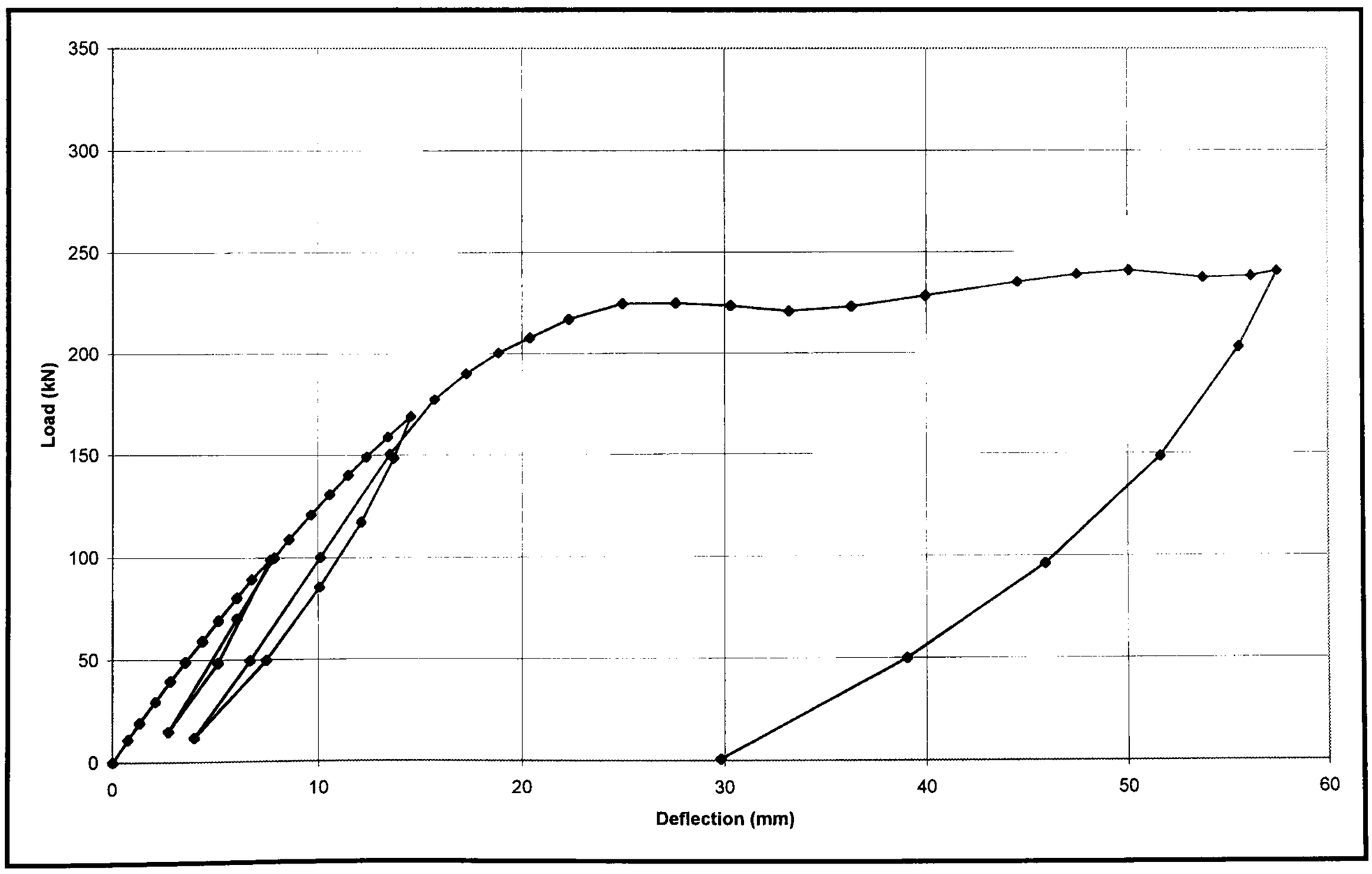

Fig. 5.30 Applied load vs. vertical mid-span deflection of Test CB3

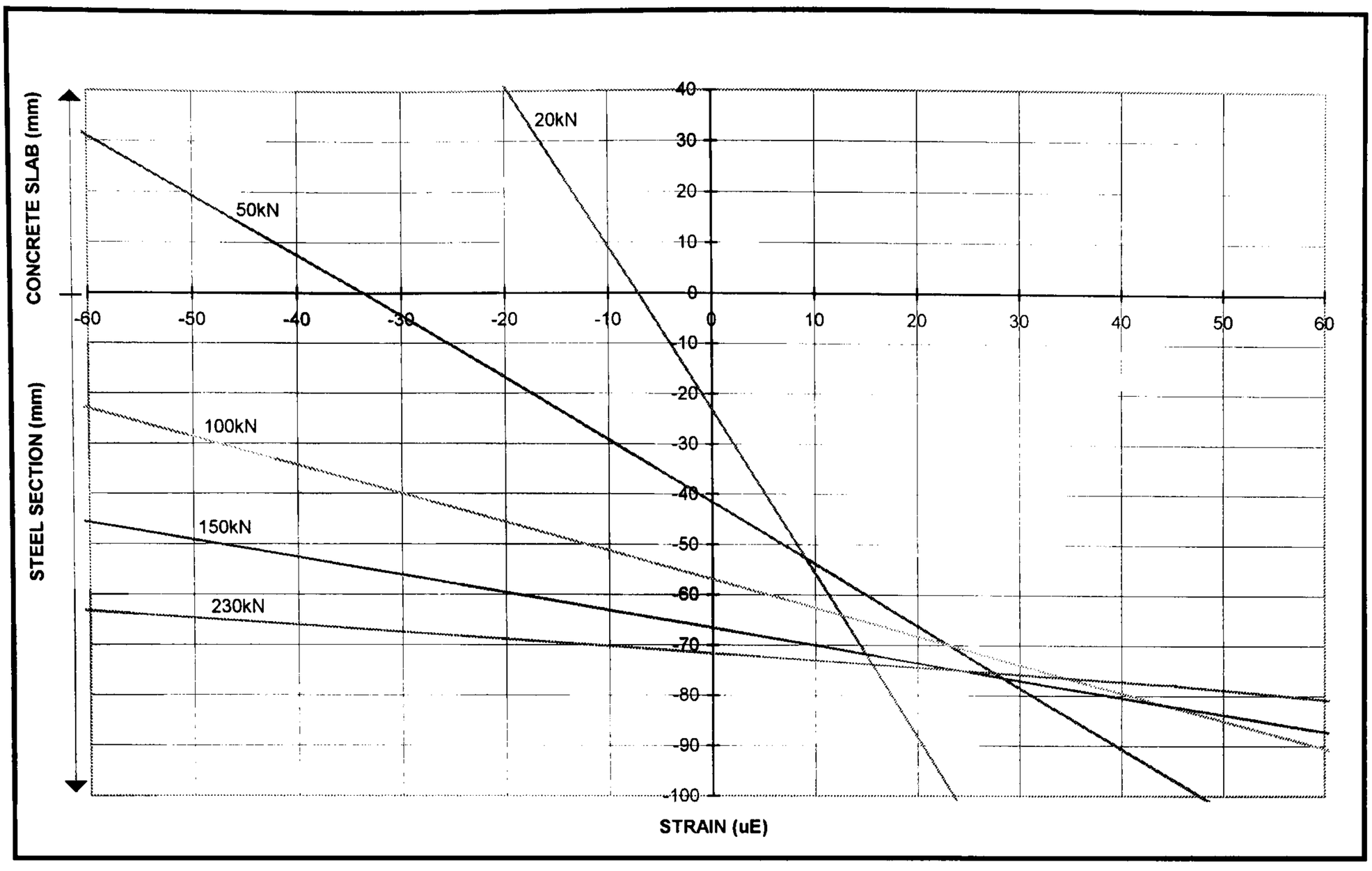

Fig. 5.31 Strain distributions for Test CB3

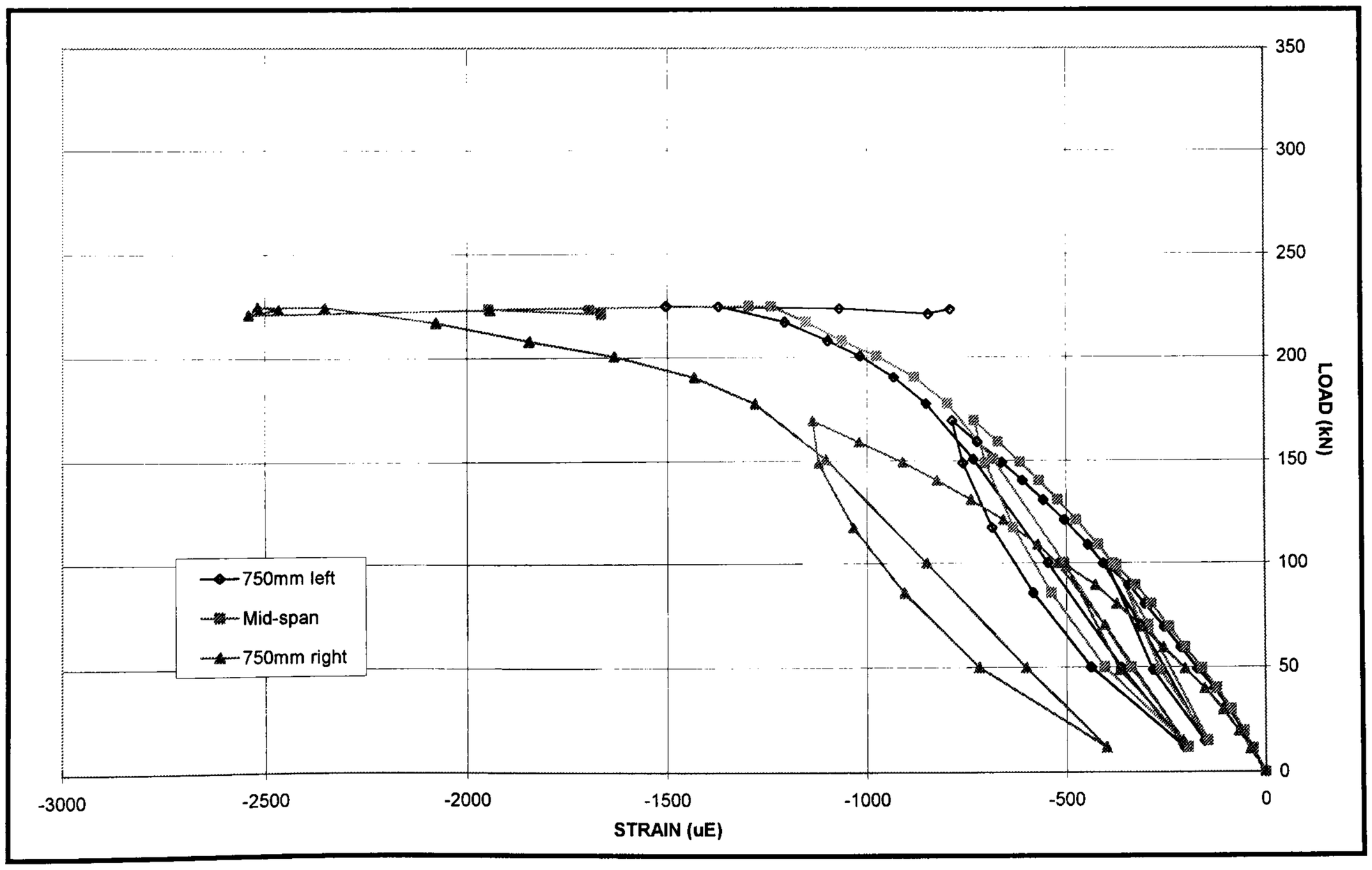

Fig. 5.32 Applied load vs. concrete surface strain of Test CB3

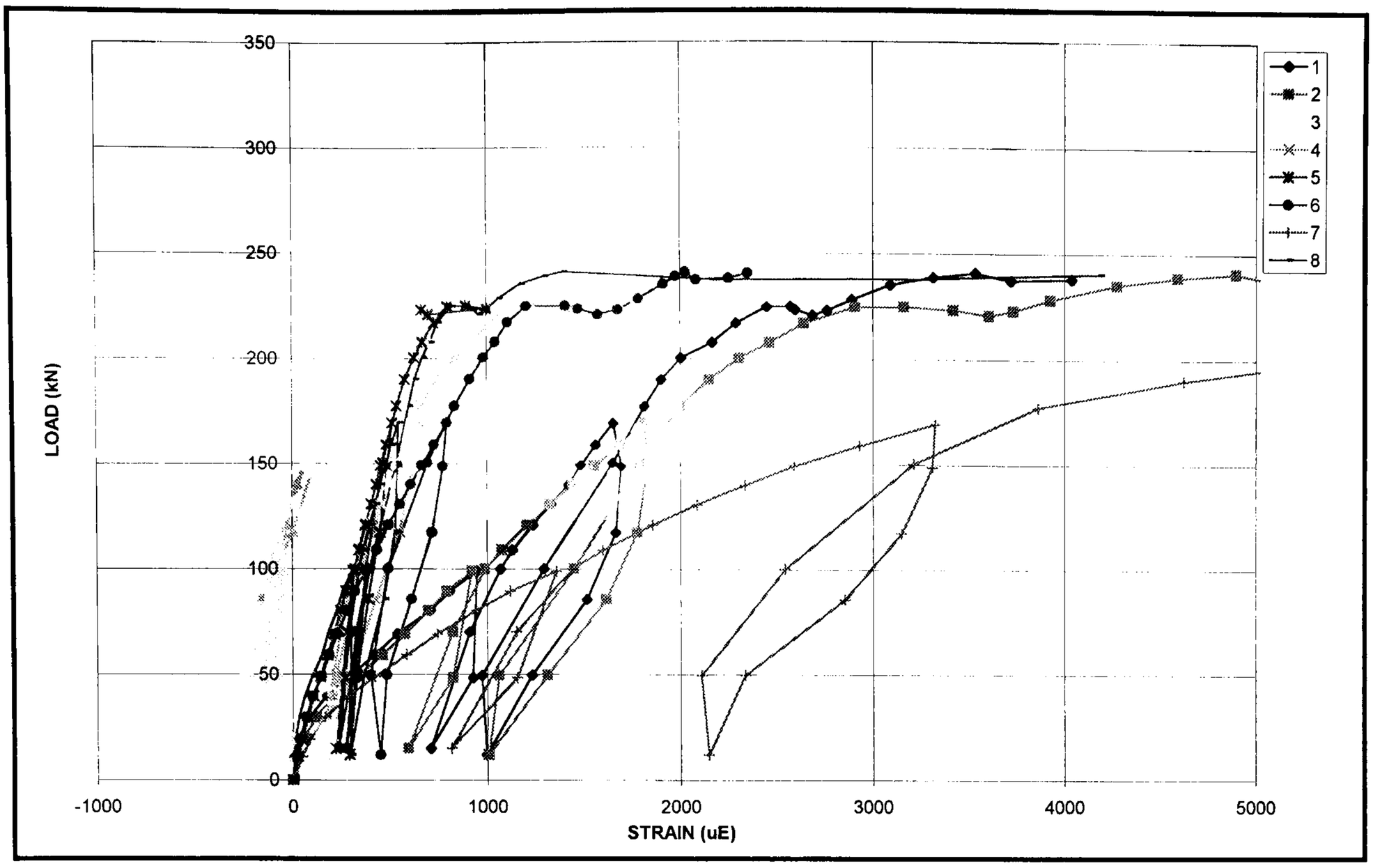

Fig. 5.33 Applied load vs. transverse reinforcement strain of Test CB3

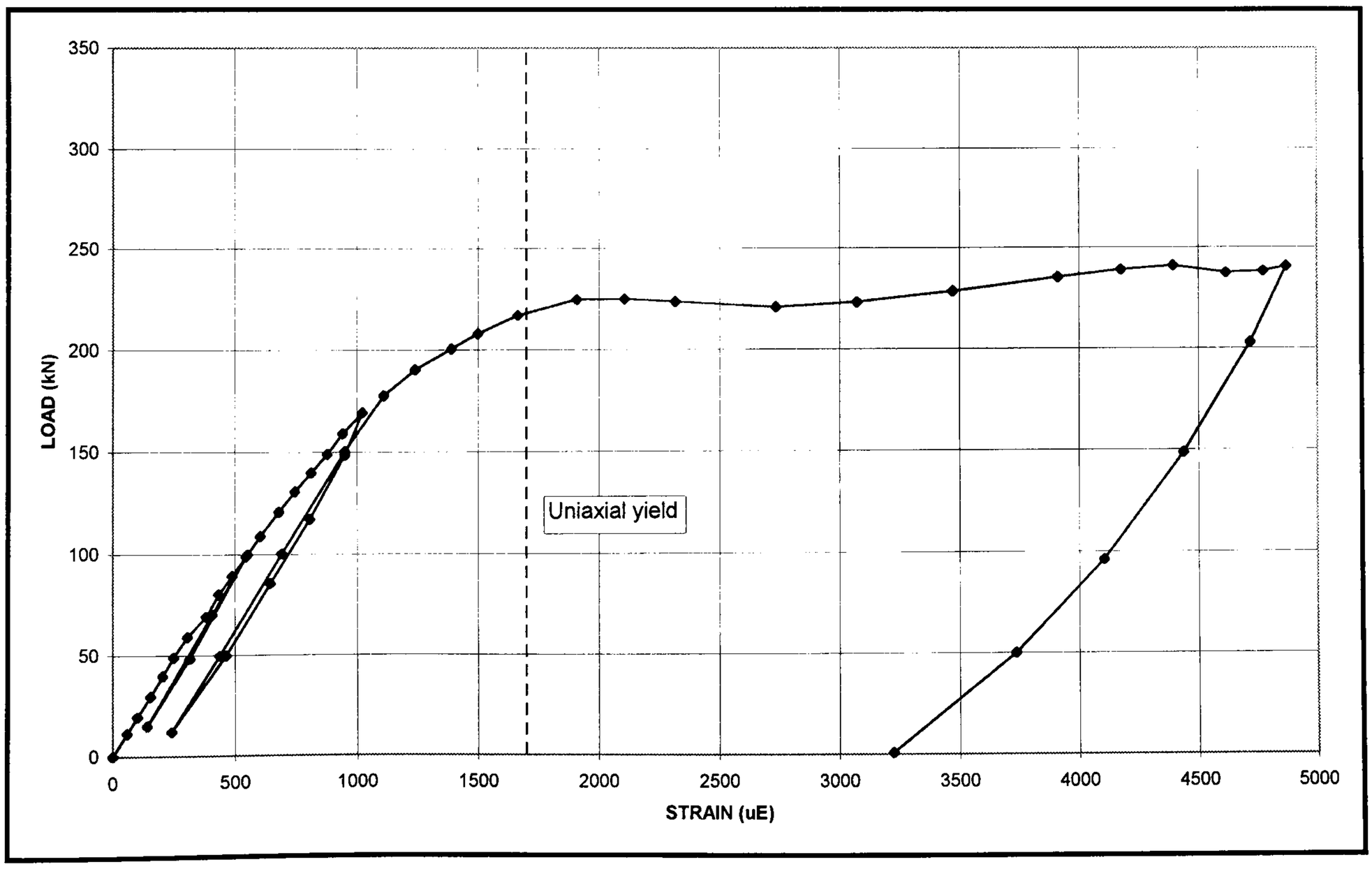

Fig. 5.34 Applied load vs. strain of steel bottom flange of Test CB3

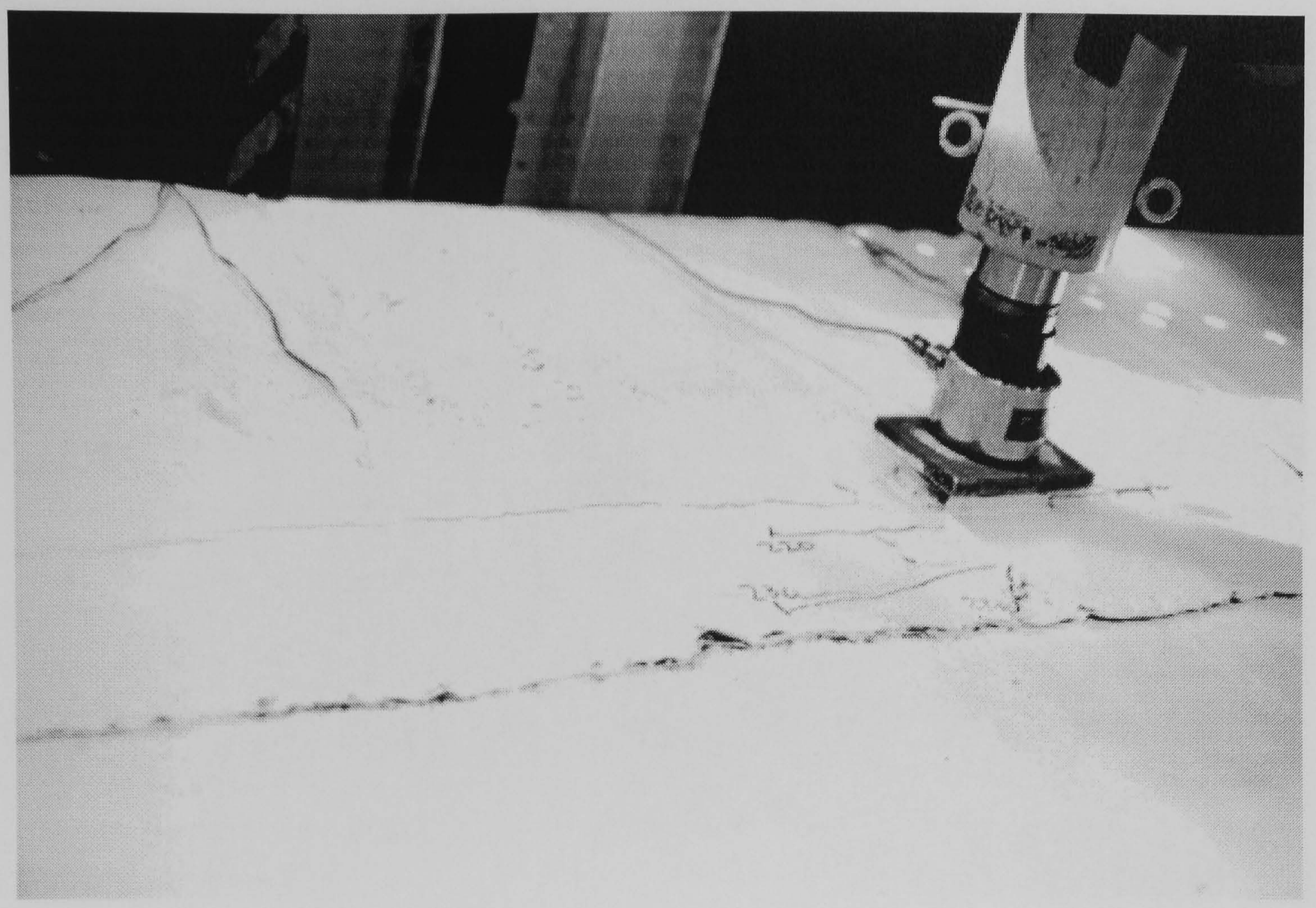

Fig. 5.35 Cracks at slab surface of Test CB3

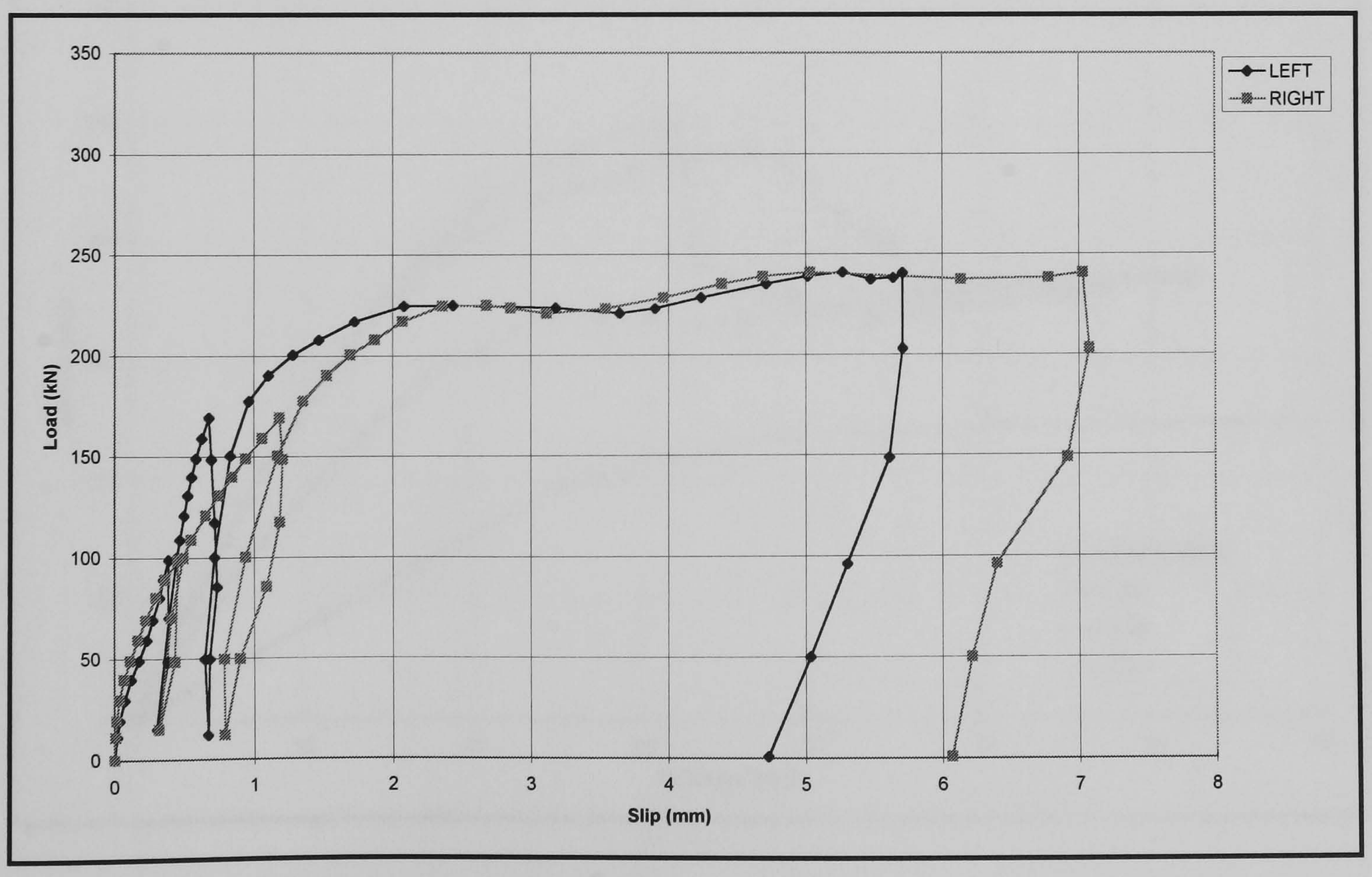

Fig. 5.36 Applied load vs. end slip of Test CB3

Fig. 5.37 Cracks at transverse joint between hcu of Test CB3

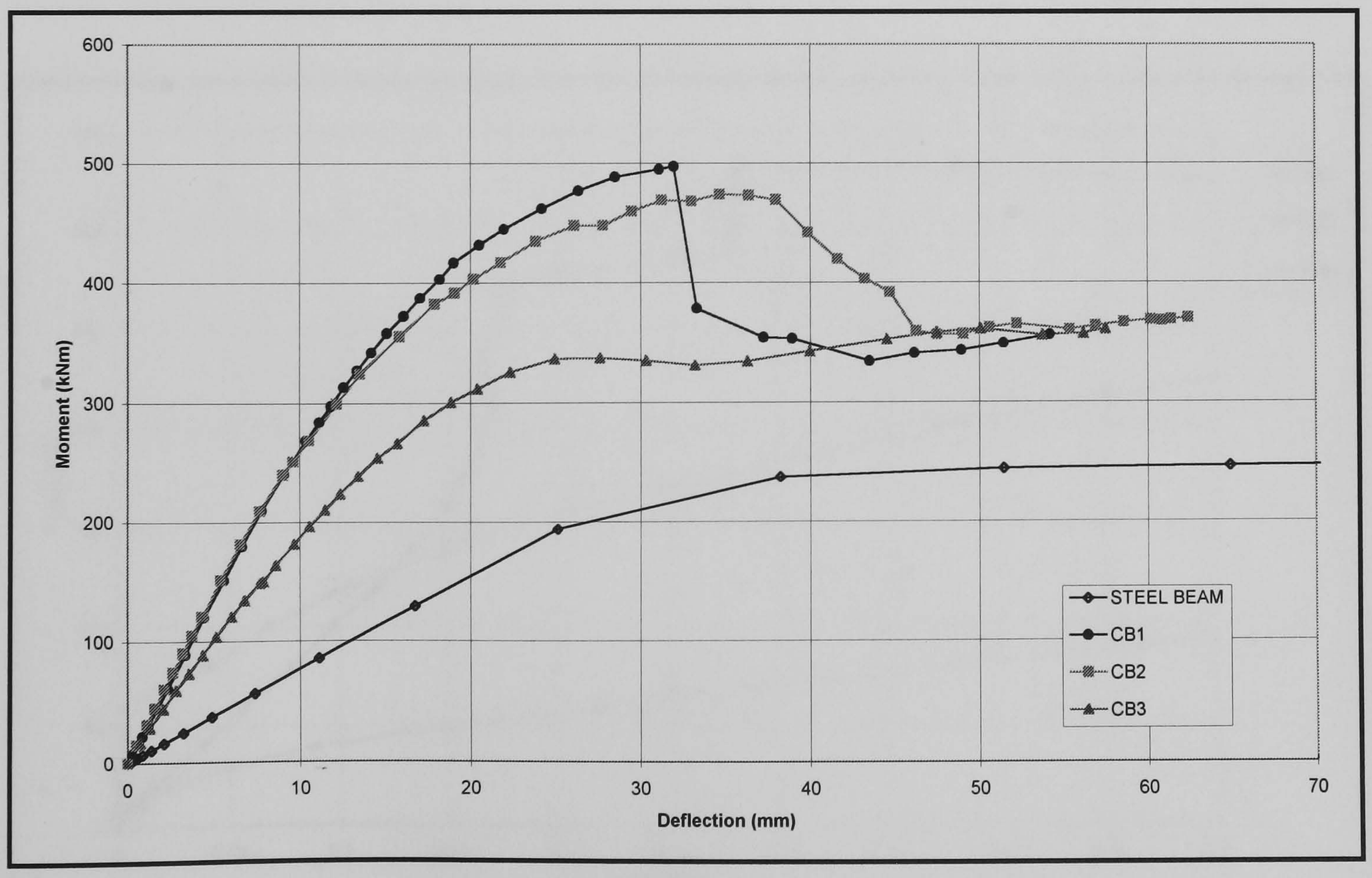

Fig. 5.38 Applied moment vs. vertical mid-span deflection curves of bending tests

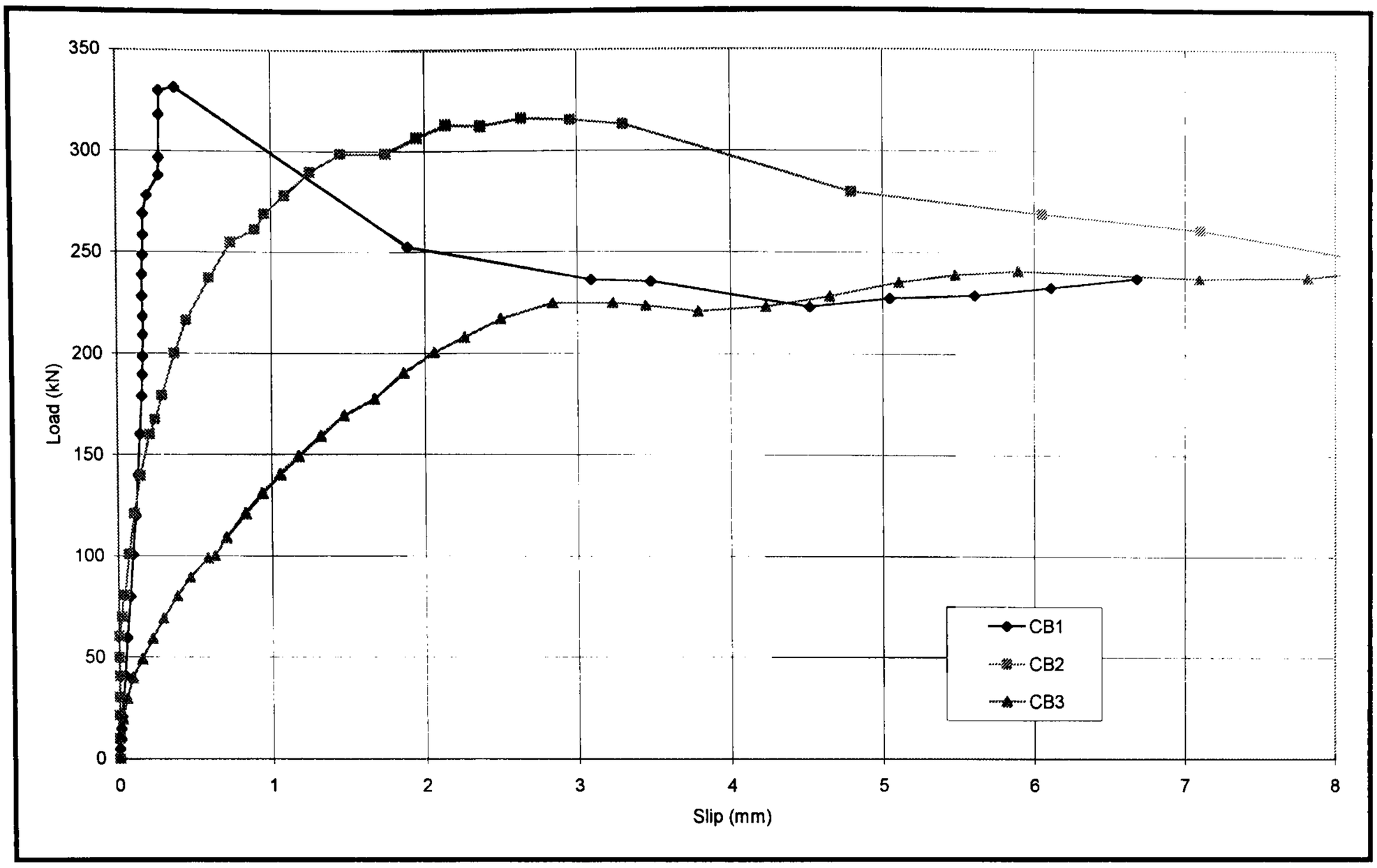

Fig. 5.39 Applied load vs. end slip curves of bending tests

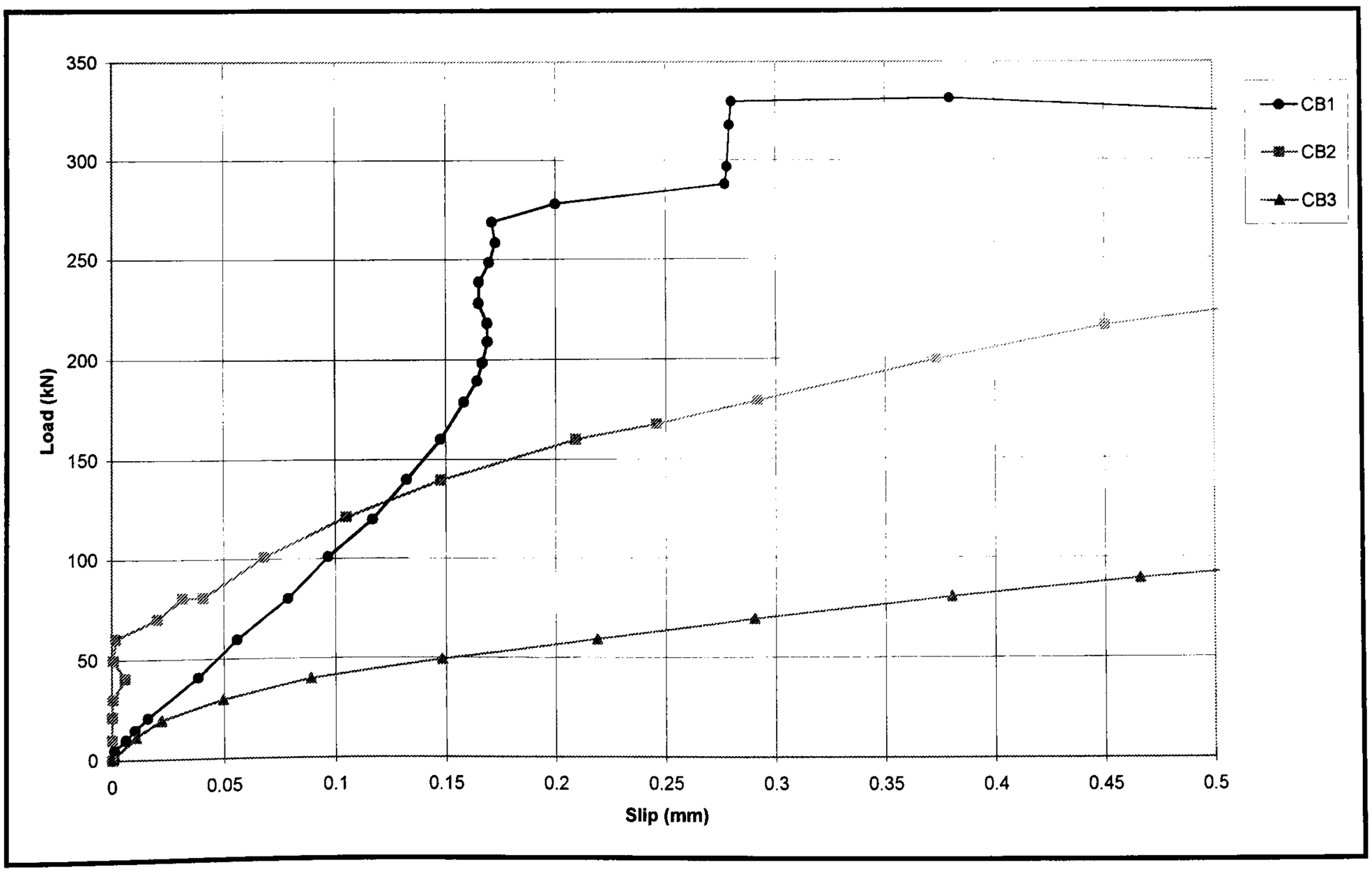

Fig. 5.40 Applied load vs. end slip of bending tests upto 0.5mm slip

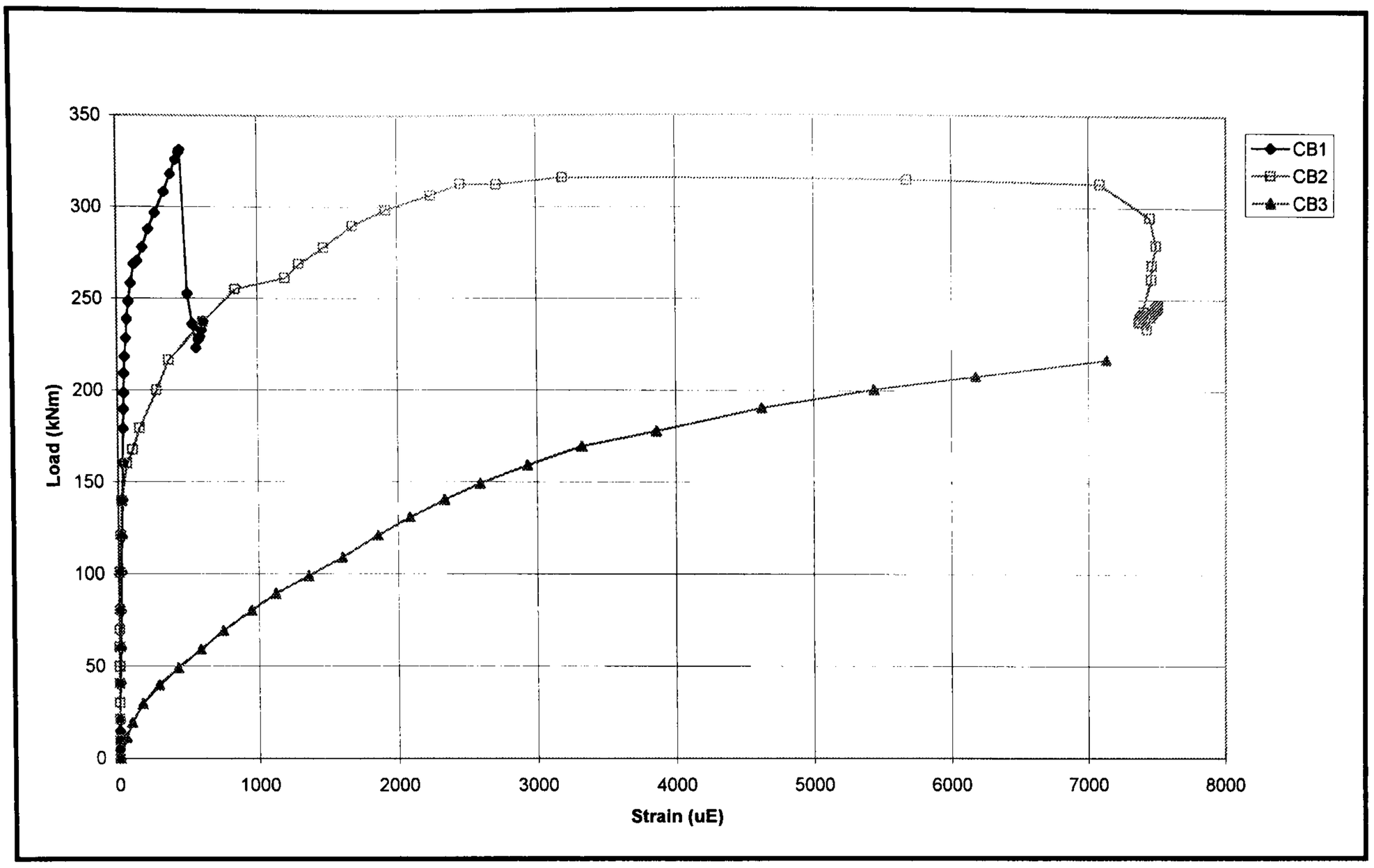

Fig. 5.41 Applied load vs. strain curves of rebar for bending tests

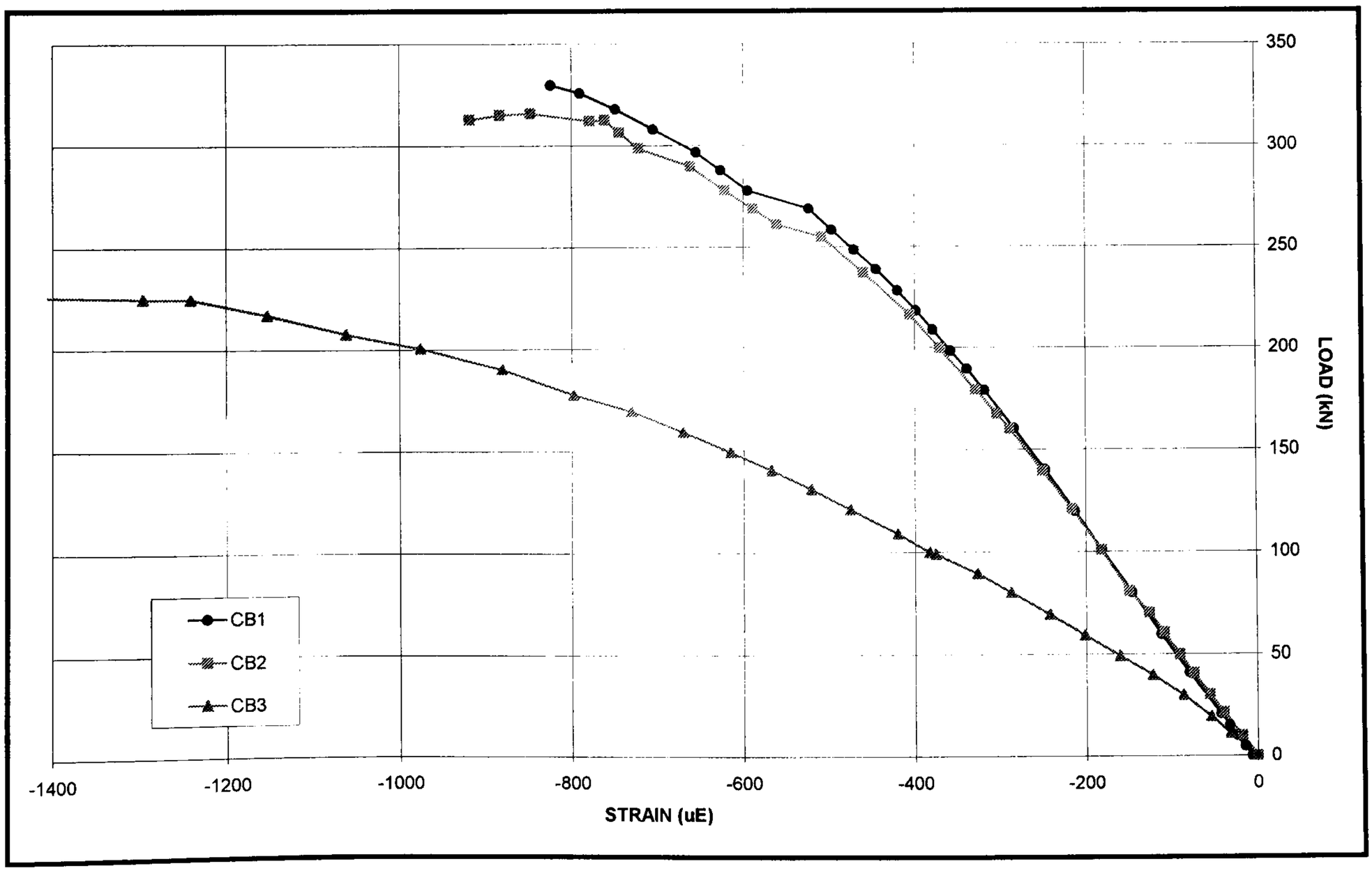

Fig. 5.42 Applied load vs. concrete surface strain for bending tests

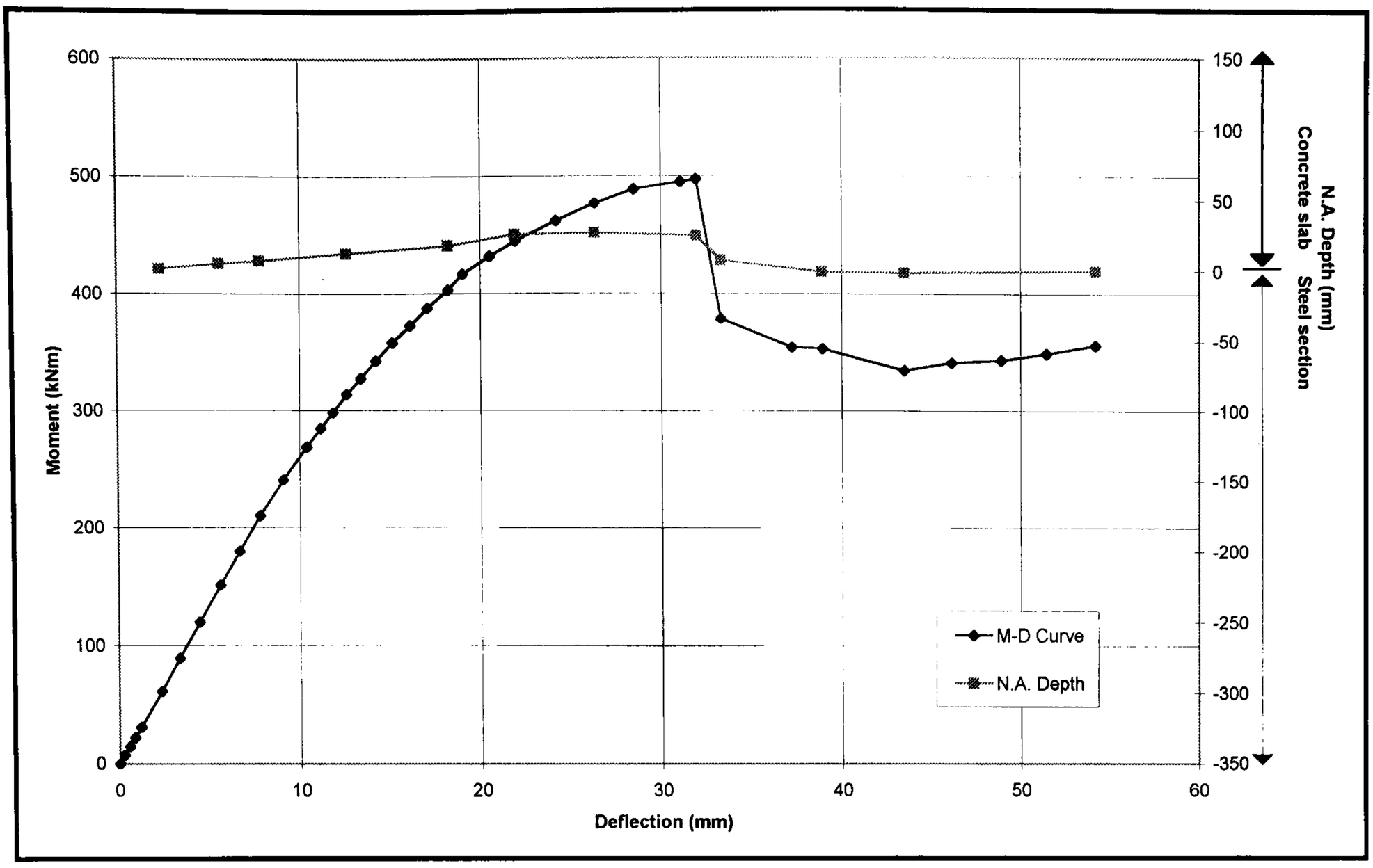

Fig. 5.43 Position of neutral axis during Test CB1

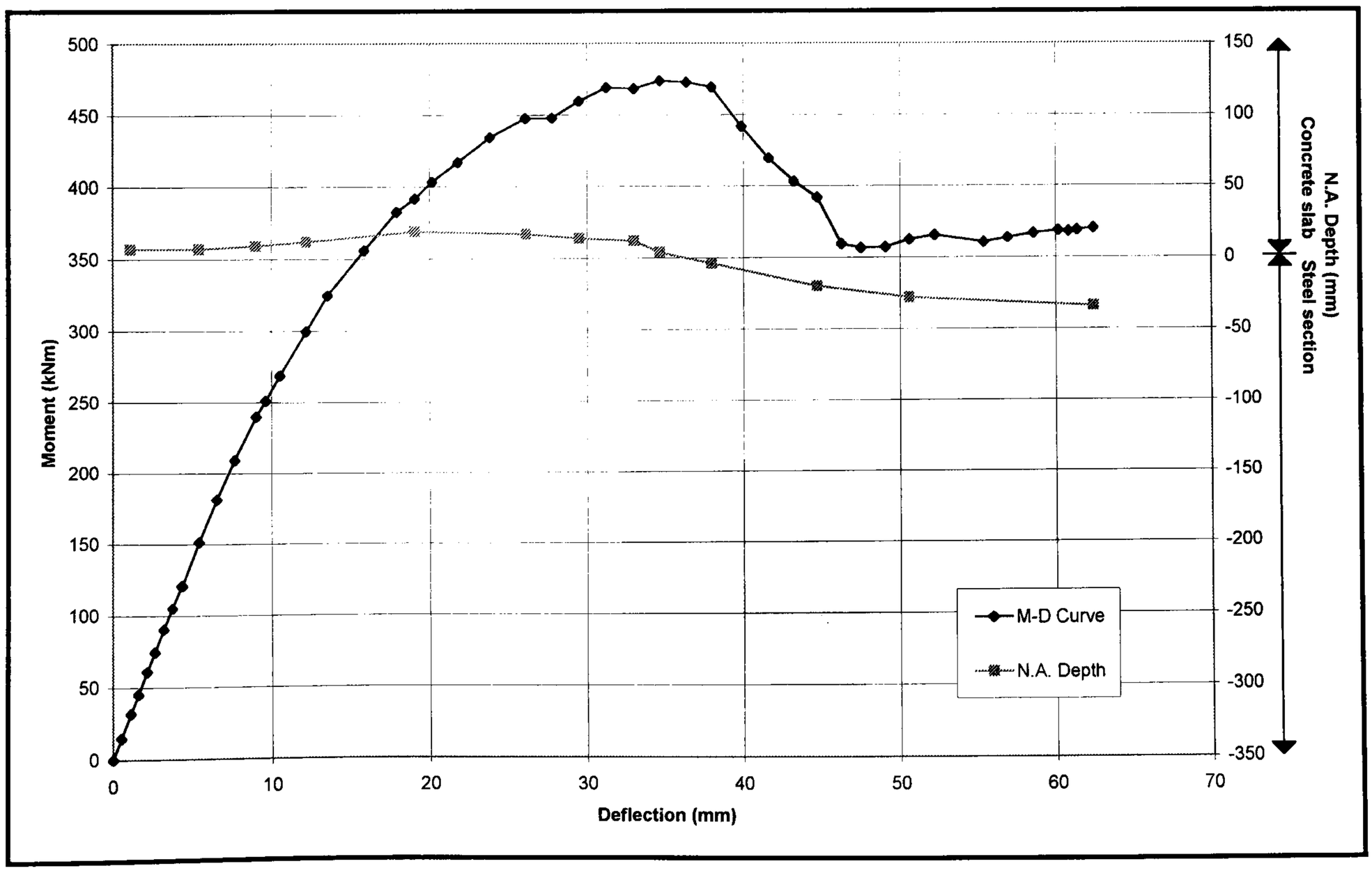

Fig. 5.44 Position of neutral axis during Test CB2

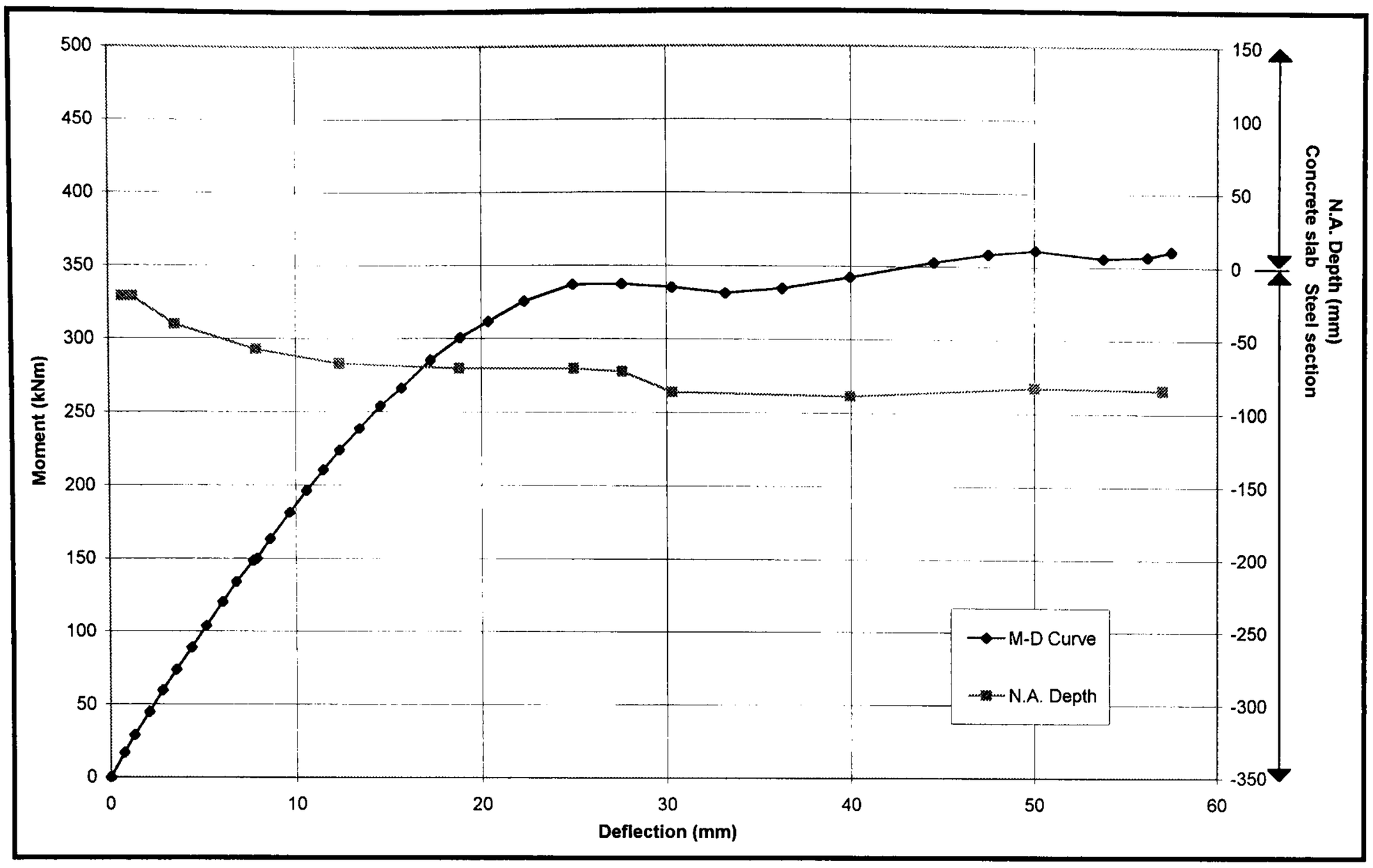

Fig. 5.45 Position of neutral axis during Test CB3

Chapter 6

Finite Element Modelling

6.1 Introduction

Although the experimental results provide valuable insight into the problem, it is not possible to cover the range needed for a complete study. In order to extend the range of parameters covered, the most suitable tool available at present is the finite element(FE) method. The method provides a cost effective alternative to full scale experimental testing.

A two dimensional FE model is used to simulate the structural behaviour of the precast hollow core composite construction. This describes the modelling of the composite slab in compression (as discussed from an experimental viewpoint in Chapter 3) and of the complete composite beam (as described in the experimental work in Chapter 5). The precast-insitu slab was modelled as a flat horizontal plate with no beam in order to investigate the ultimate compressive stress in the composite slab, and then a full composite beam was modelled for the flexural behaviour. The geometrical properties of the hcu were not modelled. The two models are unrelated and information from each model is validated with the experimental tests described in the previous chapters.

6.2 Finite element method

The FE method, which is a numerical technique for modelling a continuum by discretizing it into a finite number of components or elements, has both a mathematical and a physical counterpart in the solution of actual discrete problems such as, for example, a beam, where nodes connect standard units of the element. In the case of a continuum, however, the implicit assumption is usually made that, in order to attain the exact solution, the discretization process should be extended indefinitely, although for engineering purposes a finite degree of subdivision will eventually be sufficiently accurate. By far the most popular FE method in structural problems is based on assumed displacement fields. Consider an individual element, having a given number of nodal points along its boundaries. Then the displacement field within the element, $\boldsymbol{u}$ (where the components of $\boldsymbol{u}$ depend on the dimensions of the problem), is deemed to be obtainable by interpolating between the relevant nodal parameter $\boldsymbol{d}$ in a matrix form:

$$\boldsymbol{u} = [\mathrm{N}]\,\boldsymbol{d} \tag{6.1}$$

where [N] is the matrix of the shape functions relating the continuous field $\boldsymbol{u}$ to the discrete set of $\boldsymbol{d}$. The shape functions represent the approximating interpolation to the actual function within the element (i.e. between nodes) with the known nodal values $\boldsymbol{d}$ providing the basis for interpolation. Once the displacement field $\boldsymbol{u}$

has been obtained throughout a given element, the vector of strains, ε, follows upon operating on $\boldsymbol{u}$ by means of a suitable linear operator [**L**], i.e.

$$\varepsilon = [\mathbf{L}]\,\boldsymbol{u} \tag{6.2}$$

and, through the use of (6.1)

$$[\mathbf{B}] = [\mathbf{L}]\,[\mathbf{N}] \tag{6.3}$$

i.e. [**B**] is made up of differentials of the shape functions contained in [**N**].

Finally, the stress state σ in the finite element may be obtained upon specification of the matrix of constitutive relations, [**D**], which links stresses and strains. In general form

$$\sigma = [\mathbf{D}]\,(\varepsilon - \varepsilon_o) + \sigma_o \tag{6.4}$$

where for completeness, the vectors of the initial strains, ε_o, and stresses, σ_o, have been included, although these are seldom considered. Therefore, the computation of the stresses directly from the nodal parameters $\boldsymbol{d}$ may be written as

$$\sigma = [\mathbf{D}]\,[\mathbf{B}]\,\boldsymbol{d} \tag{6.5}$$

The equilibrium of finite element subject to nodal action $\boldsymbol{p_n}$, as well as loads $\boldsymbol{p_e}$ which are distributed throughout the element, may be tackled by means of a virtual-work approach. The application of a set of virtual displacements $\delta\boldsymbol{d}$ at the nodes will produce element displacements

$$\delta\boldsymbol{u} = [\mathbf{N}]\,\delta\boldsymbol{d} \tag{6.6}$$

and internal strains

$$\delta\boldsymbol{\varepsilon} = [\mathbf{B}]\,\delta\boldsymbol{d} \tag{6.7}$$

W_i , the internal work done by the stresses through the volume V of the element, is then

$$W_i = \int_v \delta\varepsilon^T \sigma \, dV \tag{6.8}$$

while W_e, the external work done by the nodal actions and distributed forces, amounts to

$$W_e = \delta \boldsymbol{d}^T \boldsymbol{p_n} + \int_v \delta \boldsymbol{u}^T \boldsymbol{p_e} \, dV \tag{6.9}$$

On equating W_i and W_e, and recalling that the result must hold for all values of $\delta \boldsymbol{d}^T$, the following is obtained

$$(\int_v [\mathbf{B}]^T [\mathbf{D}] [\mathbf{B}] \, dV) \, d = \boldsymbol{p_n} + \int_v [N]^T \boldsymbol{p_e} \, dV \tag{6.10}$$

As a final preliminary, the definition of the stiffness matrix for the element is

$$[\mathbf{k}] = \int_v [\mathbf{B}]^T [\mathbf{D}] [\mathbf{B}] \, dV \tag{6.11}$$

so that the equilibrium statement sought becomes

$$[\mathbf{k}] \, \boldsymbol{d} = \boldsymbol{p}$$

where $\boldsymbol{p}$ is denoted as total nodal actions.

So far, it has been assumed implicitly that $\boldsymbol{d}$ is known so that computation of $\boldsymbol{u}$, ε and σ can proceed. Such an analysis is based on the so-called stiffness or displacement method, which requires the solution of the system of linear equations

$$[\mathbf{K}] \, \boldsymbol{d} = \boldsymbol{f} \tag{6.12}$$

where $\boldsymbol{d}$ is now understood to represent all the generalised nodal displacements to be determined, while $\boldsymbol{f}$ consists of the vector of generalised forces acting on these nodes, which is obtained by summing the contributions of all elements at every node.

A non-linear structural problem, which has been discretized in accordance with the stiffness formulation, still proceeds through the solution of the set of equations

(6.12), but now the stiffness matrix is a function of the load/ displacement level.

The equation for non-linear problem can be written as

$$[\mathbf{K}(d)]\, d = f \qquad (6.13)$$

6.3 Modelling techniques

The finite element program used for this work is called ABAQUS[1]. Its applications include material linear and non-linear analysis; static and dynamic analysis; thermal stress analysis, etc. Because of its versatility, ABAQUS cannot deal with some of the special problem very well. For instance, it is widely recognised that the application of non-linear finite element packages like ABAQUS to the analysis of concrete structures has met so far with limited success[2]. Even though this drawback existed, provided special consideration is given when modelling the concrete, ABAQUS can still deal with the present problem satisfactory. This chapter describes the development of the finite element model and later modelling of the composite slab and beam using a plane stress condition, where the limiting yield stress is based on the 2-D Von Mises yield criterion.

The use of a plane stress approach is justified as the assumption of plane stress is applicable for bodies whose dimension is relatively small in one of the coordinate directions. (i.e. analysis of thin plates loaded in the plane of the plate) In a plane

stress distribution, it is assumed that in the direction perpendicular to the plane of the plate, the stress components do not vary through the thickness of the plate.

6.3.1 Geometry Definition

To construct the geometry of the finite element model, i.e. FE mesh, the co-ordinates of all nodes must first be defined. It is not essential to label all the nodes, provided the principal ones are labelled, because ABAQUS can generate the intermediate nodes between using the special commands (*NGEN, *NFILL, *NCOPY). Once all the nodes are identified, elements can be defined. To define each element, it is required to input the element number, type of element and the numbers of nodes required to form the element. As in the case of generating nodes, ABAQUS can copy and generate elements from the principal elements initially defined using special commands (*ELCOPY, *ELGEN). Fig. 6.1 shows a 4-nodes plane stress element, CPS4, used for the modelling.

6.3.2 Boundary conditions

To define the support condition and to establish symmetry, appropriate restraints on nodes are required. It can de done by specifying displacement restraints by assigning a value to the relevant degree of freedom of the nodal point using special

command (*BOUNDARY). By using this special command, symmetry about the x and y axes can also be assigned.

6.3.3 Material properties

To assign the correct material properties to the FE mesh, it is essential to divide the elements into specific sets, for example, steel, concrete, rebar, etc. For each set, it is possible to define the individual material properties. Material properties for modelling purposes are usually obtained from material testing, i.e. coupon tests, cube tests, etc. From these tests, Young's modulus of elasticity, stress-strain curves together with the yield strength of the materials can be defined and input into the finite element program.

6.3.3.1 Concrete

The most characteristic feature of the behaviour of concrete is that associated with the fracture processes which concrete undergoes under increasing load. Concrete is a brittle material and cracks under tension. Crack extension and propagation occurs in order to relieve high tensile stress concentrations which develop under increasing load in the region of the crack tips. Brittle failure is a highly discontinuous and unstable phenomenon and is not well suited to the incremental

Newton-Raphson solution method used in ABAQUS or other packages. The special command (*CONCRETE) is intended for modelling plain and reinforced concrete subjected to essentially monotonic straining. The stress-strain curve for the concrete models is derived from the short term design stress-strain curve in BS8110[3] and is input into the program using the (*CONCRETE) command. Fig. 6.2 shows the stress-strain curve for the concrete model. The (*CONCRETE) command can be used with most of the structural elements in ABAQUS, including beams, shells, and two and three-dimensional solid elements.

The interaction between the reinforcement and the concrete, such as bond slip and dowel action, are modelled approximately by introducing "tension stiffening" into the concrete model. Tension stiffening means that the direct stress across a crack does not immediately fall to zero as soon as the crack occurs. Instead it gradually reduces as the crack opens. The command (*TENSION STIFFENING) is used to specify this gradual reduction in the direct stress. The choice of tension stiffening is often critical for a successful analysis. Choosing the appropriate values is not easy as the amount of tension stiffening depends on factors such as the amount of reinforcement, the quality of bond and the mesh. Tension stiffening can be defined in two ways: stress-strain data or as stress-displacement data, the former method is used throughout the modelling as the later approach can lead to the results being mesh sensitive. Even so, care should still be taken with the FE mesh design. In the modelling of the compression slab, when the concrete cracks and is no longer capable of carrying tensile loading normal to the crack direction, the load is

transferred to the reinforcement via the tension stiffening command. The response of the concrete is highly discontinuous and large amounts of cracking can also lead to local instabilities in the analysis.

For the slab model, the compression slab is modelled as a 2-D plate using 4-node plane stress elements i.e. the thickness of the slab is assumed to be small relative to the other dimension of the slab and the stress components do not vary through the thickness of the slab. Since the extreme stresses occur at the uppermost surface of the slab, that is where the slab is modelled. Voids in the precast hollow core slab are not considered in the slab model.

For the beam model, the concrete slab that is directly on top of the steel beam is modelled using the 8-node concrete elements. 4-node elements with an aspect ratio of 1 were used initially, but the model gives the moment capacity values only in the initial stage; when the concrete reached its tensile capacity, numerical problems were encountered. These phenomena were similar to those reported by Ahmed[4]. It would appear from the results when concrete first cracks that the model stiffness matrix became singular and the load increment needed for a convergent solution became too small and led to termination of the analysis. Then 8-node elements with an aspect ratio of 2 were tried and the result was much improved. The expected ultimate load and sufficient plastic deformation were achieved. The reason is believed that ABAQUS recognises the percentage of cracking within an element, and with a larger element size, the analysis can

continue even after the first crack is formed. As before, due to the limitation of the two-dimensional model, the breadth of the concrete slab is represented by the thickness of the concrete element. Material properties of the concrete slab are input as combined properties of the insitu concrete infill and the precast hollow core concrete. This takes into account the hollow core of the precast slab and the insitu infill within the composite slab, but does not necessarily recognise the presence of the hollow cores in the slab nor the longitudinal joints between them.

6.3.3.2 Transverse reinforcement

In a precast hollow core composite beam, no longitudinal reinforcement is required, only transverse reinforcement is needed to provide the composite action between the precast and insitu interface and the steel concrete interface.

In the compression slab model, the reinforcement was uniformly distributed in the concrete element to give an effective tensile strength. Tensile strength of the concrete was ignored.

In the 2-D FE composite beam model, there is no provision using ABAQUS to input transverse reinforcement explicitly in the model. Therefore the characteristic of the transverse reinforcement has to be input by other means. As described earlier in Chapter 4, transverse reinforcement has a major influence on the

characteristic of the shear connectors, therefore it is assumed that the characteristic of the shear connector is a combined effect of the transverse reinforcement, the insitu precast interface and the strength of the shear connectors. Although the assumption is made because of the limitation of the FE model, it is not an unrealistic approximation as the results from the push off tests are a combination of these factors.

6.3.3.3 Steel element

The steel section used in the composite beam model is modelled using 4-node plane stress elements. The top and bottom flange of the steel beam are represented by one set of elements of thickness equal to the breadth of the flange. The web of the steel beam is subdivided into five rows of elements with an aspect ratio of 3.0. The thickness of the web is again represented by the element thickness. Being a 2-D model, the modelling of the third dimension is restricted and can only be represented by the thickness of the elements. The mechanical properties of the flange and web sections of the steel beam are input separately and are taken from the coupon test results shown in Appendix A, so that validation of the model can be made more accurate. Effect of strain hardening in steel was not utilised in the model.

6.3.3.4 Shear connector

In a composite steel and concrete beam, shear connectors must be provided throughout the length of the beam. The shear connectors transmit the longitudinal shear force between the steel beam and concrete slab ignoring the effect of frictional bond between the two materials. The shear connector is modelled and defined in ABAQUS using a spring element (*SPRING). The spring element is of zero length which can bear only shear force, and obeys the load-slip characteristic of the shear connector used. The positions of the spring elements coincide with the positions of the shear connectors used in the composite beam i.e. at 150c/c. Because the load-slip characteristic of the shear connector is non linear, the force is assumed to be a function of relative displacement in the spring and is defined by giving a table of force values in ascending values of relative displacement. The load-slip characteristic of the shear connector is obtained from the corresponding push off test described in Chapter 4. Fig. 6.3 shows a typical load-slip curve used in the analysis.

6.3.4 Loads

The type of loads, i.e. concentrated, uniformly distributed, etc., magnitude and direction can be defined by assigning the load to a node number for a concentrated load or an element for a uniformly distributed load using the command (*CLOAD,

*DLOAD). In ABAQUS, the load is applied in an iterative procedure and the condition for termination of the analysis can be set manually if required when specified displacements or rotations at certain node are reached.

6.3.4.1 Loading procedure

For the nonlinear analysis, proportional loading is used where the load magnitudes are considered to be part of the solution. In this case, the variation of the loading magnitude over the step is considered to be an unknown, to be determined as part of the solution. Irrespective of the updating strategy adopted, its basic formulation may be summarized in flow-chart form as depicted in Fig. 6.4.

The external-load vector is applied in the load steps $\Delta \boldsymbol{f}_e$ (typically, $\Delta \boldsymbol{f}_e \approx$ 5-10% of the load), to which the unbalanced nodal forces (i.e. the vector of residual forces, $\Delta \boldsymbol{f}_r$) of the previous iteration must be added. Then a decision on whether or not to update the various **D**-matrices and hence, the incremental stiffness matrices [**k**] is made. If the current iteration is an updating iteration, the result is an update of the incremental stiffness matrix of the structure. If the system of equations can be solved, the increments of the nodal-increments vector $\Delta \boldsymbol{d}$ are obtained, from which the new increments in strain ($\Delta\varepsilon$) and stresses ($\Delta\sigma$) at all Gauss points are calculated through the matrices [**B**] and [**D**] respectively; thus the total strain (ε) and stress (σ) may be obtained. The new total stresses are now balanced, (i.e. they

are in equilibrium at this stage) but they are not compatible with the actual material stress-strain relationships. Therefore, these equilibrated stresses are corrected so as to satisfy the constitutive equations, and this requires the additional stress increments $\Delta\sigma_r$, which lead to the total stresses σ' that are now unbalanced (as equilibrium is no longer satisfied since $\int [\mathbf{B}]^T \sigma' \, dV = \boldsymbol{f}_i \neq \boldsymbol{f}_e$). These corrective stresses $\Delta\sigma_r$ create new residual or unbalanced forces $\Delta\boldsymbol{f}_r$ which are applied to the structure in the next iteration in order to re-establish equilibrium conditions. If unbalanced forces do not satisfy convergence criteria, the external load is kept constant and further iterations are carried out; otherwise a new external load increment is applied and the whole procedure repeated. There are only two possible reasons for stopping the analysis: unrealistic solutions to the set of equations, or divergence of residual forces.

6.3.5 Output files

ABAQUS runs as a batch application (i.e. not interactively). A data file containing all the necessary information for a complete analysis is prepared and ABAQUS executes the data file in a batch mode. After a complete run, several files are generated that contain the requested output details. Outputs can be created in TEXT format or in ASCII format which can be post processed. By using the *RESTART option, graphic outputs can be obtained for the deformed shape and stress contours etc.

6.4 Compression slab model

A 2-D FE model was first set up to investigate the various factors influencing the behaviour of the precast slab with insitu infill. The main objectives of these analyses were to gain some insight into the influence of the transverse reinforcement and the insitu concrete strength and to form a direct comparison with the experimental work describe in Chapter 3.

6.4.1 Modelling of the compression slab

A mesh of 160 4-node plane stress elements was generated to model the precast slab and insitu infill, Fig. 6.5 shows the compression slab model. A finite element mesh, representing one quarter of the compression slab, was generated using two planes of symmetry through the x-x and y-y axes. Elements 1 to 40 represented the insitu concrete infill and elements 41 to 140 represented the precast slab as shown in Fig. 6.6. There is no debonding plane present between the insitu and precast concrete. A steel bearing strip (elements 1,21,41,61,81,101& 121) was introduced to act as a loading beam to transfer the uniformly distributed load and minimised any local bearing failure which caused the analysis to terminate prematurely.

The primary parameters of this series were the strength of insitu concrete infill and the area and strength of transverse reinforcement according to Table 6.1. Insitu

infill concrete of C25, C30 and C40 was chosen for the series, and a characteristic compressive concrete strength of 50 N/mm^2 was used for the precast concrete throughout. Typical concrete stress-strain curve model used for the ABAQUS is shown in Fig. 6.7. Transverse reinforcement of R6, T8, T10, T12 T16 and T25 were chosen to observe the influence to the compression slab. Transverse reinforcement input by equally distributed throughout the finite element mesh using the (*TENSION STIFFENING) command. It was uniformly distributed in the concrete element to give an effective tensile strength, f_t'

$$f_t' = \frac{A_s f_y}{A_c} \tag{6.14}$$

where A_s = area of transverse reinforcement per metre length

f_y = characteristic strength of reinforcement

A_c = area of concrete per metre length

The tensile strength of the concrete was ignored. Incremental compressive uniformly distributed pressure was applied using proportional loading through the loading strip and both the compressive stresses and tensile stresses were recorded. Failure was defined when convergence is not achieved. This is caused by cracking in the concrete that resulted in a noticeable loss of continuity in the finite element mesh. Such an abrupt discontinuity in geometry is considered to be the predominant cause of failure in the analysis.

6.4.2 Results of analysis

Two types of failure were observed, as in the experimental work. The slab either failed by tensile splitting when the effective tensile strength, f_t' was reached, or by compression when the ultimate compressive strength was exceed, i.e. $0.67f_{cu}$. Proportional loading was used and failure was recorded when convergence was not possible due to cracking and discontinuity of the FE mesh. Maximum tensile stress, σ_t and maximum compressive stress, σ_c were recorded. Typical tensile stress contours are shown in Fig. 6.8. The results have been normalised with respect to the strength of the concrete and steel reinforcement and are shown in Table 6.1. The maximum compressive stress versus type of reinforcement for each analysis are shown on Fig. 6.9. Fig. 6.10 gives the compressive stress ratios, σ_c/f_{cu} versus effective tensile strength, f_t'. The results may be expressed by the following equations:

$$\sigma_c = (0.23 f_t' + 0.27) f_{cu} \qquad \text{for } f_t' \le 2.3 N/mm^2 \qquad (6.15)$$

$$\sigma_c = 0.85 f_{cu} \qquad \text{for } f_t' > 2.3 N/mm^2 \qquad (6.16)$$

The result once again confirmed that percentage of transverse reinforcement strongly influences the mode of failure of the composite slab with little contribution from the increase of the insitu infill strength. The results in Fig. 6.10 showed a fairly close correlation between the finite element analyses and the experimental work, with the experimental results being slightly higher in general. The main reason for this was that the ABAQUS model only considered the tension

stiffening effect caused by the reinforcement, no effect of concrete interlocking and bond strength was taken into account. In the experimental work, it was found that the tensile strength of concrete contributed to the initial strength and stiffness of the composite slab, so the finite element results would tend to be conservative and similar to the Test SPC4 where the interface between the insitu infill and the precast slab was pre-cracked.

6.5 Composite beam model

6.5.1 The FE mesh

A two-dimensional model of the composite steel-concrete beam is shown in Fig. 6.11. The model is set up to the same dimension as the full scale bending test specimens described in Chapter 5. Although a 2-D model has its limitations when dealing with a 3-D structure, (i.e. the 2-D model used preclude the 3rd dimensional effect where certain failure mechanisms might be critical.) it is extremely useful when the modelling is admissible on account of economy (computational time, input/output), ready visualization and the relative ease with which parametric studies may be conducted. Three types of elements were used; 4-node plane stress elements were used to model the steel beam, 8-node concrete elements were used for the concrete slab, and spring elements were used to model the shear connectors. Each node of the steel element is connected to the node of the concrete

element at the interface, i.e. at 150c/c. The modelling technique for the steel element, concrete element, transverse reinforcement and shear connector was described earlier in Section 6.3. The test parameters used are identical to the ones used for the full scale bending tests, all the actual material properties for the bending tests were used for the analysis. Table 6.2 shows the material properties used for each analysis.

6.5.2 Boundary condition and loading procedure

To take advantage of the symmetry of the FE model and reduce the size of the FE mesh, symmetry at the centre line of the beam is taken. The nodes at the centreline were restrained from movement along the direction 1, i.e. the direction of the beam axis, in addition the node at the support was restrained from movement along the direction 2, i.e. vertically. Two point loading is used to simulate the same loading condition as the full scale beam test. Point load is applied at 1.5m from support as shown in Fig. 6.11 using proportional loading, and failure is defined when convergence is not possible.

6.5.3 Results of composite beam model

The results of the composite beam FE analysis are shown in Table 6.3. The load vs. mid-span deflection curves of FE-CB1, FE-CB2 and FE-CB3 are shown in Fig.

6.12. The results corresponded very closely with the experimental findings, failure of the beams was either due to failure of the steel-concrete interface, i.e. the spring element, or failure due to cracking in the concrete elements. The maximum load capacity of all three beams was accurately predicted, but the post failure conditions were not able to be followed for the tests FE-CB1 and FE-CB2.

FE-CB1: The load vs. vertical mid-span deflection curve is shown in Fig. 6.12. The load-deflection behaviour is elastic up to 150kN. Failure occurred at a maximum load of 330kN. The cause of failure is due to tensile cracks in the concrete elements causing discontinuity in the FE mesh, that led to termination of the analysis. At failure, the maximum mid-span vertical deflection was 33mm.

FE-CB2: The load vs. vertical mid-span deflection curve is shown in Fig. 6.12. The load-deflection curve is elastic up to 130kN. Failure occurred when a maximum load of 320kN was reached. The cause of failure was due to failure of the spring elements which led to separation and discontinuity in the FE mesh. At failure, a maximum mid-span vertical deflection of 41mm was recorded. The mode of failure is due to interface spring elements failure. The applied load-deflection stiffness of both analyses are similar to FE-CB1 with FE-CB1 being slightly higher.

FE-CB3: The load vs. vertical mid-span deflection curve is shown in Fig. 6.13. Load-slip curve from the push off test T8-25-65P was input into the model. The

results were expected to be lower than the previous two models. The load-deflection curve was elastic up to 75kN which is 50% lower than the previous analyses. Failure occurred when a maximum load of 243kN was reached. The analysis was terminated due to discontinuity in the FE mesh caused by cracking in the concrete elements. The ultimate compressive stress of concrete was exceed in the concrete element. At failure, a maximum mid-span vertical deflection of 40mm was recorded. The applied load-deflection stiffness of this analysis was 30% lower than the previous analyses.

6.5.4 Composite beam model verification

This section describes the verification of the finite element analyses against the three full scale composite beam tests.

Analysis [i]: The comparison for the moment vs. mid-span deflection behaviour of the finite element model (FE-CB1) and experimental test CB1 is made in Fig. 6.13. The results are in good agreement up to the failure of the shear studs in Test CB1. Although the differences between the test and the model results are less than 1%, maximum moment capacity of the test is predicted accurately, the post failure characteristic of the experimental test was not able to be followed.

Analysis [ii]: The moment-deflection behaviour of FE-CB2 and the experimental test CB2 is shown in Fig. 6.14. The results are almost identical up to the maximum moment capacity, although the FE result at maximum is about 2% greater than the result in the experimental test. The point of failure almost coincides with the failure of the concrete and yielding in the transverse reinforcement which led to the reduction of moment capacity in the full scale test.

Analysis[iii]: The moment-deflection behaviour of FE-CB3 and the experimental test CB3 are shown in Fig. 6.15. The maximum moment capacity of the experimental test was considerably lower than the previous tests due to the pre-cracked arrangement. The comparison shows a small difference of about 7% between the test and the FE analysis, with the FE analysis being slightly higher throughout. The reason is believed to be that the behaviour of the pre-cracked model may not be accurately represented by just the spring element alone, the ultimate compressive strength of the slab may also be over estimated which led to the higher capacity in the analysis.

6.5.5 Conclusion

From the above analyses, it is concluded that the composite precast hollow core beam can be modelled in a simplified way. The results obtained from the model were compared against the full scale test results which showed that the model is

suitable for the analysis purpose. The main objective of the analysis is to obtain reliable moment-deflection data. The comparison showed that the model can predict the maximum applied load and hence the maximum moment capacity of the composite beam very well. This model will be used in Chapter 7 to carry out parametric studies on composite beam with different parameters.

6.6 References

1. *ABAQUS user manual,* Version 5.3.1 (1994), Hibbitt, Karlsson & Sorensen, inc., 1080 Main Street, Pawtucket, RI 02860-4847, USA.

2. Kotsovos, M. D. & Pavlovic, M. N., Non-linear finite element modelling of concrete structures: basic analysis, phenomenological insight, and design implications., *Engineering Computing,* Vol. 3, September, 1986, pp243-250.

3. BS8110, Part 1 (1997) Structural Use of Concrete, British Standards Institution, London.

4. Ahmed, B. Numerical Modelling of Semi-rigid Composite Joints, Ph.D. thesis, 1996, University of Nottingham, UK.

Concrete Grade	Tie bars	Tensile Strength, f_t' (N/mm^2)	Failure Mode	Compressive		Tensile	
				Max. Stress, σ_c (N/mm^2)	σ_c/0.67fcu ratio	Max. Stress, σ_t (N/mm^2)	σ_t / f_t' ratio
C25	R6	0.16	Tensile	9.40	0.56	0.18	1.13
	T8	0.51	Tensile	11.42	0.68	0.42	0.82
0.67fcu	T10	0.80	Tensile	13.14	0.78	0.58	0.73
=16.8 N/mm^2	T12	1.16	Tensile	14,83	0.88	0.86	0.74
	T16	2.05	Comp.	19.50	1.16	1.05	0.51
	T25	5.02	Comp.	21.7	1.29	0.97	0.19
C30	R6	0.16	Tensile	9.00	0.45	0.15	0.94
	T8	0.51	Tensile	12.53	0.62	0.46	0.90
0.67fcu	T10	0.80	Tensile	14.07	0.70	0.67	0.84
=20.1 N/mm^2	T12	1.16	Tensile	17.32	0.86	0.84	0.73
	T16	2.05	Comp.	22.55	1.12	1.06	0.52
	T25	5.02	Comp.	24.41	1.21	1.09	0.22
C40	T8	0.51	Tensile	12.53	0.47	0.46	0.90
	T10	0.80	Tensile	14.00	0.52	0.67	0.84
0.67fcu	T12	1.16	Tensile	17.32	0.65	0.84	0.73
=26.8 N/mm^2	T16	2.05	Comp.	30.81	1.15	1.03	0.50
	T25	5.02	Comp.	32.23	1.20	1.05	0.21

Table 6.1 Results of finite element model of precast slab and insitu infill

Test Ref.	Precast concrete strength (N/mm^2)	Insitu concrete strength (N/mm^2)	Load-slip curve of push off test taken	Tensile strength of steel flange (N/mm^2)	Young's modulus for steel flange (N/mm^2)	Tensile strength of steel web (N/mm^2)	Young's modulus for steel web (N/mm^2)
FE-CB1	50.0	33.0	T16-25-65	312.1	186.2	354.5	202.6
FE-CB2	50.0	25.5	T8-25-65F	312.3	191.1	355.8	203.3
FE-CB3	50.0	28.5	T8-25-65P	316.3	193.4	355.8	202.9

Table 6.2 Material properties used for the composite beam model

Reference	At first yield				At maximum load			
	Moment (kNm)	Mid-span Deflection (mm)	Stiffness, M_y/δ (kNm/mm)	End slip (mm)	Moment (kNm)	Mid-span Deflection (mm)	M_y/δ (kNm/mm)	End slip (mm)
FE-CB1	225	8.0	28.1	0.15	505	33.0	15.3	1.1
FE-CB2	195	7.0	26.0	0.12	480	41.0	11.7	2.6
FE-CB3	113	5.5	20.5	0.1	365	40.0	9.1	1.8

Table 6.3 Results of FE analyses

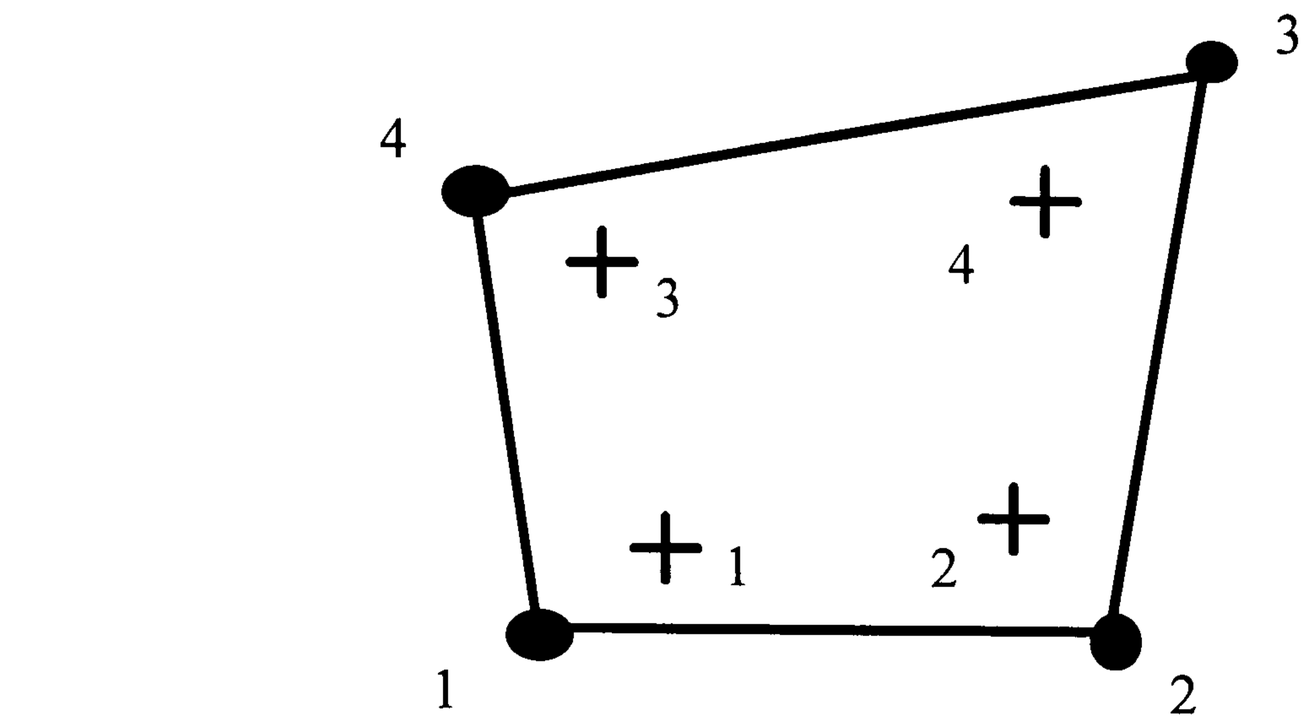

Fig. 6.1 4-nodes plane stress element (CPS4)

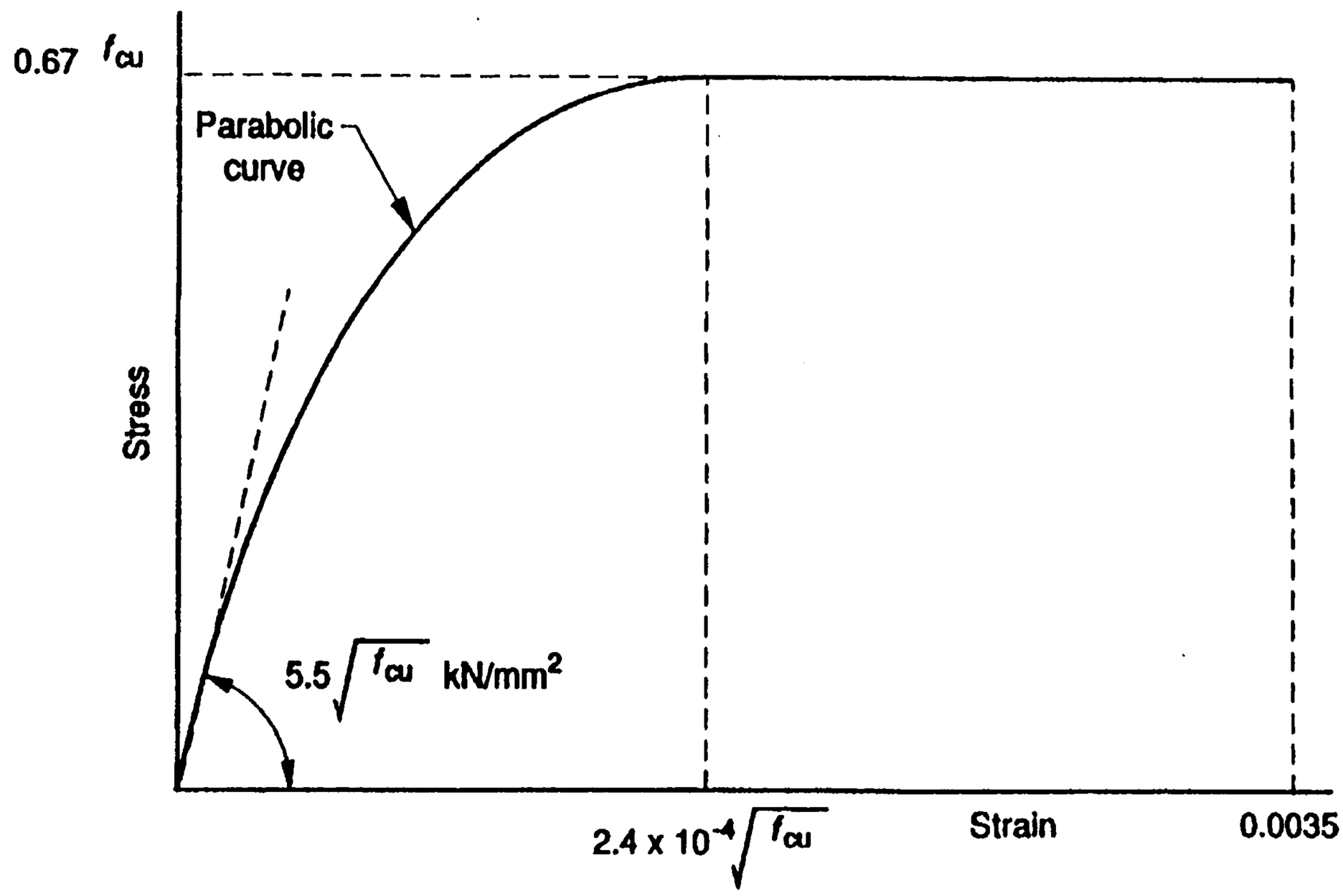

NOTE 1. 0.67 takes account of the relation between the cube strength and the bending strength in a flexural member. It is simply a coefficient and not a partial safety factor.
NOTE 2. f_{cu} is in N/mm^2.

Fig. 6.2 Stress-strain curve used for the concrete model (BS8110:1985)

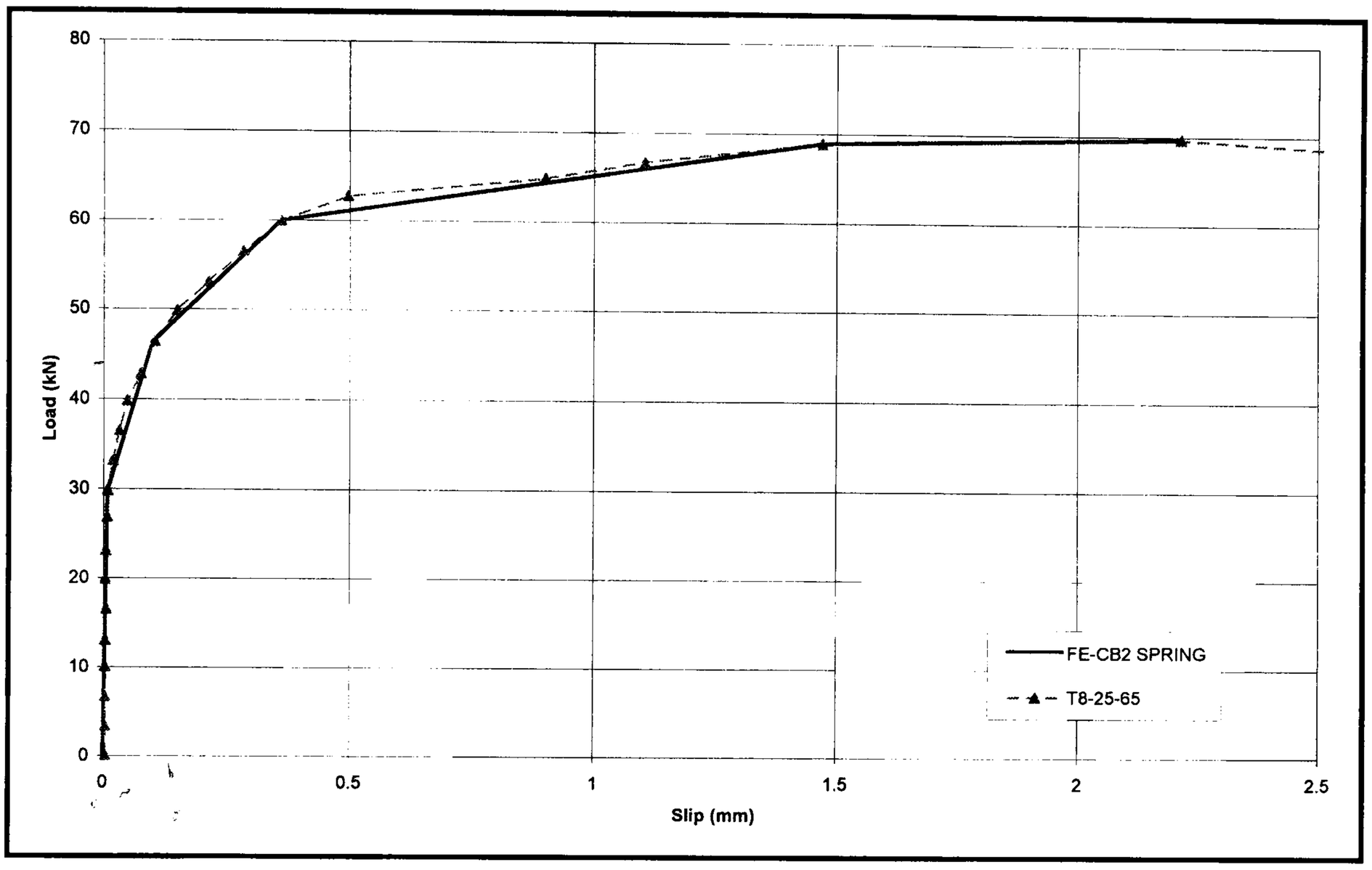

Fig. 6.3 Typical load-slip curve used for the FE analysis

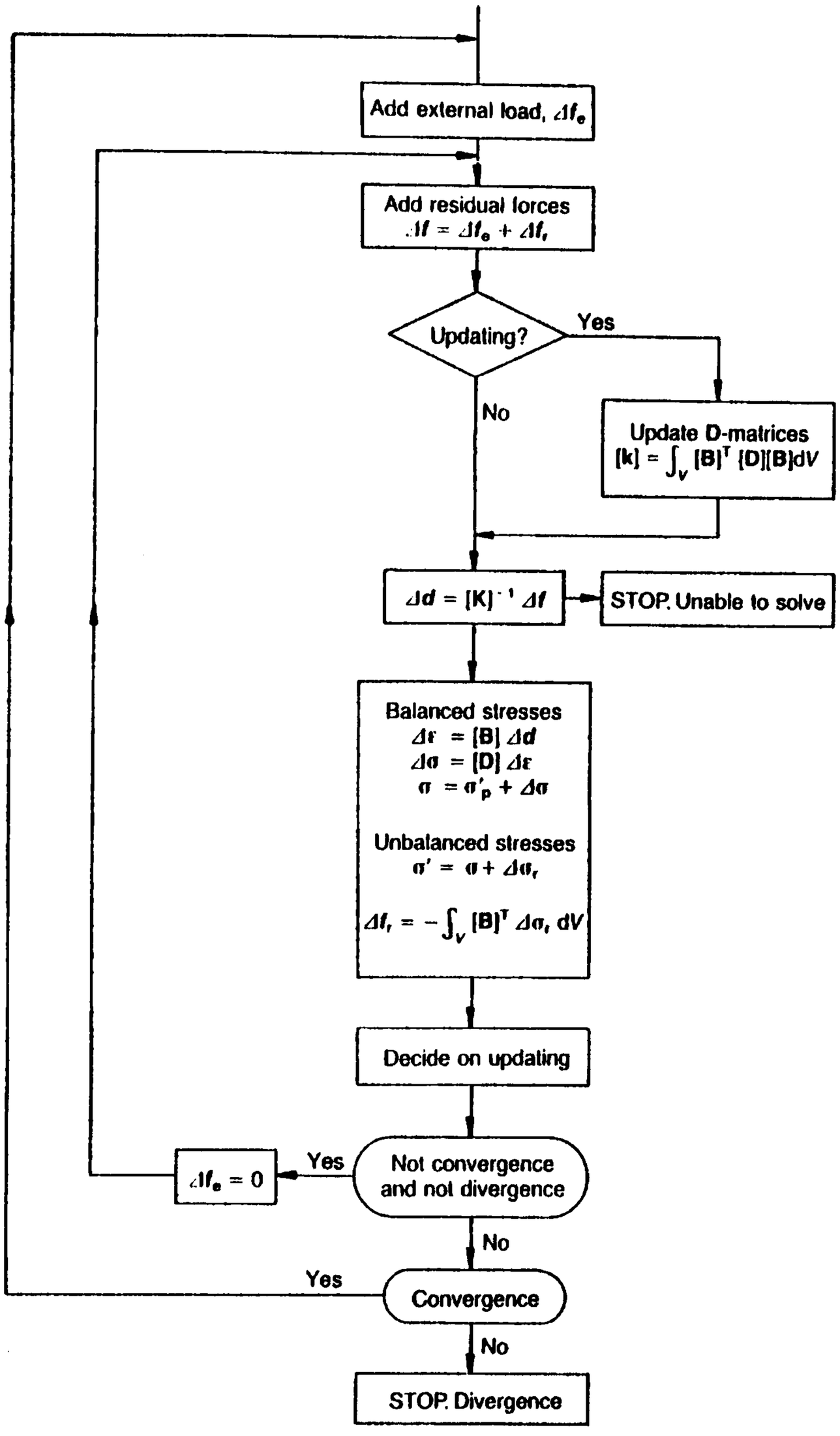

Fig. 6.4 Flow chart for non-linear finite element analysis procedure

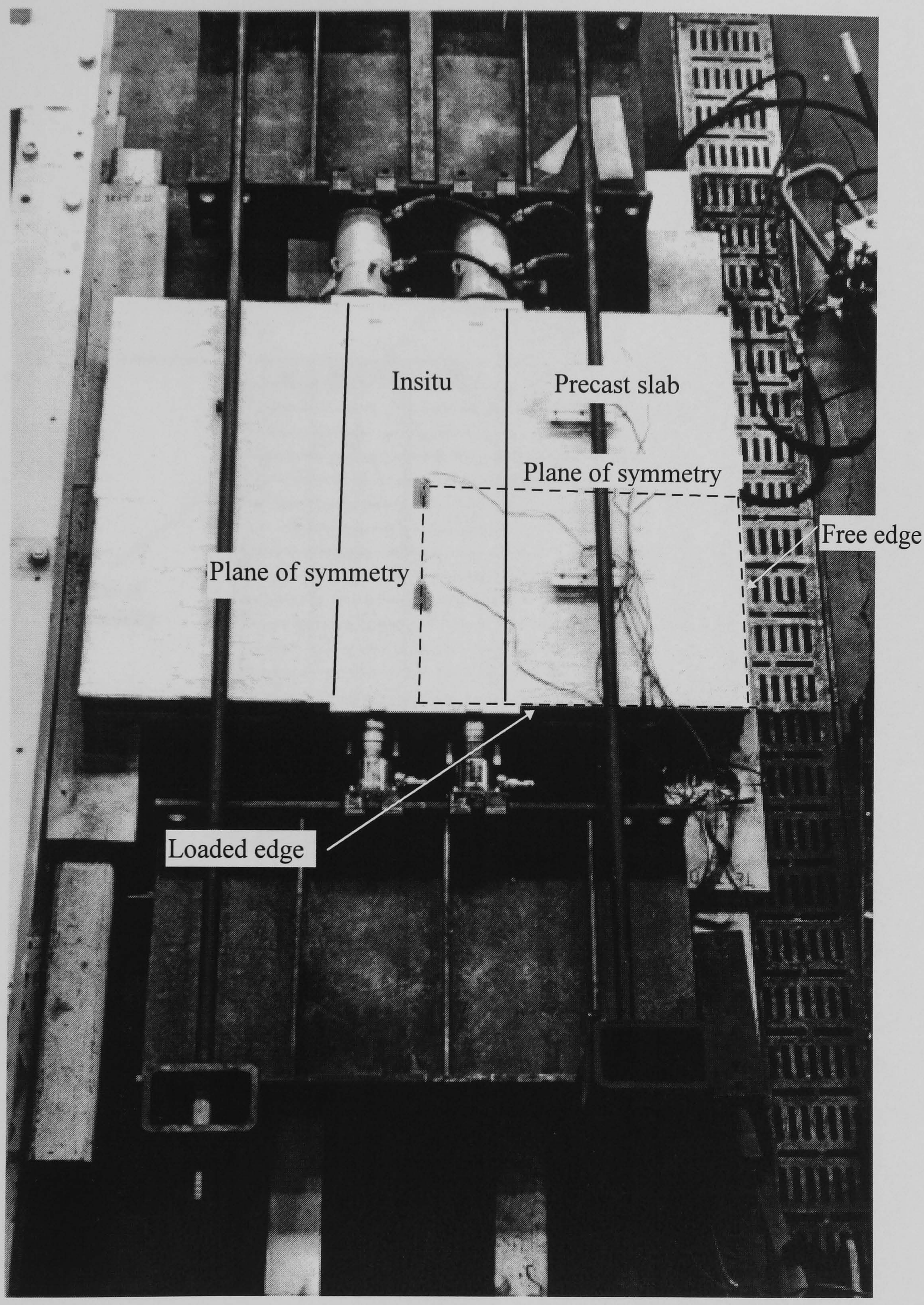

Fig. 6.5 Compression slab modelled as quarter of the top surface of the test assembly

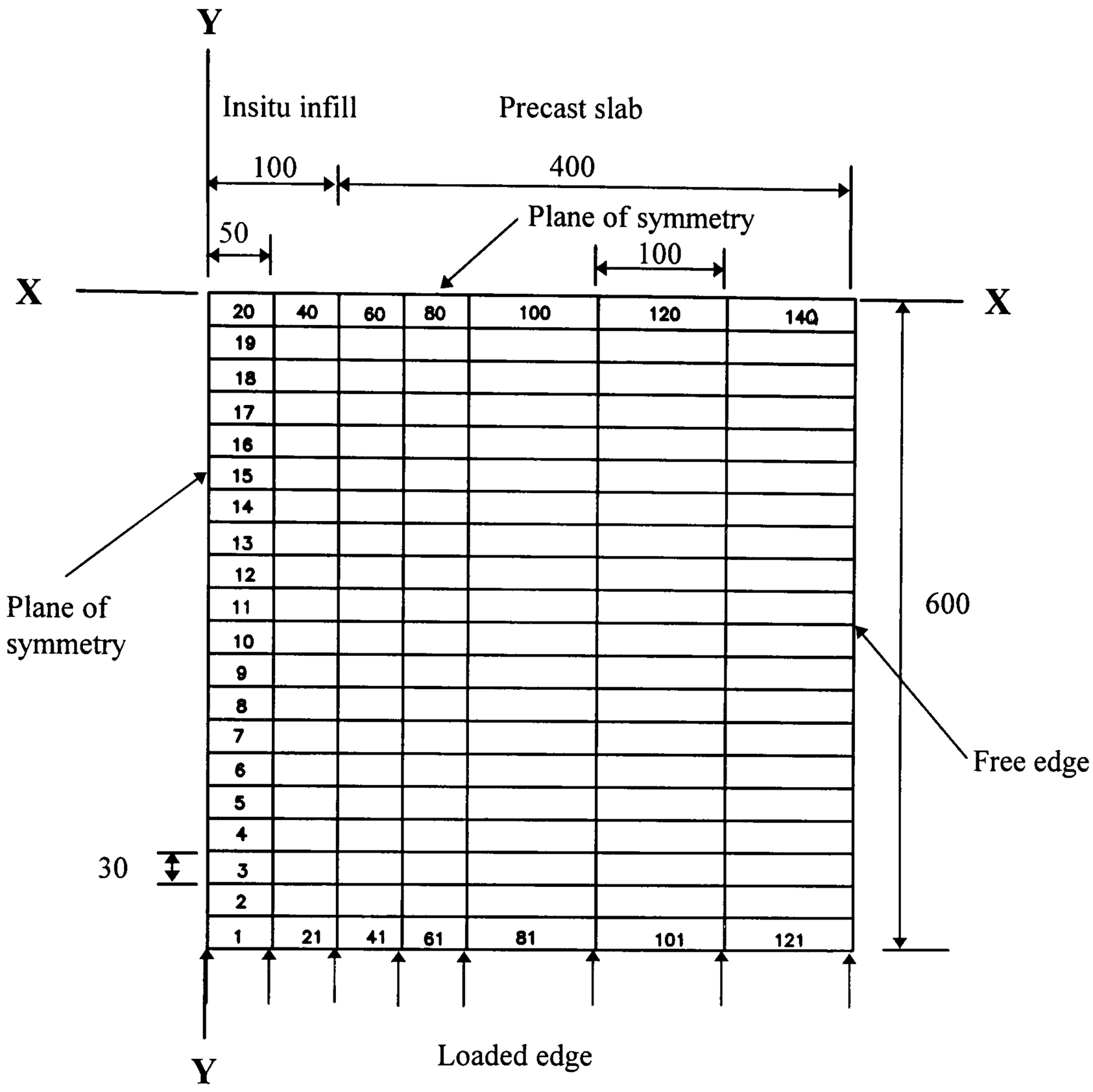

Fig. 6.6 Finite element mesh of composite slab model

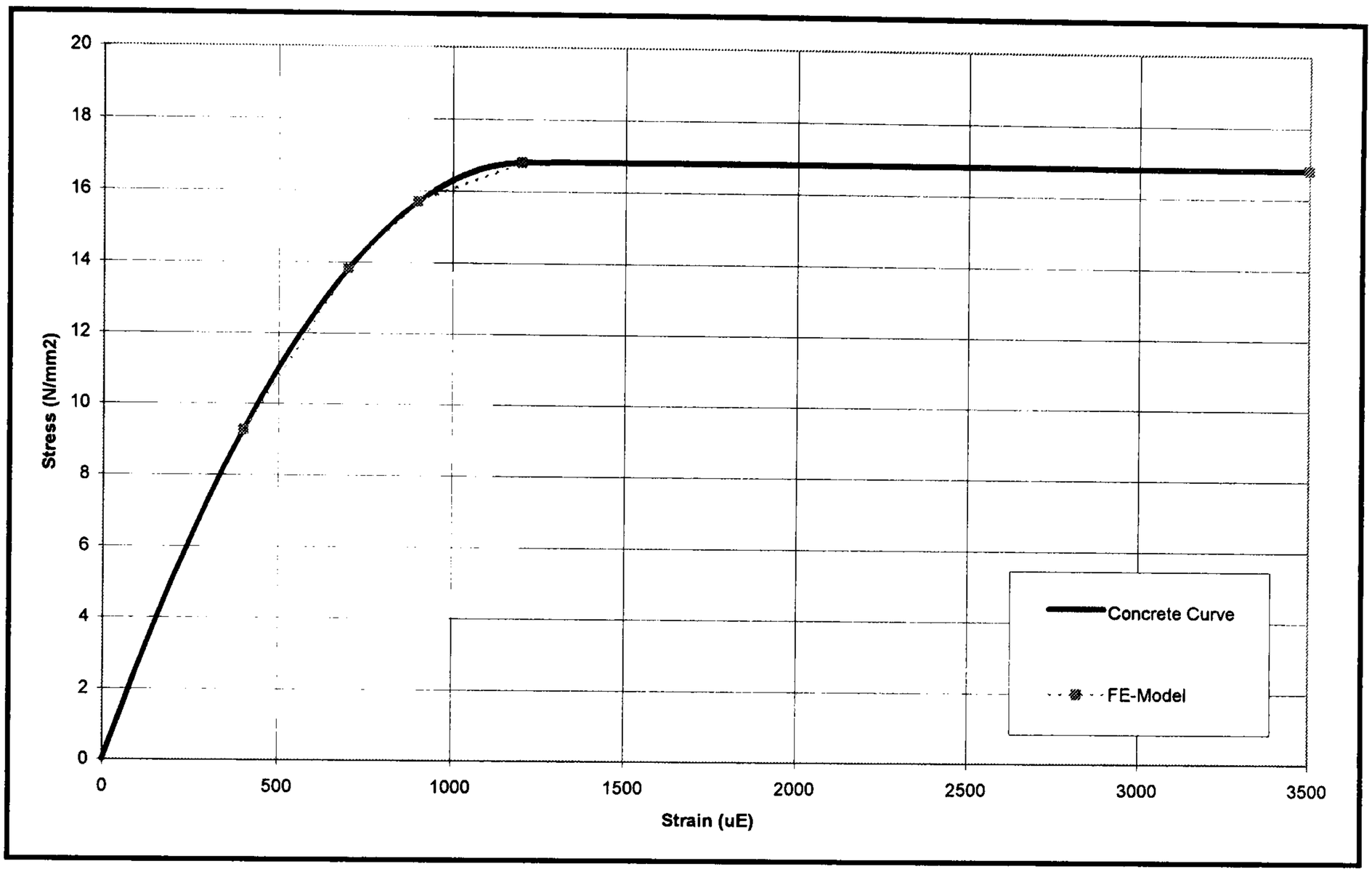

Fig. 6.7 Typical concrete stress-strain curve used for the concrete model

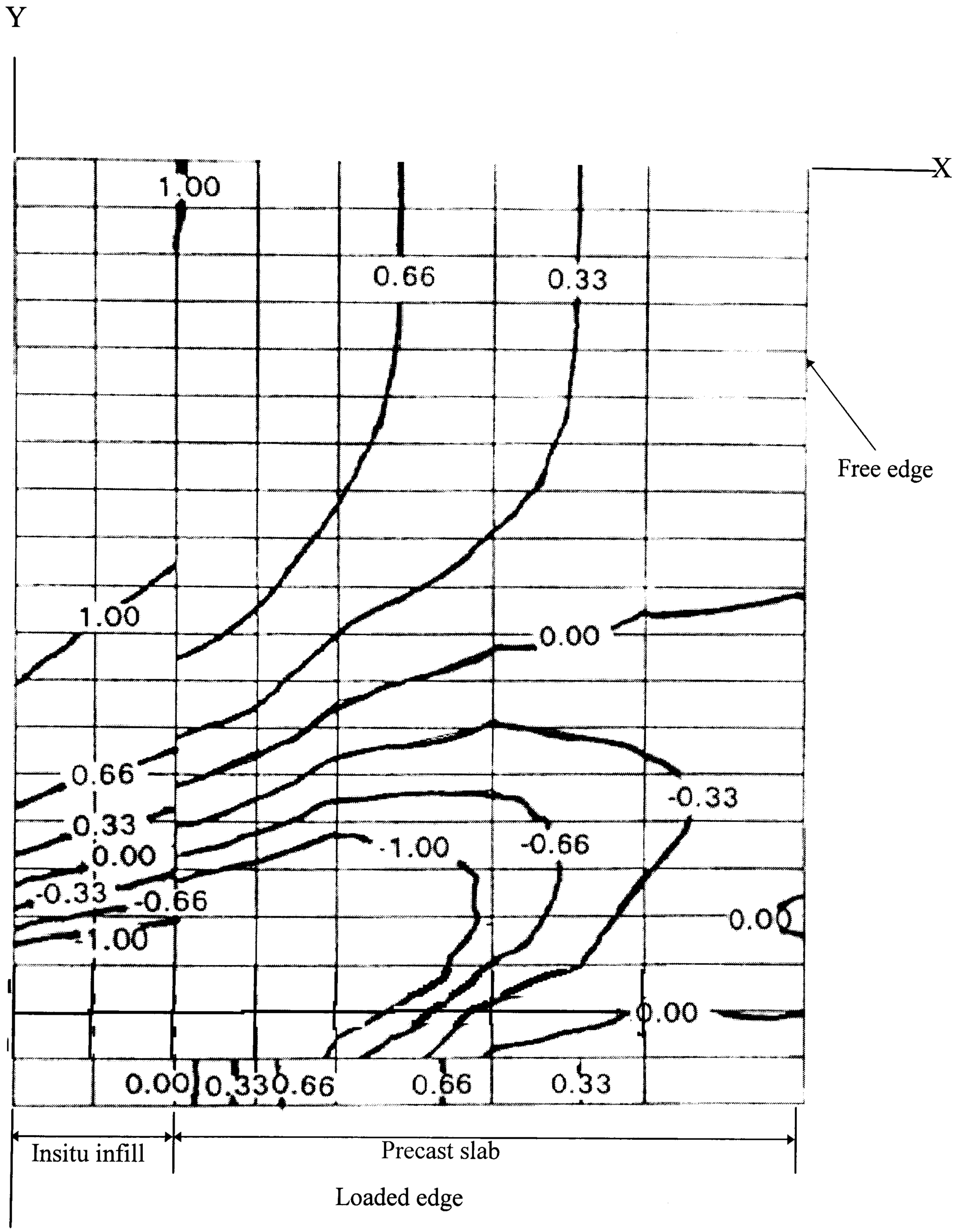

Fig. 6.8 Typical stress contours of composite slab model

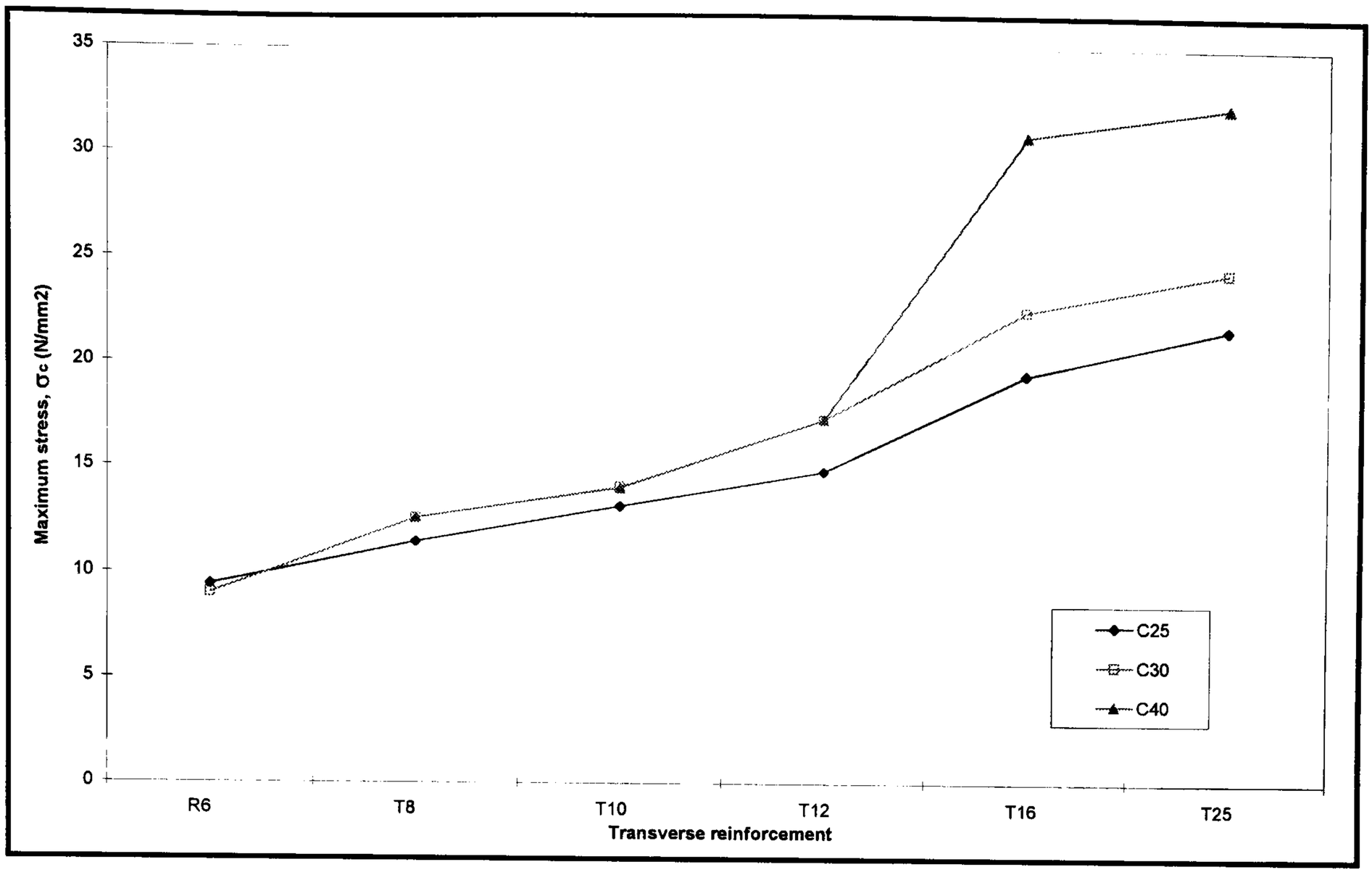

Fig. 6.9 Maximum compressive stress vs. transverse reinforcement

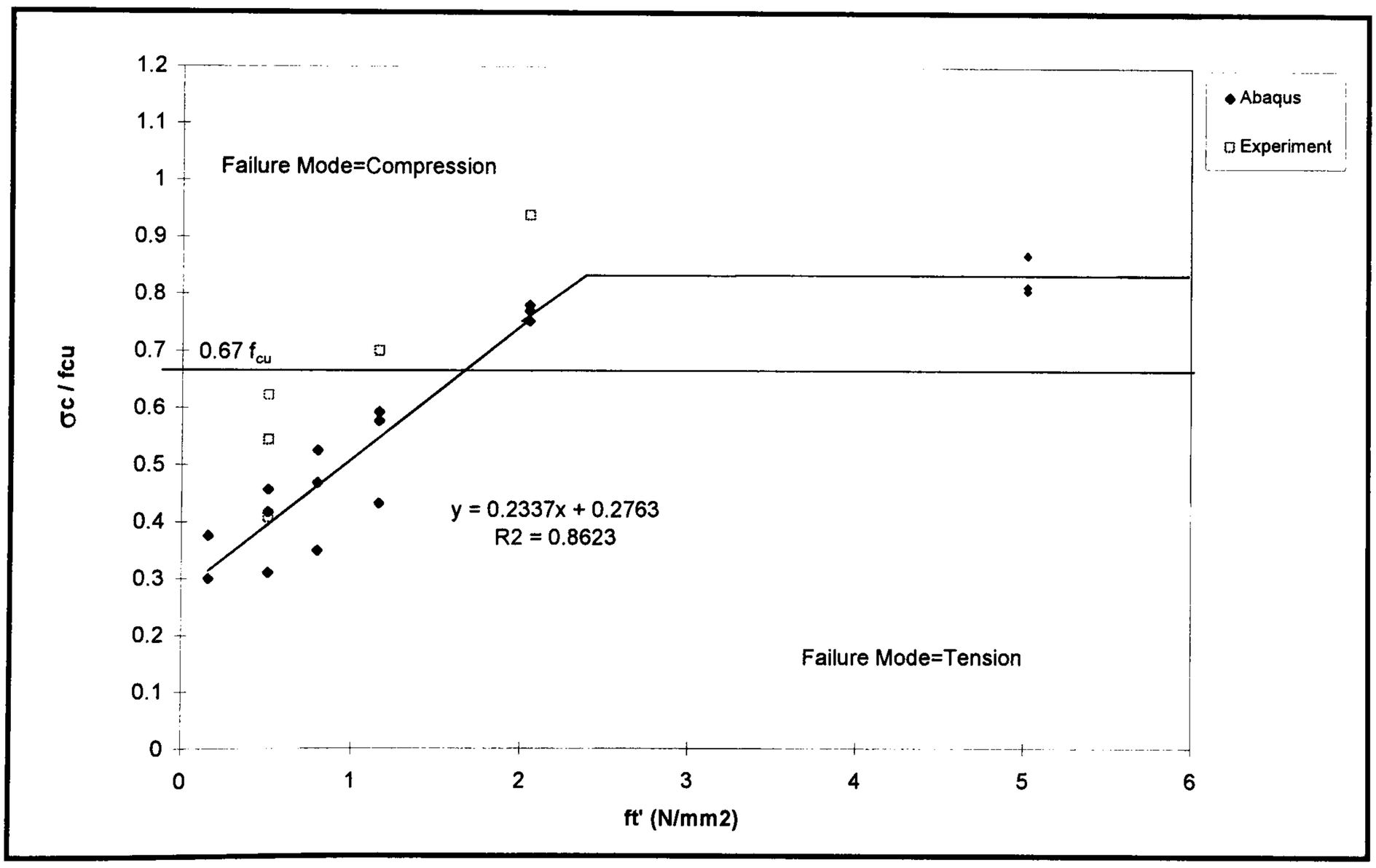

Fig. 6.10 Compressive stress ratio, σ_c/f_{cu} vs. effective tensile strength, f_t'

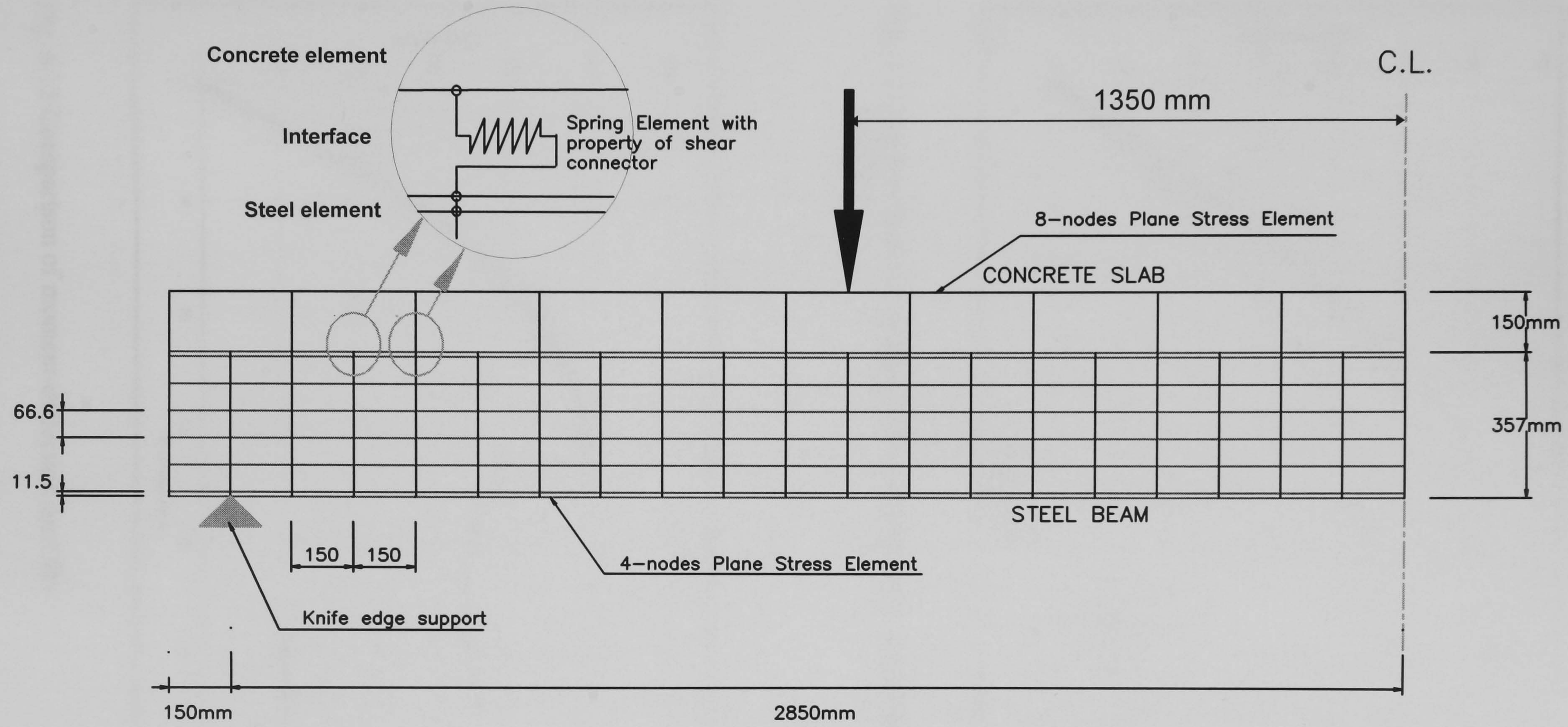

Fig. 6.11 Finite element mesh of composite beam

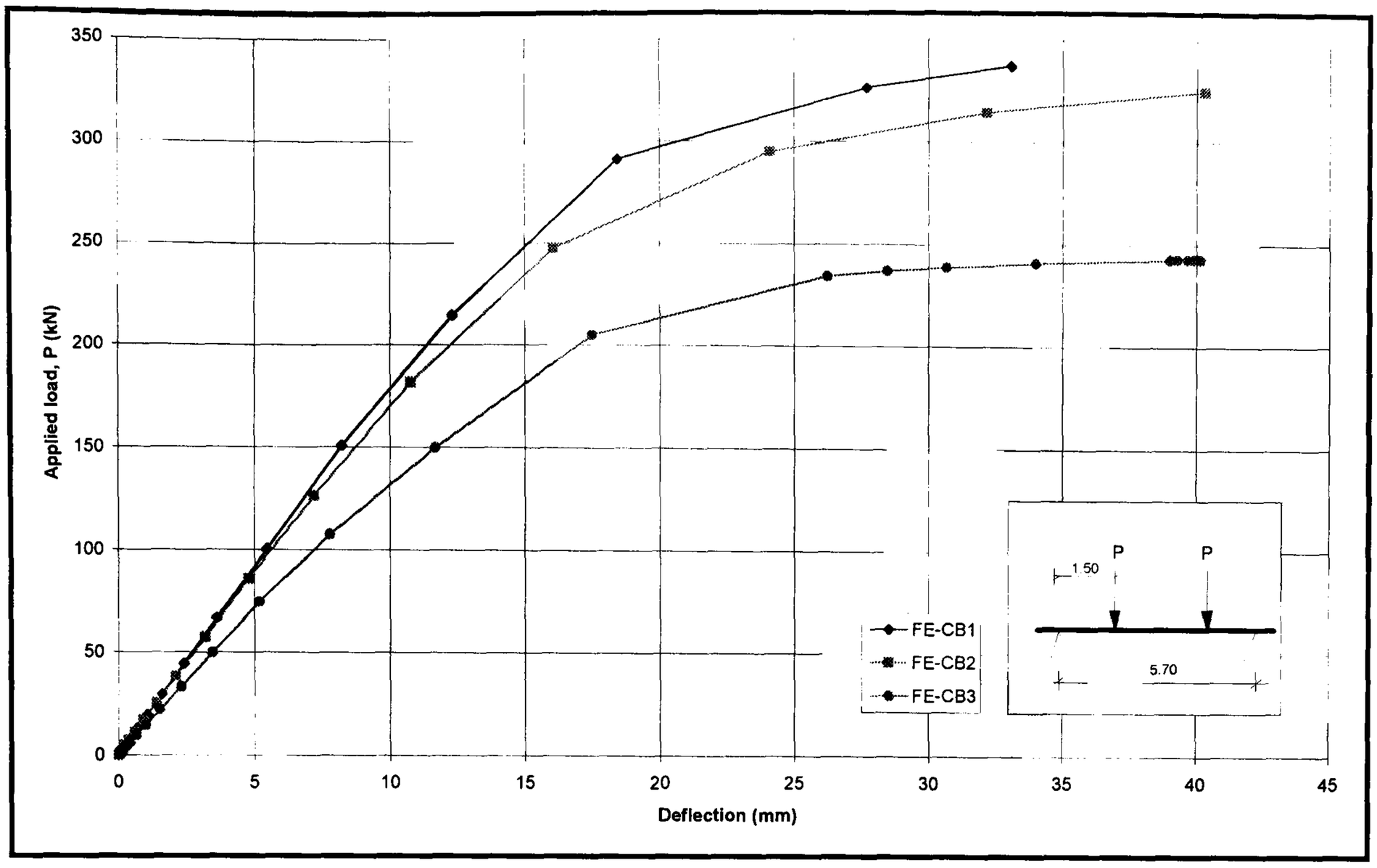

Fig. 6.12 Applied load vs. vertical mid-span deflection of FE-CB1, FE-CB2 & FE-CB3

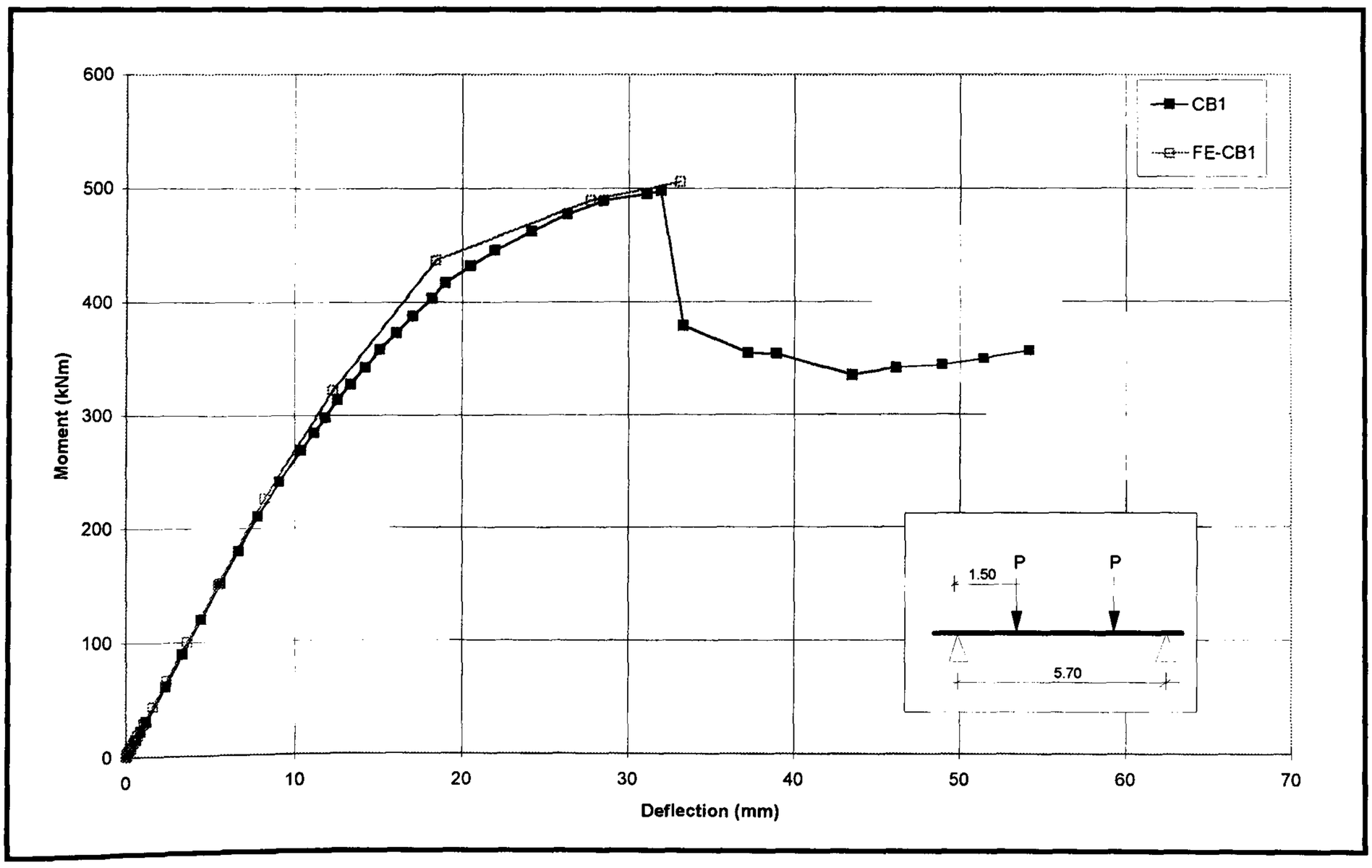

Fig. 6.13 Comparison of moment-deflection for CB1

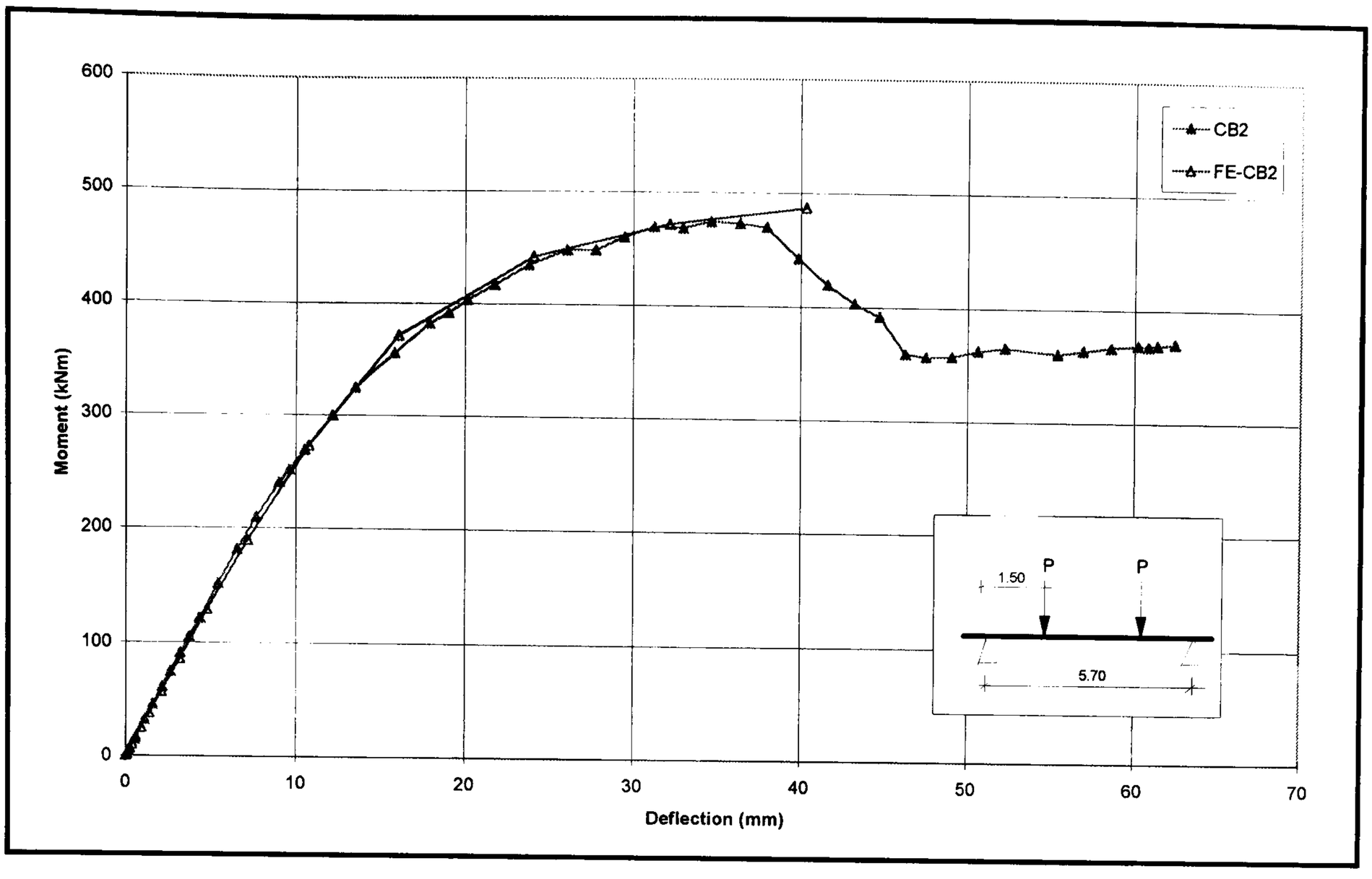

Fig. 6.14 Comparison of moment-deflection for CB2

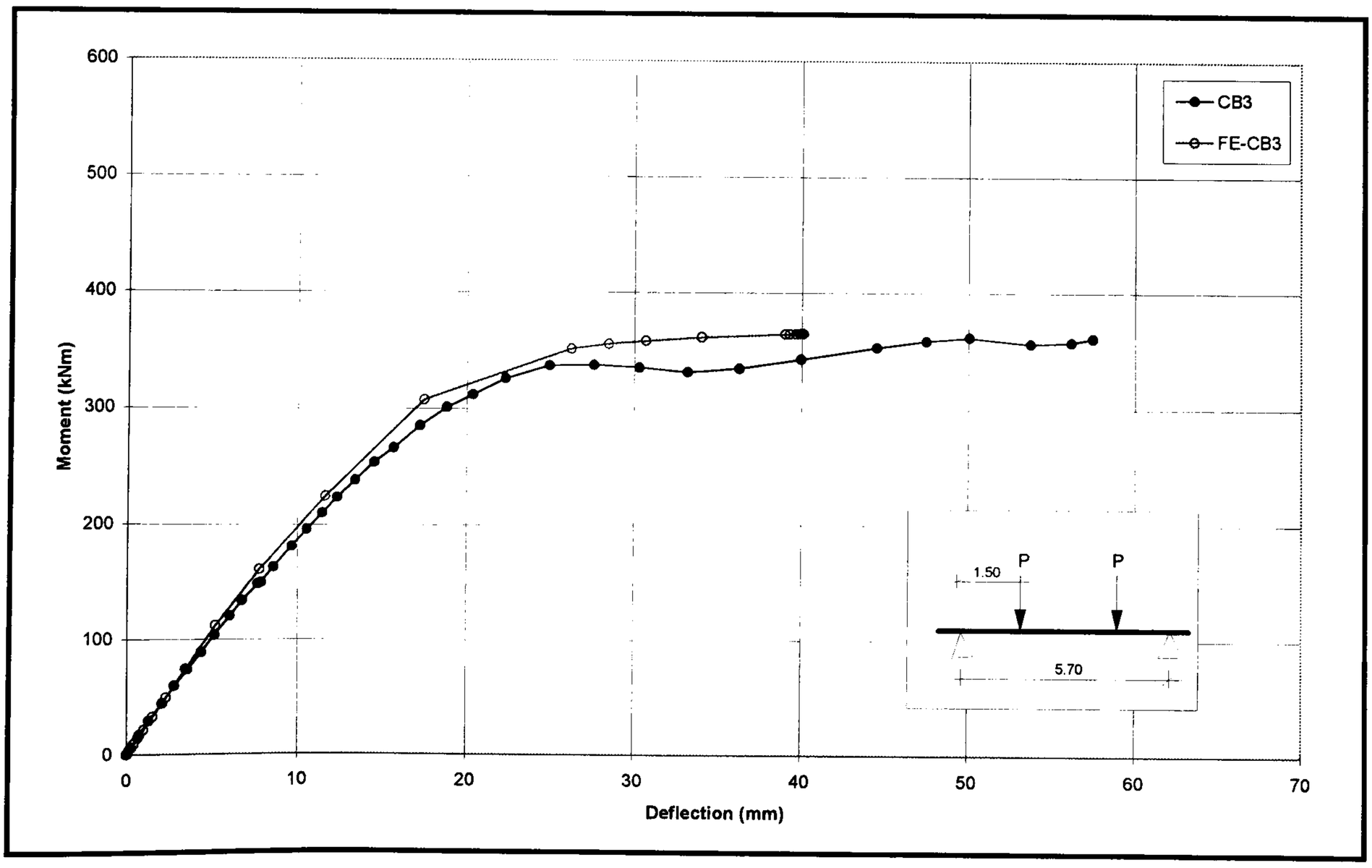

Fig. 6.15 Comparison of moment-deflection for CB3

Chapter 7

Parametric studies of composite beams

7.1 Introduction

Understanding the behaviour of the composite beam with hollow core slab construction is so far based on test evidence and subsequently a development of an FE model. Because of the large number of variables and potential modes of failure associated with this type of construction, it is unlikely that all aspects of the problem have been thoroughly examined. A finite element model to simulate the structural behaviour of the composite beam was described in detail in Chapter 6, and, having been verified against the full scale tests, it is now used to study the behaviour of a wide range of composite beams and to gain an insight into the load-deflection characteristic and moment capacity. Parametric studies were carried out to investigate the flexural behaviour with variations in: transverse reinforcement ratio; depth of precast hollow cored slab; stud spacing, η and steel UB section. Results were analysed and beam design charts formulated.

7.2 Parametric study

Table 7.1 shows the values of parameters selected for the FE analysis. They are considered to be the most influential for this type of construction. Two sizes of transverse reinforcing bar were used, i.e. T8 and T16 at 300mm spacing, with the percentage of reinforcement being 0.11% and 0.45%, respectively. It is reckoned to be the most common type of rebar used for this construction. Three depths of the hollow core slab, 150mm, 200mm and 250mm were used. These depths are commonly used in floors spanning up to ten metres. Shear stud centres of η = 150mm, 300mm and 450mm were used. Finally, with the variation in steel section, three sections of grade 43a universal beam were chosen, i.e. 356 x 171 x 51 UB, 533 x 210 x 82 UB and 762 x 267 x 147 UB. This represented the range of section sizes likely to be used for composite beams. Standard section properties of section size and material yield strength are used for the parametric studies (i.e. E_s = 205kN/mm^2, p_y = 275N/mm^2, f_{cu}=37.5N/mm^2, E_c=33.6kN/mm^2).

Forty-five analyses were conducted with one variable parameter each time, according to Table 7.2. Parametric studies for 762 x 267 x 147 UB with T16 transverse reinforcement were not performed after the analyses were carried out for 762 x 267 x 147 UB with T8 transverse reinforcement because it was felt that the effect of composite action for such a beam is not influential. Although the shear stud push off data were generated only for 150mm deep hcu, it has to be assumed that the results are similar for the 200mm and 250mm deep hcu.

7.3 Results and discussion

The results of the FE analysis are shown in Table 7.3. Plastic moment capacity of the fully restrained steel beam, $M_{R(steel)}$ is obtained from steelwork design guide[1] (i.e. $M_{R(steel)} = P_y \times S_x$). The increases in moment capacity due to composite action over the bare steel counterpart is discussed in detail according to changes in transverse reinforcement; slab depth; stud spacing and UB size.

7.3.1 Increases in moment capacity due to composite action

Table 7.4 shows the M_R / $M_{R(steel)}$ ratio for the parametric study. The study showed an increase in moment capacity for all the analyses carried out with up to 130% increase over the bare steel counterpart for the 356 x 171 x 51 UB section. The contribution from the composite action is less significant for the 762 x 267 x 147 UB section with up to 21% increase in moment capacity.

7.3 2 Change in transverse reinforcement

Two sizes of reinforcing bar were used in the parametric studies, i.e. T16 & T8. Fig. 7.1 shows moment-deflection curves for the different cases. No significant increases in stiffness were recorded, although an increase in the transverse

reinforcement ratio increased the maximum moment capacity of the composite beam. The ductility of the beam was reduced leading to a sudden failure. The span / deflection ratio at failure was 125 to 175. Table 7.5 shows the percentage increase in moment capacity due to increase in percentage of transverse reinforcement varied from 2.3% to 9.8%. This is comparable with the full scale test results of CB2 and CB1 with M_R of 474.0kNm and 497.3kNm respectively, an increase of 4.9 percent. As compared with the FE results for *PS1* and *PS19* with M_R of 451.7kNm and 471.3kNm respectively, an increase of 4.3 percent. The difference in the increases in M_R between experimental results and FE results are possibly due to the effect of the other parameters.

7.3.3 Change in slab thickness

To study the effect of changes in slab thickness, FE analyses with 150mm, 200mm and 250mm slab thickness were conducted. Fig. 7.2 and 7.3 show examples of moment-deflection curves with variation in slab thickness.

Table 7.6 shows that an increase in slab thickness led to increases in moment capacity. This is to be expected as an increase in thickness of slab would raise the neutral axis of the composite beam and increases the overall depth of the section, hence increasing the lever arm of the section. As shown in Fig. 7.2, the stiffnesses of the composite beams were 58%, 110% and 163% higher than the stiffnesses of

the bare steel with 150mm slab, 200mm slab and 250mm slab, respectively. As the steel section became comparatively deep compared with the slab, this contribution became less significant as shown in Fig. 7.3. The stiffnesses of the composite beams were 17%, 21% and 26% higher than the stiffnesses of 762 x 267 x 147 UB with 150mm, 200mm and 250mm slab respectively. From the FE analysis, it is also shown that the composite beam with a 250mm slab failed at a much lower mid span deflection. It is difficult to conclude that this effect is solely caused by the increase in slab thickness, but the mode of failure of these tests are caused by tensile failure of the concrete. As the neutral axis moved above the steel concrete interface, the bottom part of concrete slab is in tension. As concrete is weak in tension this would lead to tensile failure in concrete.

With the deeper steel section of 762 x 267 x 147 UB, see Fig. 7.3, the neutral axis is located in the steel section, even with a 250mm slab, and the concrete slab is therefore always in compression. Thus the failure mode of the composite beam with 150mm, 200mm and 250mm slabs are similar and no significant increase in M_R or stiffness is noticed; the slight increase in M_R is mainly due to the increase in overall depth of the composite section with the variation in depth of the concrete slab.

Although the finding is not conclusive, future experimental works of full scale beam test and push off test with different slab thickness should be carried out to verify these FE results.

7.3.4 Change in stud spacing, η

To study the effect of changes in stud spacing, FE analyses with η = 150mm, 300mm and 450mm were conducted. Fig. 7.4 shows a comparison of moment-deflection curves with variation in stud spacing. The decreases in M_R with increases in stud spacing are presented in Table 7.7. The results showed that increases in stud spacing caused significant reductions in moment capacity and increases in mid-span deflection at the same load level. For example, in Fig. 7.4, the mid-span deflection of the composite beam at moment = $M_{R(Steel)}$ was increased from 10mm to 13mm and 15.5mm when stud spacing increased from 150mm to 300mm and to 450mm, respectively, a 18% and 43% reduction in stiffness compared to the composite beam with η = 150mm.

The moment capacity ratios from the FE analyses with variation in stud spacing are shown in Fig. 7.5 and Fig. 7.6. Reduction in moment capacity is less noticeable with increases in η for composite beam with 762 x 267 x 147 UB, it is because the composite action between the steel beam and concrete slab is relatively less significant. The moment capacity ratio, $M_R/M_{R(steel)}$, varied from 1.15 to 1.21 for composite beam with 762 x 267 x 147 UB compared to 1.41 to 2.23 for composite beam with 356 x 171 x 51 UB.

7.3.5 Change in steel section

It is clear that increases in steel section size will increase the M_R of the composite beam, but it is interesting to note the $M_R/M_{R(steel)}$ ratio is reduced with increase in steel section. For example, for 150mm slab, T8 rebar and η = 150mm, $M_R/M_{R(steel)}$ ratio reduced from 1.84 to 1.49 and down to 1.21 with steel section increased from 356UB to 533UB and then to 762UB. Fig. 7.7 shows the moment-deflection curves with variation in steel section for 150mm slab; T8 rebars and 150mm stud spacing. It is also interested to notice for the mode of failure for both 356UB and 533UB is caused by yielding of steel section while for the 762UB, mode of failure is due to compression failure in concrete. Therefore, it is concluded that the configuration of a composite beam with the depth of steel beam to slab ratio of more than three might lead to brittle failure and should be avoided.

7.4 Design charts

From the results of the FE analysis, design charts have been prepared for uniformly distributed ultimate "factored" loadings for the design span of the composite beam. Limitations for the data used are based on the FE model described in Chapter 6 and are summarised as follows:

1. Concrete strength of the insitu infill to be 25N/mm^2.
2. Shear connectors are 19mm x 125mm nominal TRW-Nelson headed studs.

3. T8 rebars at 300mm centres are used as transverse reinforcement.

In addition to the above limitations, the following design limitations are also made:

1. Full lateral restraint to the compression flange of steel beam is provided by the hcu.
2. Maximum span of the composite beam is limited by the moment capacity and the deflection limit of span/200 at the construction stage.
3. Maximum floor span of 7.5m for 150 hcu (self weight = 2.46 kN/m^2); 9m for 200 hcu (self weight = 2.94 kN/m^2) and 11m for 250 hcu (self weight = 3.49 kN/m^2) is allowed in the design.
4. A construction load of 0.5kN/m^2 is allowed for the supported floor area.
5. Serviceability stresses in the steel beam is limited to 50% of the yield strength of steel beam at construction stage.

Fig. 7.8 to Fig. 7.10 show the design charts for composite beams with 150mm, 200mm and 250mm precast hollow core slabs. The plateau on each curve is the limiting span based on the moment capacity and the serviceability stresses of the steel section and/or the deflection limit at the non-composite stage, i.e. construction stage.

7.5 Conclusions

The finite element model described in Chapter 6 was used to study the effects of changes in transverse reinforcement ratio, slab thickness, stud spacing and steel section. In this chapter, FE analyses have shown that increased transverse reinforcement significantly increases the moment capacity of the composite beam but ductility of the beam is reduced leading to brittle failure of the composite beam. It is also evident that increases in slab thickness would lead to increases in moment capacity, though slab failure might occur due to direct tensile force in the slab. The increases in stud spacing greatly reduced the moment capacity and increased deflection of the composite beam. It is also noted that a composite beam with steel beam to slab depth ratio over 3.0 is not effective and could lead to compressive failure of the concrete slab.

The general conclusion to be drawn from all the analyses is that this FE modelling can accurately predict the flexural behaviour and moment capacity of the precast hollow core composite beam. It offers a reliable and very cost-effective alternative to full scale laboratory testing as a way of generating results. Based on the results of the FE analyses, design charts are developed and used for design of this type of composite beam.

7.6 References

1. Steelwork Design Guide to BS 5950: Part 1 (1990): Volume 1, Section Properties, Member Capacities, 3rd Edition. The Steel Construction Institute.

Variable	Range of variable selected
Transverse Reinforcement	T8 @ 300 c/c, T16 @ 300 c/c
Depth of precast concrete slab	150mm, 200mm, 250mm
Shear connector spacing, η	150mm, 300mm, 450mm
Size of steel section	356 x 171 x 51 UB, 533 x 210 x 82 UB, 762 x 267 x 147 UB

Table 7.1 Values of parameters selected for parametric studies

UB serial size	Studs spacing, η (mm)	Slab depth (mm) and transverse bar size					
		150		200		250	
		T8	T16	T8	T16	T8	T16
356 x 171 x 51UB	150	*PS1*	*PS19*	*PS4*	*PS22*	*PS7*	*PS25*
	300	*PS2*	*PS20*	*PS5*	*PS23*	*PS8*	*PS26*
	450	*PS3*	*PS21*	*PS6*	*PS24*	*PS9*	*PS27*
533 x 210 x 82UB	150	*PS10*	*PS28*	*PS13*	*PS31*	*PS16*	*PS34*
	300	*PS11*	*PS29*	*PS14*	*PS32*	*PS17*	*PS35*
	450	*PS12*	*PS30*	*PS15*	*PS33*	*PS18*	*PS36*
762 x 267 x 147UB	150	*PS37*	-	*PS40*	-	*PS43*	-
	300	*PS38*	-	*PS41*	-	*PS44*	-
	450	*PS39*	-	*PS42*	-	*PS45*	-

Table 7.2 Schedule for the parametric study

UB serial size	Studs spacing, η (mm)	Slab depth (mm) and transverse bar size					
		150		200		250	
		T8	T16	T8	T16	T8	T16
356 x 171 x 51UB	150	*451.7*	*471.3*	*501.3*	*529.8*	*547.8*	*566.7*
$M_{R(steel)}$ = 246 kNm	300	*376.5*	*403.4*	*407.4*	*437.7*	*439.4*	*482.3*
	450	*346.0*	*367.5*	*389.0*	*398.0*	*401.6*	*420.8*
533 x 210 x 82UB	150	*842.3*	*868.2*	*875.0*	*920.9*	*915.6*	*937.8*
$M_{R(steel)}$ = 566 kNm	300	*724.5*	*779.3*	*758.7*	*817.2*	*788.3*	*854.7*
	450	*687.6*	*729.6*	*711.6*	*750.3*	*752.6*	*806.7*
762 x 267 x 147UB	150	*1659.0*	-	*1633.5*	-	*1657.7*	-
$M_{R(steel)}$ = 1370 kNm	300	*1609.5*	-	*1630.5*	-	*1638.0*	-
	450	*1557.0*	-	*1555.5*	-	*1579.5*	-

Table 7.3 Results of moment capacity, M_R (kNm) for the parametric study

UB serial size	Studs spacing, η (mm)	Slab depth (mm) and transverse bar size					
		150		200		250	
		T8	T16	T8	T16	T8	T16
356 x 171 x 51UB	150	*1.84*	*1.92*	*2.04*	*2.15*	*2.23*	*2.30*
	300	*1.53*	*1.64*	*1.66*	*1.78*	*1.79*	*1.96*
	450	*1.41*	*1.49*	*1.58*	*1.62*	*1.63*	*1.71*
533 x 210 x 82UB	150	*1.49*	*1.53*	*1.55*	*1.63*	*1.62*	*1.66*
	300	*1.28*	*1.38*	*1.34*	*1.44*	*1.39*	*1.51*
	450	*1.21*	*1.29*	*1.26*	*1.33*	*1.33*	*1.43*
762 x 267 x 147UB	150	*1.21*	-	*1.19*	-	*1.21*	-
	300	*1.17*	-	*1.19*	-	*1.20*	-
	450	*1.14*	-	*1.14*	-	*1.15*	-

Table 7.4 Moment capacity ratio, M_R / $M_{R(steel)}$ for the parametric study

UB Serial size	η (mm)	Depth of slab (mm)		
		150	200	250
356 x 171 x 51UB	150	*4.3*	*5.7*	*3.5*
	300	*7.1*	*7.4*	*9.8*
	450	*6.2*	*2.3*	*4.8*
533 x 210 x 82UB	150	*3.1*	*5.2*	*2.4*
	300	*7.6*	*7.7*	*8.4*
	450	*6.1*	*5.4*	*7.2*

No comparison for 762 x 267 x 147 UB

Table 7.5 Percentage increase in M_R for T8 to T16 rebars. (All other parameters constant)

UB Serial size	η (mm)	Percentage increase in M_R for 200mm to 150mm deep slab		Percentage increase in M_R for 250mm to 150mm deep slab	
		T8	T16	T8	T16
356 x 171 x 51UB	150	*11.0*	*12.4*	*21.3*	*20.2*
	300	*8.2*	*8.5*	*16.7*	*19.6*
	450	*12.4*	*8.3*	*16.1*	*14.5*
533 x 210 x 82UB	150	*3.9*	*6.1*	*8.7*	*8.0*
	300	*4.7*	*4.9*	*8.8*	*9.7*
	450	*3.5*	*2.8*	*9.5*	*10.6*
762 x 267 x 147UB	150	*-1.5*	-	*0.0*	-
	300	*1.3*	-	*1.8*	-
	450	*0.0*	-	*1.4*	-

Table 7.6 Percentage increase in M_R for depth of slab expressed in term of M_R for 150 mm slab (All other parameters constant)

UB Serial size	Depth of slab (mm)	Percentage decrease in M_R for increases in η from 150mm to 300mm		Percentage decrease in M_R for increases in η from 150mm to 450mm	
		T8	T16	T8	T16
356 x 171 x 51UB	150	*-16.7*	*-14.4*	*-23.4*	*-22.0*
	200	*-18.7*	*-17.4*	*-22.4*	*-24.9*
	250	*-19.8*	*-14.9*	*-26.7*	*-25.7*
533 x 210 x 82UB	150	*-14.0*	*-10.2*	*-18.4*	*-16.0*
	200	*-13.3*	*-11.3*	*-18.7*	*-18.5*
	250	*-13.9*	*-8.9*	*-17.8*	*-14.0*
762 x 267 x 147UB	150	*-3.0*	-	*-6.1*	-
	200	*-0.2*	-	*-4.8*	-
	250	*-1.2*	-	*-4.7*	-

Table 7.7 Percentage decrease in M_R for increases in shear stud spacing, η (All other parameters constant)

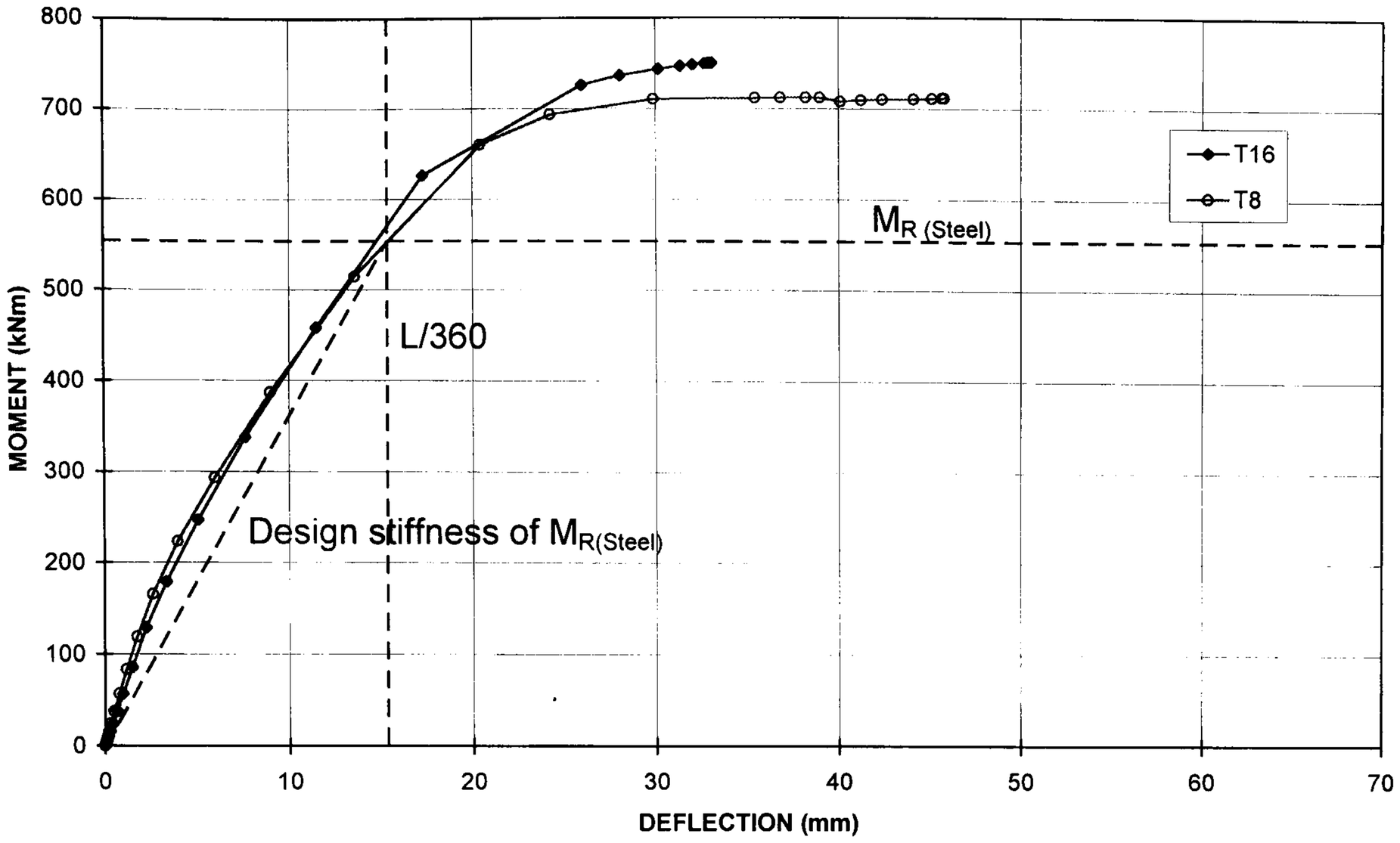

Fig.7.1 Moment-deflection curves for variations of transverse reinforcement for 533 x 210 x 82UB, 200mm slab and η = 450mm

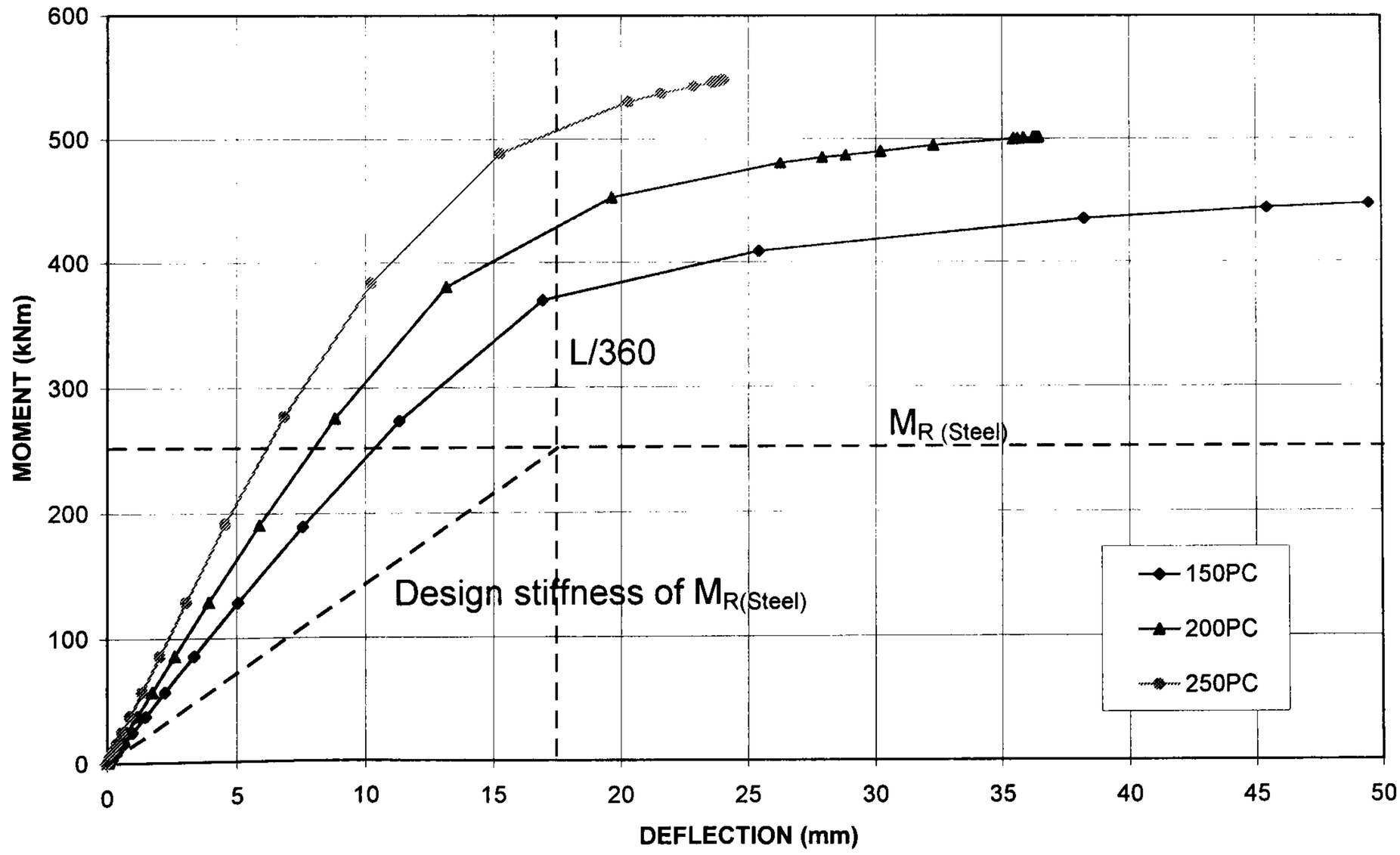

Fig.7.2 Moment-deflection curves for variations of slab thickness for 356 x 171 x 51UB, T8 rebar and η = 150mm

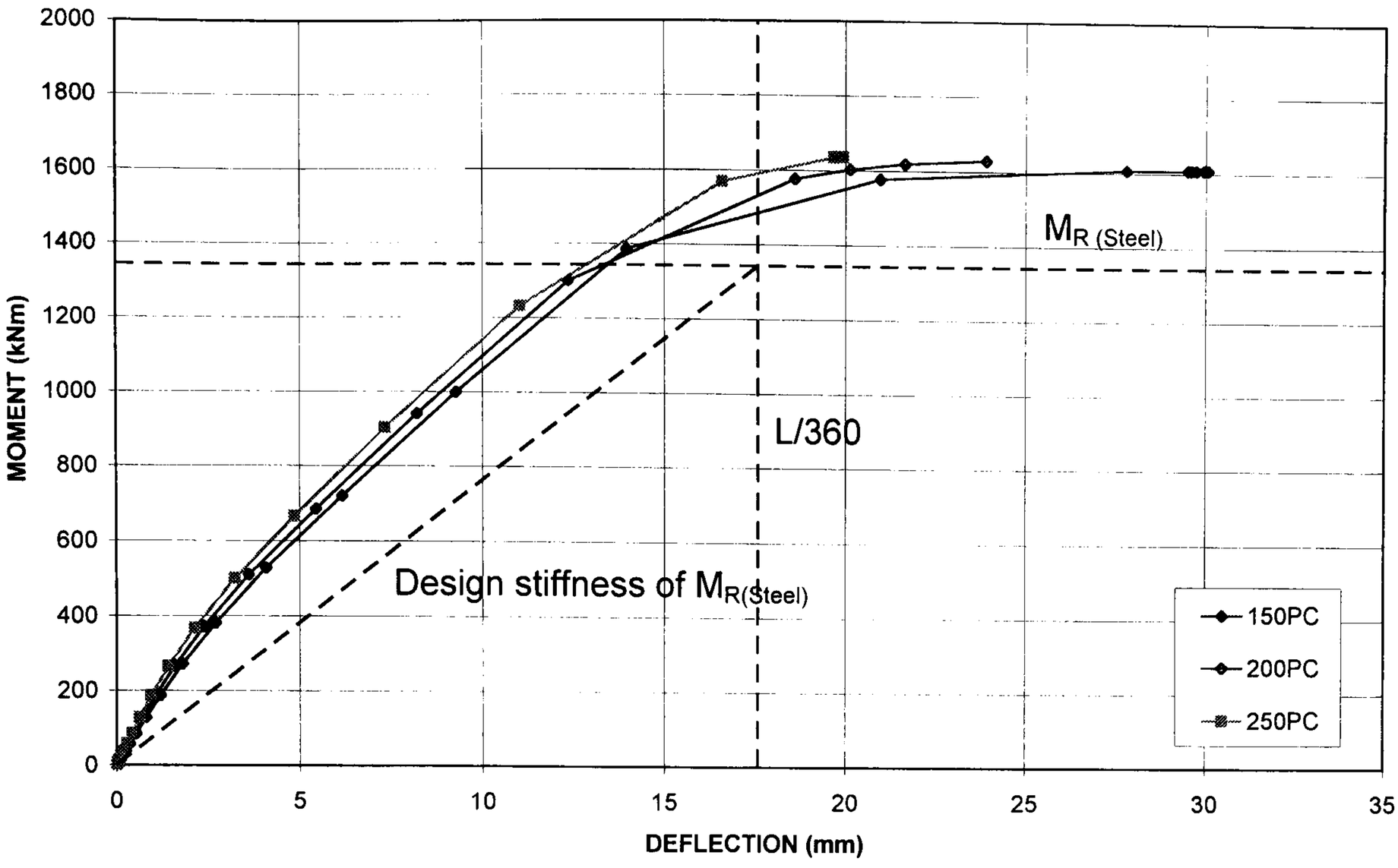

Fig.7.3 Moment-deflection curves for variations of slab thickness for 762 x 267 x UB, T8 rebar and η = 300mm

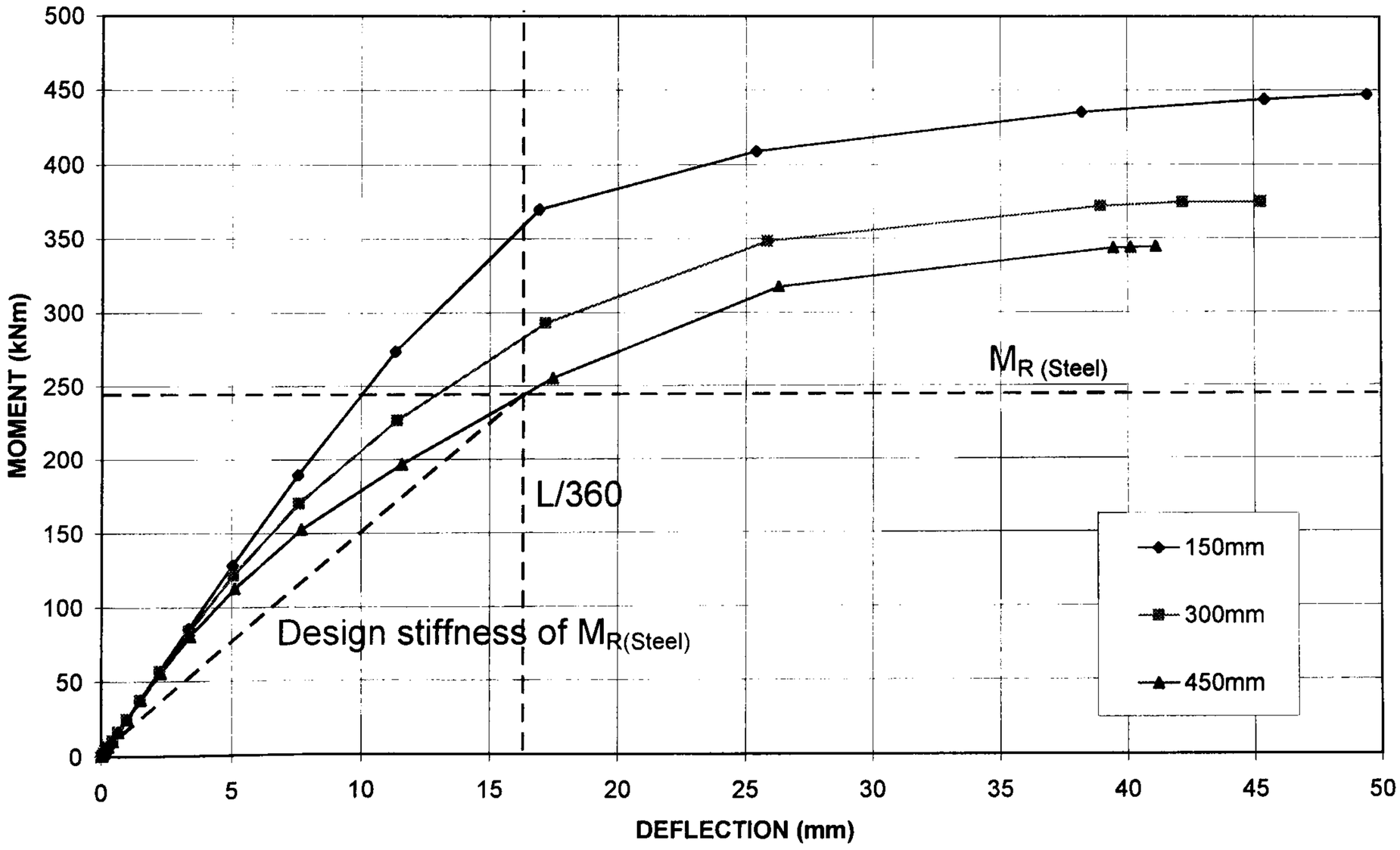

Fig.7.4 Load-deflection curves for variations of stud spacing, η for 356 x 171 x 51UB, T8 rebar and 150mm slab

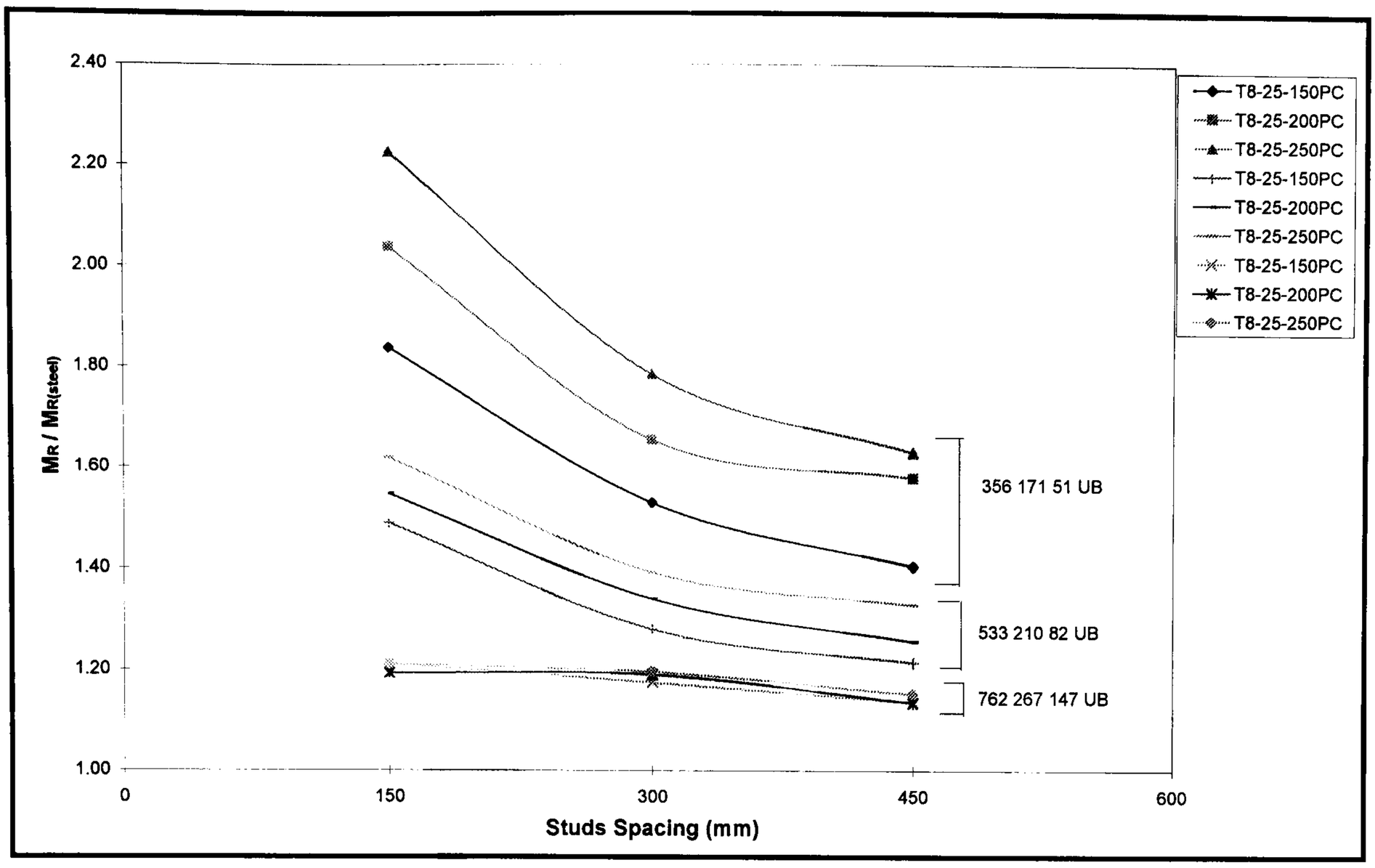

Fig. 7.5 Moment capacity ratio, $M_R/M_{R(steel)}$ for variations of stud spacing for T8 rebar

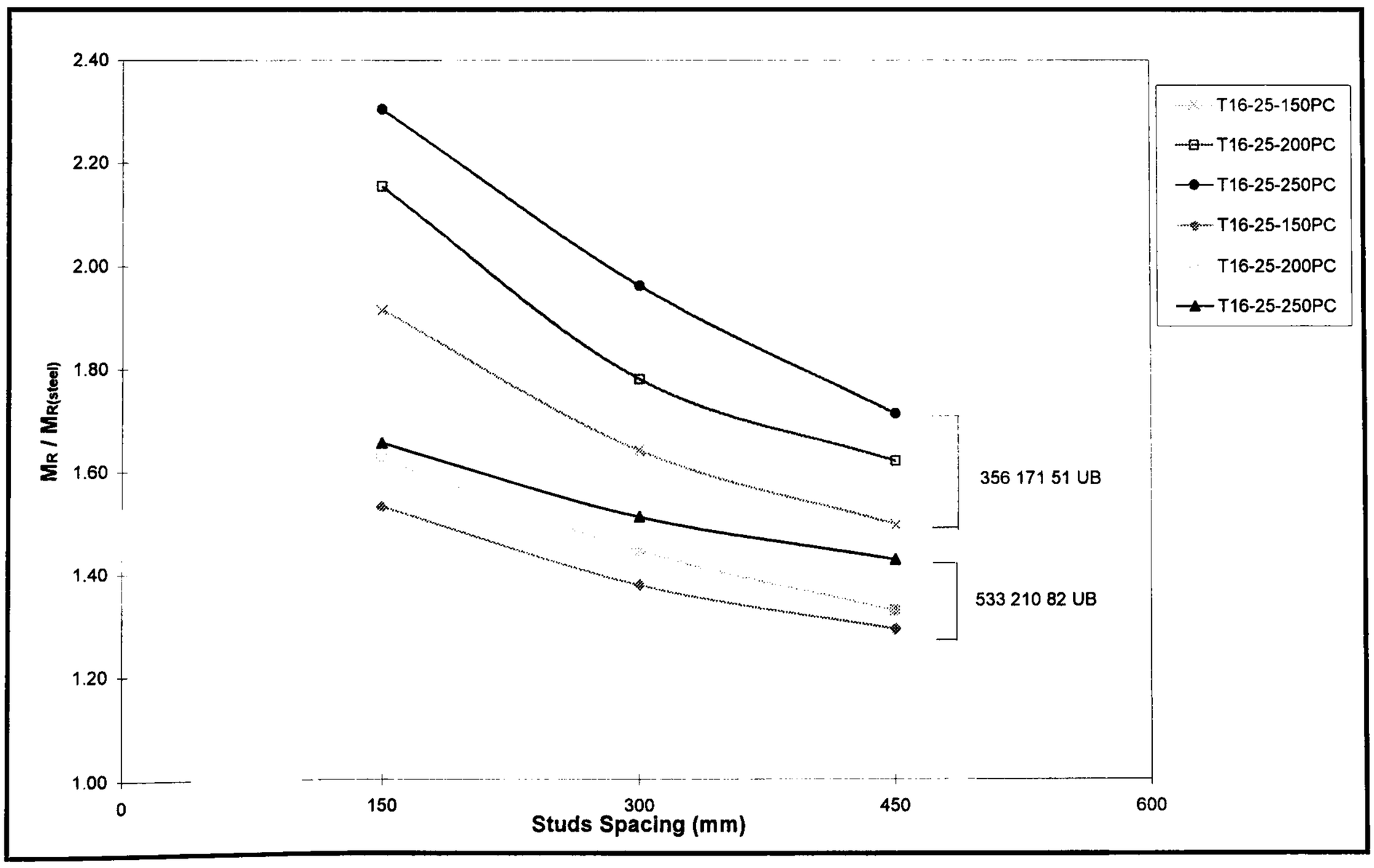

Fig. 7.6 Moment capacity ratio, $M_R/M_{R(steel)}$ for variations in stud spacing for T16 rebar

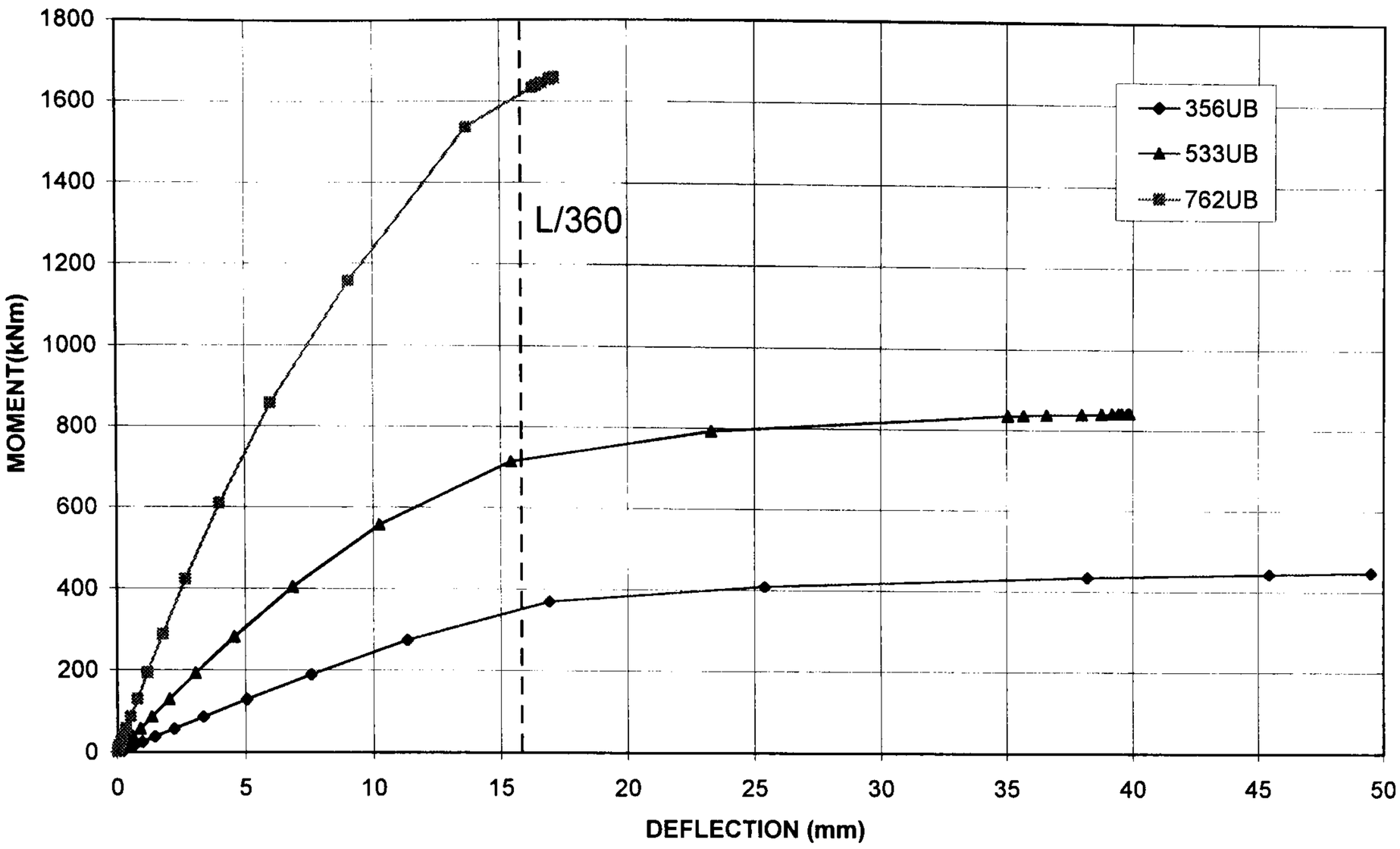

Fig.7.7 Moment-deflection curves for variations in steel section for 150mm slab, T8 rebar and η = 150mm

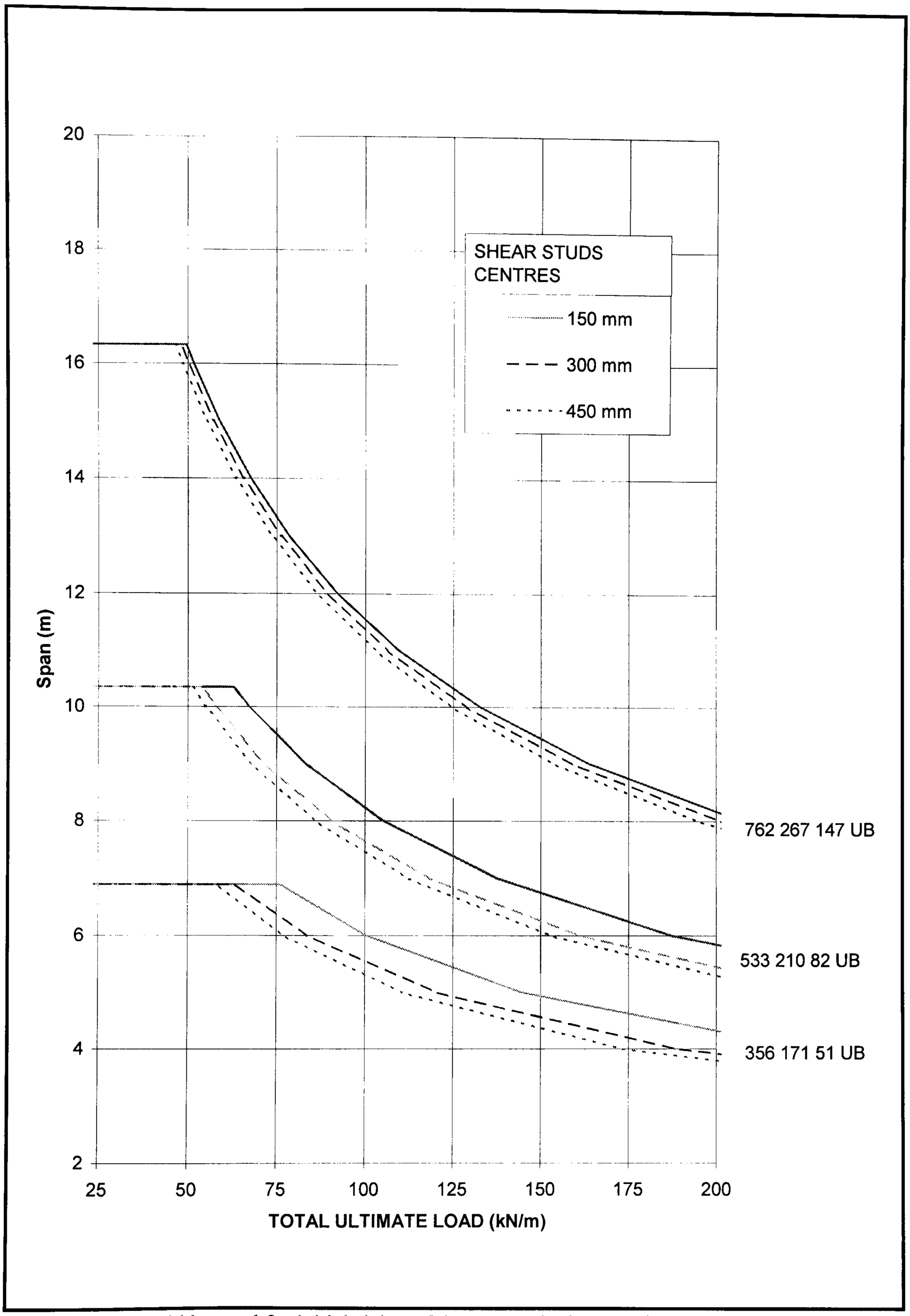

Design chart should be used for initial sizing of the composite beam only.
Design chart is based on 2-D FE analyses which preclude certain failure mechanisms which might be critical. Full design check should be carried out in accordance to the proposed equations in Chapter 8.

Fig. 7.8 Design chart for composite beam with 150mm hollow core slabs

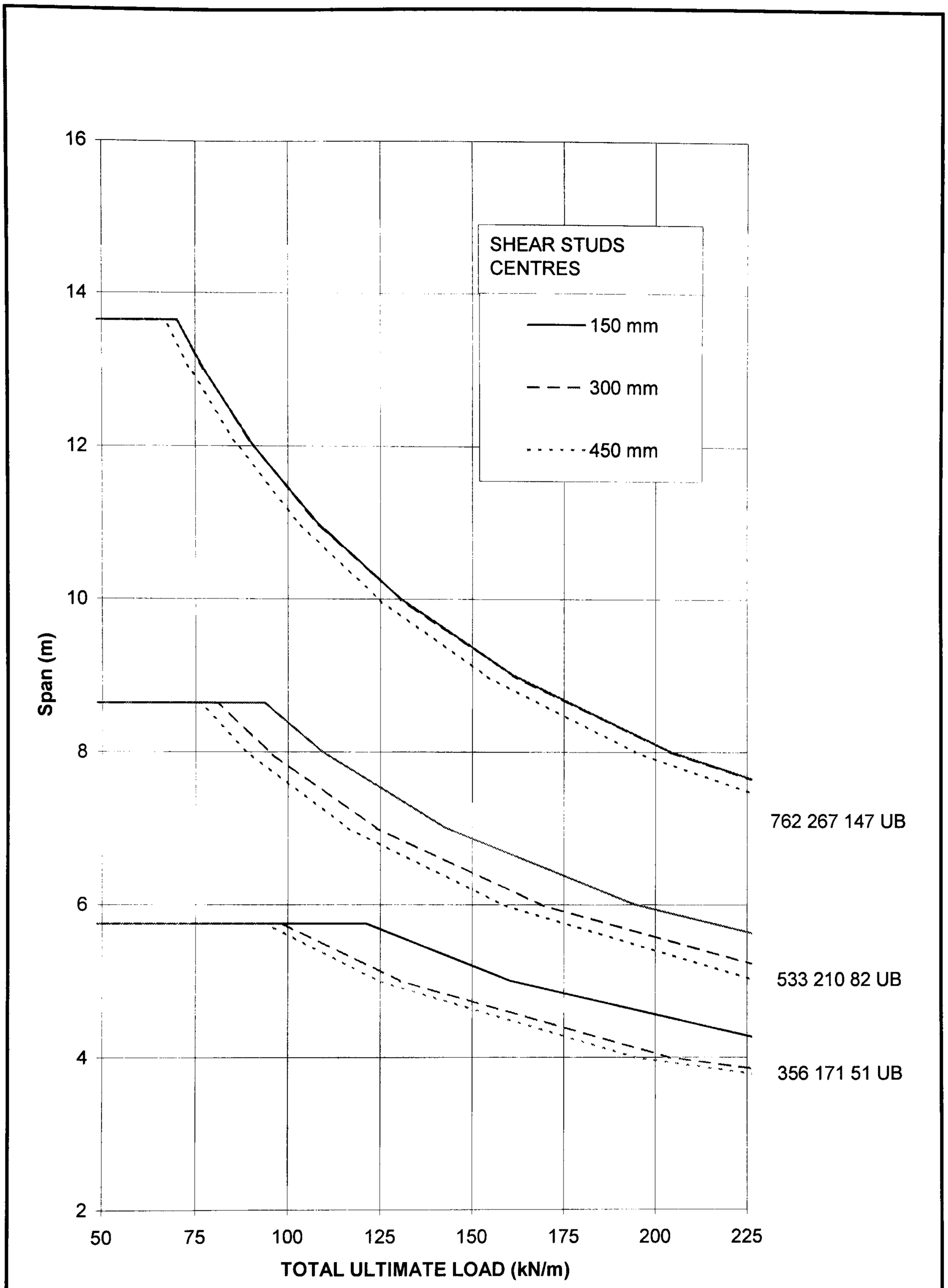

Design chart should be used for initial sizing of the composite beam only.
Design chart is based on 2-D FE analyses which preclude certain failure mechanisms which might be critical. Full design check should be carried out in accordance to the proposed equations in Chapter 8.

Fig. 7.9 Design chart for composite beam with 200mm hollow core slabs.

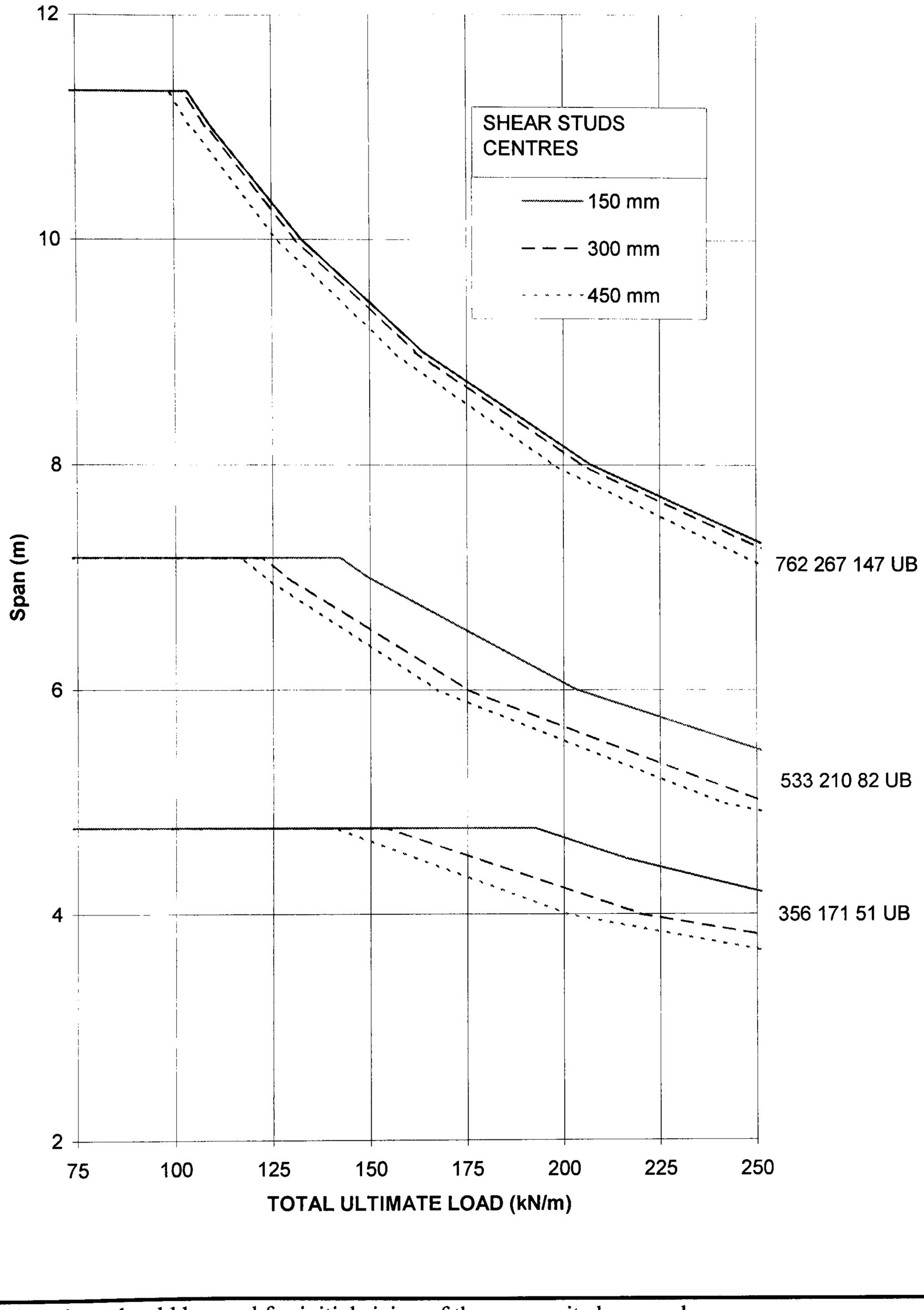

Design chart should be used for initial sizing of the composite beam only.
Design chart is based on 2-D FE analyses which preclude certain failure mechanisms which might be critical. Full design check should be carried out in accordance to the proposed equations in Chapter 8.

Fig. 7.10 Design chart for composite beam with 250mm hollow core slabs.

Chapter 8

Discussion and theoretical comparisons of test results

8.1 Introduction

In order to determine the moment capacity of the composite beam, plastic analysis principles are used. This assumes that very high strains are developed in the cross-section so that the section may be analysed as a series of 'rectangular' stress blocks. The concrete slab is assumed to be fully stressed over its effective breadth. Transverse reinforcement across the section is neglected in the moment capacity calculations but it is needed for resistance against tensile splitting. Shear capacity of the shear studs is the other important factor required for the design calculation of the moment capacity of the composite beam. For the serviceability limit state, second moment of area of the composite section is required for the calculation of the deflection of the beam. It is the intention of this research programme to investigate the behaviour of the precast hollow core composite beam and to propose design equations for use in design.

Compression slab tests were first carried out to investigate the behaviour of the slab and hence to determine the effective breadth of the concrete slab. Push off tests were then carried out to investigate the shear capacity of the shear studs for

this type of construction, and finally, full scale flexural tests were carried out so as to provide test results against which theoretical comparisons could be made.

8.2 Compression slab tests

The main purpose of the compression slab tests was to observe the behaviour and measure the horizontal compressive strength of the combined insitu - precast slab, and hence to determine the effective breadth of the compression flange to use in design and the second moment of area of the composite section for the serviceability check.

8.2.1 Effective breadth, b_{eff}

The effective breadth, b_{eff} is defined in general to allow for a non-uniform distribution of stress due to shear lag. Fig. 8.1 shows typical horizontal longitudinal stress contours of the composite slab. Considering the cross-section A-A in Fig. 8.2, it is assumed that the concrete element is narrower such that the rectangular stress block of area $b_{eff} \times \sigma_{max}$ is equal to the area under the curvilinear stress block σ_x over the width ℓ. This is equivalent to integrating the rigorously

calculated horizontal longitudinal stress σ_x in the concrete slab over the width ℓ, and dividing by the peak value of the stress σ_{max}.

Thus

$$b_{eff} = \frac{\int_{b_l}^{b_r} \sigma_x dx}{\sigma_{max}} \qquad (8.1)$$

where b_r = half the transverse spans of the slab on the right of the steel beam.

b_l = half the transverse spans of the slab on the left of the steel beam.

x = coordinate transverse to the centreline of the steel.

Although the phenomenon of shear lag is not so important for the composite beam design[1], it is still important to proportion the concrete element to incorporate the non-linear effects of shear lag. In simple T-beam theory, based primarily on the engineering assumption that plane sections remain plane after bending, the idealised T-beam consists of the steel element with a certain width of slab referred to as effective breadth that is stressed uniformly.

Alternatively, the effective breadth, b_{eff} can be derived from the strain measurement of the compression slab tests as described in Chapter 3, using the following formula:

$$\sigma_c = \frac{F}{A_c} + \frac{Fe}{Z_c} \qquad (8.2)$$

where σ_c = longitudinal concrete stress at the extreme fibre (top of the slab).

F = applied eccentric load.

e = eccentricity of load from the slab neutral axis.

A_c = area of concrete. i.e. $b_{eff}\, d_p$

Z_c = elastic modulus of concrete slab. i.e. $b_{eff}\, d_p^2 / 6$

d_p = depth of slab.

Therefore,

$$b_{eff} = \frac{F}{\varepsilon_c E_c}\left(\frac{1}{d_p} + \frac{6e}{d_p^2}\right) \qquad (8.3)$$

If e, E_c and d_p are known, F and ε_c can be obtained from the load vs. concrete strain curve of the compression slab tests (given in Figs. 3.8, 3.11, 3.14, 3.16 and 3.18), therefore the effective breadth of the compression flange can be derived as given in Table 8.1.

For the consideration of the compression flange of the composite beam, it is important that the precast hcu and the insitu infill act compositely. Therefore, it is to be expected that the effective breadth will be influenced by the strength of concrete and the transverse reinforcement and will be a function of the following parameters:

$$b_{eff} = f\left(f_{cu}, E_c, A_s, f_y\right) \qquad (8.4)$$

where f_{cu} = compressive concrete cube strength.

E_c = modulus of elasticity of insitu concrete.

A_s = area of transverse reinforcement.

f_y = yield strength of transverse reinforcement.

As the elastic modulus of concrete, E_c is dependent on the cube strength, f_{cu}, it is suggested that b_{eff} is affected by the cube strength and tensile force of the transverse reinforcement (i.e. $A_s f_y$). From the results of the compression slab tests described in Chapter 3 and FE analysis results as described in Chapter 6, the following empirical equation for b_{eff} is proposed:

$$b_{eff} = \left(\frac{25}{f_{cu}}\right)^2 * \left(\frac{0.4}{f'_t}\right) * 1000 + 300 \qquad (8.5)$$

where b_{eff} = effective breadth of compression flange in mm.

f_{cu} = compressive concrete cube strength in N/mm^2.

f_t' = effective tensile strength in N/mm^2.

The equation is based on the equation (8.4) and the experimental work and FE analyses carried out in this research programme. Table 8.2 shows that the calculated b_{eff} values based on equation (8.5) give a reasonable estimate of the effective breadths as determined from strain measurements. Results from Table 8.1 show the calculated values of b_{eff} to all be within 10% of the value derived from compression slab tests.

8.2.2 Second moment of area

Second moment of area, I_{com} of the composite section is needed for the calculation of the deflection of the composite beam. To evaluate I_{com}, elastic analysis using the transformed section method is used, where the following assumptions are made:

1. The beam and slab materials are both linearly elastic.
2. These two materials are related by the modular ratio, α_e.
3. The shear connection provides full interaction between the steel and concrete.

The equation for the second moment of area, I_{com} is modified from the equation given in BS5950[2] and is obtained by summing the area of each element times the

f_{cu} = compressive concrete cube strength in N/mm^2.

f_t' = effective tensile strength in N/mm^2.

The equation is based on the equation (8.4) and the experimental work and FE analyses carried out in this research programme. Table 8.2 shows that the calculated b_{eff} values based on equation (8.5) give a reasonable estimate of the effective breadths as determined from strain measurements. Results from Table 8.1 show the calculated values of b_{eff} to all be within 10% of the value derived from compression slab tests.

8.2.2 Second moment of area

Second moment of area, I_{com} of the composite section is needed for the calculation of the deflection of the composite beam. To evaluate I_{com}, elastic analysis using the transformed section method is used, where the following assumptions are made:

1. The beam and slab materials are both linearly elastic.
2. These two materials are related by the modular ratio, α_e.
3. The shear connection provides full interaction between the steel and concrete.

The equation for the second moment of area, I_{com} is modified from the equation given in BS5950[(2)] and is obtained by summing the area of each element times the

distance squared from the elastic neutral axis using the 'parallel axis theorem' as follows:

$$I_{com} = I_s + \frac{b_{eff} d_p^{\,3}}{12\alpha_e} + \frac{A_{steel} b_{eff} d_p (D + d_p)^2}{4[A_{steel}\alpha_e + b_{eff} d_p]} \qquad (8.6)$$

where I_s = second moment area of the steel of cross sectional area, A_{steel}.

α_e = ratio of the elastic moduli of steel to insitu infill concrete (modular ratio).

D = depth of steel section.

d_p = depth of concrete slab

Once the I_{com} of the composite section is determined, the deflection of the composite beam can be calculated using the appropriate deflection formulae.

8.3 Push off tests

Because of the complexity of the dowel action, the strength and ductility of shear connectors are always determined experimentally. It is very difficult, if not impossible, to determine the behaviour of the shear connectors from composite beam tests. This is because the connectors are loaded indirectly from the flexural

forces within the beam, and it is clear that the force on a connector is not directly proportional to the load applied to the beam, but depends on the stiffness of various components of the composite beam[3]. Even if the connector strength could be determined from a composite beam test, it would be uneconomical to carry out such a test. Instead, the behaviour of the connectors is determined from push-off tests in which the connectors are loaded directly. Details of push-off test are described in Chapter 4.

8.3.1 Shear strength of headed stud connector

From the push-off test results in Chapter 4, it is suggested that the shear strength of the shear connectors is affected by the insitu concrete gap width, the amount of transverse reinforcement and the strength of the concrete. The equations for the shear connector capacity, P_{RD} for composite precast construction which take into account the effect of the strength of the insitu infill, the gap width g, the diameter ϕ of transverse reinforcement and the presence of transverse joints between the hcu are proposed:-

$$P_{RD} = 0.29\alpha\beta\lambda d^2\sqrt{\omega f_{cp}E_{cp}} / \gamma_v \qquad (8.7)$$

$$P_{RD} = 0.8 f_u \frac{\pi d^2}{4\gamma_v} \qquad (8.8)$$

where α = $0.2\ (h/d + 1) < 1.0$

β = gap width factor and is given as $0.5\ (g/70 + 1) < 1.0$, and $g >$ 30 mm (5mm aggregate + stud dia. + 5mm aggregate);

λ = transverse reinforcement factor (grade 460) and is given by $0.5\ (\phi/20 + 1) < 1.0$, and bar diameter, $\phi > 8$ mm;

ω = transverse joint factor $= 0.5(w/600 + 1) < 1.5$,

w = width of hcu.

f_{cp} = average concrete cylinder strength = 0.8 x average cube strength of the insitu and precast concrete (N/mm^2).

E_{cp} = average value of elastic modulus of the insitu and precast concrete (N/mm^2).

γ_v = partial safety factor (normally taken as 1.25 at ultimate accordance to EC4[4]).

f_u = ultimate tensile strength of the headed stud material, e.g. 450 N/mm^2.

The equation (8.7) is modified from the equation in EC4[4] and takes into account the other parameters affecting the shear capacity in precast hcu composite construction. No modification to equation (8.8) is proposed as the tensile strength of the shear stud is thought not to be influenced by the precast construction, nor is there any experimental evidence to justify making any change. The coefficients β,

ε and ω are based on the push off tests results described in Chapter 4, Section 4.8. Table 8.3 presents a comparison of the predicted unfactored shear capacity P_{RD} given by equation (8.7) (i.e. $\gamma_V = 1.0$) with the ultimate test capacity Q_T in the push-off tests. In each case, the predicted value is within 6 per cent of the test result except for the solid r.c. specimen T8-38-RC which over-predicts the test result by 20 per cent. The equation may therefore be accepted for the hollow core composite specimens. Table 8.4 gives a schedule of factored values (i.e. $\gamma_V = 1.25$) for P_{RD} for a range of typical construction and material parameters.

8.3.2 Mechanisms of longitudinal shear transfer

It is necessary in the design of composite beams to ensure that the longitudinal shear transmitted by the shear connection can be resisted by the concrete. The mechanism by which shear is transferred across the insitu / precast interface is illustrated in Fig. 8.3, which shows the longitudinal shear crossed by transverse reinforcement. The shear forces cause the interfaces to slip relative to each other, and this shear distortion is resisted along the line of the interface by a combination of dowel action, interface interlock and friction.

The relative slip between the interfaces is resisted by bending of the transverse reinforcement, as shown in Fig. 8.3. This resistance to shear is referred to as dowel action, which is similar to the dowel action associated with the stud connector.

Therefore the dowel strength of the transverse reinforcement, v_{dow} can be written as

$$v_{dow} = 0.8\rho f_y \qquad (8.9)$$

where ρ = area of reinforcement across the plane as a proportion of the area of concrete.

f_y = yield strength of transverse reinforcement.

The transfer of shear by interface interlock, v_{lock}, depends on the passive restraint of the transverse reinforcement that allows for both faces of the concrete protrusions at the interface. Fracture of the interface protrusion will be a function of the concrete tensile strength, f_{ct}.

For the concrete tensile strength, f_{ct} can be expressed as $0.36\sqrt{f_{cu}}$ where f_{cu} is the compressive cube strength of concrete. v_{lock} for interface interlock as proposed by Mattock[5] can be written in the form

$$v_{lock} = 0.66 f_{ct} \qquad (8.10)$$

Shear is also resisted across the shear plane by friction, v_{fric}, of the aggregate particles that protrude from each shear surface. This mechanism of shear transfer can only occur when the two surfaces are held together by transverse confinement

pressure, p as shown in Fig. 8.3. The interface interlock mechanism generated by the transverse reinforcement across the interface will allow the shear to be transferred by friction. It will be assumed that

$$v_{fric} = \mu p_r \qquad (8.11)$$

where μ = coefficient of friction = 0.4 as determined by Walraven[6].

p_r = transverse reinforcement stress

Hence the total shear strength across the interface, v_u consists of the sum of the following components

$$v_u = v_{dow} + v_{lock} + v_{fric} \qquad (8.12)$$

Therefore, the equation (8.12) to determine the shear strength across the shear interface can be written as

$$v_u = 0.8\rho f_y + 0.66 f_{ct} + 0.4\rho f_y$$

$$v_u = 1.2\rho f_y + 0.66 f_{ct} \qquad (8.13)$$

where the units are in N and mm.

8.3.3 Shear plane

It is necessary to determine the length of shear plane, L_s where the shear force is acting. Fig. 8.4 shows the shear plane that encompasses the shear connector. This is influence by the height of the headed stud and the gap of the insitu infill. From the proposed equation (8.7) which is confirmed by the push-off tests, the shear strength is also influenced by the height of the headed studs and the gap of the insitu infill. Therefore substituting equation (8.13) for L_s, the shear force across the shear plane, V_u is equal to

$$V_u = 1.2 A_s f_y + 0.66 f_{ct} L_s \qquad (8.14)$$

where A_s = area of transverse reinforcement.

Hence, the equation (8.14) can be used to determine the amount of transverse reinforcement required to ensure a smooth transfer of longitudinal shear force from the shear connectors into the slab without causing splitting failure of the concrete.

8.3.4 Worked example

To calculate the shear force resistance across the shear plane for beam CB2:

Total longitudinal shear force per unit length = $P_{RD} / \eta = 68.1/150 = 0.454$kN/mm

For shear resistance, $V_u = 1.2A_sf_y + 0.66f_{ct}L_s$

$V_u = 1.2 \times (2 \times 50.2) / 300x460 + 0.66x0.36\sqrt{25.5}x246 = 480$N/mm $= 0.48$kN/mm

Therefore, transverse reinforcement of T8 @ 300 c/c is satisfactory.

8.4 Composite beam tests

8.4.1 Moment capacity

The ultimate moment capacity of the composite beam may be determined by plastic analysis principles. The concrete is assumed to be fully stressed (i.e. $0.67f_{cu}$) over its effective breadth sufficient to provide a total compressive force which is equal to the total tensile force provided by the steel section at its fully yielded state assuming full interaction between steel and concrete. The moment capacity of the composite beam is obtained by summing the resistances of each element times the distance from the plastic neutral axis. Based on the formulae for calculating section properties in BS5950[(2)], the resistances of the various elements of the composite section are expressed as follows:

Resistance of concrete flange, F_{conc}

$$F_{conc} = 0.67 f_{cu} b_{eff} d_p \qquad (8.15)$$

Resistance of steel beam, F_{steel}

$$F_{steel} = A_{steel} p_y \qquad (8.16)$$

Provided there are sufficient shear connectors to transfer the horizontal force between the concrete slab and the steel beam at the ultimate state, moment capacity of the composite beam, M_{comp} for full shear connection can be written as

For plastic neutral axis in concrete flange, $F_{conc} > F_{steel}$

$$M_{comp} = F_{steel}\left(\frac{D}{2} + d_p - \frac{F_{steel}}{F_{conc}}\frac{d_p}{2}\right) \qquad (8.17a)$$

For plastic neutral axis in the steel section, $F_{steel} > F_{conc}$

$$M_{comp} = F_{steel}\frac{D}{2} + F_{conc}\frac{d_p}{2} - \frac{\left(F_{steel} - F_{conc}\right)^2}{F_{flange}}\frac{T}{4} \qquad (8.17b)$$

where F_{flange} = axial capacity of one steel flange of thickness, T

If the capacity of the shear connectors, F_{con} is less than the smaller of F_{conc} or F_{steel}, then the beam should be designed for 'partial shear connection'. The moment

capacity of the composite beam, M_{comp} for partial shear connection can be written as

$$M_{comp} = F_{con}\frac{D}{2} + F_{con}\left[d_p - \frac{F_{con}}{F_{conc}}\frac{d_p}{2}\right] - \frac{(F_{steel} - F_{con})^2}{F_{flange}}\frac{T}{4} \qquad (8.18)$$

where F_{con} = resistance force of shear connectors = n P_{RD}

n = number of shear connector in half span

Table 8.5 shows the comparison of measured moment capacity and calculated moment capacity with values used for f_{cu}, f_y and p_y from the full scale composite beam tests and b_{eff} calculated using equation (8.5). All the calculated results were within 12% of the measured capacities with the calculated capacities being lower than the test results. The discrepancy is probably due to the strain hardening effect of the steel beam.

8.4.2 Load deflection analysis

In studying load deflection of a composite beam, interface slip must be taken into account. All the composite beams tested exhibited partial interaction as slip occurred even at low load levels. Linear elastic analysis is used to determine the load-deflection behaviour. This load deflection analysis is based on the theory for partial interaction presented by Newmark[7]. The strain distribution associated with

partial interaction is shown in Fig. 8.5 and from the assumption of linear elastic behaviour, the stress distribution will have a similar shape.

Consider the load-slip relationship for a shear stud connection. Considering linear elastic behaviour, the shear stiffness, k_s is given as

$$k_s = \frac{P}{s} \tag{8.19}$$

where P = shear force per stud from push-off test.

s = slip of shear stud.

and hence under a uniform spacing, l_s of the connectors (i.e. stud centre),

$$P = ql_s \tag{8.20}$$

where q = shear force transmitted per unit length of beam.

Consider a composite beam with the axial force and moment acting on each element as shown in Fig. 8.6. The force and moment for the concrete element act through the centroid of the concrete element at a distance h_c from the steel/concrete interface, and the force and moment for the steel element act at the centroid of the steel element at a distance h_s from the interface. The elastic strain at the bottom of the concrete element, ε_c as shown in Fig. 8.5 is given by

$$\varepsilon_c = \frac{M_{conc} h_c}{E_c I_c} - \frac{F_{conc}}{E_c A_{conc}} \qquad (8.21a)$$

and the elastic strain at the top of the steel element, ε_s as shown in Fig. 8.5 is given by

$$\varepsilon_s = \frac{F_{steel}}{E_s A_{steel}} - \frac{M_{steel} h_s}{E_s I_s} \qquad (8.21b)$$

where A_{conc}= area of concrete element.

A_{steel}= area of steel element.

I_c = second moment of area of the concrete element about its centroidal axis.

I_s = second moment of area of the steel element about its centroidal axis.

From the push-off test,

$$F_{shear} = F_{conc} = F_{steel} \qquad (8.22)$$

where F_{shear} = total shear force on the shear connectors in the shear span of length x.

The shear connection force, F_{shear} = qx, the shear force per unit length of the beam, q can be written as

$$q = \frac{dF_{shear}}{dx} \tag{8.23}$$

By combining equations (8.19), (8.20) and (8.23), the slip strain in the composite beam, ds/dx, as shown in Fig. 8.5 becomes

$$\frac{ds}{dx} = \frac{d^2F_{shear}}{dx^2}\frac{l_s}{k_s} = \varepsilon_c - \varepsilon_s \tag{8.24}$$

and combine equations (8.21), (8.22) and (8.24) to give equation (8.25),

$$\frac{l_s}{k_s}\frac{d^2F_{shear}}{dx^2} = \frac{M_{conc}h_c}{E_cI_c} + \frac{M_{steel}h_s}{E_sI_s} - F_{shear}\left[\frac{1}{E_cA_{conc}} + \frac{1}{E_sA_{steel}}\right] \tag{8.25}$$

The composite moment, M_{com} is equal to,

$$M_{com} = M_{conc} + M_{steel} + F_{shear}\left(h_c + h_s\right) \tag{8.26}$$

Since the shear connection is required to prevent any separation between the steel and concrete, the curvatures, κ for the concrete and the steel must be the same, so that

$$\kappa = \frac{M_{conc}}{E_c I_c} = \frac{M_{steel}}{E_s I_s} = \frac{d^2 y}{dx^2} \qquad (8.27)$$

Therefore, $M_{conc} = \kappa E_c I_c$ and $M_{steel} = \kappa E_s I_s$, and by substitution into equations (8.25) and (8.26) gives

$$\frac{l_s}{k_s}\frac{d^2 F_{shear}}{dx^2} = \kappa h_c + \kappa h_s - F_{shear}\frac{1}{\overline{\overline{EA}}} \qquad (8.28)$$

and

$$\kappa = \frac{M_{com} - F_{shear}(h_c + h_s)}{\sum EI} = \frac{d^2 y}{dx^2} \qquad (8.29)$$

where $$\frac{1}{\overline{\overline{EA}}} = \frac{1}{E_c A_{conc}} + \frac{1}{E_s A_{steel}}$$

and $$\sum EI = E_c I_c + E_s I_s$$

Equating equations (8.28) and (8.29) gives equation (8.30),

$$\frac{l_s}{k_s}\frac{d^2 F_{shear}}{dx^2} = \frac{M_{com}(h_c + h_s)}{\sum EI} - \frac{F_{shear}(h_c + h_s)^2}{\sum EI} - \frac{F_{shear}}{\overline{\overline{EA}}} \qquad (8.30)$$

Using parallel axis theorem,

$$\overline{EI} = \sum EI + \overline{EA}\left(h_c + h_s\right)^2$$

therefore,

$$(h_c + h_s)^2 = \frac{\overline{EI} - \sum EI}{\overline{EA}} \qquad (8.31)$$

so that equation (8.30) becomes

$$\frac{l_s}{k_s}\frac{d^2F_{shear}}{dx^2} = \frac{M_{com}(h_c + h_s)}{\sum EI} - \frac{F_{shear}\overline{EI}}{\sum EI\,\overline{EA}} + \frac{F_{shear}}{\overline{EA}} - \frac{F_{shear}}{\overline{EA}} \qquad (8.32)$$

or

$$\frac{l_s}{k_s}\frac{d^2F_{shear}}{dx^2} = \frac{M_{com}(h_c + h_s)}{\sum EI} - \frac{F_{shear}\overline{EI}}{\sum EI\,\overline{EA}} \qquad (8.33)$$

i.e. Shear slip strain is due to the difference between the strain due to the moment M_{com} and that due to the interface force F_{shear}.

Multiply each term in equation (8.33) by a geometric ratio, R

$$R = \frac{\overline{EA}(h_c + h_s)}{\overline{EI}}$$

gives,

$$\frac{M_{com}(h_c + h_s)^2}{\sum EI}\frac{\overline{EA}}{\overline{EI}} - \frac{F_{shear}(h_c + h_s)}{\sum EI} = \left(R\frac{l_s}{k_s}\right)\frac{d^2F_{shear}}{dx^2} \qquad (8.34)$$

and substituting equation (8.31) gives

$$\frac{M_{com} - F_{shear}(h_c + h_s)}{\sum EI} = \frac{M_{com}}{EI} - \left(R\frac{l_s}{k_s}\right)\frac{d^2F_{shear}}{dx^2} \qquad (8.35)$$

Substitutes equation (8.32) and letting slip coefficient, $S = R\, l_s/k_s$ gives,

$$\frac{d^2y}{dx^2} = \frac{M_{com}}{\overline{EI}} + S\frac{d^2F_{shear}}{dx^2} \qquad (8.36)$$

By integrating d^2y/dx^2 twice with respect to x gives

$$\delta_{part} = \delta_{full} + SF_{shear} \qquad (8.37)$$

where δ_{part} = deflection of composite beam with part interaction.

δ_{full} = deflection of composite beam with full interaction.

S = slip coefficient, for $S = \frac{l_s}{k_s}(h_c + h_s)\frac{\overline{EA}}{\overline{EI}}$

For full interaction, shear stiffness, k_s approaches infinity and the slip coefficient would become zero, therefore, $\delta_{part} = \delta_{full}$ is expected.

Fig. 8.7 shows a typical load-deflection curve of the test result vs. theoretical result. In general, a finite element analysis as described in Chapter 6 may be used to solve the differential equation numerically for the deflection of a beam with partial interaction.

8.4.3 Worked example

To calculate partial interaction deflection of beam CB2:

$$\delta_{part} = \delta_{full} + SF_{shear}$$

For 4 point loading, where point load F acts at distance *a* from supports and L is effective span:-

$$\delta_{part} = \frac{FL^3}{6EI_{com}}\left[\frac{3a}{4L} - \left(\frac{a}{L}\right)^3\right] + SF_{shear}$$

Using equation (8.6),

b_{eff}= 999mm from Table 8.5, d= 150mm, α_e= 7.4, A_{steel}= 6460 mm^2,

$I_x = 14118x10^4$ mm^4, D= 356mm

$$I_{com} = I_x + \frac{b_{eff}d^3}{12\alpha_e} + \frac{A_{steel}b_{eff}d(D+d)^2}{4[A_{steel}\alpha_e + b_{eff}d]}$$

$I_{com} = 49264 \times 10^4$ mm^4

For slip coefficient, $S = \frac{l_s}{k_s}(h_c + h_s)\frac{\overline{EA}}{\overline{EI}}$

where for test CB2: l_s= 150 mm, h_c = d/2 = 75 mm, h_s = D/2 = 178 mm

$E_c = 5.5x10^3\sqrt{f_{cu}} = 5.5x10^3\sqrt{25.5} = 27773$ N/mm^2

From push off test T8-25-65F, k_s = 260000 N/mm

For $\frac{1}{\overline{EA}} = \frac{1}{E_cA_{conc}} + \frac{1}{E_sA_{steel}}$

$$\frac{1}{\overline{EA}} = \frac{1}{27773(1012 \times 150)} + \frac{1}{205000(6460)} = 9.92 \times 10^{-10}$$

$\overline{EA} = 10.1 \times 10^8\ N$

$$\overline{EI} = \sum EI + \overline{EA}\left(h_c + h_s\right)^2$$

$$\sum EI = E_c I_c + E_s I_s$$

$$\sum EI = 27773 \times \frac{1012 \times 150^3}{12} + 205000 \times 14118 \times 10^4 = 3.68 \times 10^{13}\, Nmm^2$$

Therefore,

$$\overline{EI} = 3.68 \times 10^{13} + 10.1 \times 10^8 (178 + 75)^2 = 1.0 \times 10^{14}\, Nmm^2$$

and slip coefficient,

$$S = \frac{150}{260000} \times \frac{10.1 \times 10^8}{1.0 \times 10^{14}}\left(178 + 75\right) = 1.47 \times 10^{-6}\, mm / N$$

Let F = 100kN,

$$\delta_{part} = \frac{100000 \times 5700^3}{6 \times 205000 \times 49264 \times 10^4}\left[\frac{3(1500)}{4(5700)} - \left(\frac{1500}{5700}\right)^3\right] + 1.47 \times 10^{-6} \times 600000$$

$$\delta_{part} = 5.46 + 0.89 = 6.35mm$$

Therefore, for M = 1.5F = 150 kNm, δ_{part} =6.35 mm

The deflection caused by the slip is approximately 15% of the full deflection of the composite beam.

8.5 Conclusion

The main objective of this research is to investigate the behaviour of the composite beam with precast hollow core slab and to propose design recommendations for this type of construction.

Theoretical analysis is made and design equations are proposed for the effective breadth for the hollow core slab, shear capacity for the shear stud, and hence moment capacity of the composite beam. Equations are also proposed for checking the amount of transverse reinforcement and for conducting a serviceability analysis for the beam deflection. All prediction equations were compared with the test results and gave values within 12% of the experimental results. Therefore, the design equations can be recommended for use in the design of precast hollow core composite beams.

8.6 References

1. Heins, C.P. and Fan, H.M., 'Effective composite beam width at ultimate load', *Journal of the Structural Division, Proceedings of American Society of Civil Engineers,* Vol. 102, No. ST11, November, 1976, pp2163-2179.

2. BS5950: Part 3: Section 3.1: Code of practice for design of simple and continuous composite beams, British Standard: Structural Use of Steelwork in Building, British Standards Institution, London, 1990.

3. Oehlers, D.J. and Johnson, R.P., 'The strength of stud shear connections in composite beams.', The Structural Engineer, Vol. 65B, No.2, June, 1987, pp44-48.

4. DD ENV 1994-1-1 (1994) Eurocode 4: Design of composite steel and concrete structures, British Standards Institution, London.

5. Mattock, A.H. and Hawkins, N.M., 'Shear transfer in reinforced concrete recent research', *Precast Concrete Institute Journal,* April, 1972, pp55-75.

6. Walraven, J.C. and Reinhardt, H.W., 'Concrete Mechanics, Part A. Theory and experiments on the mechanical behaviour of cracks in plain and reinforced concrete subjected to shear loading', *Heron*, Vol. 26, No. 1A, 1981, pp1-68.

7. Newmark, N.M., Siess, C.P. and Viest, I.M., 'Studies of slab and beam highway bridges, Part III - Small scale tests of shear connectors and composite T-beams', *Bulletin 396,* University of Illinios, Urbana, Illinios.

Test Reference	P/ε_c (kN/με)	b_{eff} (mm) from compression test	b_{eff} (mm) from equation (8.5)	Percentage of differences, %
SPC1	1.4	474	471	1
SPC2	2.0	594	649	8
SPC3	2.3	805	993	9
SPC4	2.3	776	823	6
SPC5	1.61	561	615	9

Table 8.1 Effective breadth, b_{eff} for compression slab tests

Test Reference	f_{cu}, (N/mm^2)	A_s, (mm^2)	f_y, (N/mm^2)	A_c, (mm^2)	f'_t, (N/mm^2)	b_{eff}, (mm)
SP1	25.1	197.2	530	45000	2.32	471
SP2	32.7	50.1	600	45000	0.67	649
SP3	23.2	50.1	600	45000	0.67	993
SP4	26.7	50.1	600	45000	0.67	823
SP5	23.8	110.8	570	45000	1.40	615

Table 8.2 Calculated effective breadth, b_{eff} based on equation (8.5)

Test reference	Experimental shear capacity, Q_T (kN)	β	ε	ω	f_{cp} (N/mm^2)	E_{cp}* (N/mm^2)	Predicted P_{RD} Equ. (8.7) with $\gamma_v = 1.0$ (kN)	Ratio Q_T / P_{RD}
T8-25-40	56.5	0.786	0.7	1.0	31.4	34457	59.9	0.94
T8-25-65	69.7	0.964	0.7	1.0	29.4	33342	69.9	1.00
T8-25-65P	54.3	0.964	0.7	1.5	18.4[x]	23592	57.0	0.95
T8-25-65F	78.0	0.964	0.7	1.5	29.2	33228	85.2	0.92
T8-25-120	72.8	1.0	0.7	1.0	29.8	33568	73.3	0.99
T16-25-65*	60.5	0.964	0.9	1.0	29.4	33342	89.9	N/A
T16-25-65	88.7	0.964	0.9	1.0	29.8	33568	90.8	0.98
T16-25-40F	88.4	0.786	0.9	1.5	29.2	33228	89.3	0.99
T25-25-40F	97.1	0.786	1.0	1.5	29.2	33228	99.3	0.98
T25-25-65	100.8	0.964	1.0	1.0	30.2	33793	102.0	0.99
T8-38-RC	72.9	1.0	0.7	1.5	30.0	33904	91.1	0.80
T16-25-RC	97.0	1.0	0.9	1.5	20.0	27500	95.1	1.02

* $E_{cp} = 5.5x10^3\sqrt{(f_{cp} / 0.8)}$

[x] f_{cp} of insitu infill only

Table 8.3 Comparison of predicted capacity with test results.

Gap width (mm)	T8 at 300 c/c	T12 at 300 c/c	T16 at 300 c/c	T20 at 300 c/c
40	53.7	61.3	69.0	76.7
50	58.5	66.9	75.2	*81.5*
60	63.4	72.5	81.5	*81.5*
> 70	68.3	78.0	*81.5*	*81.5*

Values are given for f_{cu} = 25 N/mm^2 for the insitu infill. For f_{cu} = 30 N/mm^2 increase the tabulated values by 1.05, and for f_{cu} = 35 N/mm^2 increase the tabulated values by 1.10, but $P_{RD} \leq$ 81.5 kN max. (i.e. $0.8f_u \times \pi d^2/4$).

Shear stud parameters have been taken as 125 mm long x 19 mm dia. at 150 mm minimum spacing; f_u = 450 N/mm^2; tie steel f_y = 460 N/mm^2; precast hollow cored slabs grade C50 x 150 mm minimum depth.

Table 8.4. Shear stud capacities P_{RD} (kN) for precast composite construction.

Test Ref.	Measured moment capacity, M_c (kNm)	f_{cu} (N/mm^2)	b_{eff} from Eq (8.5) (mm)	p_y (N/mm^2)	F_{conc} (kN)	F_{steel} (kN)	F_{con} (kN)	F_{flange} (kN)	Calculated moment capacity, M_{comp} (kNm)	M_{comp} / M_c
CB1	497.3	32.5	390	312.1	1274	2016	1725	615	451.8	0.91
CB2	474.0	25.5	999	312.3	2560	2017	1619	616	453.5	0.96
CB3	361.5	28.0	902	316.3	2538	2043	1083	624	316.7	0.88

Table 8.5 Comparison of measured and calculated moment capacity

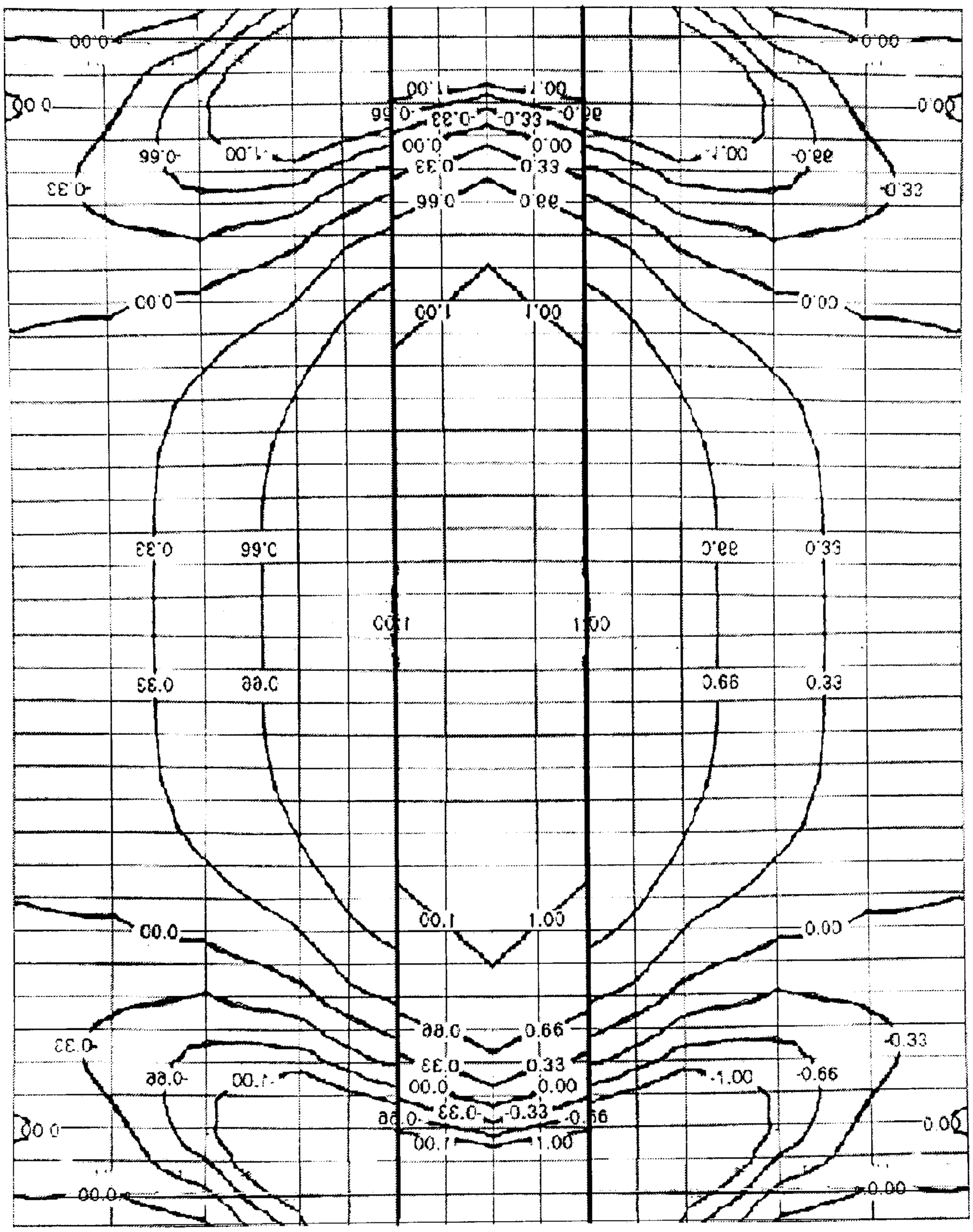

Numbers represents stress / ultimate stress ratio
-ve: compression
+ve: Tension

Fig. 8.1 Typical stress contours of the composite slab model, see Fig. 8.2 for Section A-A

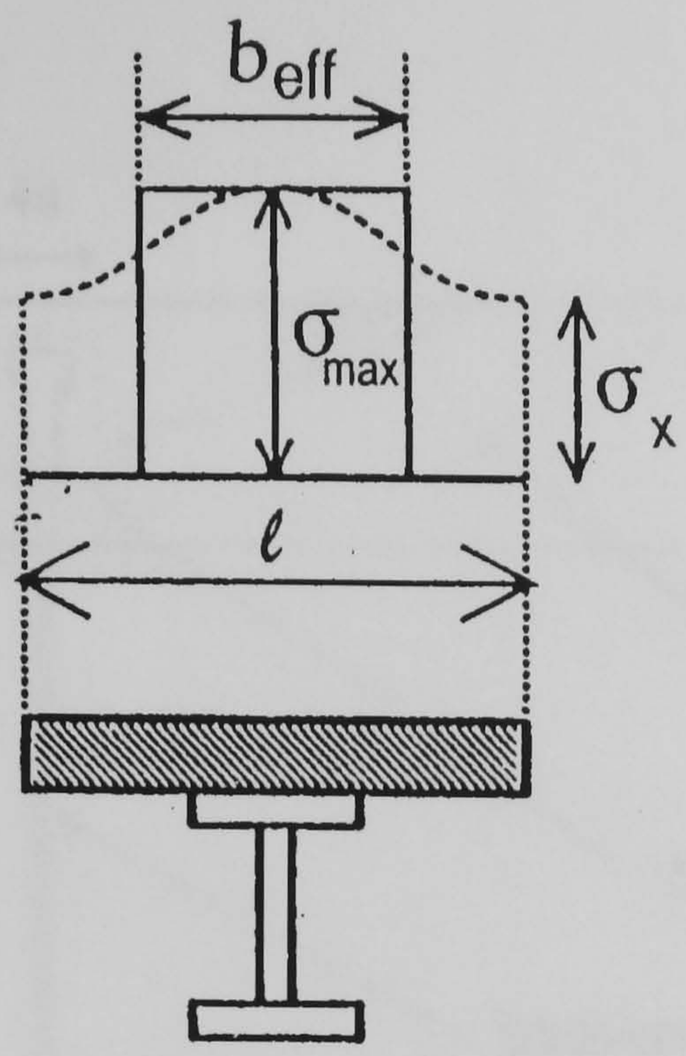

Section A-A in Fig. 8.1

Fig. 8.2 Effective breadth, b_{eff} of composite section

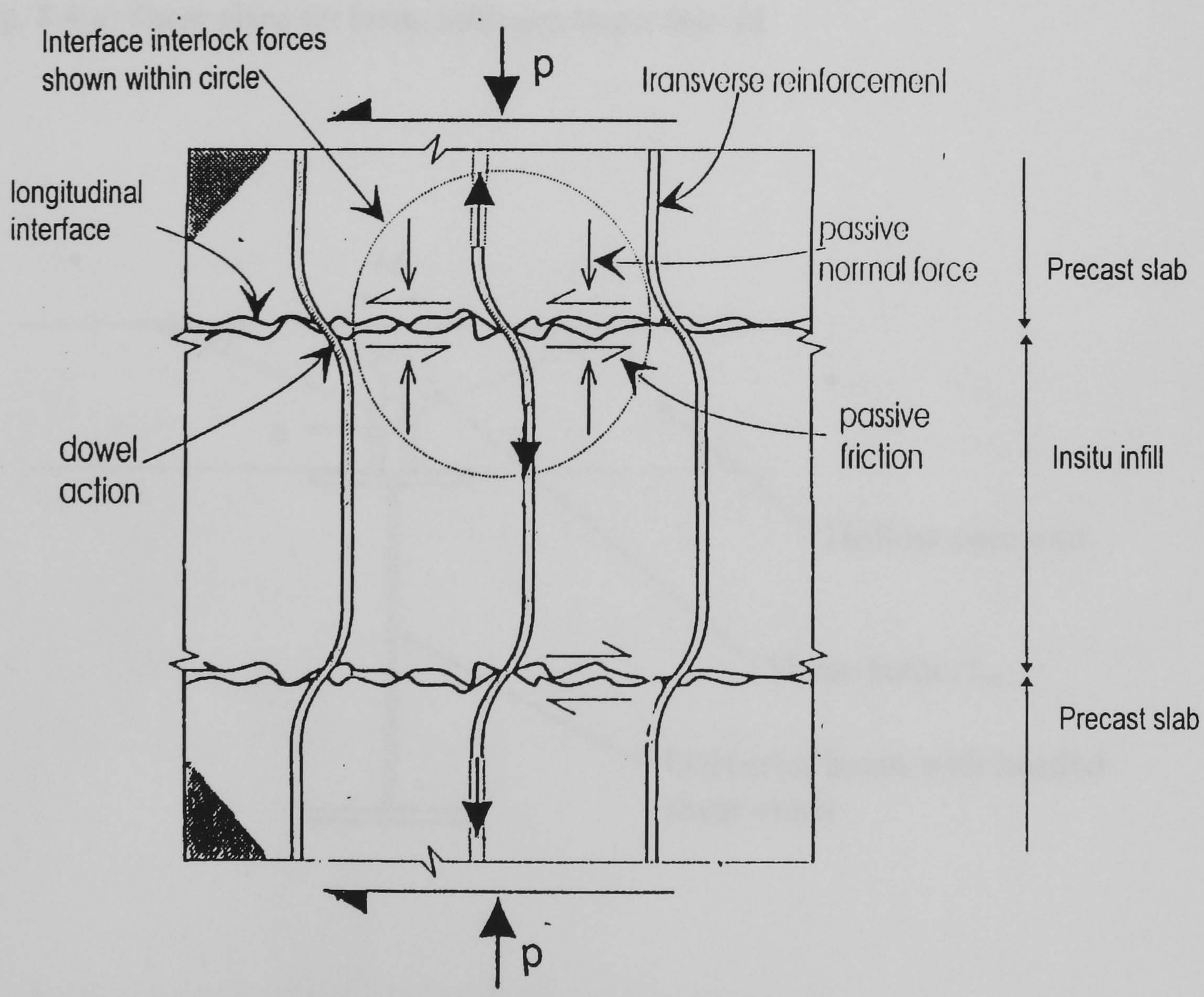

Fig. 8.3 Mechanisms of longitudinal shear transfer

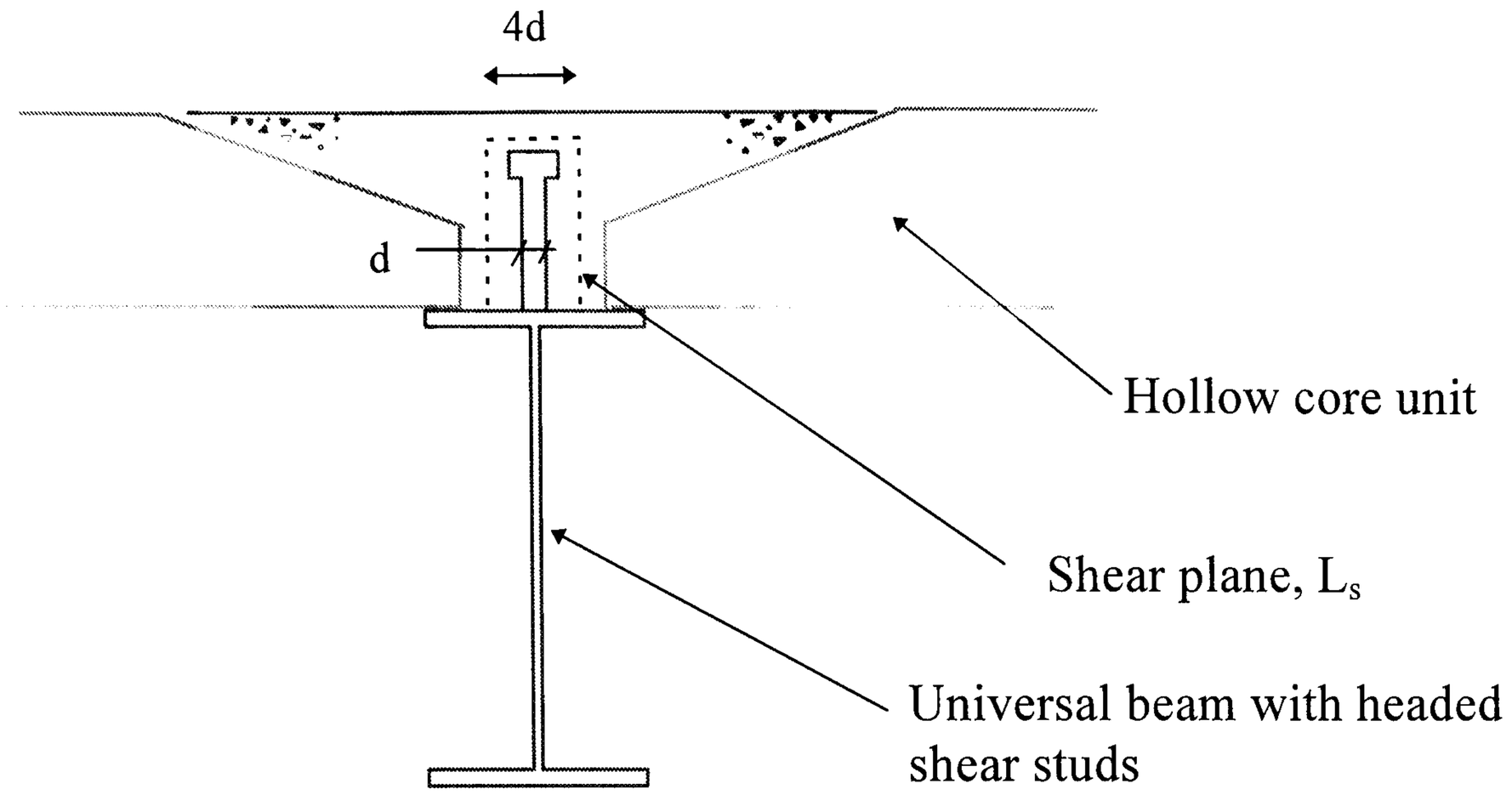

Fig. 8.4(a) Shear plane for insitu infill gap larger than 4d

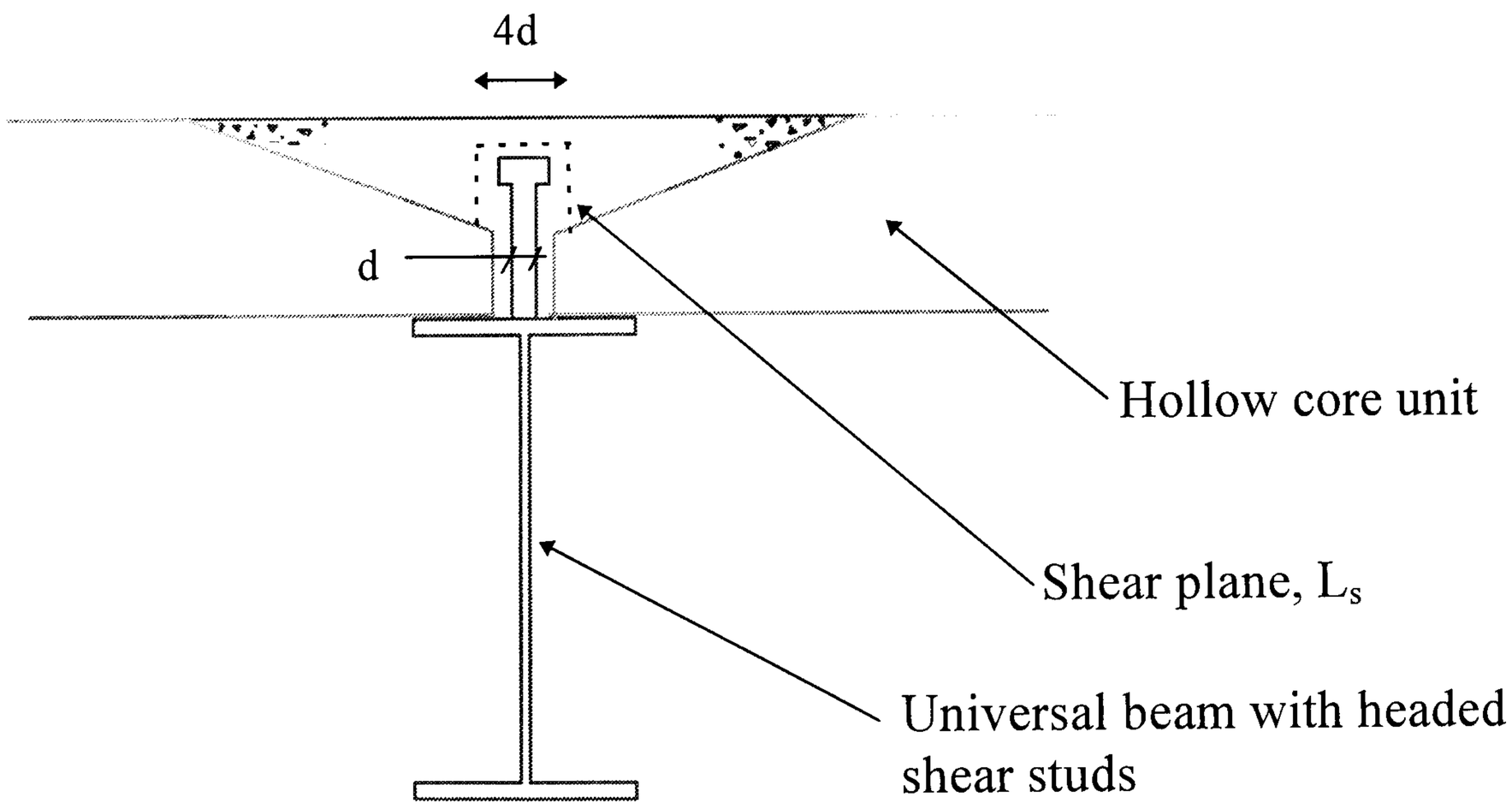

Fig. 8.4(b) Shear plane for insitu infill gap less than 4d

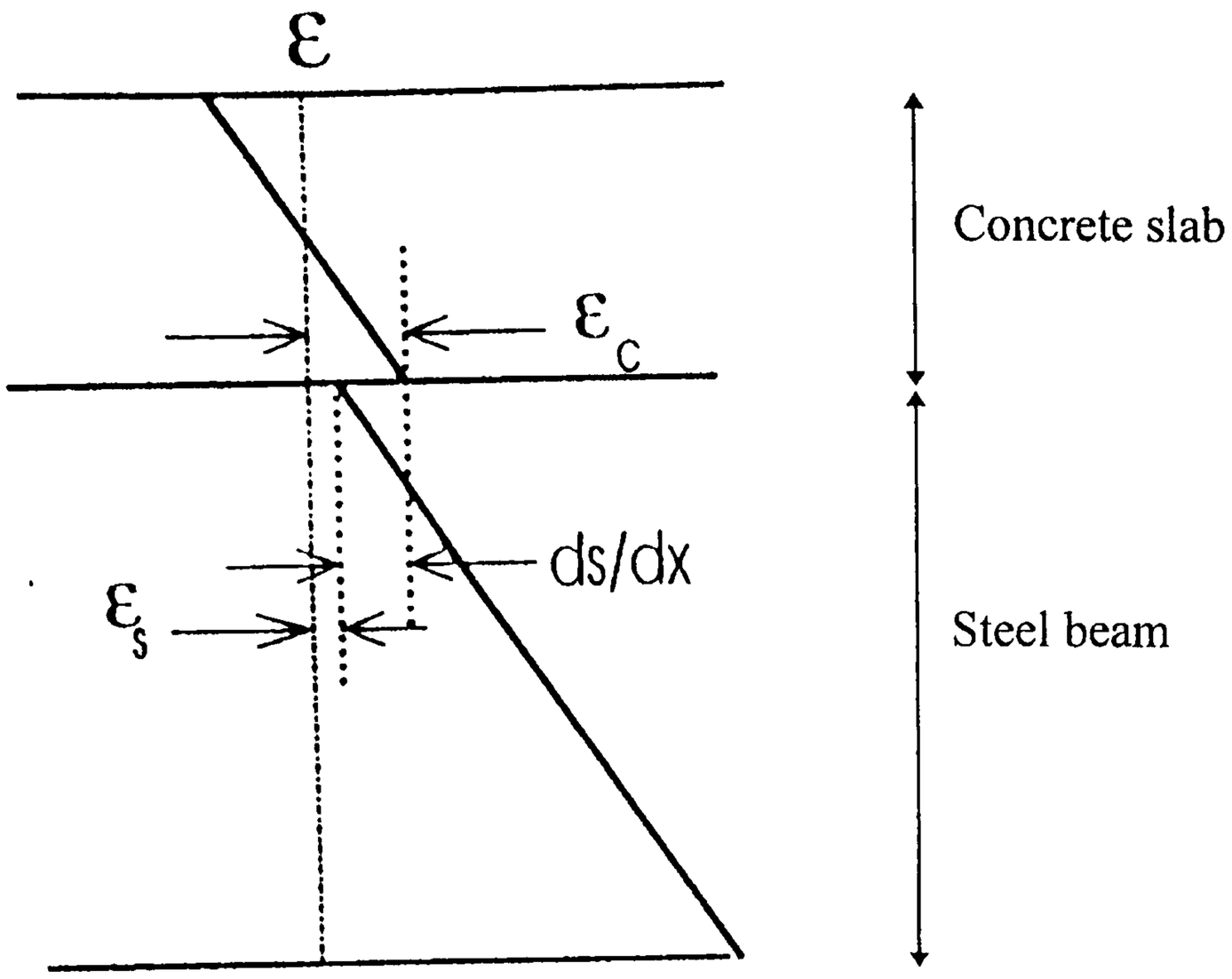

Fig. 8.5 Strain distribution for partial interaction

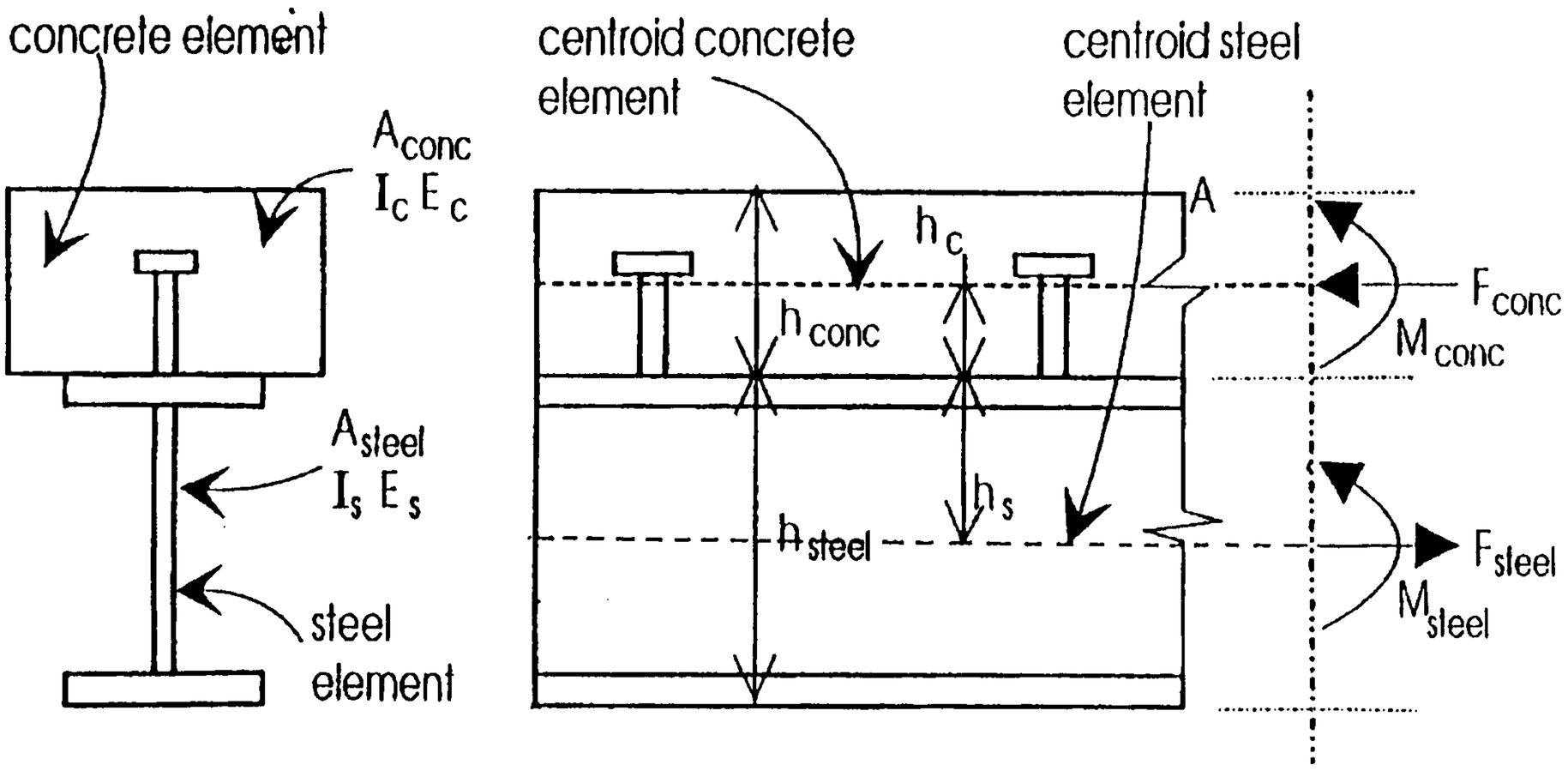

Fig. 8.6 Force and moment distribution of composite beam

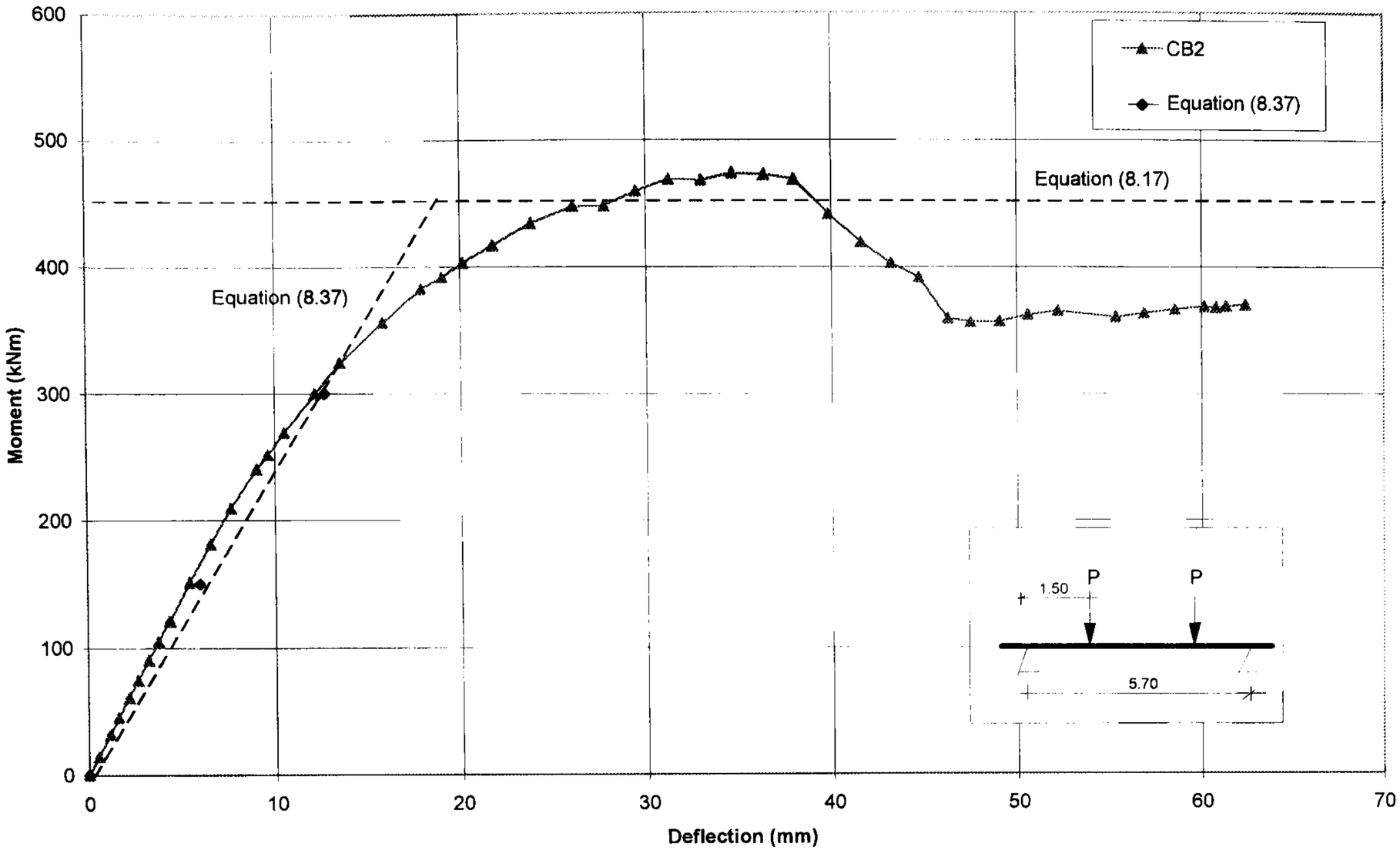

Fig. 8.7 Moment deflection curves of test result vs. theoretical analysis

Chapter 9

Conclusions and Future Work

9.1 Conclusions from the research programme

The behaviour of composite beams with precast hollow core slabs has been investigated by a combination of experimental and analytical study, and the following conclusions can be extracted from this research:

(i) Full scale experimental tests have shown that composite action between steel beams and precast concrete hollow core slabs may be achieved using headed shear stud connectors and small quantities of grade C25 (minimum) insitu concrete placed at the end of the floor slabs.

(ii) For typical sizes of UB and hcu slab, the flexural strength of the composite beam is between 50% to 100% greater than the strength of the bare steel beam. The flexural stiffness is up to 300% greater than the stiffness of the steel beam.

(iii) An adequate amount of insitu concrete, reinforced with at least 0.11 per cent area of high tensile bars, should be compacted around the headed

studs. The grade of insitu concrete should be C25 minimum. The effects of supply of over-strength materials might introduce brittle failure and should be avoided.

(iv) Eccentric compression slab tests and push-off tests have been used to develop empirical design equations for the effective breadth of the precast-insitu concrete slab, and for the horizontal shear capacity of the headed shear studs and predications are within 10 per cent of the experimental results.

(v) A parametric study using 45 finite element analyses has given the strength and stiffness of a wide range of composite beam sections. These results have been used to develop design rules. Also, load/span design charts for the 150mm, 200mm and 250mm precast hollow cored slab are formulated for use by the designer for initial sizing purpose only.

9.2 Proposed future work

Additional work needed for a complete understanding of the composite steel beam using hollow cored floor slabs is as follows:

(i) *Further experimental study on shear capacity and flexural behaviour with variation of depth of hollow cored floor slabs.* All the experimental studies in this research program were based on 150mm deep hcu and shear studs at 150mm centres. The properties of the deeper hcu are similar and it is believed that the arguments presented have shown that they can applied in more general situations. However, certain areas require further investigation. For example, the shear stud capacity with variation in hcu depth; the flexural behaviour of a composite beam with variation in stud spacing and deep hcu with shallow steel beam. These additional studies not only can verify the design equations and the FE design charts proposed but also increase the understanding of the behaviour of this type of construction.

(ii) *Finite element modelling of shear stud in hcu.* The finite element modelling work showed that the FE method provided a valuable and cost effective alternative to full scale experimental study. Although the simple 2-D FE model showed in this research can accurately predict the moment capacity for the composite beam, however, it is still reliant on the experimental load-slip curve obtained from the push off test. Although the push off test has been established as a basic method for the determination of shear capacity of shear connection, FE model of shear stud in hcu will eliminate the need for future experimental work which has some

disadvantages in term of time and costs and the need for specialized laboratories.

(iii) *To study the behaviour of continuous composite beams using hollow cored floor slabs.* To study continuous construction would seem to be a natural progression from the simple support construction. The construction is more complex because columns and connections are involved and the design of the hogging moment regions of the composite beam with hcu may require special attention as the hcu is weak in tension. Longitudinal reinforcement may be required in the hogging moment regions.

(iv) *To study the behaviour of composite beam-column connections with hcu.* For continuous composite construction, it is very important to develop an understanding of the behaviour of the composite beam-column connection. Experimental and analytical studies on the moment-rotation characteristics of the composite beam-column connection are needed so as to provide some insight into the potential for improved performance of beams in continuous construction and beams and columns in non-sway frames.

(v) *To study the diaphragm action in the hollow core slab with composite steel beam.* Research on diaphragm action of floors in precast concrete frames[1] has been carried out in the past. It showed the floor diaphragms consisting entirely of a hollow core slab would satisfy the strength and stiffness

requirements of most multi-storey precast building. The research based on the precast concrete beam where the neutral axis coincided with the neutral axis of the hcu and the lateral movement of the slabs were restrained by the beams. With the composite steel beam with hcu construction, the hcu is placed on top of the steel beam, therefore the load transfer between the beam and the hcu can only rely on the shear connection. The finding from this work may enable elimination of horizontal bracing for this type of construction.

(vi) *To study the torsional effect of the composite beam due to edge loading condition.* Eccentric loading on the edge beam would induce torsional effects in the composite beam and hence cause torsional buckling of the steel beam. Current practice in simple construction suggests the use of a steel hollow section for the edge beam design which may not be always desirable. With the composite construction, the neutral axis is further away from the bottom flange, therefore the torsional effect will be more critical.

9.3 References

1. Elliott, K.S., Davies, G., and Omar, W., 'Experimental and theoretical investigation of precast concrete hollow-cored slabs used as horizontal

floor diaphragms', *The Structural Engineer*, Vol. 70, No. 10, May, 1992, pp175-187.

Appendix A

Test Ref.	Member	No.	Size of coupon		Yield Strength (N/mm^2)	Ultimate Tensile Strength (N/mm^2)	Young Modulus (N/mm^2)
			Width (mm)	Thickness (mm)			
CB1	Flange	1	20.02	10.58	313.82	580.10	183.21
		2	20.01	10.55	310.90	569.09	187.57
		3	19.99	10.50	311.59	569.78	187.81
CB1	Web	1	20.06	7.51	345.46	589.12	203.92
		2	20.02	7.50	355.85	609.28	198.16
		3	19.98	7.44	362.30	603.00	205.67
CB2	Flange	1	20.01	10.55	312.55	578.90	190.87
		2	19.99	10.50	310.78	565.60	189.86
		3	20.01	10.60	313.50	580.02	192.50
CB2	Web	1	20.01	7.51	355.05	609.28	198.51
		2	19.99	7.53	356.43	602.58	205.82
		3	20.01	7.52	355.88	610.33	205.55
CB3	Flange	1	20.01	10.58	316.70	562.42	198.86
		2	20.00	10.59	315.60	580.55	193.50
		3	19.97	10.59	316.55	589.35	187.85
CB3	Web	1	19.99	7.51	355.84	595.06	204.46
		2	20.01	7.50	355.50	602.15	205.12
		3	20.01	7.50	356.13	609.45	199.13

Table A.1 Yield strength, ultimate tensile strength and Young's modulus of steel coupon tests

Test Ref.	Rebar	No.	Diameter of rebars (mm)	Yield Strength (N/mm^2)	Ultimate Tensile Strength (N/mm^2)	Young's Modulus (kN/mm^2)
CB1	T16	1	16.2	585	748	202
		2	16.1	585	746	202
CB2	T8	1	8.1	471	805	198
		2	8.05	464	754	198
		3	8.15	509	841	199
CB3	T8	1	8.1	462	750	199
		2	8.0	470	757	197
		3	8.05	465	755	199

Table A.2 Yield strength, ultimate tensile strength and Young's modulus of transverse reinforcement

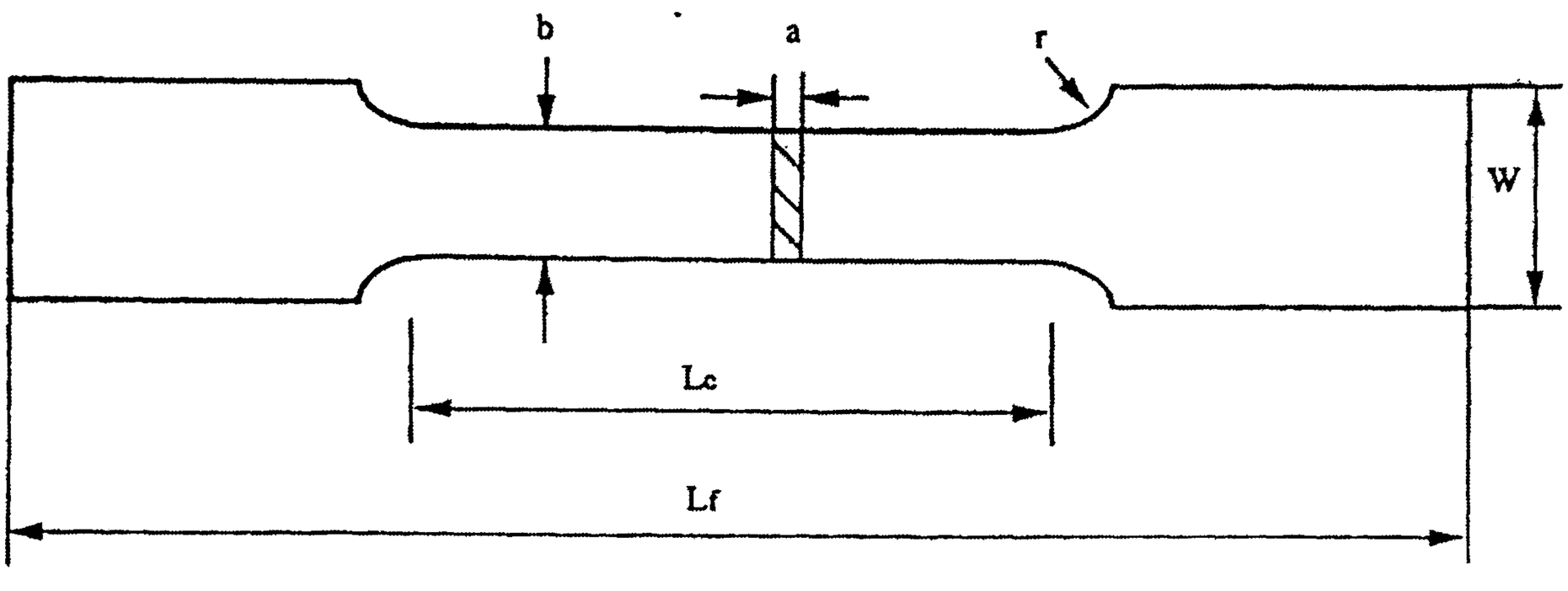

a = steel member thickness
b = 20 mm
Lc = 90 mm
Lf = 250 mm
W = 50 mm
r = 25 mm

Fig. A.1 Dimensions of coupon test specimen

UNIVERSITY OF NOTTINGHAM DEPT OF CIVIL ENGINEERING

TENSILE TESTING OF COUPONS FROM ROLLED STEEL SECTIONS

TEST RESULTS:

Young's modulus kN/mm^2	0.1% Proof Stress N/mm^2	0.2% Proof Stress N/mm^2	0.5% Proof Stress N/mm^2	U T S N/mm^2
198.86	311.72	316.70	330.31	562.42

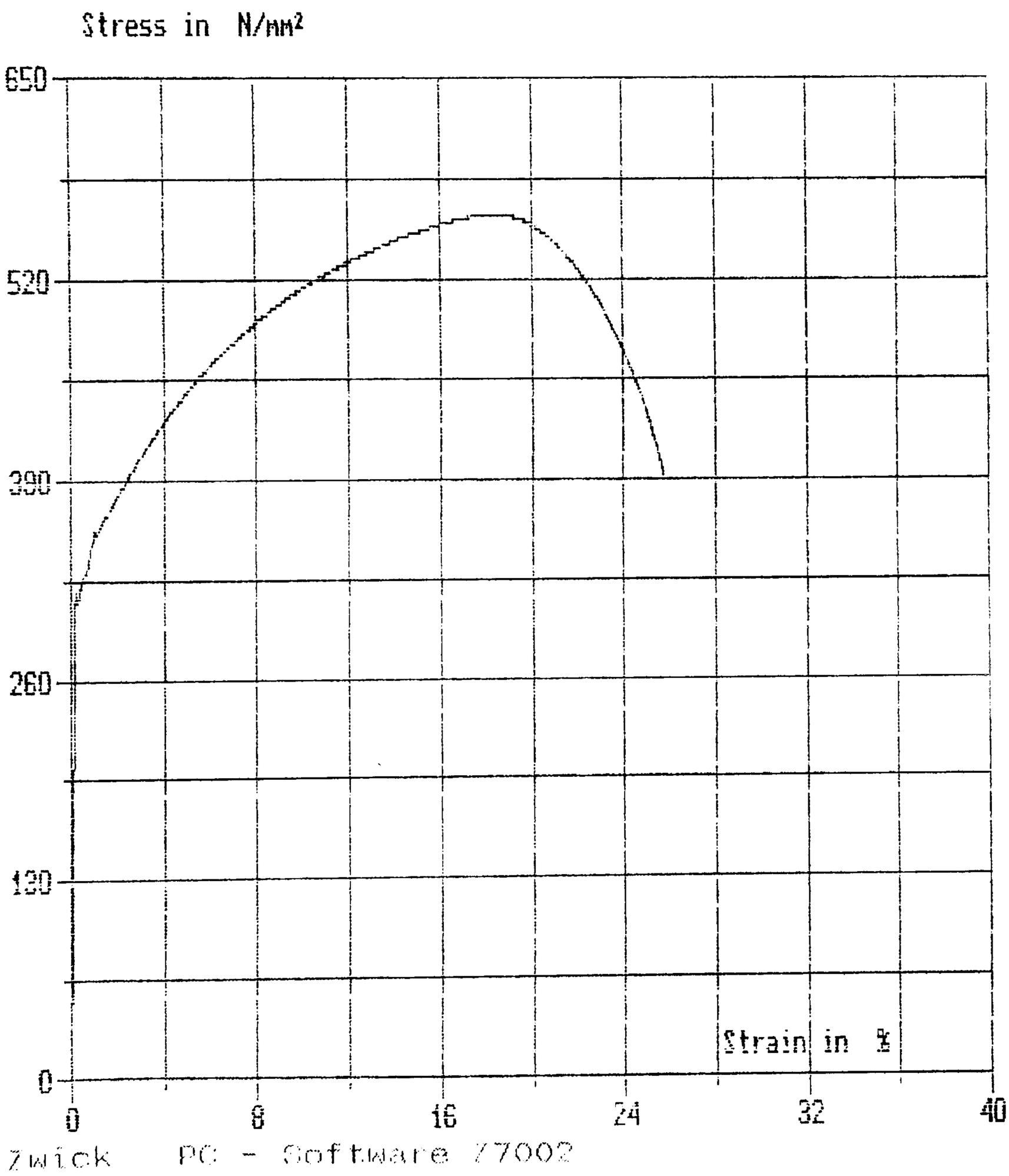

Fig. A.2 Standard coupon test curve for beam flange

UNIVERSITY OF NOTTINGHAM DEPT OF CIVIL ENGINEERING

TENSILE TESTING OF COUPONS FROM ROLLED STEEL SECTIONS

TEST RESULTS:

Young's modulus kN/mm^2	0.1% Proof Stress N/mm^2	0.2% Proof Stress N/mm^2	0.5% Proof Stress N/mm^2	U T S N/mm^2
204.46	357.14	355.84	347.88	595.06

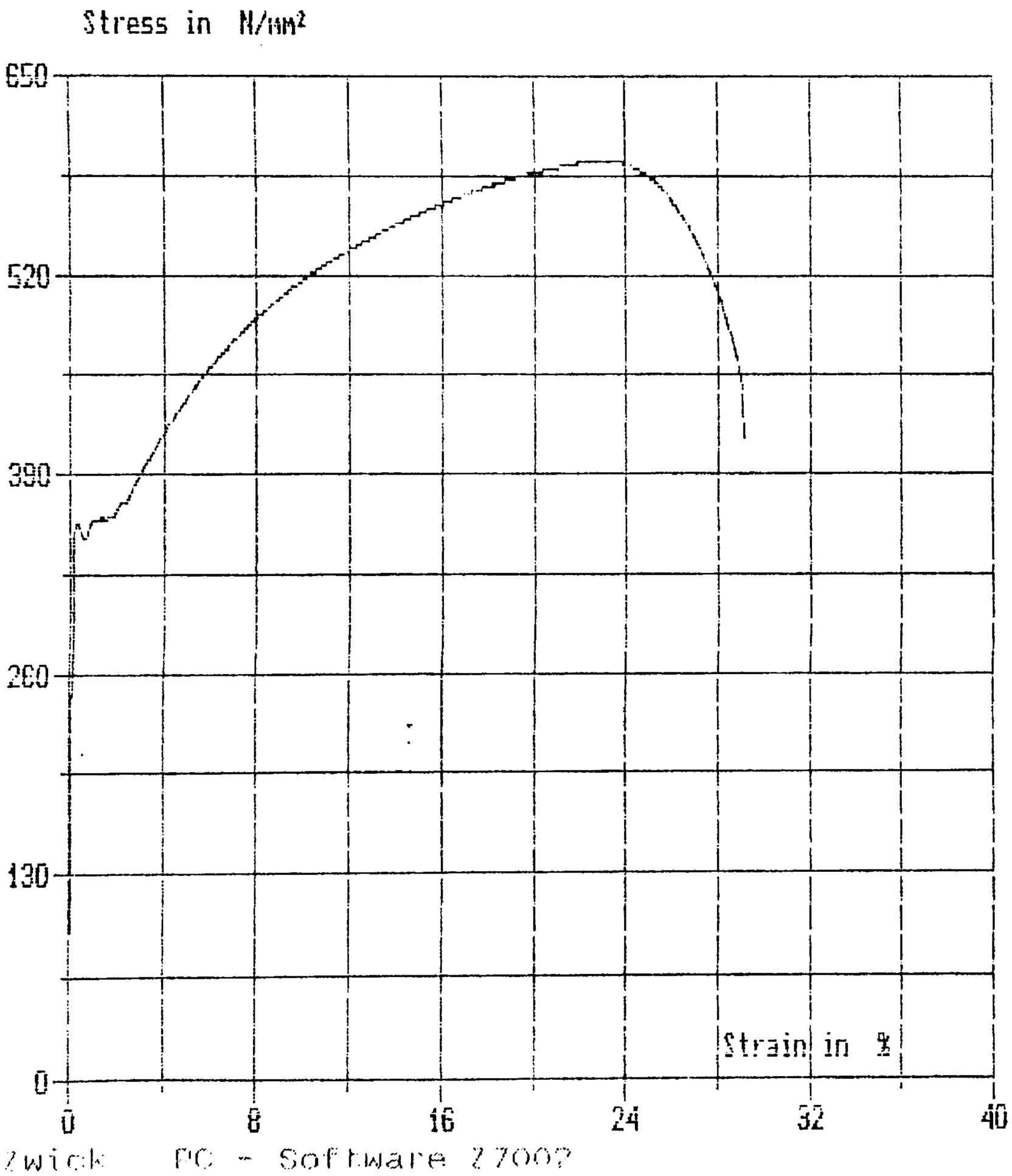

Fig. A.3 Standard coupon test curve for beam web